Novel Ferrocenyl benzoyl peptide esters as anti-cancer agents and Ferrocenoyl self assembled monolayers as anion sensors.

by

Alan J. Corry B.Sc. (Hons)

A thesis presented for the degree of Doctor of Philosophy

at

Dublin City University

Under the supervision of Dr. Peter T. M. Kenny

Ollscoil Chathair Bhaile Atha Cliath

School of Chemical Sciences

January 2009

To my family

Declaration

I hereby certify that this material, which I now submit for assessment on the programme of study leading to the award of Ph.D is entirely my own work, that I have exercised reasonable care to ensure that the work is original, and does not to the best of my knowledge breach any law of copyright, and has not been taken from the work of others save and to the extent that such work has been cited and acknowledged within the text of my work.

Signed: _____

Alan J. Corry

ID No.: _____

Date: _____

Acknowledgements

I would like to thank Dr. Peter T. M. Kenny for giving me the opportunity to conduct research under his supervision and for being supportive and patient during my three years in the lab.

I would also like to thank:

IRCSET and the Embark Initiative for funding this research.

Dr. Norma O'Donovan, Dermot O'Sullivan and Aine Mooney for conducting the biological studies.

Colm T. Mallon for being my electrochemistry guru and for answering all my questions and for his help throughout, also to Dr Mary Pryce for the use of her potentiostat and PC.

To all the technical and academic staff for their help, especially John McLoughlin, Damien McGuirk and Ambrose May.

A special thank you to all the PKRG (Peter Kenny Research Group), members, past and present especially Brian, Paula, Aine, Will and Andy.

Also to my fellow postgraduates especially Debbie, Neil, Lorraine, Saibh, Ewa, Dan, Brian Deegan, Liz, Emma K and Shelly, also to Sonia, Laura, Yvonne, Nicola, Emma, Sarah, Fadi, Tom, Lynda 1&2 and Bruce. Big thanks also to Michael Ryan.

Thanks to all the lads from home Ambrose, Ronny, Mick, Ged, Brady and Warren, even though they never really understood what I was doing.

Also, to all my family, especially Mam, Niamh, Pat, Kieran, Margaret and Ann, for all their support in every way possible over the past 24 years. Also, to the all the members of the Devine, Hand and Mathews families. I can start paying them back now.

Abstract

A series of novel *N*-(ferrocenyl)benzoyl peptide esters have been synthesized, characterized and screened *in vitro* against the non-small cell lung cancer cell line, H1299 (cisplatin and carboplatin resistant variant). The potential production of hydroxyl radicals would be enhanced by the benzoyl spacer as this lowers the redox potential of the ferrocene moiety thus making the iron atom easier to oxidize. The peptide chain would also be able to interact with biomolecules *via* hydrogen bonding.

A series of *N*-(ferrocenyl)$_2$ and *N*-(ferrocenoyl)$_2$ cystine dimethyl esters have also been synthesized, characterized and immobilized onto gold electrodes. The electroactivity of the ferrocene and the hydrogen bonding ability of the peptide amide bonds will be exploited in the sensing of anions in aqueous media.

The synthesis of each series of compounds was achieved by coupling the free *N*-terminus of various amino acid and peptide esters to the carboxyl group of ferrocenyl benzoic acid (*ortho*, *meta* and *para*) or ferrocenecarboxylic acid using *N*-(3-dimethylaminopropyl)-*N'*-ethylcarbodiimide hydrochloride (EDC) and 1-hydroxybenzotriazole (HOBt) coupling protocol. All compounds were characterized by a range of spectroscopic techniques including: ^{1}H, ^{13}C, DEPT 135 and HMQC NMR in addition to IR, UV-Vis, MS and CV.

The biological effects of orientation around the central benzoyl moiety, increasing peptide chain length and lipophilicity were investigated for the *N*-(ferrocenyl)benzoyl peptide esters. The most active compound was found to be *N*-{*meta*-(ferrocenyl)-benzoyl}-glycine-L-alanine ethyl ester with an IC_{50} value of 4.0 μM while *N*-{*ortho*-(ferrocenyl)-benzoyl}-glycine-L-alanine ethyl ester induced a block in the G2/M phase of the cell cycle.

{*N-ortho*-(ferrocenyl)-benzoyl}$_2$-L-cystine dimethyl ester displayed a linear amperometric response to chloride anions in aqueous media while {*N*-(ferrocenoyl)-β-alanine}$_2$-L-cystine dimethyl ester exhibited a linear response to nitrate, dihydrogen phosphate and adenosine nucleotides. For adenosine nucleotides {*N*-(ferrocenoyl)-β-alanine}$_2$-L-cystine dimethyl ester showed a nanomolar sensitivity in aqueous media.

Table of Contents

Section 1

Ferrocenyl benzoyl peptide esters as anti-cancer agents

Chapter 1

Biologically active ferrocene derivatives

1.1 Introduction.

Over the past 40 years organometallic chemistry has developed into a vibrant and important area linking organic and inorganic chemistry. Applications of organometallic compounds are varied and numerous. They include catalysts for industrial syntheses and anti-knocking agents for fuel. The interest in metal complexes in a biological sense was initiated by the success of cisplatin against various types of cancer [(1)]. Organometallic compounds containing transition metals, such as Co, Cu, Fe, Ga, Ge, Mo, Pt, Sn, Rh, Ru, Ti, and V are known to have anti-proliferative (*in vitro*) and anti-neoplastic (*in vivo*) activities. Platinum coordination compounds, such as cisplatin, carboplatin and other derivatives are used in the treatment of a variety of tumours [(2)]. However, problems with toxicity, harsh side effects during administration, together with acquired drug resistance problems has prompted the search for alternative anti-cancer drugs with better pharmacological profiles whilst retaining therapeutic efficacy. Some of the most promising novel non-platinum anti-cancer agents are emerging from the field of bioorganometallic chemistry. Bioorganometallic chemistry is a field devoted to the synthesis and study of organometallic species of biological and medical interest. Notably, the field of medicinal chemistry has benefited considerably from the incorporation of organometallic moieties into potential drug molecules. In the wake of the success of platinum complexes, coordination and organometallic compounds are possible alternative therapeutics for the treatment of cancer [(3)]. The resistance of some cancers to cisplatin emphasises the need for new drugs with differing modes of action in order to overcome this resistance. Colon and non-small-cell lung cancer are intrinsically resistant while ovarian and small-cell lung cancers acquire resistance over time. Resistance is due to decreased drug accumulation and an increased ability of DNA to tolerate the damage caused by cisplatin. Deactivation of cisplatin also occurs upon binding to proteins. A number of the severe side effects of cisplatin are attributed to this protein binding [(4)]. The ultimate aim of this research is the discovery of compounds that are active against a wide

range of cancers but that have fewer side effects than cisplatin [5]. This is highlighted by the recent entry of ruthenium compounds into Phase I clinical trials for the treatment of colorectal carcinoma, for example imidazolium-trans-tetrachloro(dimethylsulphoxide) imidazoleruthenium(III) [6].

Metallocenes, including ferrocene, are also known to have a wide range of biological applications. Ferrocene has attracted particular attention due to its aromatic character, stability and low toxicity. It can also be easily derivatized and the central iron atom is also easily oxidised from Fe(II) to Fe(III). The medicinal application of ferrocene is currently an active area of research with many reports showing its activity *in vivo* and *in vitro* and its potential as an anti-tumour, anti-malarial and anti-fungal agent [5].

1.2 Redox properties of ferrocene.

The electron transfer-reactive oxygen species-oxidative stress theory (ET-ROS-OS) has been implicated in the mechanism of action of a wide variety of biologically active compounds, for example nitroaromatics and quinones. Therefore the development of drugs that enhance Reactive Oxygen Species (ROS) has increased in importance. Also the fact that cancer tissue is known to be in a state of oxidative stress further increases the need for new drugs that can exploit this fact [7]. Increasing the concentration of ROS may overwhelm the cancer cells but leave normal cells unaffected. Elevated levels of ROS are also known to induce apoptosis. Current attention is concentrated on increasing concentration of ROS to lethal levels in cells, interfering with anti-oxidant enzymes and the promotion of catalysts that enhance the toxicity of the ROS.

The loss of an electron from a high energy, non-bonding orbital to yield the ferricenium cation, ($Fc \rightarrow Fc^{+}$), is an important aspect of the chemistry of ferrocene and is often implicated in its cytotoxicity [2]. This is demonstrated in Figure 1.1

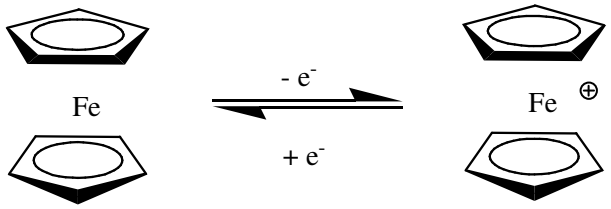

Fig. 1.1 One electron oxidation of ferrocene to yield the ferricenium ion and reverse reduction reaction.

In biological systems ferrocene can be oxidised by hydrogen peroxide in the presence of horseradish peroxidase. The hydroxyl radicals formed from Fc^+ under physiological conditions are proposed to act as DNA damaging agents for biologically active ferrocene derivatives. The ferricenium cation has been shown to form charge transfer complexes with donor groups in proteins. The reverse reaction, ($Fc^+ \rightarrow Fc$), is known to proceed through oxidation of metalloproteins, in the presence of glutathione forming hydroxyl radicals and through oxidation of NADH to NAD^+ [(2)]. The oxidation of NADH to NAD^+ is a good indicator of the ferricenium cations capacity for interfering with biologically important, enzyme controlled electron transfer reactions.

The redox status of a given biological system is vitally important as numerous processes in living cells are mediated by redox reactions. For example, cellular respiration whereby ATP is formed involves a series of reactions including the reduction of NAD^+ and oxygen and the oxidation of sugars. Redox activation of otherwise inactive prodrugs coupled with further chemical modification e.g. hydrolysis, can lead to highly reactive electrophilic compounds. A suitable bio-redox prodrug should have minimal toxicity to healthy cells, stability to metabolism in aerobic cells and suitable bioavailability and pharmacological properties.

1.3 Ferricenium salts as anti-cancer agents.

As early as 1984 the potential of ferricenium salts as anti-cancer candidates was observed [(8)]. In tests against Ehrlich ascites tumour cells in mice, ferricenium salts exhibited remarkable anti-neoplastic potency. Ferricenium picrate **1** and trichloroacetate salts were

responsible for a 100% cure rate using an optimal dose of 220-300 mg/kg. The colon R85 carcinoma displayed a 60-80% inhibition of tumour growth in the presence of **1**.

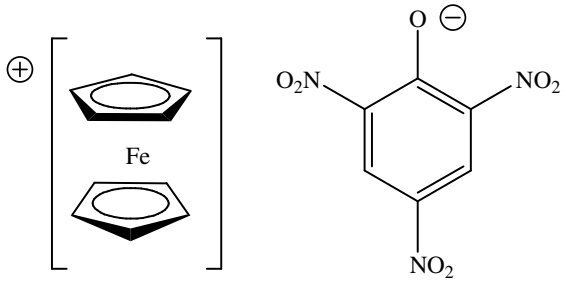

1

Osella *et al* continued this initial work and prepared ferricenium salts, for example $[FcCOOH]^+$ $[PF_6]^-$, for *in vivo* studies on Ehrlich ascites tumours. They observed that ferrocenes with a Fe(II) centre were unable to inhibit cell growth but Fe(III) ferricenium salts were cytotoxic. This cytotoxicity was independent of redox potential, at least in the range of 175 to 330 mV. It was also observed that there was no intercalation between the ferricenium salts and DNA. Interactions between the salts and the phosphate backbone of DNA were proposed to be electrostatic following observations from ^1H and ^{31}P NMR studies. Using electron spin resonance (ESR) experiments, it was proposed that the ferricenium salts produced hydroxyl radicals under physiological conditions, which in turn resulted in DNA damage [9]. The success of this initial work led to the preparation of different ferricenium salts for screening versus MCF-7 breast cancer cells [10]. The most active of these salts, with an IC_{50} value of 35 μM, was decamethylferricenium tetrafluoroborate **2**.

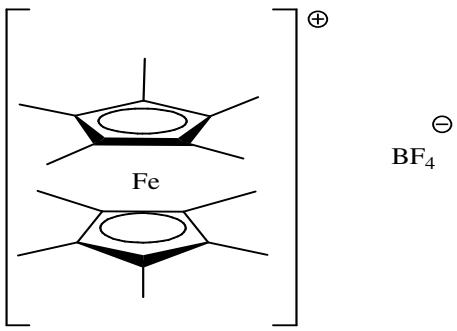

2

ESR experiments confirmed that compound **2** is able to produce oxygen radical species as a consequence of its degradation in aqueous media. From the ESR pattern it is suggested that there is a Haber-Weiss like process followed by a Fenton reaction to yield a hydroxyl radical, •OH. Compound **2** was also used in tandem with the clinically used anti-tumour drug bleomycin. Bleomycin is known to be activated in the presence of iron. A synergistic effect between compound **2** and bleomycin was observed. This corresponds to the DNA damage inflicted by compound **2** and the accompanying increased level of bleomycin activation by the Fe(II)/Fe(III) species.

Early cytotoxic results indicate that azaferrocenyl phosphanates, for example compound **3**, show anti-metabolite activity in HeLa cervical cancer cells. This data is preliminary and concentrations are in the millimolar range, however, azaheterocyclic metallocene derivatives are a logical starting point in the search for new anti-cancer agents [(11)]. The *in vitro* toxicity of compound **3** was determined by measuring its activity against the non-cancerous NIH 3T3 cell line and the cancerous HeLa cell line. Compound **3** produced significant inhibition of metabolic activity in the HeLa cell line, whilst it was ineffective against the non-cancerous cell line.

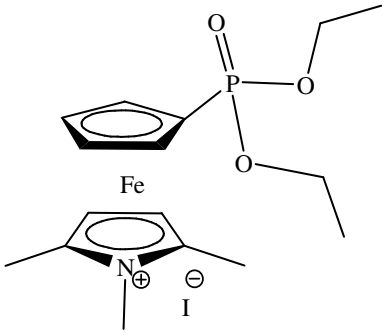

3

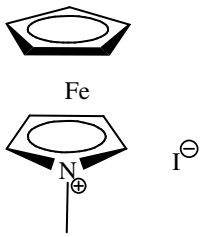

4

In the wake of *in vitro* experiments the potential of azaferrocenes, for example compound **4**, to trigger DNA scission was confirmed. Compound **4** caused a complete degradation of the plasmid at the lowest concentration used, namely 6.25 μM. ESR spectroscopy suggests a free radical mechanism of DNA scission by azaferrocenes. The strength of the iron-heteroatom ring bonding and the release of redox active metal cations that can generate free radicals were found to be important in DNA scission [(12)].

1.4 Metallocene based selective estrogen receptor modulators and anti-androgens.

Tamoxifen is a widely prescribed selective estrogen receptor modulator (SERM). It is used against hormone dependent breast cancer, where the estrogen receptor (ER), is present. These are known as ER positive cells, ER(+) [13]. SERMs are capable of interacting with estrogen binding sites despite their non-steroidal structure.

The effect of tamoxifen in the body is as a result of the hydroxylated form **5** which causes an anti-estrogenic effect following binding to the ER. However, some breast cancer cells do not have ER present. These are referred to as ER(-). Following prolonged exposure to tamoxifen some cells develop resistance. Hillard *et al* have prepared a series of ferrocene substituted tamoxifen derivatives [13]. These hydroxyferrocifens, for example compound **6** (n = 2, 3 or 5), were screened against ER(-) and ER(+) cell lines. In the ER(+) lines, the effect was comparable to that of tamoxifen showing significant anti-proliferative behaviour. When tested on the ER(-) cell line an IC_{50} value in the order of 0.5 μM was obtained where tamoxifen had previously been inactive.

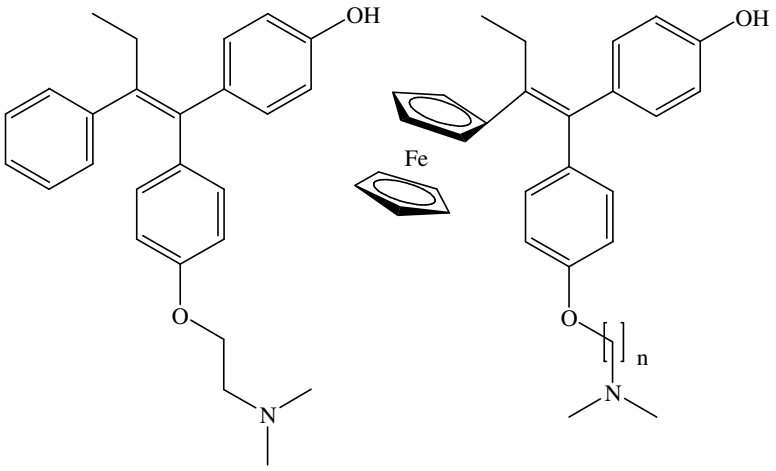

5 **6** n = 2, 3 or 5

Pigeon *et al* prepared the ruthenocene analogue of hydroxytamoxifen, compound **7**. This compound was found to be active towards ER(+) MCF-7 cells, whereas it had no effect on MDA-MB231 cells which are ER(-) [14]. The derivative of **7** where n = 3-5 is more

effective than tamoxifen on the ER(+) cells. These results contrast surprisingly with those of ferrocifen. Electrochemical experiments revealed that upon oxidation the ruthenocene radical cation decomposes. This is a possible explanation for the difference in activity between the two analogues, **6** and **7**.

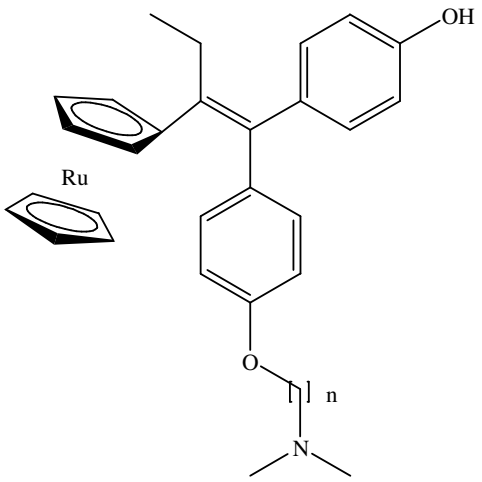

n = 2-8

7

The activity of compound **6** had been attributed to intracellular oxidation resulting in hydroxyl radical formation and cell death. However it was demonstrated using fluorescence activated cell sorting (FACS) that even at high concentrations ferrocifens caused negligible oxidative DNA damage. FACS monitors the presence of 8-oxo-guanine which is a marker for nucleobase oxidative damage.

Hilliard and Jaouen used cyclic voltammetry experiments to propose another possible mechanism for the cytotoxic effect of hydroxyferrocifens. The addition of pyridine to electrochemical solutions caused two changes in the observed voltammograms. The Fc/Fc^+ redox couple became irreversible, which is possibly due to the scavenging of the ferricenium cation before the reverse sweep. This observation was accompanied by a large increase in the ferrocene oxidation wave. This is representative of a second electron transfer following reaction of the primary cation. They proposed that following oxidation to Fc^+ the electron is delocalized over the π system resulting in a slight positive charge on the hydroxyl group. This proton is then easily removed in the presence of pyridine. The resulting phenoxy radical can then be oxidized, which is then followed by another proton

abstraction from the ethyl group furnishing a quinone methide. In the presence of a basic species like DNA the quinone methide species **8** will be formed which in turn will lead to cell death [13].

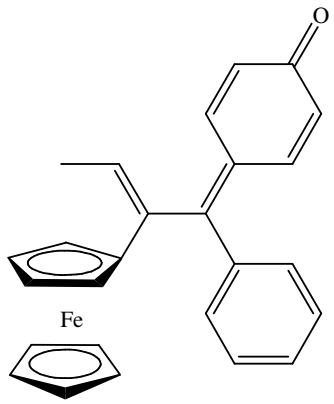

8

This mechanism of action is further validated electrochemically, as derivatives that were inactive showed no electrochemical changes upon addition of pyridine to solution. The oxidation of tamoxifen and other SERMs to quinoids is also a recognised pathway for their cytotoxicity [15].

Vessieres *et al* have prepared a series of diphenolic compounds derivatized with ferrocene and studied their anti-cancer activity against ER dependent and independent breast cancer cell lines [16]. Derivative **9** had strong anti-proliferative activity against MCF-7 and MDA-MD231 breast cancer cells with IC_{50} values of 0.7 and 0.6 μM respectively. Conversely compound **10**, which is a regioisomer of compound **9**, displays only modest activity against both cell lines. There are two main differences between compounds **9** and **10** in terms of structure. In compound **9** one of the two phenol groups is always orientated *trans* to ferrocene, whereas in compound **10** there is a *cis* relationship between ferrocene and the phenol group. Secondly, in compound **9** the two phenol rings are bonded to the same carbon of the alkene, whereas in compound **10** each carbon of the alkene is attached to a phenol ring.

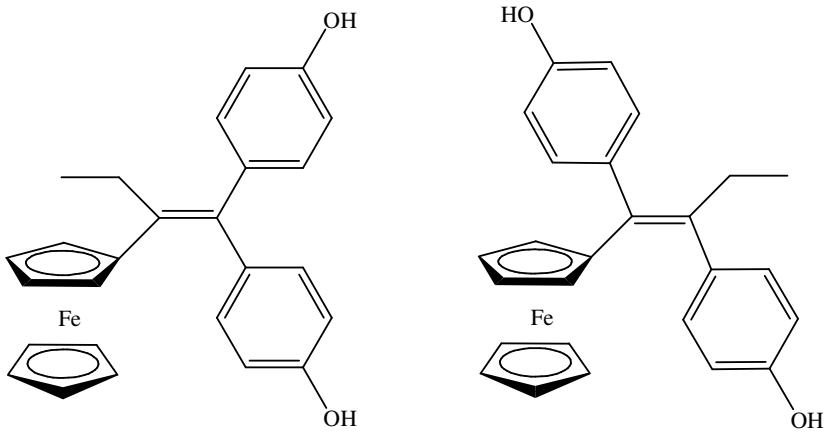

9 **10**

The different biological results indicate that the ferrocene moiety is not solely responsible for activity. The relationship between ferrocene and the rest of the molecule must be considered. Vessieres used derivatives of **9** and **10**, where one -OH of each compound was replaced with an -OMe group, to show the importance of the position of the ferrocene. Only the compound in which the ferrocene and ethyl groups were attached to the same carbon showed irreversible redox activity upon addition of pyridine. The position of the ferrocene in relation to the ethyl group is therefore essential to form the quinone methide derivative **8**.

Compound **9** has recently been successfully incorporated into two types of nanoparticles, namely nanocapsules and PEG/PLA (polyethyleneglycol/poly-D-lactic acid) nanospheres with the aim of finding an *in vivo* drug delivery model. These nanoparticles can protect the drug against hydrolysis and oxidation and prevent degradation [17]. After compound **9** was appended to nanoparticles, cell cycle assays were performed in the presence of α-tocopherol **11**.

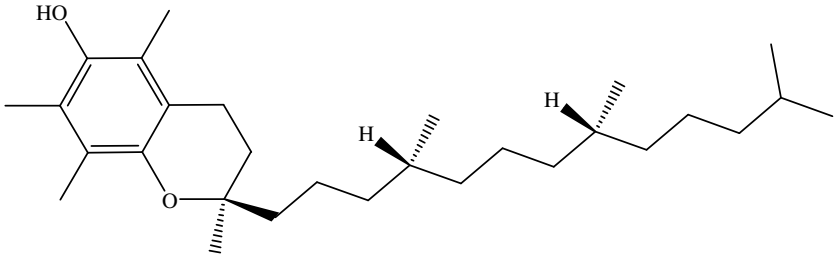

11

Compound **11** is the vitamin E form that is preferentially absorbed by humans and is a well known anti-oxidant. In the presence of compound **11** the anti-proliferative effect of compound **9** was reversed as there was a drop in the population of cells in the sub G1 phase of the cell cycle, the stage where damaged cells would be found. The presence of an anti-oxidant may prevent oxidation of ferrocene to ferricenium and therefore prevent the formation of compound **8** leading to a loss in anti-proliferative effect.

The importance of conjugation to the activity of these compounds is evident from biological results of a series of unconjugated ferrocenyl phenols, for example **12**. The anti-proliferative effect of the unconjugated derivatives was markedly lower than for compound **9**. For both cell lines compound **9** was 5-7 times more active than any of the unconjugated derivatives [4]. Cyclic voltammetry was again used to probe the mechanism of action of these derivatives. For the unconjugated derivatives there was no major change in the ferrocene/ferricenium redox couple observed when pyridine was added. These results suggest that the π system of compound **9** facilitates the generation of a reactive quinoid species **8**. Due to the absence of a π system in compound **12** it is unable to mediate electron transfer. However the significant IC_{50} values for these derivatives of less than 5 μM in each case represents significant cytotoxicity. As they do not give rise to quinine methide species it is possible that Fenton type chemistry is responsible for their activity.

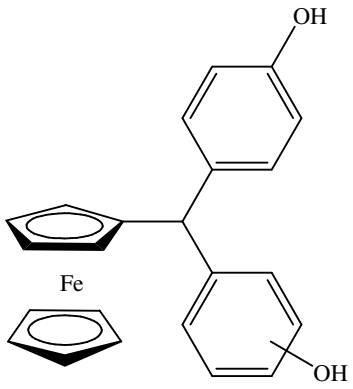

12

The importance of the hydroxyl group of ferrocifen was again demonstrated when Jaouen prepared thioether and thioester derivatives. The presence of thioesterases in breast cancer cells was expected to hydrolyse compound **13** and possibly lead to formation of the cytotoxic quinone methide. However, no anti-proliferative effect was observed in ER(+) or ER(-) cells for the thioether or thioester derivatives [18].

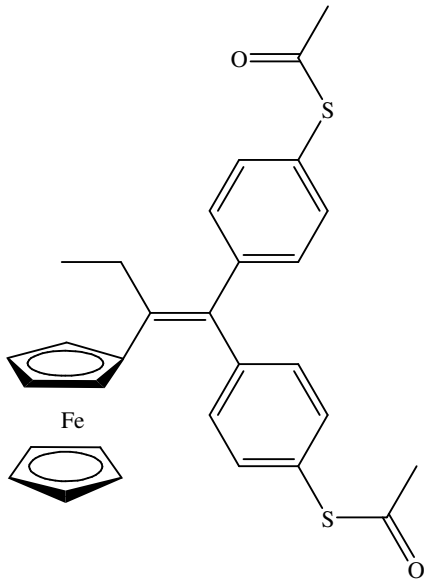

13

Investigating the mechanism of action of hydroxyferrocifens is further complicated by the fact that there are two ER sub groups, namely ERα and ERβ [19]. One possible role of the ERβ sub group is the control of intracellular oxido-reduction. Therefore when designing potential cytotoxic agents for ER(+) cells it is important to consider the relative binding affinities (RBA) of the drug for each ER, α and β. A relative binding affinity (RBA), of 3.4, ERβ/ERα, was observed for the *ortho* form of **12**. This agrees with the theory that the β form is more suitable for accommodating small ligands than the α form [20].

Molecules with an affinity for estrogen receptors have been used as vectors for cytotoxic agents. A number of platinum derivatives have been prepared. For example, the active moiety of oxaliplatin used in the treatment of colorectal cancer was coupled to tamoxifen to form derivative **14** [21]. This compound (R = OH) had an IC_{50} value of 4.0 μM, whereas

oxaliplatin had an IC_{50} value of 7.4 μM against MCF-7 breast cancer cells. Therefore the anti-proliferative effect of **14** is similar to that observed for the parent platinum complex.

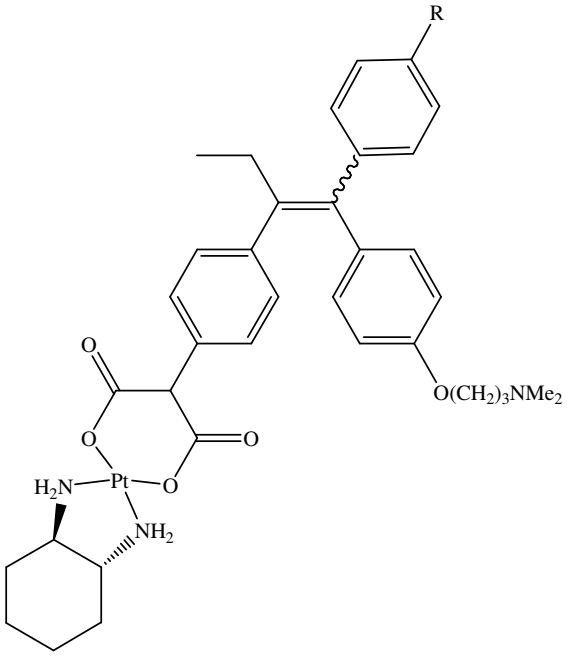

14, R = H, OH

Tamoxifen has also been appended to the potentially cytotoxic titanocene dichloride [22]. However the most important finding was the proliferative effect of **15** and titanocene dichloride on ER(+) MCF-7 cells. Compound **15** exhibited an estrogenic effect almost as powerful as that of estradiol, even at low concentrations. This effect concealed any anti-proliferation that may have been caused by the tamoxifen scaffold. The proliferative effect caused by titanocene dichloride has been attributed to the Ti(IV) ion. The parent molecule undergoes hydrolysis of the chloride ligands and also the cyclopentadienyl groups leading to the complete release of Ti(IV). A molecular modelling study indicated that the Ti(IV) ion had a similar effect to estradiol on the ER.

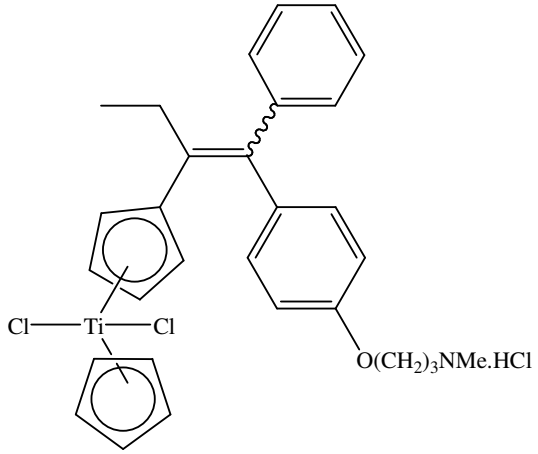

15

The stable cyclopentadienyl rhenium tricarbonyl ($CpRe(CO)_3$) moiety was also integrated into the tamoxifen scaffold, compound **16**. Exchange of the phenol ring for the bulkier ($CpRe(CO)_3$) is likely to change the active receptor site and the interactions of the dimethyl amino side chain. These interactions are known to be responsible for the anti-estrogenic effect of tamoxifen [23].

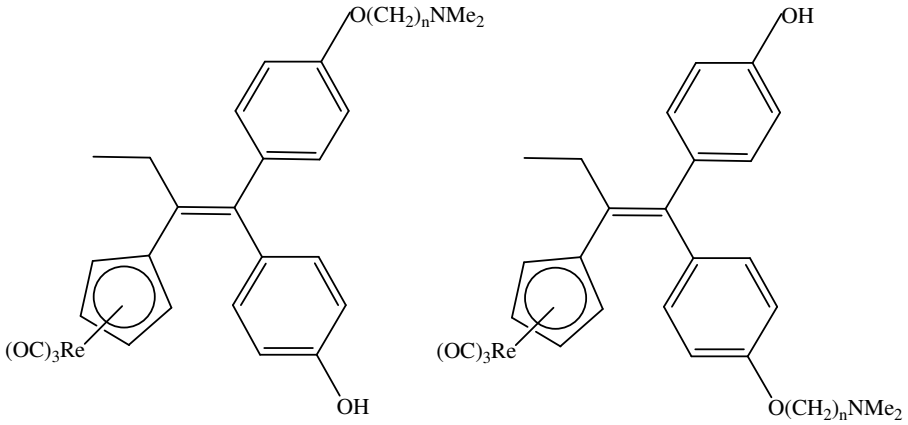

16, Z and E isomers

Compound **16** displayed an increase in lipophilicity compared to hydroxytamoxifen, an important feature in terms of its permeability through lipid membranes. The decrease observed for the RBA of **16** for the estrogen receptor does not appear to impact on its anti-proliferative ability. For ER(+) MCF-7 cells the anti-proliferative effect is slightly better than that of hydroxytamoxifen while there was only a marginal effect on the ER(-) MDA-MD231 cell line [23].

Payen *et al* also prepared ferrocene derivatives of the non steroidal anti-androgen nilutamide, used in the treatment of prostrate cancer. Analogues of nilutamide were prepared where the C-5 position of the hydantoin ring was substituted with ferrocene, **17**, and a *para*-anisyl group, **18** [24]. Both analogues showed negligible binding affinity for the androgen receptor (AR) which is claimed to play a vital role in cancer development. These derivatives were found to be the most active when tested *in vitro* versus the hormone independent PC-3 cell line. IC_{50} values of 5.4 µM for compound **17** and 5.6 µM for compound **18** respectively indicate that the effect of the ferrocene is due to its aromatic character and is independent of its organometallic nature.

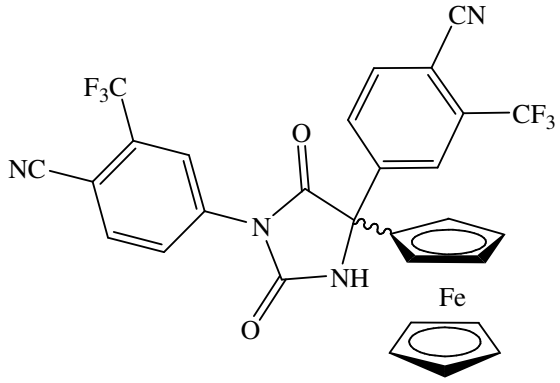

17

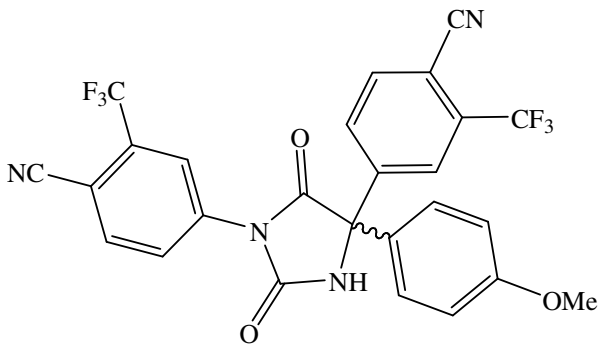

18

It may be possible for compounds **17** and **18** to act *via* recognition by receptors other than the AR. A higher level of the cannabinoid receptor is observed in the cancerous prostrate relative to a healthy organ therefore it is suggested that **17** and **18** interact with this receptor.

1.5 Ferrocenyl peptide conjugates as anti-cancer agents.

Standard peptide coupling procedures were used by Kelly *et al* to prepare a series of *N*-(ferrocenylmethyl)fluorobenzene-carboxamide derivatives. The inclusion of fluorine is a recognized strategy in the development of various drug types [25]. This series was screened against ER(+) MDA-MB-435-S-F breast cancer cells. Compound **19** was found to be the most active with an IC_{50} value of between 11 and 14 µM. As the concentration

of compound **19** was increased, cytotoxicity increased, indicating a dose dependent relationship.

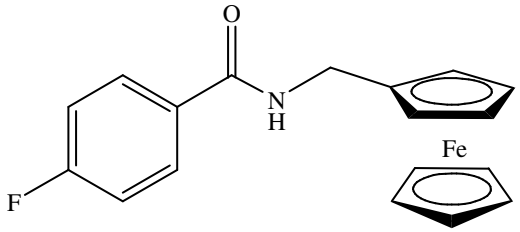

19

N-(ferrocenyl)benzoyl dipeptide esters have also been shown to be highly active *in vitro* [26, 27, 28]. *N*-{*ortho*-(ferrocenyl)-benzoyl}-glycine ethyl ester was initially tested for its *in vitro* anti-proliferative activity towards lung cancer cells (H1299 and H1299 carboplatin resistant variant). This compound was found to be cytotoxic and had an IC_{50} value of 48 μM, whereas the starting material, *ortho*-ferrocenyl ethyl benzoate, was completely inactive against this cell line. Therefore other derivatives were evaluated for their anti-cancer activity against lung cancer cells. The dipeptide derivative *N*-{*ortho*-(ferrocenyl)-benzoyl}-glycine-glycine ethyl ester was shown to have an IC_{50} value of approximately 20 μM, while *N*-{*ortho*-(ferrocenyl)-benzoyl}-glycine-L-alanine ethyl ester **20** had an IC_{50} value of 5.3 μM (RSD 8%) [26]. The *meta* and *para* analogues of **20** were also assayed and gave results of 4.0 μM and 6.6 μM respectively. This indicates that orientation around the central benzoyl moiety is not a crucial factor for activity [27].

The activity of these compounds is possibly due to their low redox potentials and their ability to form reactive oxygenated species (ROS) under physiological conditions. The activity of compound **20** is not solely due to ferrocene so it is plausible that the peptide chain is involved in a secondary mode of action. The lipophilic ferrocene group may anchor to the cell membrane and the peptide chain may block the opening of channels in the cell membrane leading to cell death [28]. Cell cycle assays were also performed on a control sample and on cells treated with *N*-{*ortho*-(ferrocenyl)-benzoyl}-glycine-L-alanine ethyl ester, compound **20**, at concentrations of 5 μM, 10 μM, 20 μM and 40 μM. As the concentration of compound **20** increases, the percentage of cells in the G1 phase

of the cell cycle decreases, suggesting a block in the G2/M phase, preventing the cells re-entering the G1 phase [27].

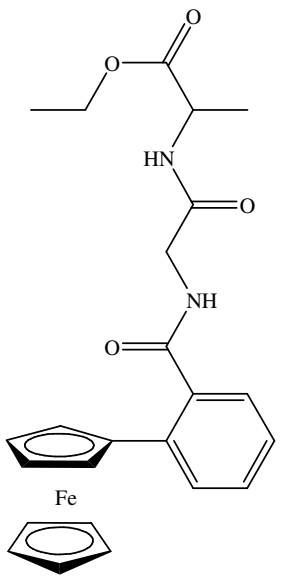

20

1.6 Other metallocene complexes as anti-cancer agents.

Johnson *et al* have developed water soluble and biocompatible polymers with a ferrocene side chain for treatment of colon cancer [29]. Cancers of the intestinal system are known to be insensitive to many treatments. These ferrocene conjugates have demonstrated excellent activity against Colo 320 DM colon cancer cells. The IC_{50} values represent the mean polymer concentration to achieve 50% cell growth inhibition. The cell growth inhibition is expressed as a function of polymer concentration in µg Fe/ml. Compounds **21** and **22** displayed significant activity with IC_{50} values of 0.22 and 0.55 µg Fe/ml respectively compared with an IC_{50} value of 1.00 µg Pt/ml for cisplatin.

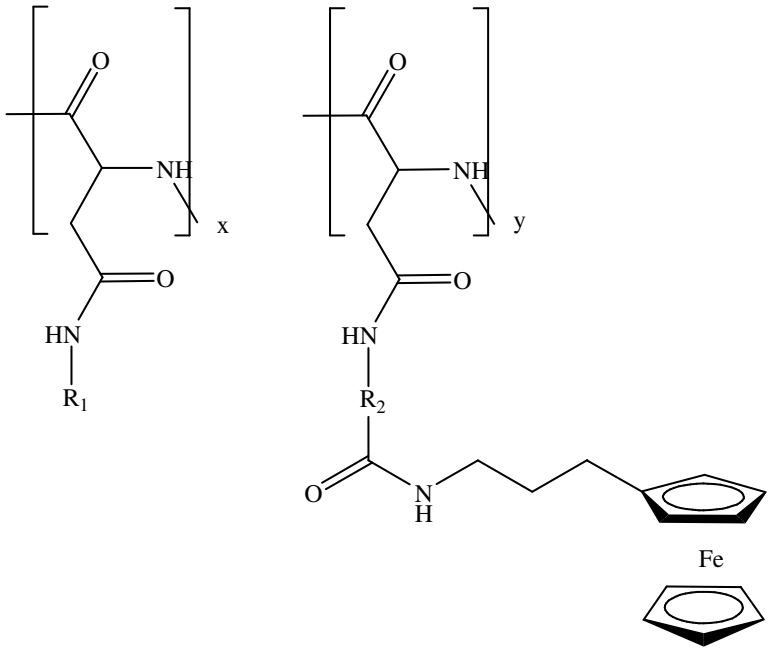

21: R_1 = 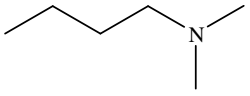 , R_2 = 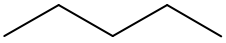 , x and y = 4

22: R_1 = 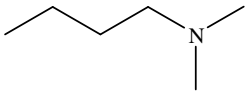 , R_2 = direct bond, x and y = 9

The activity of these conjugates was attributed to the tertiary amine side chain (R_1). This enables the polymer to become cationic at physiological pH through nitrogen protonation. Cationic polymers of this type are known to enter cells more favourably than polymers in a neutral state.

Topoisomerases are enzymes that are crucial in DNA replication, transcription and repair. They can be divided into two categories, topoisomerase I and topoisomerase II. Due to their crucial role in DNA function their loss can make cells vulnerable. As a result of this topoisomerase I and topoisomerase II inhibitors have become important targets for researchers. Several ferrocenyl derivatives have been prepared as topoisomerase inhibitors [(30)].

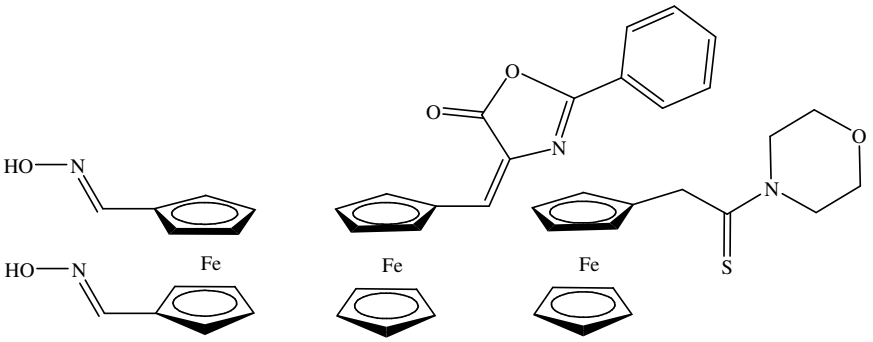

23 **24** **25**

The carboxaldoxime derivative **23** had a strong anti-proliferative effect against human Colo 205 colon carcinoma. It is proposed that enzyme complexation is as a result of nitrogen and oxygen interaction between **23** and the topoisomerase. The azalactone derivative **24** inhibits DNA passage activity leading to the formation of a cleavage complex, while thiomorpholideamidomethyl ferrocene **25** competes with ATP binding and inhibits the catalytic activity of the enzyme [(31)]. The exact role of ferrocene in these examples is unclear. Metallocene dihalides have also shown topoisomerase inhibition. The metallocene dihalide derivatives undergo halide hydrolysis to form coordination complexes. It is possible that there is then binding between the metallocene and coordination sites on the topoisomerase resulting in loss of activity of the enzyme.

Metallocene dichlorides with Ti, V and Nb metal centres have also shown anti-tumour activity [(32)]. Titanocene dichloride reached Phase II clinical trials for patients with renal cell carcinoma and metastatic breast cancer. The anti-proliferative effects of dimethyl-amino functionalised titanocenes were observed *in vitro* and *ex vivo*. These derivatives demonstrated that prostrate, cervix and renal cell cancer were prime targets. Compound **26** displays an IC_{50} of 5.5 μM against LLC-PK renal cell lines. Against this particular cell line it is approximately 400 times more active compared to Cp_2TiCl_2. The IC_{50} value also compares favourably with cisplatin which has a value of 3.3 μM. The increase in cytotoxicity is attributed to the two *N,N*-dimethylamino groups. After the drug has passed the cell membrane a mono or dication may be formed after hydrolysis of either or both of the chloride ligands. Coordination of the N-Me_2 groups to the titanium centre would then stabilise the metal cation and lead to more titanococene-DNA interactions.

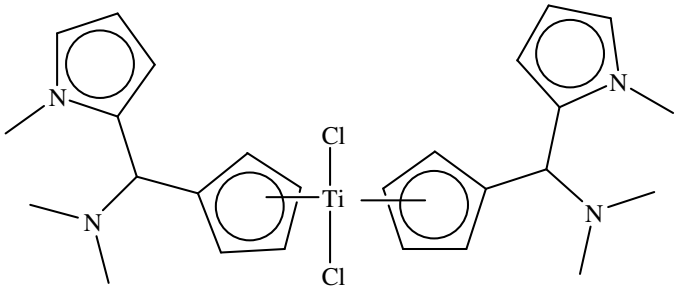

26

Another titanocene derivative **27** has demonstrated significant activity against various cancer types and caused an increase in apoptosis of prostrate cancer cells when compared to cisplatin [33]. It also has an IC_{50} value of 21 μM *in vitro* against LLC-PK renal cells, whereas other mono, di and trimethoxy derivatives had very little activity against this cell line with IC_{50} values between 88 μM and 253 μM [34].

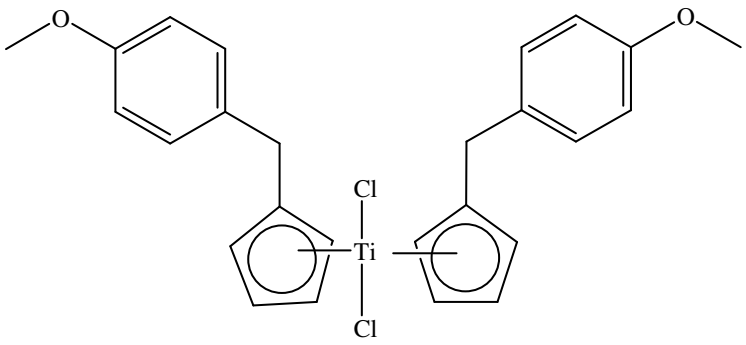

27

1.7 Ferrocene derivatives as anti-malarial agents.

Malaria is a tropical disease with 40% of the world's population believed to be at risk [5]. It is estimated that the number of deaths ranges from 1.5 to 2.7 million per annum [35], the majority of these deaths occur in Africa. Resistance of parasites that cause human malaria to chloroquine, the main malaria treatment, has led to a desperate need for new anti-malarial agents with novel modes of action [36]. Ferroquine **28**, a ferrocene analogue of

chloroquine, has recently entered Phase I clinical trials [37]. It is hoped that compound **28** will overcome the problem of chloroquine resistance.

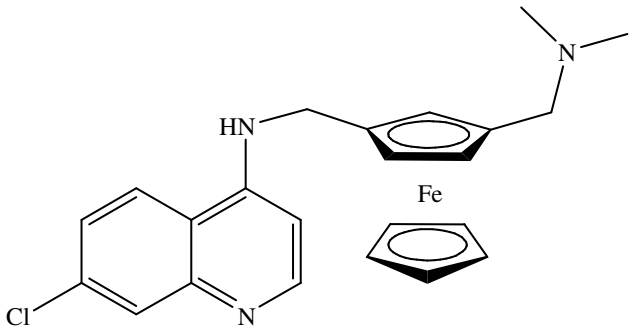

28

Compound **28** was found to be more active than chloroquine against four strains of *Plasmodium falciparum*, a chloroquine resistant parasite. When tested *in vitro* IC_{50} values in the nanomolar range were obtained [35]. Biot *et al* have also recently prepared ferrocenyl derivatives of triazacyclononanes [38]. The bis quinoline derivative **29** showed promising activity against the chloroquine resistant Dd2 strain of *P. falciparum*. The IC_{50} value of 62 nM compares favourably with the value for chloroquine of 94 nM.

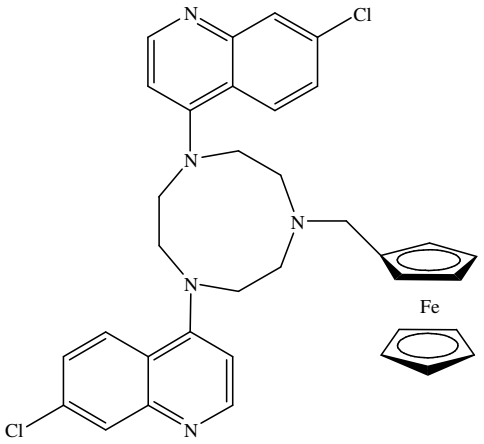

29

The mechanism of action of ferroquine was found to be similar to that of chloroquine [39]. In red blood cells the drug becomes protonated, subsequently it binds to heme to form a drug-heme complex that is highly toxic to the cell. Ferroquine activity against chloroquine resistant parasites is attributed to an increase in lipophilicity and differences

in electronic and geometric structure. Ferrocenyl sugars have also displayed activity towards *P. falciparum* with compound **30** displaying an EC_{50} of 0.6 µM when tested *in vitro* [40].

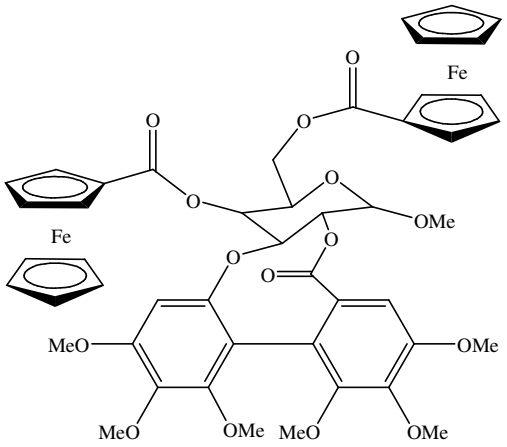

30

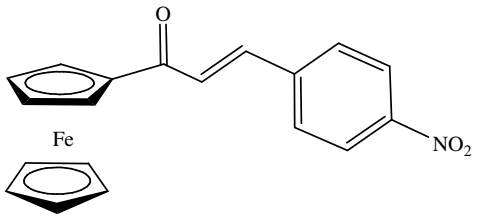

31

The role of the ferrocene in the anti-malaria activity of ferrocenyl chalcones was investigated by Wu *et al* [41]. The most active of these compounds was **31** with an IC_{50} value of 4.6 µM when tested *in vitro* against *P. falciparum*. The location of the ferrocene and the polarity of the carbonyl link influenced the oxidation of the iron atom. These ferrocenyl chalcones also exhibited radical quenching and hydroxyl adduct formation. It is therefore plausible that ferrocene is involved in redox cycling, contributing further to anti-plasmodial activity.

Replacement of the Fe atom with another metal is a well established strategy in organometallic chemistry. Chemically, ruthenoquine **32** is quite similar to ferroquine and shows comparable anti-malarial activity [42].

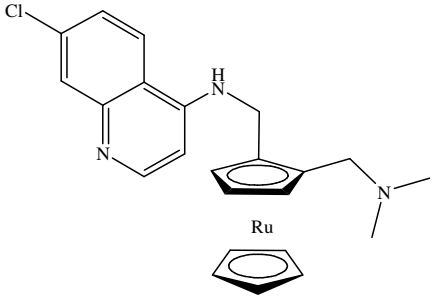

32

There is a clear variation in activity of compound **32** when compared to chloroquine as compound **32** is known to accumulate in the parasitic membrane. Such a build up is not evident with chloroquine. The similarity in activity of ferroquine **28** and ruthenoquine **32** suggests that the difference in effect of the metallocene moiety is insignificant. The lipophilicity and size of these functionalities may aid membrane permeability and lead to a greater affinity for haematin.

1.8 Conclusions.

The use of organometallics for targeted medical purposes is a flourishing area of research [(43)]. Metallocenes, of which ferrocene is the standard, are small, rigid lipophilic molecules that can easily penetrate the cell membrane. The metallocenes' external surface also resembles that of the aromatic nucleus. Biologically active ferrocene derivatives can be classified into two groups, namely novel ferrocene compounds that exert a biological effect and ferrocene analogues of known drugs that have been prepared in order to overcome the problem of resistance.

The well established redox properties of ferrocene have been utilized in preparing various electrochemical sensors, and this redox activity has been strongly associated with the biological activity of ferrocenyl complexes.

Ferrocifens have shown promising results *in vitro* against ER(+) and ER(-) breast cancer cells, whereas the parent drug tamoxifen only expresses an effect on ER(+) cells. Ferroquine is a unique malaria drug candidate, which is currently being developed by Sanofi-Aventis. It is extremely active against both chloroquine sensitive and chloroquine resistant parasites. It has completed Phase I clinical trials and will begin Phase II trials in a combination treatment with artesunate [(44)]. The ferrocifens and ferroquines are currently the most advanced ferrocene based drug candidates

References.

1. Yang, P., Guo, M., *Coor. Chem. Rev.*, **1999**, *185*, 189.
2. Neuse, E. W., *J. Inorg. Organomet. Polym. Mat.*, **2005**, *15*, 3.
3. Alderden, R. A., Hall, M. D., Hambley, T. W., *J. Chem. Ed.*, **2006**, *83*, 728.
4. Hillard, E., Vessieres, A., Le Bideau, F., Plazuk, D., Spera, D., Huche, M., Jaouen, G., *Chem. Med. Chem.*, **2006**, *1*, 551.
5. Fouda, M. F. R., Abd-Elzaher, M. M., Abdelsamaia, R. A., Labib, A. A., *Appl. Organomet. Chem.*, **2007**, *21*, 613.
6. Kaptiza, S., Pongratz, M., Jakupec, M. A., Heffeter, P., Berger, W., Lackinger, L., Keppler, B. K., Marian, B., *J. Cancer Res. Clin. Oncol.*, **2005**, *131*, 101.
7. Hillard**,** E. A., de Abreu, F. C., Ferreira, D. C. M., Jaouen, G., Goulart, M. O. F., Amatore, C., *Chem. Comm.*, **2008**, 2612.
8. Kopf-Maier, P., Kopf, H., Neuse, E. W., *Angew. Chem. Int. Ed. Eng.*, **1984**, *23*, 456.
9. Osella, D., Ferrali, M., Zanello, P., Laschi, F., Fontani, M., Nervi, C., Cavigiolio, G., *Inorg. Chim. Acta.*, **2000**, *306*, 42.
10. Tabbi, G., Cassino, C., Lavigiolio, G., Colangelo, D., Ghiglia, A., Viano, I., Osella, D., *J. Med. Chem.*, **2002**, *45*, 5786.
11. Kowalski, K., Zakrzewski, J., Long, N. J., Suwaki, N., Mann, D. J., White, A. J. P., *Dalton Trans.*, **2006**, 571.
12. Kowalski, K., Suwaki, N., Zakrzewski, J., White, A. J. P., Long, N. J., Mann, D. J., *Dalton Trans.*, **2007**, 743.
13. Hillard, E., Vessieres, A., Thouin, L., Jaouen, G., Amatore, C., *Angew. Chem. Int. Ed.*, **2006**, *45*, 285.
14. Pigeon, P., Top, S., Vessieres, A., Huche, M., Hillard, E. A., Salomon, E., Jaouen, G., *J. Med. Chem.*, **2005**, *48*, 2814.
15. Fan, P. W., Zhang, F., Bolton, J. L., *Chem. Res. Toxicol.*, **2000**, *13*, 45.
16. Vessieres, A., Top, S., Pigeon, P., Hillard, E., Boubeker, L., Spera, D., Jaouen, G., *J. Med. Chem.*, **2005**, *48*, 3937.

17. Nguyen, A., Marsaud, V., Bouclier, C., Top, S., Vessieres, A., Pigeon, P., Gref, R., Legrand, P., Jaouen, G., Renoir, J-M., *Inter. J. of Pharmaceutics*, **2008**, *347*, 128.
18. Heilmann, J. B., Hillard, E. A., Plamont, M-A., Pigeon, P., Bolte, M., Jaouen, G. Vessieres, A., *J. Organomet. Chem.*, **2008**, *693*, 1716.
19. Osella, D., Mahboobi, H., Colangelo, D., Cavigiolio, G., Vessieres, A., Jaouen, G., *Inorg. Chim. Acta.*, **2005**, *358*, 1993.
20. Plazuk, D., Vessieres, A., Le Bideau, F., Jaouen, G., Zakrzewski, J., *Tett. Lett.*, **2004**, *45*, 5425.
21. Vessieres, A., Top, S., Beck, W., Hillard, E., Jaouen, G., *Dalton Trans.*, **2006**, 529.
22. Top, S., Kaloun, E. B., Vessieres, A., Laios, I., Leclerq, G., Jaouen, G., *J. Organomet. Chem.* **2002**, *643-644*, 350.
23. Top, S., Vessieres, A., Pigeon, P., Rager, M-N., Huche, M., Salomon, E., Cabestaing, C., Vaissermann, J., Jaouen, G., *Chem. Bio. Chem.,* **2004**, *5*, 1104.
24. Payen, O., Top, S., Vessieres, A., Brule, E., Plamont, M-A., McGlinchey, M. J., Muller-Bunz, H., Jaouen, G., *J. Med. Chem.*, **2008**, *51*, 1791
25. Kelly, P. N., Pretre, A., Devoy, S., O'Reilly, J., Devery, R., Goel, A., Gallagher, J. F., Lough, A. J., Kenny, P. T. M., *J. Organomet. Chem.*, **2007**, *692*, 1327.
26. Corry, A. J., Goel, A., Alley, S. R., Kelly, P. N., O'Sullivan, D., Savage, D., Kenny, P. T. M., *J. Organomet. Chem.*, **2007**, *692*, 1405.
27. Corry, A. J., O'Donovan, N., Mooney, A., O'Sullivan, D., Rai, D. K., Kenny, P. T. M., *J. Organomet. Chem.*, **2008**, doi: 10.1016/j.jorganchem.2008.09.072.
28. Goel, A., Savage, D., Alley, S. R., Kelly, P. N., O'Sullivan, D., Mueller-Bunz, H., Kenny, P. T. M., *J. Organomet. Chem.*, **2007**, *692*, 1292.
29. Johnson, M. T., Kreft, E., N'Da, D. D., Neuse, E. W., van Resberg, C. E. J., *J. Inorg. Organomet. Polym.*, **2003**, *13*, 255.
30. Basnet, A., Thapa, P., Karki, R., Na, Y., Jahng, Y., Jeong, B. S., Jeong, T. C., Lee, C. S., Lee, E. S., *Biorg. Med. Chem.*, **2007**, *15*, 4351.
31. Sai Krishna, A. D., Panda, G., Kondapi, A. K., *Arch. Biochem. Biophys.*, **2005**, *438*, 206.

32. Pampillon, C., Sweeney, N. J., Strohfeldt, K., Tacke, M., *J. Organomet. Chem.*, **2007**, *692*, 2153.
33. O'Connor, K., Gill, C., Tacke, M., Rehmann, F. J. K., Strohfeldt, K., Sweeney, N., Fitzpatrick, J. M., Watson, R. W. G., *Apoptosis*, **2006**, *11*, 1205.
34. Claffey, J., Hogan, M., Muller-Bunz, H., Pampillon, C., Tacke, M., *J. Organomet. Chem.*, **2008**, *693*, 526.
35. Biot, C., Delhaes, L., Abessolo, H., Domarle, O., Maciejewski, L.A., Mortuaire, M., Delcourt, P., Deloron, P., Camus, D., Dive, D., Brocard, J. S., *J. Organomet. Chem.*, **1999,** *589*, 59**.**
36. Ciu, X., Vlahakis, J. Z., Crandall, I. E., Szarek, W. A., *Bioorg. Med. Chem.*, **2008**, *16*, 1927.
37. Daher, W., Biot, C., Fandeur, T., Jouin, H., Pelinski, L., Viscogliosi, E., Fraisse, L., Pradines, B., Brocard, J., Khalife, J., Dive, D., *Malaria J.*, **2006**, *5*, 11.
38. Biot, C., Dessolin, J., Ricard, I., Dive, D., *J. Organomet. Chem.*, **2004,** *689*, 4678.
39. Biot, C., Taramelli, D., Forfar-Bares, I., Maciejewski, L. A., Boyce, M., Nowogrocki, G., Brocard, J. S., Basilico, N., Olliaro, P., Egan, T. J., *Mol. Pharaceut*., **2005**, *2*, 185.
40. Itoh, T., Shirakami, S., Ishida, N., Yamashita, Y., Yoshida, T., Kim, H-S., Wataga, Y., *Bioorg. Med. Chem. Lett.*, **2000**, *10*, 1657.
41. Wu, X., Wilairat, P., Go, M-L., *Bioorg. Med. Chem. Lett.*, **2002**, *12*, 2299.
42. Blackie, M. A. L., Beagley, P., Croft, S. L., Kendrick, H., Moss, J. R., Chibale, K., *Bioorg. Med. Chem.*, **2007**, *15*, 6510.
43. Jaouen, G., '*Bioorganometallics*', Wiley-VCH **2006**.
44. Dive, D., Biot, C., *Chem. Med. Chem.*, **2008**, *3*, 383.

Chapter 2
Results and Discussion

2.1 Introduction.

Organometallic compounds have been successfully incorporated in a wide variety of materials with diverse applications. Ferrocene is one such compound that is recognised as a promising candidate for use in novel materials due to its ease of use and electrochemical and spectroscopic properties [(1)]. As a result of this, ferrocene research has received an increased level of attention over the past decade. The ultimate goal of this research is the development of novel sensor compounds, peptide mimetic models and unnatural drugs [(2)]. *N*-(ferrocenyl)benzoyl amino acid and dipeptide esters were originally prepared as potential anion sensing agents [(3)] however they demonstrated cytotoxicity following *in vitro* screening. The compounds are composed of three key moieties, namely, (i) an electroactive core, (ii) a conjugated aromatic linker and (iii) an amino acid or peptide derivative that can interact with other molecules *via* hydrogen bonding. *N*-{*ortho*-(ferrocenyl)-benzoyl}-glycine ethyl ester was initially tested for its *in vitro* anti-proliferative activity towards lung cancer cells (H1299 and H1299 carboplatin and cisplatin resistant variants). This compound was found to be cytotoxic and had an IC_{50} value of 48 μM, whereas the starting material, *ortho*-ferrocenyl ethyl benzoate, was completely inactive against this cell line. Therefore other derivatives were evaluated for their anti-cancer activity against lung cancer cell lines. Initial results showed that the cytotoxicity of the *meta* dipeptide, *N*-{*meta*-(ferrocenyl)-benzoyl}-L-alanine-glycine ethyl ester is *ca.* 2 times higher than the *ortho*-glycine derivative, the IC_{50} value being 26 μM (RSD 20%) whilst the corresponding *ortho* analogue, *N*-{*ortho*-(ferrocenyl)-benzoyl}-L-alanine-glycine ethyl ester has an IC_{50} value of 21 μM (RSD 20%). The dipeptide derivative *N*-{*ortho*-(ferrocenyl)-benzoyl}-glycine-glycine ethyl ester was shown to have an IC_{50} value of approximately 20 μM, also *N*-{*ortho*-(ferrocenyl)-benzoyl}-glycine-L-alanine ethyl ester is more active than *N*-{*ortho*-(ferrocenyl)-benzoyl}-L-alanine-glycine ethyl ester with an IC_{50} value of 5.3 μM (RSD 8%). From

this it may be assumed that the glycine residue of the dipeptide that is attached to the benzoyl group is important for activity. The larger amino acid alanine as the second residue also increased activity. To assess the effects of lipophilicity, the alanine group can be replaced with residues that differ by a methylene (CH_2) unit. By incorporating the amino acid 2-aminobutyric acid (Abu) the methyl group of alanine (CH_3) is transformed to an ethyl group (C_2H_5). This process can be extended by using norvaline (Nva) and norleucine (Nle) in the synthesis to introduce propyl (C_3H_7) and butyl (C_4H_9) groups respectively. The number of methylene groups in the first amino acid of the dipeptide chain was also extended using β-alanine and γ-aminobutyric acid. As the glycine dipeptide derivative was more active than the glycine amino acid derivative the study was therefore extended to longer peptide chains with additional glycine residues. 1,1'-*N, N'*-{*ortho*-(ferrocenyl)-bisbenzoyl} amino acid and dipeptide esters were also prepared in order to assess the effect of a disubstituted ferrocene molecule on activity.

Coupling reactions were used in the preparation of the dipeptide esters and also to facilitate the introduction of the ferrocenyl benzoyl group onto the peptide esters. Ferrocenyl benzoic acids, *ortho*, *meta* and *para*, were prepared and were treated with 1-hydroxybenzotriazole (HOBt), *N*-(3-dimethylaminopropyl)-*N'*-ethylcarbodiimide hydrochloride (EDC), and triethylamine (TEA) in dichloromethane at 0 ^{o}C in the presence of the peptide esters.

The primary objective was to prepare analogues of the lead compound *N*-{*ortho*-(ferrocenyl)-benzoyl}-glycine-L-alanine ethyl ester **20** and compare their *in vitro* biological activity. This was achieved by varying the sequence and size of the peptide chain and by altering their orientation around the central benzoyl moiety.

2.2 The synthesis of dipeptide ethyl esters.

The dipeptides required in this study were not available commercially and therefore had to be prepared. Conventional peptide chemistry was employed where BOC protected glycine, β-alanine and γ-aminobutyric acid were reacted with the ethyl esters of L-alanine, L-2-aminobutyric acid, L-norvaline and L-norleucine *via* the EDC/HOBt coupling protocol. Subsequent deprotection of the BOC group using trifluoroacetic acid

allows for reaction at the *N*-terminus between the free amino group and ferrocenyl benzoic acids.

In the formation of the peptide bond between two amino acids, protection of the *N*-terminus of one amino acid and the *C*-terminus of the other amino acid is required to ensure regiospecific coupling. All compounds were subsequently characterized using a variety of NMR and spectroscopic techniques. As they were intermediates in the synthesis of *N*-(ferrocenyl)benzoyl dipeptide esters they will not be included in the experimental section. Figure 2.1 describes the synthesis and deprotection of the dipeptide esters. For example, glycine-L-norvaline n = 1 and R = C_3H_7.

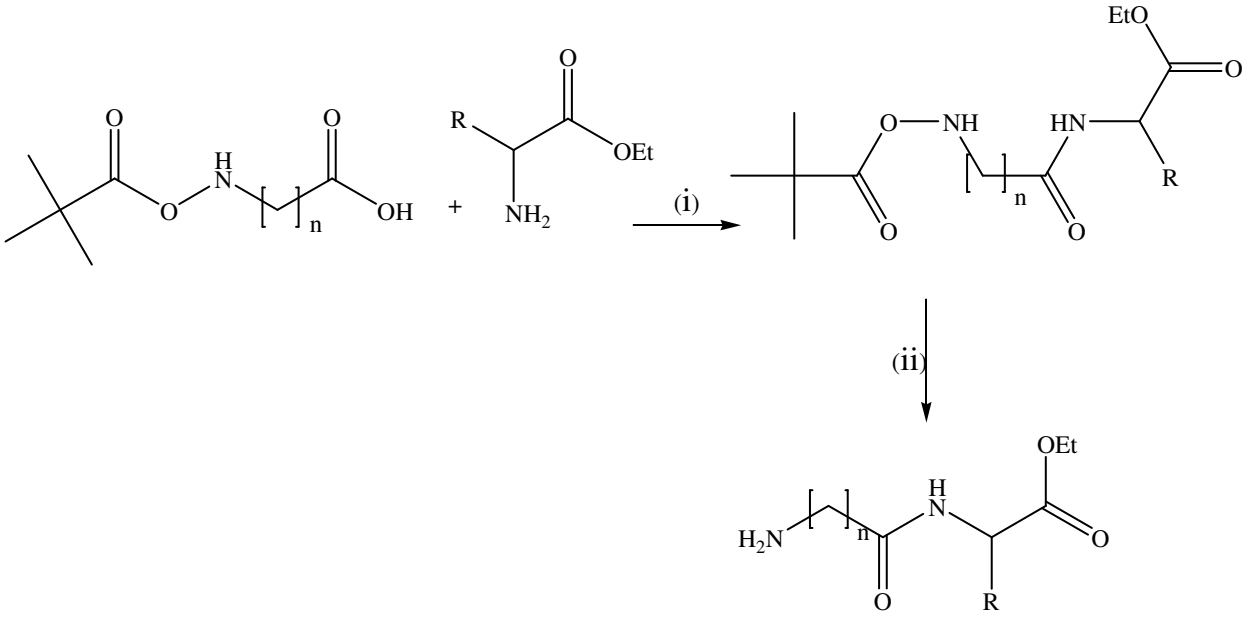

n = 1, 2, 3, R= CH_3, C_2H_5, C_3H_7, C_4H_9

(i) EDC, HOBt, Et_3N, (ii) TFA, DCM

Fig. 2.1 The synthesis and deprotection of dipeptides.

2.2.1 Amino protecting groups

The protection of the amino group guarantees that only the desired dipeptide product is obtained. Characteristic protecting groups contain carbamate units that have a low degree of nucleophilicity and are easily deprotected. The most effective protecting groups are labile to mild cleaving conditions that will not affect the peptide bond or disturb chiral

centres [4]. Common carbamate protecting groups include the benzyloxycarbonyl (Z) **33** and *t*-butoxycarbonyl (BOC) **34** groups. These groups are introduced onto the amino acid using benzyl chloroformate and di-*t*-butyl carbonate respectively.

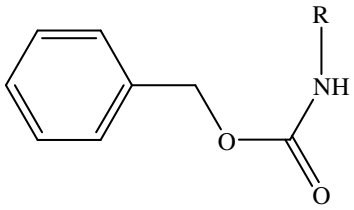

33

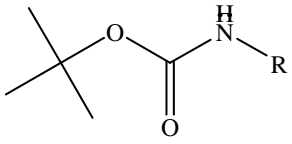

34

These protecting groups are stable to basic conditions but are easily removed using acid. In each case a carbamic acid is formed followed by the loss of CO_2. The deprotection of the BOC group is illustrated in Figure 2.2.

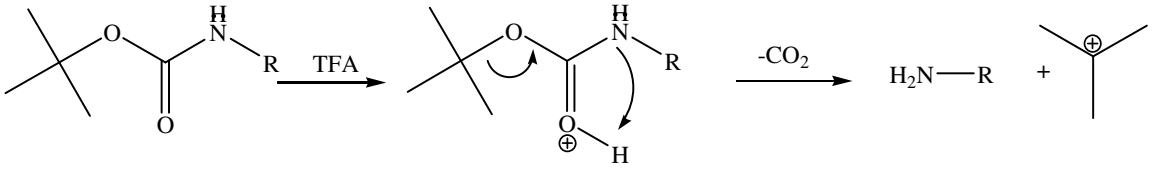

Fig. 2.2 Deprotection of BOC group.

The 9-fluorenylmethoxycarbonyl (FMOC) protecting group **35** is a variant that is acid stable and base labile. It can be introduced onto the amino acid using its chlorformate derivative and removed using a base, for example piperidine.

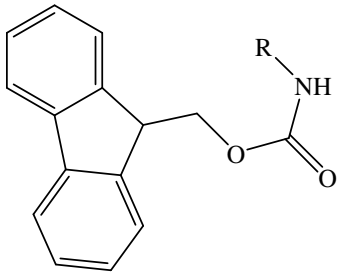

35

2.2.2 Carboxyl protecting groups

To ensure that an anhydride linkage is not formed during the coupling process it is also necessary to protect the carboxyl group of the second amino acid. Amino acids are known to react readily with thionyl chloride in alkyl alcohols to give the corresponding alkyl ester hydrochloride salts (Figure 2.3) [5]. The free amino group is generally generated *in situ* upon reaction with a tertiary base as the free base can decompose rapidly.

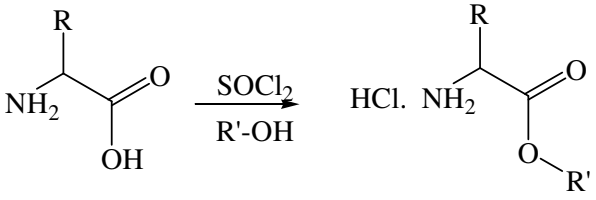

Fig. 2.3 Esterification of amino acids.

2.2.3 Amide bond formation.

The key step in peptide synthesis is the formation of the amide bond. This requires the activation of the carboxylic acid i.e., attachment of a leaving group to the acyl carbon of the carboxyl group. This is achieved using peptide coupling reagents [6]. Activation of the carboxyl group is necessary as carboxylic acids and amines do not ordinarily form amide bonds at ambient temperatures [7].

2.2.3.1 Acyl chlorides

Conversion of the carboxyl group to its corresponding acyl chloride is the most straightforward form of activation. The usefulness of acyl chlorides is hampered by the cyclization of simple amino acid chlorides to oxazolones (Figure 2.4).

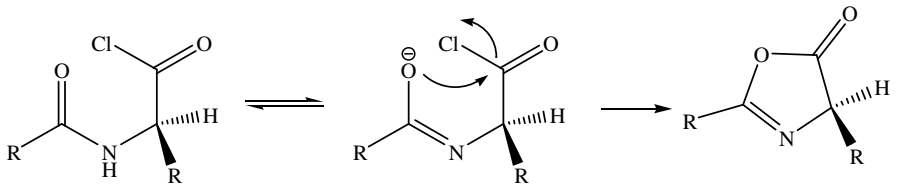

Fig. 2.4 Cyclization of amino acid chlorides to oxazolones.

Although oxazolones are reactive towards aminolysis, racemization is known to occur and the rate is faster than that of amide bond formation (Figure 2.5). The need for optically pure products means this method is seldom used [7].

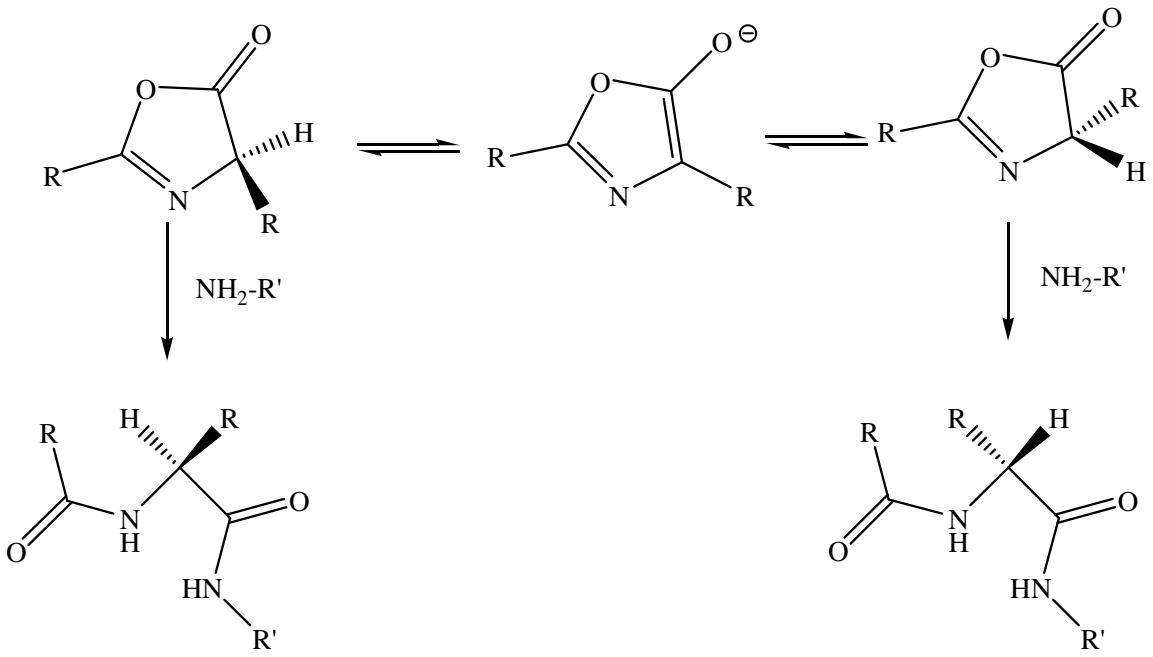

Fig. 2.5 Racemization of oxazolones.

2.2.3.2 Phosphonium Reagents

Acyloxyphosphonium reagents react readily with nucleophiles at the acyl carbon. They are formed from reaction of a carboxylate anion with phosphonium cations [(7)]. The first of these reagents was benzotriazolyl-1-oxy-tris(dimethylamino) phosphonium hexafluorophosphate (BOP). The BOP reagent reacts with the carboxylate group to give a benzotriazole ester that readily undergoes aminolysis (Figure 2.6). The success of BOP as an activating reagent is tempered by the high toxicity of the byproduct hexamethylphosphoramide. Attention has now focused on developing derivatives to overcome this problem with the uronic salt *O*-benzotriazolyl bis(dimethylamino)uronium tetrafluoroborate (TBTU) **36** an example of this.

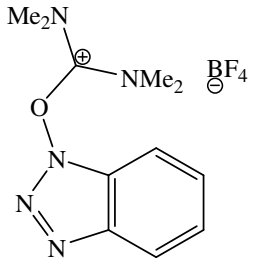

36

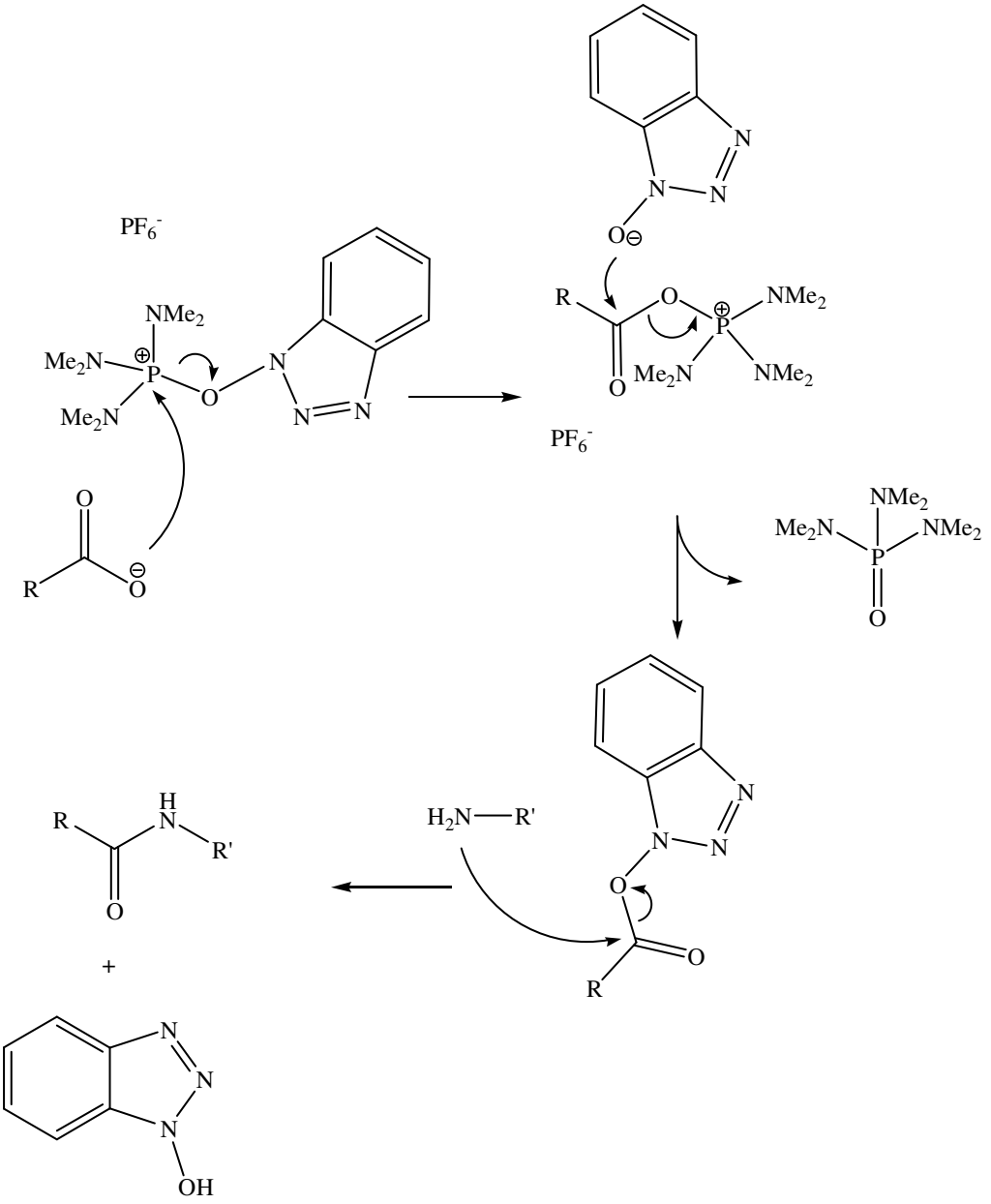

Fig. 2.6 Amide bond formation using BOP reagent.

2.2.3.3 Carbodiimides

Carbodiimides have been the most widely used carboxyl activating reagents since dicyclohexylcarbodiimide (DCC) was introduced in the 1950's. DCC and other carbodiimides can be used to generate symmetrical anhydrides and active esters or as a direct coupling reagent [(6)]. In each case the initial activating event is the formation of an *O*-acylisourea intermediate. This *O*-acylisourea is a potent acylating agent and rapidly leads to peptide formation following aminolysis. However, this high reactivity can lead to

the formation of the more inert *N*-acylurea intermediate following acyl transfer (Figure 2.7).

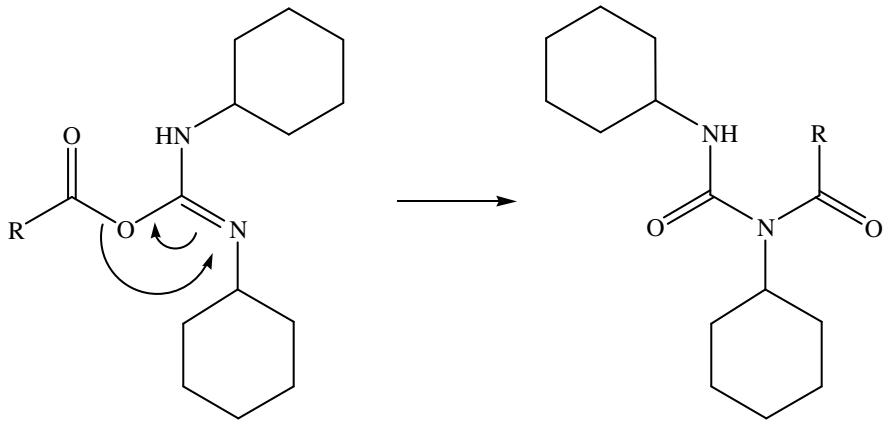

Fig. 2.7 Acyl transfer of *O*-acylisourea to *N*-acylurea.

Furthermore, the *O*-acylisourea intermediate is prone to racemization (Figure 2.8). This occurs when there is an intramolecular proton transfer from the chiral carbon atom to the basic centre of the *O*-acylisourea. The chiral carbon is rehybridized from sp^3 to sp^2 and when the proton returns to its original position it is equally likely to return to either face of the sp^2 hybridized carbon [7].

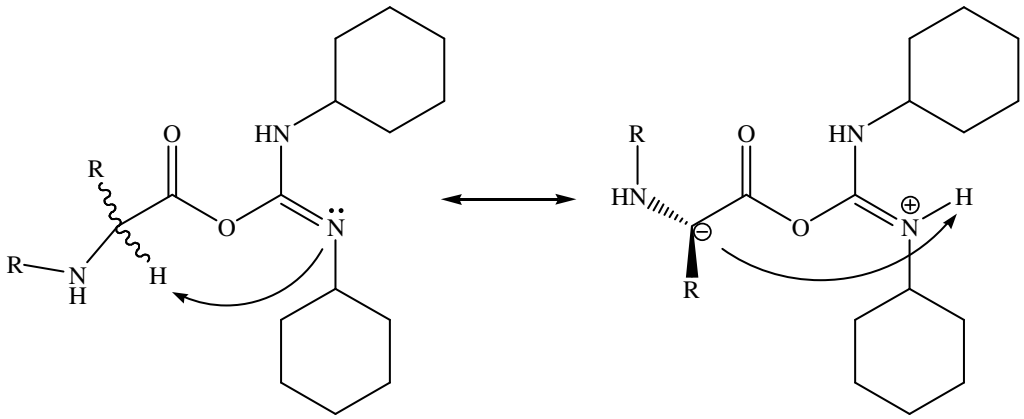

Fig. 2.8 Proton transfer resulting in racemization.

These difficulties can be overcome with the addition of a secondary nucleophile, for example HOBt, which can react with the *O*-acylisourea. This leads to the formation of an intermediate with a lower overall reactivity but that is still highly reactive to aminolysis and less susceptible to side reactions and racemization. EDC was employed in the synthesis of the dipeptide esters and the *N*-(ferrocenyl)benzoyl peptide ester products due to the problems associated with the removal of the urea by-products of DCC, namely *N*, *N*'- dicyclohexylurea (DCU). EDC produces a water soluble urea by-product i.e., 1-{3-(dimethylamino)propyl}-3 ethyl urea, and is removed during a dilute acid washing procedure. The participation of HOBt in the coupling process with EDC is outlined in Figure 2.9.

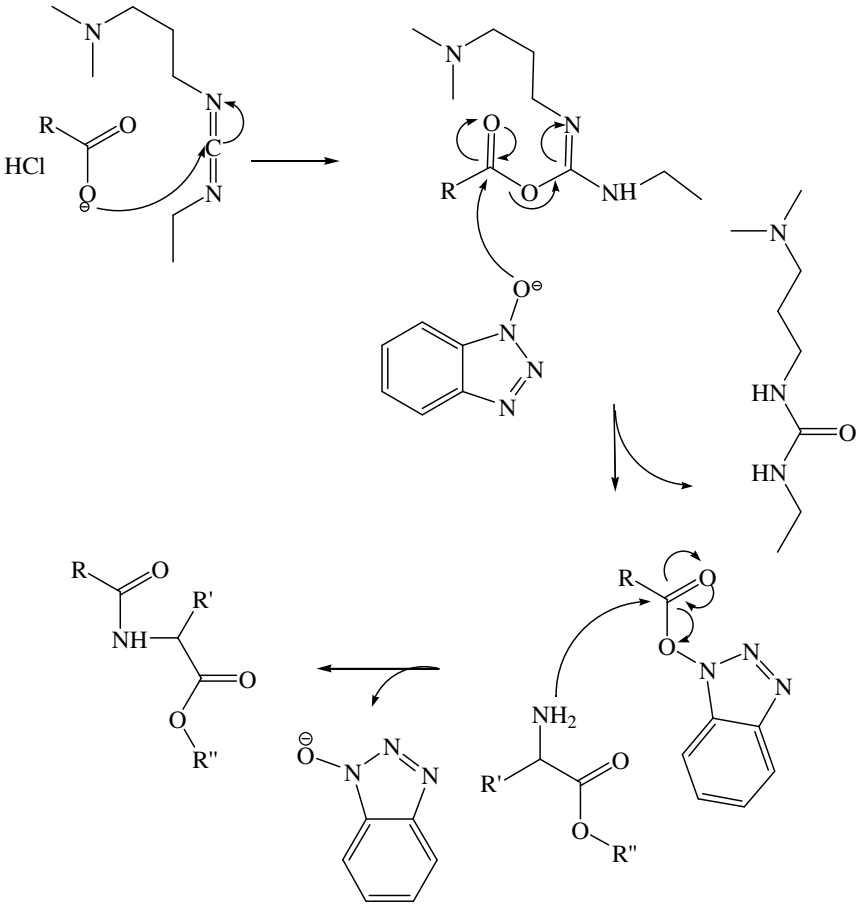

Fig. 2.9 Mechanism of dipeptide synthesis using EDC and HOBt.

2.3 The synthesis of *N*-(ferrocenyl)benzoyl peptide esters.

2.3.1 The preparation of ferrocenyl benzoic acid.

The arylation of ferrocene is readily achieved by reacting ferrocene with an aryl diazonium salt [8]. In this case ethyl-2, ethyl-3 and ethyl-4-aminobenzoate were used in order to give *ortho*, *meta* and *para*-ferrocenyl ethyl benzoates. These compounds were isolated as red crystals. The ethyl ester group was efficiently cleaved by saponification using 10% sodium hydroxide to yield the ferrocenyl benzoic acids. This procedure is outlined in Figure 2.10.

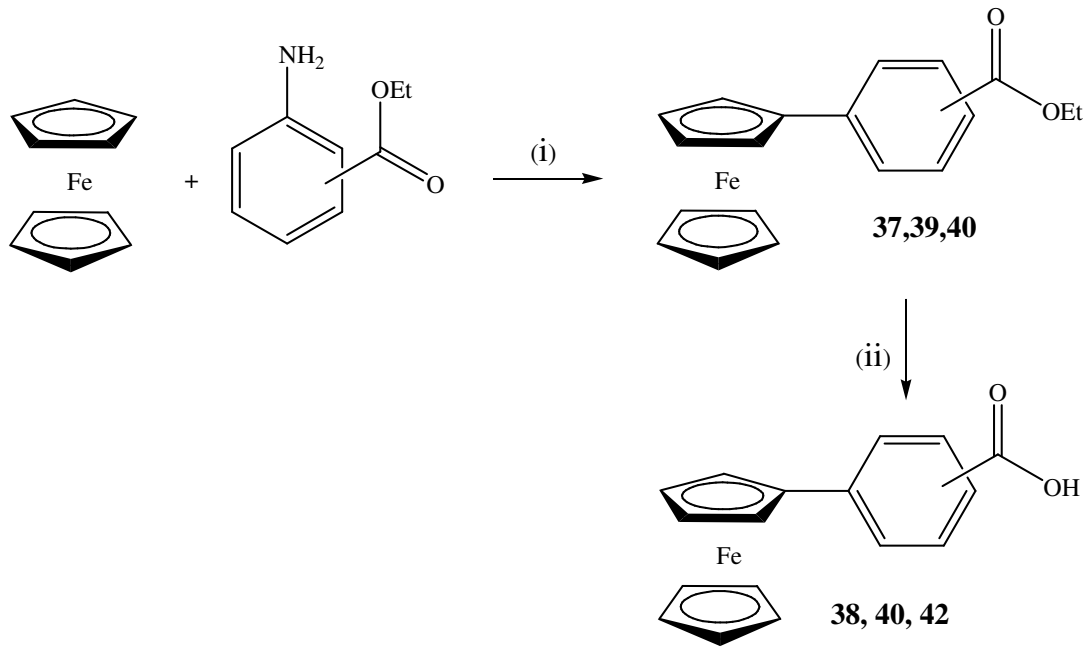

(i) $NaNO_2$, HCl, (ii) NaOH/MeOH, HCl

Fig. 2.10 Reaction scheme for the preparation of ferrocenyl benzoic acids.

2.3.2 Coupling of ferrocenyl benzoic acids to peptide esters.

Coupling reactions were used to facilitate the inclusion of the ferrocenyl benzoyl group to the peptide or amino acid ester. Ferrocenyl benzoic acids, *ortho*, *meta* and *para*, were treated with 1-hydroxybenzotriazole (HOBt), *N*-(3-dimethylaminopropyl)-*N*′-

ethylcarbodiimide hydrochloride (EDC) and triethylamine (TEA) in dichloromethane at 0 ^{o}C in the presence of the peptide esters. In the case of the dipeptide series glycine, β-alanine and γ-aminobutyric acid were the first amino acid in the sequence. L-Alanine, L-2-aminobutyric acid and L-norvaline and L-norleucine were the second amino acids in the sequence. The hydrochloride salts of triglycine and tetraglycine ethyl ester were also used. The coupling of ferrocenyl benzoic acids and peptide esters gave yields in the range of 25% to 73% and all gave spectroscopic data in accordance with their proposed structures. The general reaction scheme for the synthesis of *N*-(ferrocenyl)benzoyl dipeptide esters is outlined in Figure 2.11.

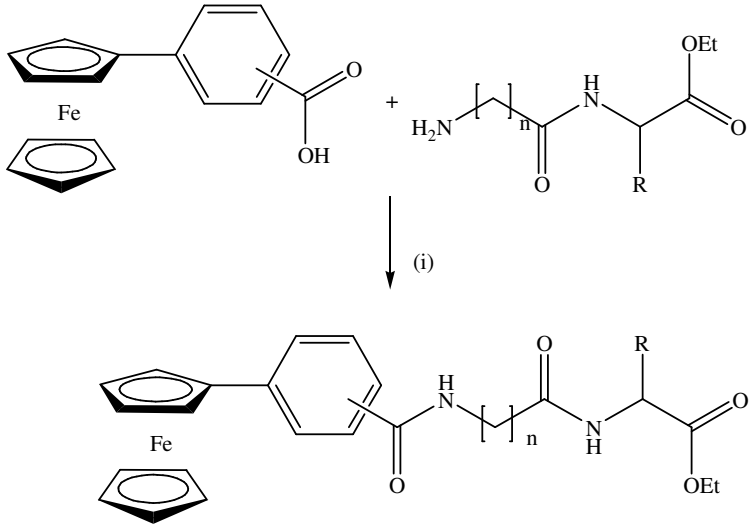

n = 1, 2, 3. R = CH_3, C_2H_5, C_3H_7, C_4H_9.

(i) EDC, HOBt, Et_3N

Fig. 2.11 The general reaction scheme for the synthesis of *N*-(ferrocenyl)benzoyl dipeptide esters. (A similar method is used for the tri- and tetrapeptide derivatives).

Subsequent to the reaction outlined in Figure 2.11 and an acid-base washing procedure, a crude *N*-(ferrocenyl)benzoyl dipeptide was isolated. Purification using column chromatography furnishes the pure product. In each case the eluant was a hexane:ethyl acetate or a petroleum ether (40-60 ^{o}C):ethyl acetate mixture.

Overall yields for the *N*-(ferrocenyl)benzoyl dipeptide esters, **20**, **45-85**, varied from 25% to 73%. Typically, the *ortho* and *meta* derivatives gave the lowest yields while the *para* derivatives gave the highest yields, however this trend is not consistent. The reason for the overall difference in yields can be rationalized by considering the respective orientations of the *ortho* and *meta*-ferrocenyl benzoic acids during the reaction. They are more sterically hindered than the *para*-ferrocenyl benzoic acid starting material. Table 2.1 summarizes the yields of all the *N*-(ferrocenyl)benzoyl dipeptide esters.

Table 2.1 *N*-(ferrocenyl)benzoyl dipeptide ethyl ester derivatives.

Compound No.	Fc-Bz	1st AA	2nd AA	% Yield
20	*Ortho*	Glycine	L-Alanine-OEt	56
45	*Ortho*	Glycine	Glycine-OEt	49
46	*Ortho*	Glycine	L-Alanine-OMe	46
47	*Ortho*	Glycine	L-Alanine-OPr	36
48	*Ortho*	Glycine	L-2-Aminobutyric acid-OEt	25
49	*Ortho*	Glycine	L-Norvaline-OEt	31
50	*Ortho*	Glycine	L-Norleucine- OEt	34
51	*Ortho*	Glycine	L-Leucine- OEt	67
52	*Ortho*	Glycine	L-Phenylalanine-OEt	28
53	*Ortho*	L-Alanine	Glycine-OEt	39
54	*Ortho*	β-Alanine	L-Alanine-OEt	36
55	*Ortho*	β-Alanine	L-2-Aminobutyric acid-OEt	50
56	*Ortho*	β-Alanine	L-Norvaline-OEt	51
57	*Ortho*	β-Alanine	L-Norleucine-OEt	49
58	*Ortho*	GABA	L-Alanine-OEt	32
59	*Ortho*	GABA	L-2-Aminobutyric acid-OEt	46
60	*Ortho*	GABA	L-Norvaline-OEt	47
61	*Ortho*	GABA	L-Norleucine-OEt	32
62	*Meta*	Glycine	L-Alanine-OEt	30
63	*Meta*	Glycine	L-2-Aminobutyric acid-OEt	39
64	*Meta*	Glycine	L-Norvaline-OEt	31

65	*Meta*	Glycine	L-Norleucine-OEt	34
66	*Meta*	β-Alanine	L-Alanine-OEt	28
67	*Meta*	β-Alanine	L-2-Aminobutyric acid-OEt	55
68	*Meta*	β-Alanine	L-Norvaline-OEt	44
69	*Meta*	β-Alanine	L-Norleucine-OEt	42
70	*Meta*	GABA	L-Alanine-OEt	32
71	*Meta*	GABA	L-2-Aminobutyric acid-OEt	36
72	*Meta*	GABA	L-Norvaline-OEt	59
73	*Meta*	GABA	L-Norleucine-OEt	55
74	*Para*	Glycine	L-Alanine-OEt	33
75	*Para*	Glycine	L-2-Aminobutyric acid-OEt	45
76	*Para*	Glycine	L-Norvaline-OEt	73
77	*Para*	Glycine	L-Norleucine-OEt	40
78	*Para*	β-Alanine	L-Alanine-OEt	52
79	*Para*	β-Alanine	L-2-Aminobutyric acid-OEt	50
80	*Para*	β-Alanine	L-Norvaline-OEt	51
81	*Para*	β-Alanine	L-Norleucine-OEt	54
82	*Para*	GABA	L-Alanine-OEt	47
83	*Para*	GABA	L-2-Aminobutyric acid-OEt	39
84	*Para*	GABA	L-Norvaline-OEt	47
85	*Para*	GABA	L-Norleucine-OEt	48

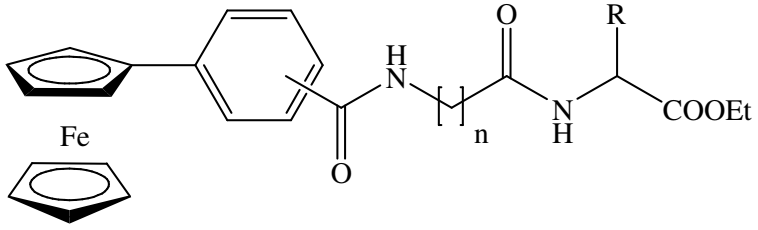

Fig. 2.12 General structure of *N*-(ferrocenyl)benzoyl dipeptide ethyl ester derivatives, n = 1, 2, 3. R = Me, Et, Pr, Bu.

2.4 ^{1}H NMR studies of *N*-(ferrocenyl)benzoyl dipeptide esters.

All the ^{1}H NMR experiments were performed in d_6-DMSO as the *N*-(ferrocenyl)benzoyl dipeptide esters showed limited solubility in other deuterated solvents. In d_6-DMSO the amide protons of the peptide chain appear between δ 8.89 and δ 8.14. The spectra have three signals in the ferrocenyl region which are typical of the mono-substituted ferrocene splitting pattern. The protons of the substituted ring appear as fine triplets or singlets between δ 4.95 and δ 4.38, while the unsubstituted cyclopentadiene ring appears as a singlet at approximately δ 4.0.

The aromatic splitting pattern present in the ^{1}H NMR spectra of *N*-(ferrocenyl)benzoyl dipeptide esters varied depending on whether *ortho*, *meta* or *para* ferrocenyl benzoic acid was used in the final coupling step. The *ortho* derivatives have a doublet, triplet, triplet, doublet splitting pattern in the majority of cases**,** with each peak integrating for one proton. The *meta* derivatives give rise to a singlet, multiplet, triplet splitting pattern where the multiplet integrates for two protons. The *para* derivatives give the archetypal *para* disubstituted aromatic splitting pattern with two doublets that both integrate for two protons with coupling constants ranging from 8.4 Hz to 8.8 Hz.

Table 2.2. Selected ^{1}H NMR spectral data (δ, d_6-DMSO) for *N*-(ferrocenyl)benzoyl dipeptide esters.

Compound	**NH's**	**αH**	***ortho* (η^5-C_5H_4)**	***meta* (η^5-C_5H_4)**
48	8.47, 8.22	4.26-4.19	4.66	4.26-4.19
63	8.77, 8.31	4.23-4.17	4.86	4.39
75	8.66, 8.27	4.22-4.17	4.89	4.41
56	8.28, 8.15	4.22-4.17	4.57	4.29
68	8.51, 8.30	4.22-4.18	4.85	4.39
80	8.50, 8.30	4.31-4.25	4.94	4.47
61	8.17-8.13	4.20-4.15	4.57	4.28
73	8.51, 8.23	4.22-4.16	4.85	4.39
85	8.49, 8.30	4.26-4.21	4.94	4.47

2.4.1 ^{1}H NMR spectroscopic study of *N*-{*ortho*-(ferrocenyl)-benzoyl}-β-alanine-L-norvaline ethyl ester 56.

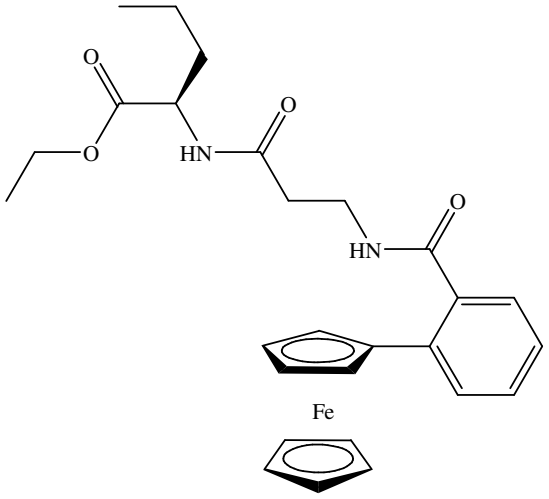

56

In the ^{1}H NMR spectrum of *N*-{*ortho*-(ferrocenyl)-benzoyl}-β-alanine-L-norvaline ethyl ester **56** the two amide protons occur at the relatively downfield positions of δ 8.28 and δ 8.15 respectively. The L-norvaline amide proton is a doublet due to coupling with the α-hydrogen at the chiral centre and has a coupling constant of 7.2 Hz. The β-alanine amide of the dipeptide is a triplet due to coupling with the adjacent methylene group of the β-alanine chain and has a coupling constant of 5.6 Hz. The splitting pattern for the *ortho* disubstituted phenyl ring is observed as a doublet, triplet, triplet, doublet between δ 7.80 and δ 7.14. Each peak integrates for one proton with coupling constants ranging from 6.6 Hz to 7.6 Hz. The *ortho* and *meta* protons of the substituted (η^5-C_5H_4) ring appear as fine triplets at δ 4.57 and δ 4.29 with coupling constants of 1.6 Hz respectively. The α-hydrogen of the L-norvaline residue occurs as a multiplet between δ 4.22 and δ 4.17 due to its position beside the amide proton and the methylene group of the L-norvaline side chain. The signal for the unsubstituted (η^5-C_5H_5) ring overlaps with the methylene of the ethyl ester resulting in a multiplet between δ 4.12 and δ 4.06 with an overall integration of seven. The remaining methylene protons of the β-alanine and L-norvaline chains are observed between δ 3.31 and δ 1.28. The most upfield signals are due to the methyl

groups of the ethyl ester and the L-norvaline side chain. These both appear as triplets between δ 1.18 and δ 0.87.

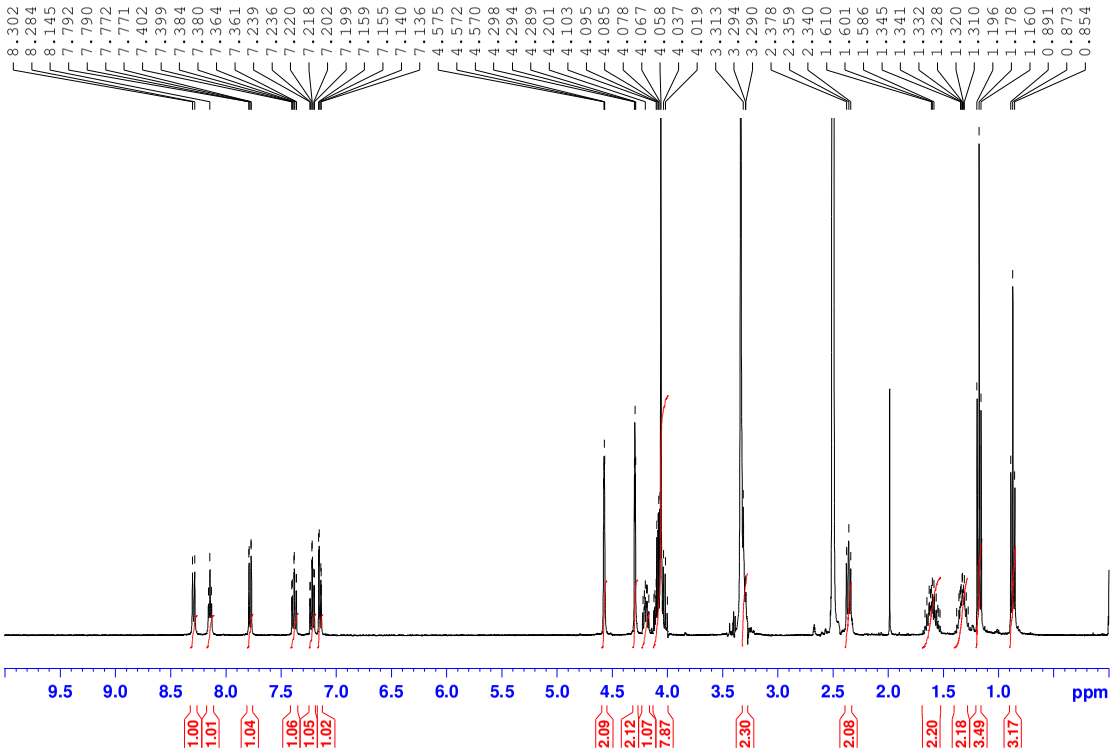

Fig. 2.13 ^{1}H NMR spectrum of *N*-{*ortho*-(ferrocenyl)-benzoyl}-β-alanine-L-norvaline ethyl ester **56**.

2.4.2 ^{1}H NMR spectroscopic study of *N*-{*meta*-(ferrocenyl)-benzoyl}-β-alanine-L-norvaline ethyl ester 68.

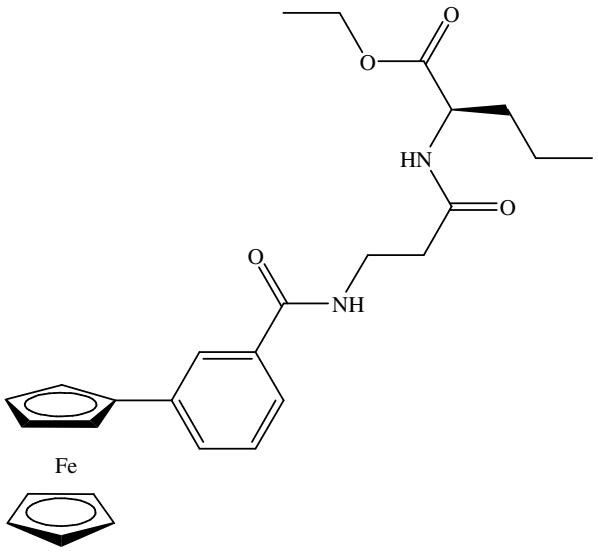

68

The amide protons of *N*-{*meta*-(ferrocenyl)-benzoyl}-β-alanine-L-norvaline ethyl ester **68** appear downfield between δ 8.51 and δ 8.30. The amide proton of the β-alanine portion of the dipeptide is split by the methylene protons of the β-alanine chain resulting in a triplet. The amide proton at δ 8.30 is split into a doublet due to coupling with the α-hydrogen at the chiral centre of L-norvaline. The *meta* disubstituted phenyl ring splitting pattern occurs as a singlet, multiplet, triplet at δ 7.94, δ 7.71-7.64 and δ 7.38 respectively. The mono-substituted ferrocenyl pattern is observed as two triplets representing the (η^5-C_5H_4) ring between δ 4.85 and δ 4.39. Both peaks integrate for two protons and have coupling constants of 1.6 Hz. The unsubstituted (η^5-C_5H_5) ring appears as a multiplet between δ 4.11 and δ 4.02 with the CH_2 group of the ethyl ester. The α-hydrogen of L-norvaline appears as a multiplet between δ 4.22 and δ 4.18 due to coupling with the amide proton and the first methylene group of the L-norvaline side chain. The remaining methylene groups of the β-alanine and L-norvaline chains occur between δ 3.49 and δ 1.24. The methyl group of the ethyl ester and the L-norvaline side chain each occur as triplets between δ 1.16 and δ 0.82 with coupling constants of 7.2 Hz.

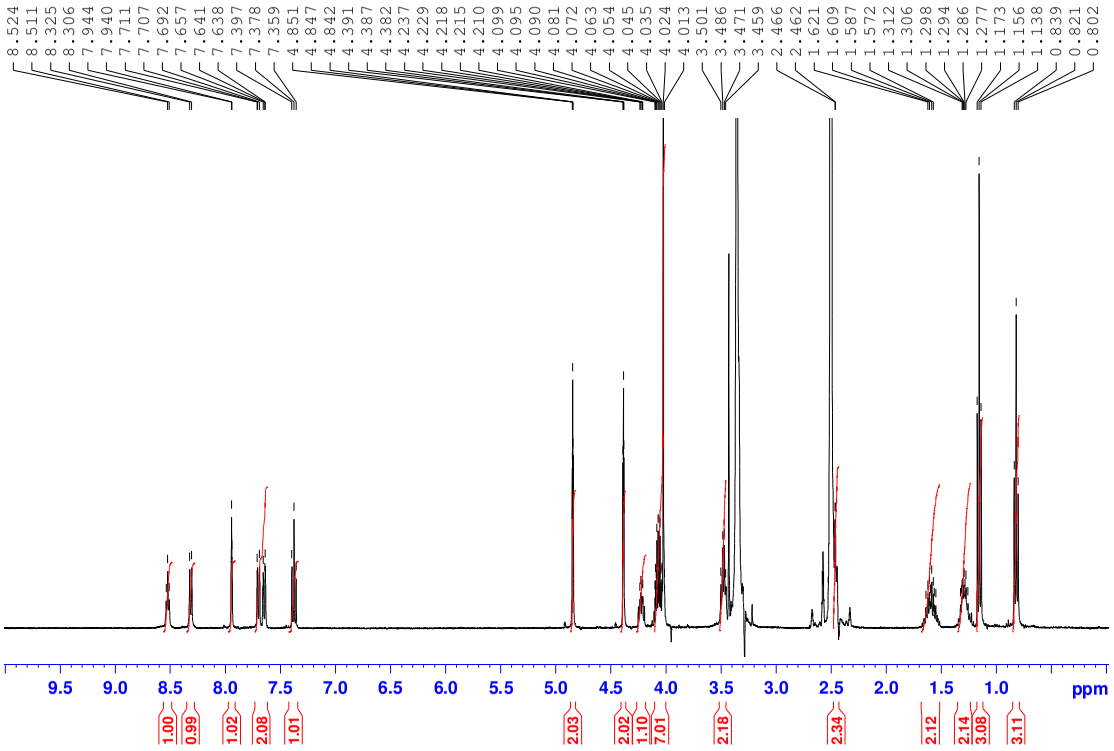

Fig. 2.14 ^{1}H NMR spectrum of *N*-{*meta*-(ferrocenyl)-benzoyl}-β-alanine-L-norvaline **68**.

2.4.3 ^{1}H NMR spectroscopic study of *N*-{*para*-(ferrocenyl)-benzoyl}-β-alanine-L-norvaline ethyl ester 80.

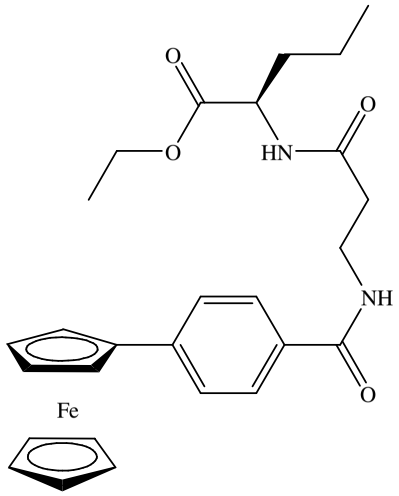

80

The amide protons of the dipeptide chain appear at δ 8.50 and δ 8.30. The triplet at δ 8.50 represents the amide of the β-alanine portion of the dipeptide while the doublet at δ 8.30 is as a result of the amide group of L-norvaline. The archetypal *para* substituted aromatic splitting pattern is observed as two doublets at δ 7.81 and δ 7.65 respectively that both integrate for two protons and have coupling constants of 8.8 Hz. The ferrocenyl peaks of the substituted ring occur between δ 4.94 and δ 4.08. The unsubstituted (η^5-C_5H_5) ring appears as a multiplet between δ 4.31 and δ 4.08 integrating for eight protons with the α-proton of L-norvaline and the methylene protons of the ethyl ester. The methylene protons of the β-alanine and L-norvaline chains occur between δ 3.38 and δ 1.31. The methyl groups of the ethyl ester and the L-norvaline side chain are triplets at δ 1.23 and δ 0.93 respectively.

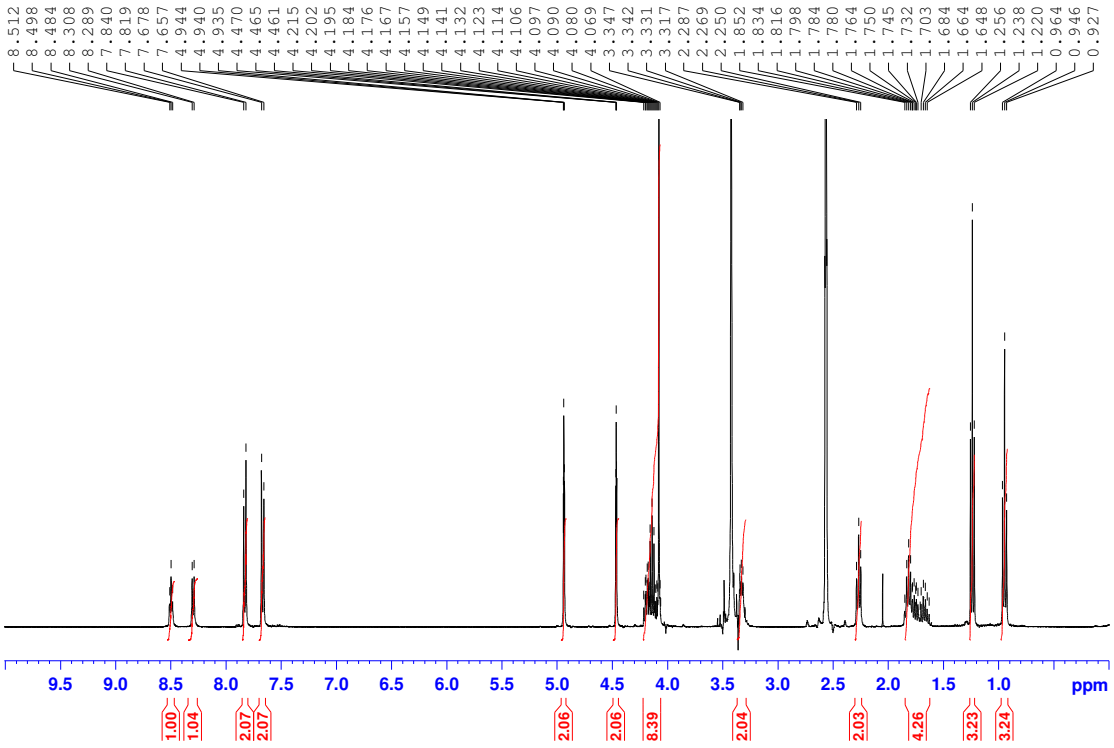

Fig. 2.15 ^{1}H NMR spectrum of *N*-{*para*-(ferrocenyl)-benzoyl}-β-alanine-L-norvaline ethyl ester **80**.

2.5 ^{13}C NMR and DEPT 135 studies of *N*-(ferrocenyl)benzoyl dipeptide esters.

In the ^{13}C NMR spectra of *N*-(ferrocenyl)benzoyl dipeptide esters the amide and ester carbonyl carbons appear between δ 172.7 and δ 166.0. The pattern observed in the aromatic region of the spectrum is dependent on whether the ferrocenyl moiety and the dipeptide chain are *ortho*, *meta* or *para* to each other. *Ortho* and *meta* derivatives give rise to six peaks due to the six non-equivalent carbons. While the *para* derivatives have four peaks representing four unique carbons. The ferrocenyl carbons appear in the range of δ 84.5 and δ 66.0 with the *ipso* carbon of the substituted (η^5-C_5H_4) appearing at the most downfield position. The methylene carbon atoms of these derivatives are easily identified from their negative resonance in DEPT 135 spectra.

Table 2.3. Selected ^{13}C NMR data (δ, d_6-DMSO) for *N*-(ferrocenyl)benzoyl dipeptide esters.

Compound	*C*=O	Ipso *C*	(η^5-C_5H_5)	-O*C*H$_2$CH$_3$	-OCH$_2$*C*H$_3$
50	172.1, 169.9, 168.9	84.3	69.4	60.4	14.1
65	172.1, 169.2, 166.3	84.0	69.4	60.4	14.0
77	172.1, 169.2, 166.5	83.2	69.5	60.4	14.0
56	172.3, 170.5, 169.7	84.4	69.4	60.3	14.1
68	172.3, 170.7, 166.1	84.0	69.4	60.3	14.0
80	172.3, 170.7, 166.0	83.2	69.5	60.3	14.0
59	172.2, 172.1, 169.7	84.5	69.4	60.3	14.1
71	172.3, 172.1, 166.1	84.1	69.4	60.3	14.1
83	172.2, 169.4, 166.0	83.3	69.5	60.3	14.1

2.5.1 ^{13}C NMR and DEPT 135 study of *N*-{*ortho*-(ferrocenyl)-benzoyl}-glycine-L-norleucine ethyl ester 50.

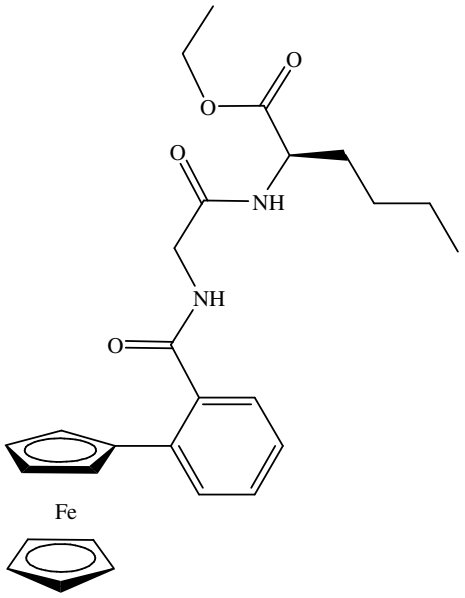

50

The ^{13}C NMR spectrum of *N*-{*ortho*-(ferrocenyl)-benzoyl}-glycine-L-norleucine ethyl ester **50** displays three carbonyl carbon atoms between δ 172.1 and δ 168.9. These signals are absent from the DEPT 135 spectrum. The aromatic region of the spectrum is characteristic of an *ortho* disubstituted benzoyl system with six signals representing the six non-equivalent carbon atoms. The absence of the carbons at δ 136.2 and δ 136.1 in the DEPT 135 spectrum indicates their quaternary nature. Similarly, the signal at δ 84.3 in the ferrocenyl region represents the *ipso* carbon of the (η^5-C_5H_4) as this does not appear in the DEPT 135 spectrum. The unsubstituted (η^5-C_5H_5) ring appears at δ 69.4 with the *meta* and *ortho* carbons occurring at δ 68.7 and δ 68.2 respectively. The methylene groups of the ethyl ester, glycine and L-norleucine moieties are easily assigned as they show negative resonance peaks in the DEPT 135 spectrum at δ 60.4, δ 41.8, δ 30.8, δ 27.3 and δ 21.7 respectively. The methyl carbons of the ester group and L-norleucine are observed in the most upfield positions. They occur at δ 14.1 and δ 13.7 respectively.

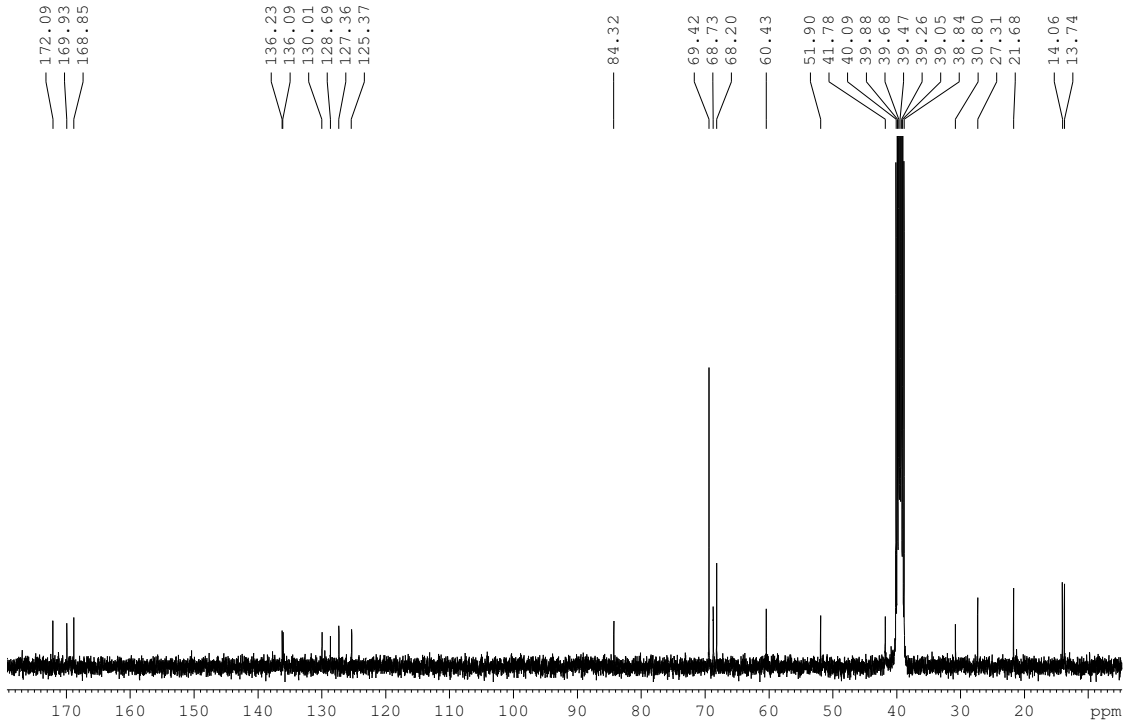

Fig. 2.16 ^{13}C NMR spectrum of *N*-{*ortho*-(ferrocenyl)-benzoyl}-glycine-L-norleucine ethyl ester **50**.

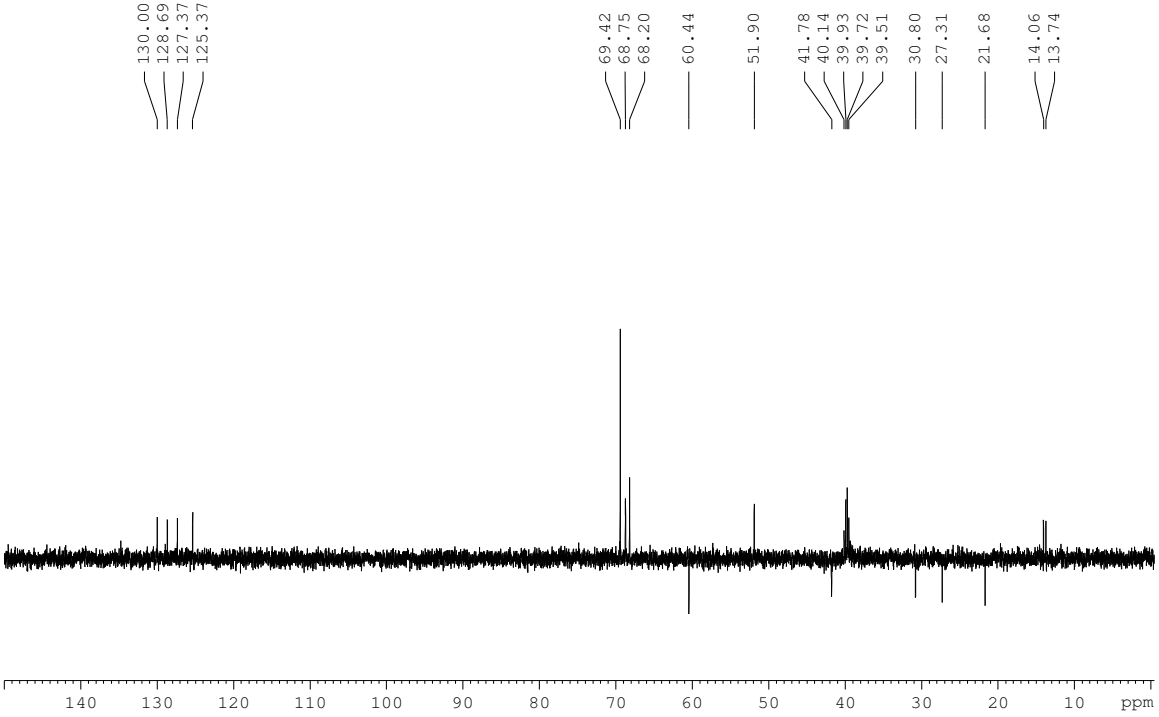

Fig. 2.17 DEPT 135 spectrum of *N*-{*ortho*-(ferrocenyl)-benzoyl}-glycine-L-norleucine ethyl ester **50**.

2.6 COSY studies of *N*-{*para*-(ferrocenyl)-benzoyl}-γ-aminobutyric acid-L-norleucine ethyl ester.

COSY (Correlation Spectroscopy) is the simplest example of a two-dimensional NMR technique. There are two coordinate axes, each representing a chemical shift range. The data is plotted as a grid with both chemical shift ranges and the third dimension shows the intensity of the observed signal [9]. In the COSY spectrum of *N*-{*para*-(ferrocenyl)-benzoyl}-γ-aminobutyric acid-L-norleucine ethyl ester **85** the proton spectrum is plotted along each axis. The spectrum shows distinct spots on the diagonal with each spot corresponding to the same peak on each coordinate axis. It is clear that the amide proton of the γ-aminobutyric acid **a** (δ 8.49) correlates with the methylene of the γ-aminobutyric acid chain **b** (δ 3.36-3.30), while the amide proton of L-norleucine **e** (δ 8.30) couples with the methine proton **f** (δ 4.21) at the chiral centre of L-norleucine. Correlation is also present between the *ortho* and *meta* protons of the substituted (η^5-C_5H_4), **l** and **k**. The first methylene group of the L-norleucine side chain **g** (δ 1.75-1.60) is identified from its coupling with the methine proton **f**. The first methylene group of L-norleucine **g** (δ 1.75-1.60) also couples with the second methylene group **h**, while the second group **h** also couples with the third methylene group **i**. The third methylene group **i** in turn couples with the methyl group of the chain **j**. The middle methylene group of the γ-aminobutyric acid **c** is easily identified due to its coupling with both remaining methylene groups, **b** and **d**. The methylene **m** and methyl protons **n** of the ethyl ester only show coupling with each other, as do the aromatic protons of the benzoyl group, **o** and **p**.

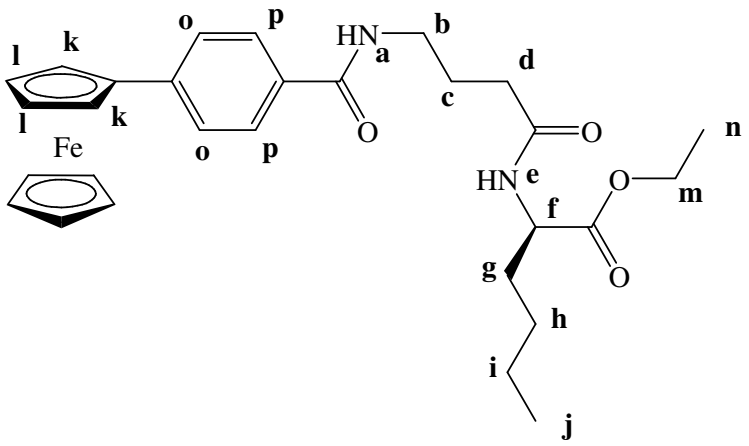

Fig. 2.18 *N*-{*para*-(ferrocenyl)-benzoyl}-γ-aminobutyric acid-L-norleucine ethyl ester **85**.

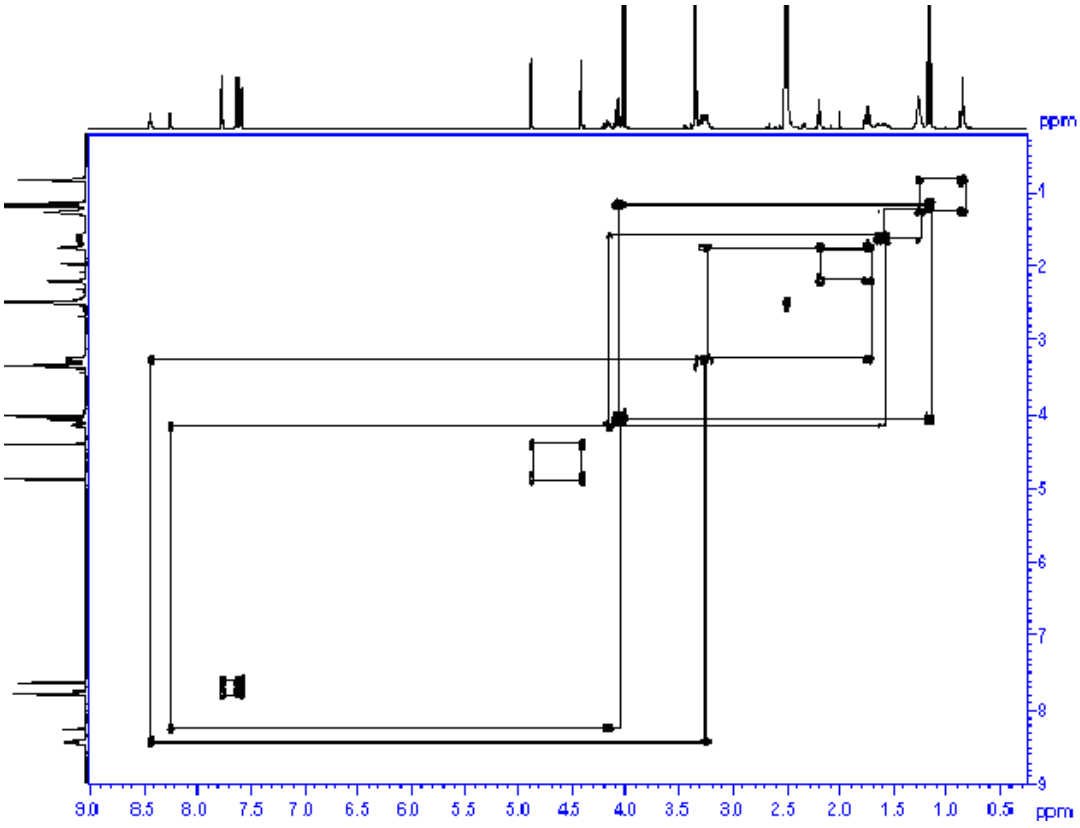

Fig. 2.19 COSY spectrum of *N*-{*para*-(ferrocenyl)-benzoyl}-γ-aminobutyric acid-L-norleucine ethyl ester **85**.

2.7 HMQC study of *N*-{*meta*-(ferrocenyl)-benzoyl}-β-alanine-L-2-aminobutyric acid ethyl ester.

Heteronuclear multiple quantum coherence (HMQC) allows for the complete assignment of proton and carbon spectra and therefore full structural elucidation may be achieved. The carbon aspect of the spectrum is very useful in resolving the often severely overlapping proton element [10]. This correlation is achieved by using a pulse sequence with a delay time set at half the value of the ^{13}C-^{1}H coupling constant, usually in the region of 100-200 Hz. This results in a correlation between the carbon atom and the proton to which it is attached. Needless to say, quaternary carbons are not present in the HMQC spectrum. A full assignment of chemical shifts for *N*-{*meta*-(ferrocenyl)-benzoyl}-β-alanine-L-2-aminobutyric acid ethyl ester **67** is outlined in Figure 2.21 and Table 2.3.

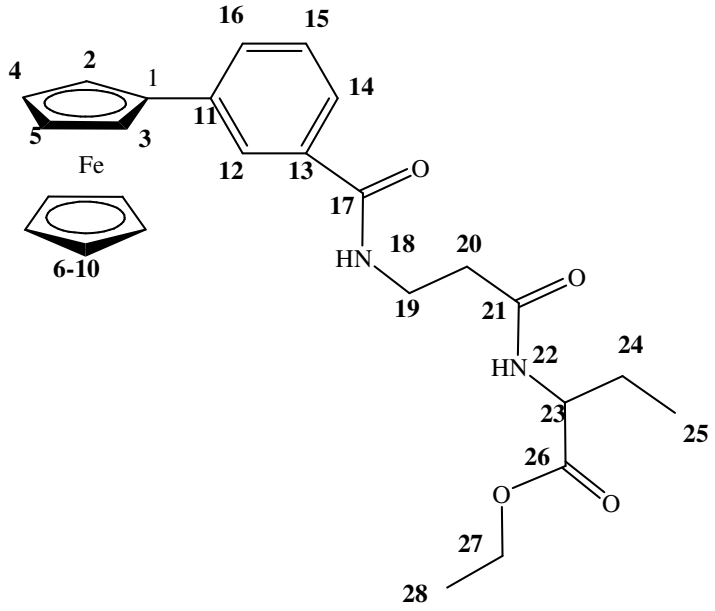

Fig. 2.20 *N*-{*meta*-(ferrocenyl)-benzoyl}-β-alanine-L-2-aminobutyric acid ethyl ester **67**.

Table 2.3 C-H correlation data from HMQC spectrum of *N*-{*meta*-(ferrocenyl)-benzoyl}-β-alanine-L-2-aminobutyric acid ethyl ester **67**.

Site	**^{1}H NMR**	**^{13}C NMR**	**HMQC**
1		84.0	
2 and 3	4.84		66.4
4 and 5	4.39		69.0
6 to 10	4.12-4.08		69.4
11		139.2	
12	7.94		124.1
13		134.5	
14	7.71-7.64*		128.4
15	4.84		128.3
16	7.71-7.64*		124.7
17		166.1	
18	8.30		
19	3.49		36
20	2.48		34.7
21		170.7	
22	8.52		
23	4.19-4.14		53.4
24	1.74-1.57		24.5
25	0.87		10.3
26		172.1	
27	4.12-4.08		60.3
28	1.16		14.0

* Note: Signals 14 and 16 appear as a multiplet in the ^{1}H spectrum.

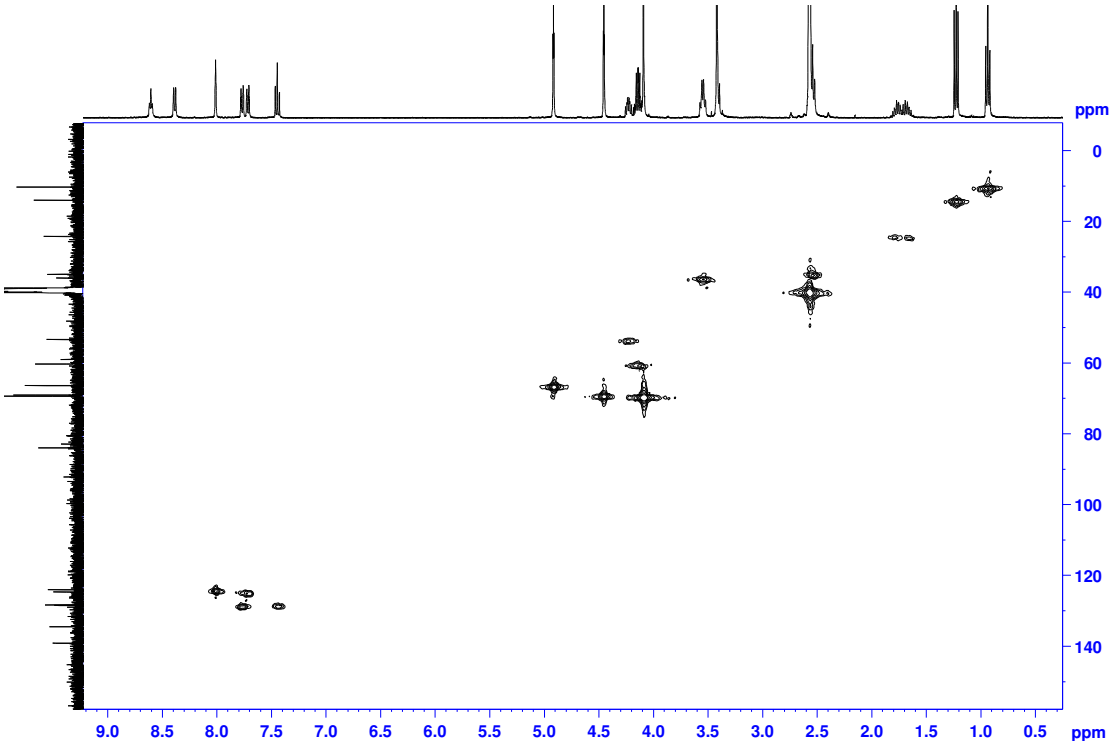

Fig. 2.21 HMQC spectrum of *N*-{*meta*-(ferrocenyl)-benzoyl}-β-alanine-L-2-aminobutyric acid ethyl ester **67**.

2.8 ^{1}H NMR studies of *N*-(ferrocenyl)benzoyl tri- and tetrapeptide ethyl esters.

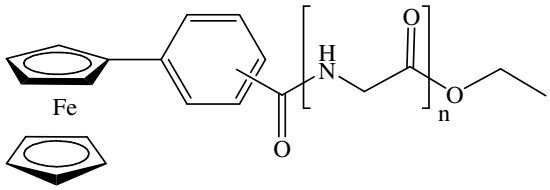

Fig. 2.22 General structure of *N*-(ferrocenyl)benzoyl tri- and tetrapeptide ethyl esters where n = 3 **86-88**, n = 4 **89-91**.

N-(ferrocenyl)benzoyl tri- and tetrapeptide esters were also synthesised and ^{1}H NMR experiments were subsequently performed. The aromatic signals of *N*-(ferrocenyl)benzoyl tri- and tetrapeptide esters varied depending on whether *ortho*, *meta*

or *para* ferrocenyl benzoic acid was used as a starting material. For the *ortho* derivatives the aromatic region displays a doublet, triplet, multiplet splitting pattern, integrating for one, one and two protons respectively. In the *meta* derivatives the pattern observed was a singlet that integrates for one proton, a multiplet that integrates for two protons and a triplet that integrates for one proton. The *para* substituted splitting pattern is two doublets that each integrate for two protons.

The chemical shift of the amide proton that forms the amide bond between the benzoyl group and the peptide is present between δ 8.9 and δ 8.5 for the tripeptides and δ 8.9 and δ 8.6 for the tetrapeptides. These downfield chemical shifts are attributed to the hydrogen bonding between the N-H of the amide and the S=O bond of the deuterated DMSO, in which the NMR studies were carried out.

The *ortho* protons of the substituted cyclopentadienyl (η^5-C_5H_4) ring appear between δ 4.90 and δ 4.70 and integrate for two protons, as does the peak for the *meta* protons of the (η^5-C_5H_4) ring. These peaks appear as fine triplets with coupling constants between 1.6 and 2.0 Hz. The unsubstituted cyclopentadienyl (η^5-C_5H_5) ring appears as a singlet between δ 4.1 and δ 4.0, with an integration of five protons. The methylene protons of the peptide chains appear between δ 4.02 and δ 3.71. They may appear as individual doublets integrating for 2 protons each or as a multiplet. Figure 2.23 displays the ^{1}H NMR spectrum of *N*-{*meta*-(ferrocenyl)-benzoyl}-glycyl-glycyl-glycine ethyl ester **87**.

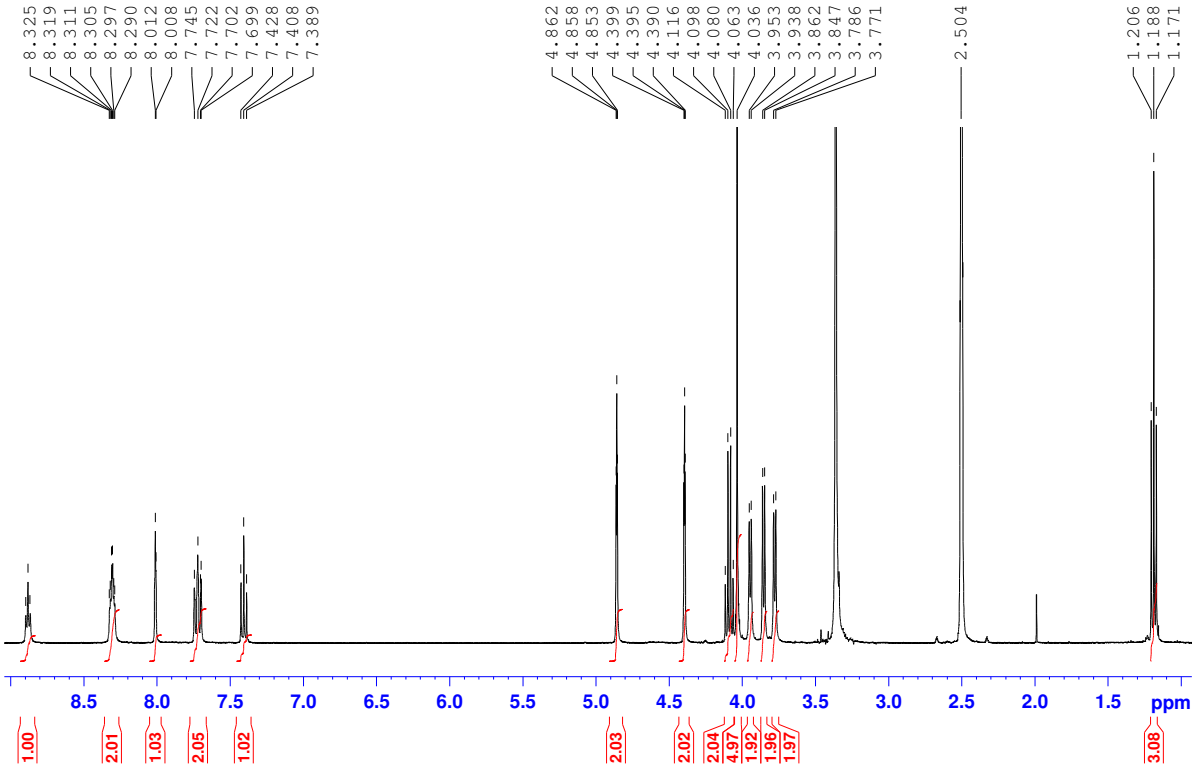

Fig. 2.23 ^{1}H spectrum of *N*-{*meta*-(ferrocenyl)-benzoyl}-glycyl-glycyl-glycine ethyl ester **87**.

2.9 ^{13}C NMR and DEPT 135 studies of *N*-(ferrocenyl)benzoyl tri- and tetrapeptide ethyl esters.

^{13}C NMR and DEPT 135 spectra were obtained for all of the compounds, **86-91**. In the DEPT 135 spectra methylene carbons appear below the resonance line while methine and methyl groups appear as positive peaks. The carbonyl and quaternary carbons of these compounds do not appear in the DEPT 135 spectra. In the ^{13}C NMR spectrum of *N*-(ferrocenyl)benzoyl tri- and tetrapeptide esters the amide and ethyl ester carbonyl carbon atoms appear in the range of δ 170.1 and δ 166.4. In the aromatic region the pattern observed depended on whether the derivatives were *ortho*, *meta* or *para* disubstituted. The *ortho* and *meta* derivatives give rise to six carbon peaks as all six carbons are non-equivalent. The *para* derivatives have four carbon peaks, two of these being quaternary carbons that were easily identified by using DEPT 135. The ferrocenyl carbons are

present between δ 84.3 and δ 66.3. The *ipso* carbon on the substituted cyclopentadienyl (η^5-C_5H_4) ring appears in the range of δ 84.3 and δ 83.1. The unsubstituted cyclopentadienyl (η^5-C_5H_5) ring is observed as an intense peak at approximately δ 69, while the *ortho* and *meta* carbons of the substituted cyclopentadienyl (η^5-C_5H_4) ring have chemical shifts between δ 68 and δ 66. The methylene group of the ethyl ester appears at δ 60.4 in all spectra. This peak and the methylene peaks of the peptide chain are easily recognised by their negative resonances in DEPT 135 spectra. The methylene carbons of the tripeptide chain appear between δ 42.7 and δ 40.0 and appear between δ 42.2 and δ 39.9 for the tetrapeptide derivatives. The methyl group of the ethyl ester is at δ 14.0 in all spectra.

Table 2.4 Selected ^{13}C data (δ, d_6-DMSO) for compounds **86** to **91.**

Compound	C=O	*Ipso* (η^5-C_5H_4)	(η^5-C_5H_5)	O-CH_2CH_3	Peptide CH_2
86	170.1-169.1	84.4	69.4	60.4, 14.0	42.3-40.6
87	170.0-166.6	83.9	69.4	60.4, 14.0	42.8-40.6
88	169.7-166.5	83.1	69.5	60.4, 14.0	42.7-40.6
89	170.1-169.1	84.4	69.4	60.4, 14.0	42.3, 40.6
90	169.6-166.6	84.0	69.4	60.4, 14.0	42.8-40.6
91	169.6-166.5	83.2	69.5	60.4, 14.0	42.8, 41.2

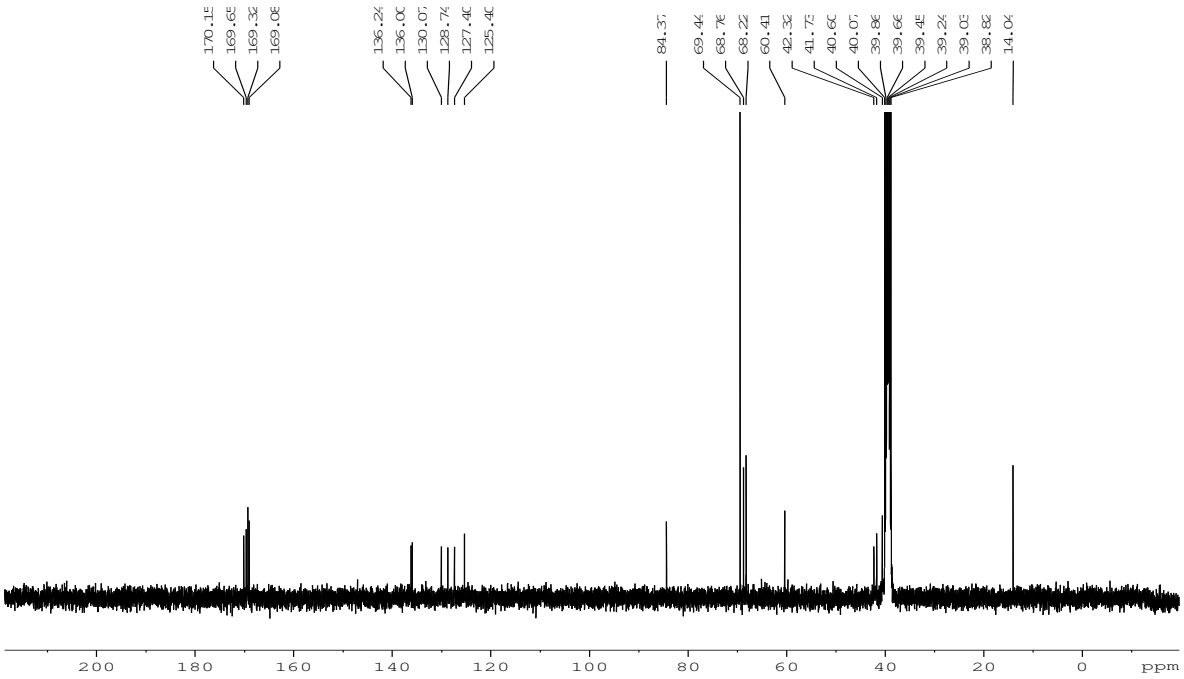

Fig. 2.24 ^{13}C NMR spectrum of *N*-{*ortho*-(ferrocenyl)-benzoyl}-glycyl-glycyl-glycine ethyl ester **86**.

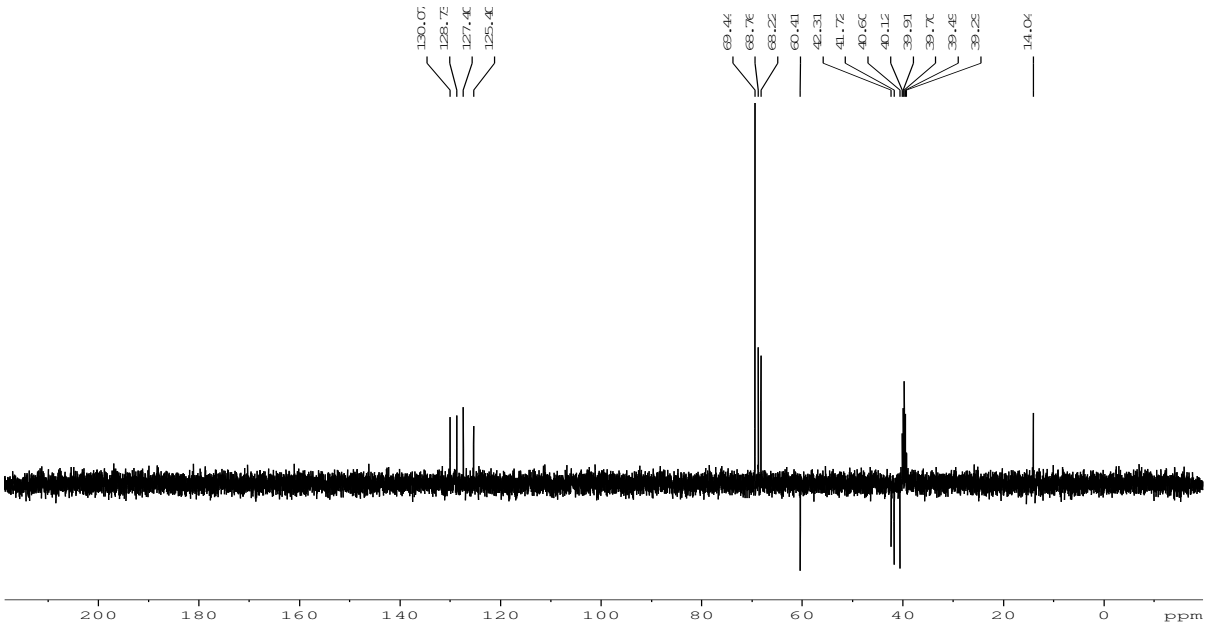

Fig. 2.25 DEPT 135 spectrum of *N*-{*ortho*-(ferrocenyl)-benzoyl}-glycyl-glycyl-glycine ethyl ester **86**.

2.10 Synthesis of 1, 1'-*N, N*'-{*ortho*-(ferrocenyl)-bisbenzoyl} amino acid and dipeptide esters 94-96.

The general procedure for the synthesis of 1,1'-*N, N*'-{*ortho*-(ferrocenyl)-bisbenzoyl} amino acid and dipeptide esters is presented in Figure 2.25. In order to prepare a 1,1'-disubstituted ferrocenyl benzoyl system two equivalents of diazonium reagents are required. In the final coupling step two equivalents of coupling reagents are also required to obtain the desired product. The yields for the 1,1'-*N, N*'-{*ortho*-(ferrocenyl)-bisbenzoyl} amino acid and dipeptide esters ranged between 14% and 35%. These overall modest yields illustrate the difficulties in preparing 1,1'-disubstituted ferrocenyl benzoyl systems.

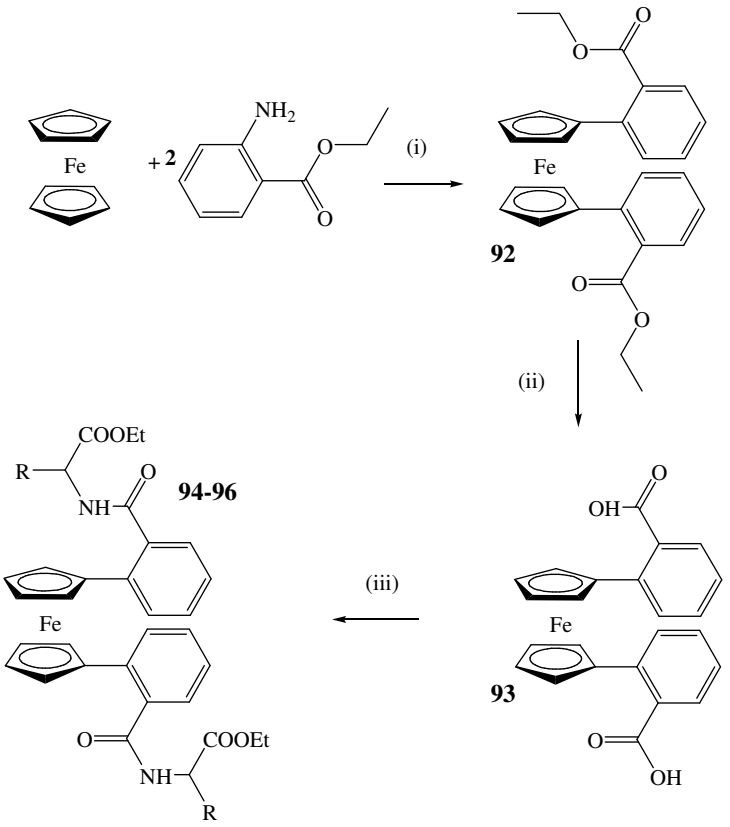

(i) $NaNO_2$ (2 equivalents), HCl, 5 ^{o}C, (ii) NaOH/MeOH, HCl, (iii) EDC, HOBt, amino acid or dipeptide ester (all 2 equivalents), TEA, R = amino acid or dipeptide ester.

Fig. 2.26 Reaction scheme for the preparation of 1,1'-*N,N*'-{*ortho*-(ferrocenyl)-bisbenzoyl} amino acid and dipeptide esters.

2.10.1 Palladium catalysed cross coupling.

The preparation of 1,1'-*ortho*(ferrocenyl)bis ethyl benzoate was performed using diazonium salt chemistry. However the low yield of 16 % and extensive purification required resulted in an alternative synthetic route being sought. A model reaction was carried out where *para*-ferrocenyl ethyl benzoate was prepared *via* the Suzuki reaction. Reaction conditions and purification procedures were optimised using commercially available ferroceneboronic acid. The reaction proceeds *via* the palladium catalysed coupling of organic halides with organoboranes under basic conditions. It is a very versatile procedure for creating new carbon-carbon bonds [(11)]. Refluxing ferroceneboronic acid in dimethoxyethane (DME) in the presence of a palladium catalyst, potassium carbonate and ethyl-4-iodo benzoate yielded *para*-ferrocenyl ethyl benzoate. The ^{1}H NMR spectrum of *para*-ferrocenyl ethyl benzoate is presented in Figure 2.27. This is a modified procedure for the palladium-catalysed arylation of ferrocene that has been previously reported [(12)].

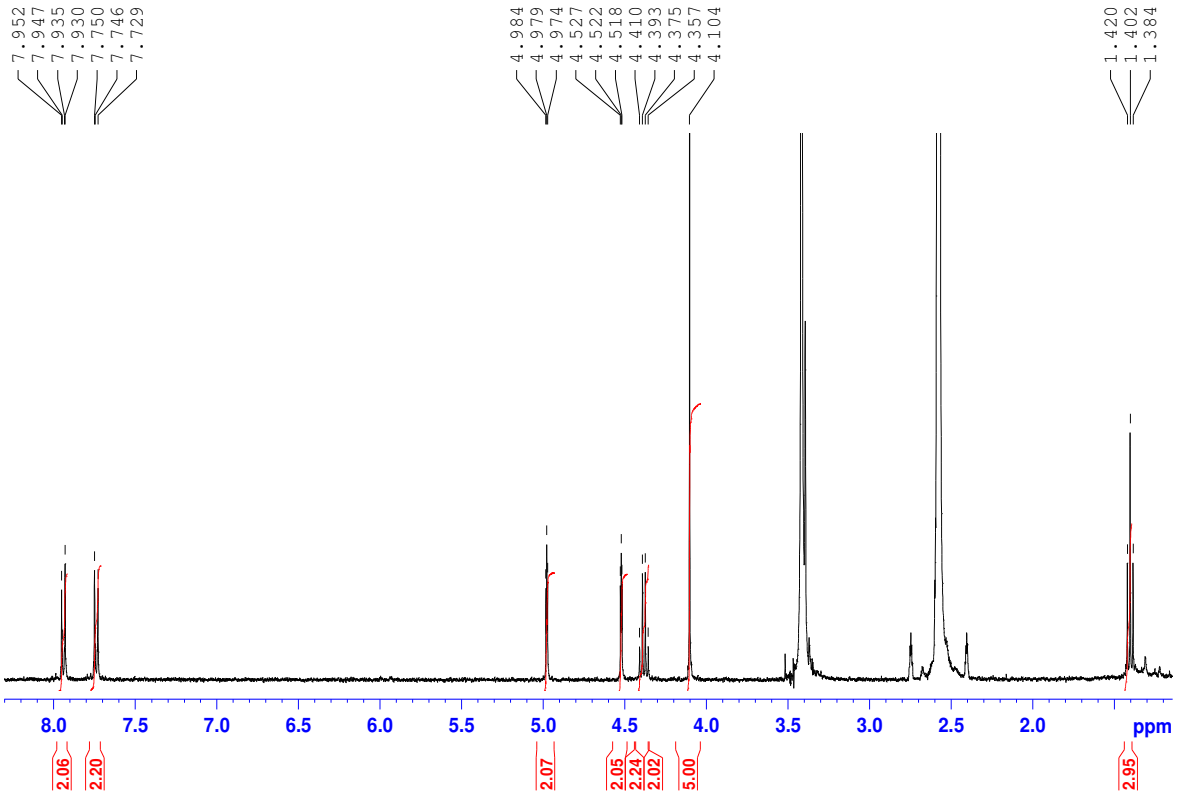

Fig. 2.27 ^{1}H NMR spectrum of *para*-ferrocenyl ethyl benzoate *via* cross coupling reaction **41b**.

The catalytic cycle proceeds *via* three steps in a complex reaction process [11].

a) There is oxidative addition of a carbon electrophile to the zero valent palladium.
b) The transmetallation of a nucleophilic carbon from boron to the palladium complex.
c) This is followed by the rapid reductive elimination of the cross coupled product to regenerate the zero valent palladium, Pd(0).

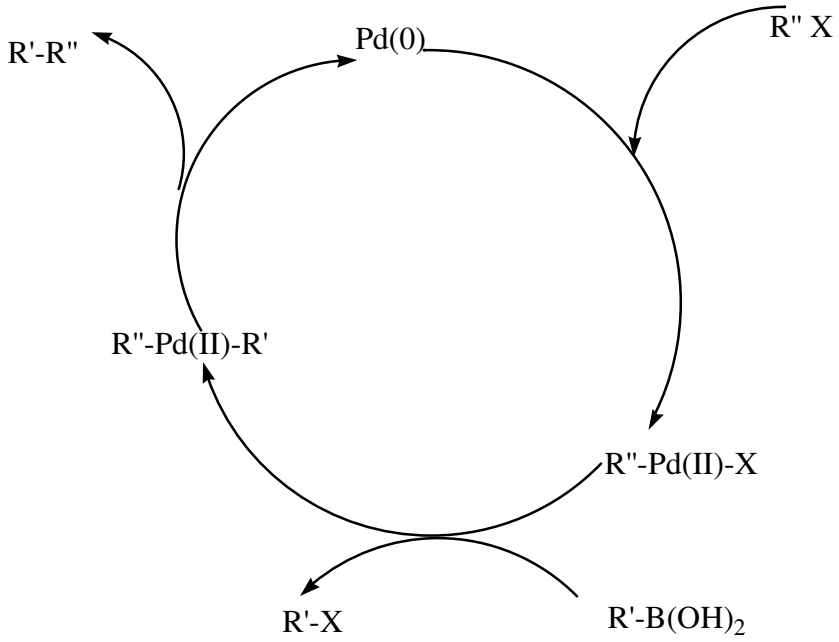

Fig. 2.28 Catalytic cycle for palladium catalysed cross coupling. R' = ferroceneboronic and R" = ethyl-4-iodobenzoate.

The overall yield for the preparation of *para*-ferrocenyl ethyl benzoate *via* the cross coupling procedure was less than that observed for the diazonium procedure, 34% and 51% respectively. However with further optimization of reaction conditions and purification procedures it is envisaged that palladium catalysed reaction may be useful in the preparation of 1,1'-disubstituted ferrocenyl benzoyl systems.

2.11 ^{1}H and ^{13}C NMR studies of 1, 1'-*N, N'*-{*ortho*-(ferrocenyl)-bisbenzoyl} amino acid and dipeptide esters.

In ^{1}H NMR studies of 1,1'-*N, N'*-{*ortho*-(ferrocenyl)-bisbenzoyl} amino acid and dipeptide esters the aromatic region is similar to that observed for *N*-{*ortho*-(ferrocenyl)-benzoyl} peptide esters with a doublet, triplet, multiplet splitting pattern observed between δ 7.72 and δ 7.91. In d_6-DMSO the amide peaks are observed between δ 8.70 and δ 8.34.

In a disubstituted ferrocenyl system two peaks are present between δ 4.6 and δ 4.0 that correspond to the *meta* and *ortho* ferrocenyl hydrogens of the substituted cyclopentadienyl (η^5-C_5H_4) rings. They can appear as a singlet or fine triplets and both peaks will integrate for four protons.

2.11.1 ^{1}H NMR study of 1,1'-*N, N'*-{*ortho*-(ferrocenyl)-bisbenzoyl}-glycine ethyl ester 94.

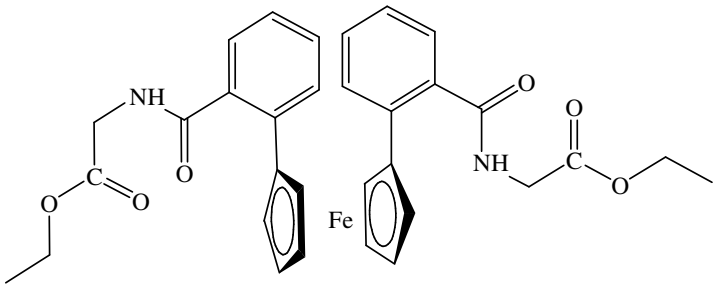

94

The amide proton of each glycine unit appears as a triplet at δ 8.72 due to coupling with the adjacent methylene protons. The appearance of one amide peak that integrates for two protons shows that the two amide protons are in the same chemical environment. The *ortho* disubstituted splitting pattern appears as a doublet, triplet, multiplet that integrates for eight protons corresponding to the eight protons on the two benzene rings. At δ 4.54 and δ 4.07 singlets with integrations of four protons are observed that correspond to the *ortho* and *meta* ferrocenyl protons of the two cyclopentadienyl (η^5-C_5H_4) rings. The methylene group of the ethyl ester overlaps with the *meta* ferrocenyl protons. This methylene group appears as a quartet and also integrates for four protons. The methyl

group of the ethyl ester is present at δ 1.21 and appears as a triplet. The doublet at δ 3.88 is due to the methylene group of the glycine. This peak integrates for four protons, corresponding to the methylene groups of each glycine unit.

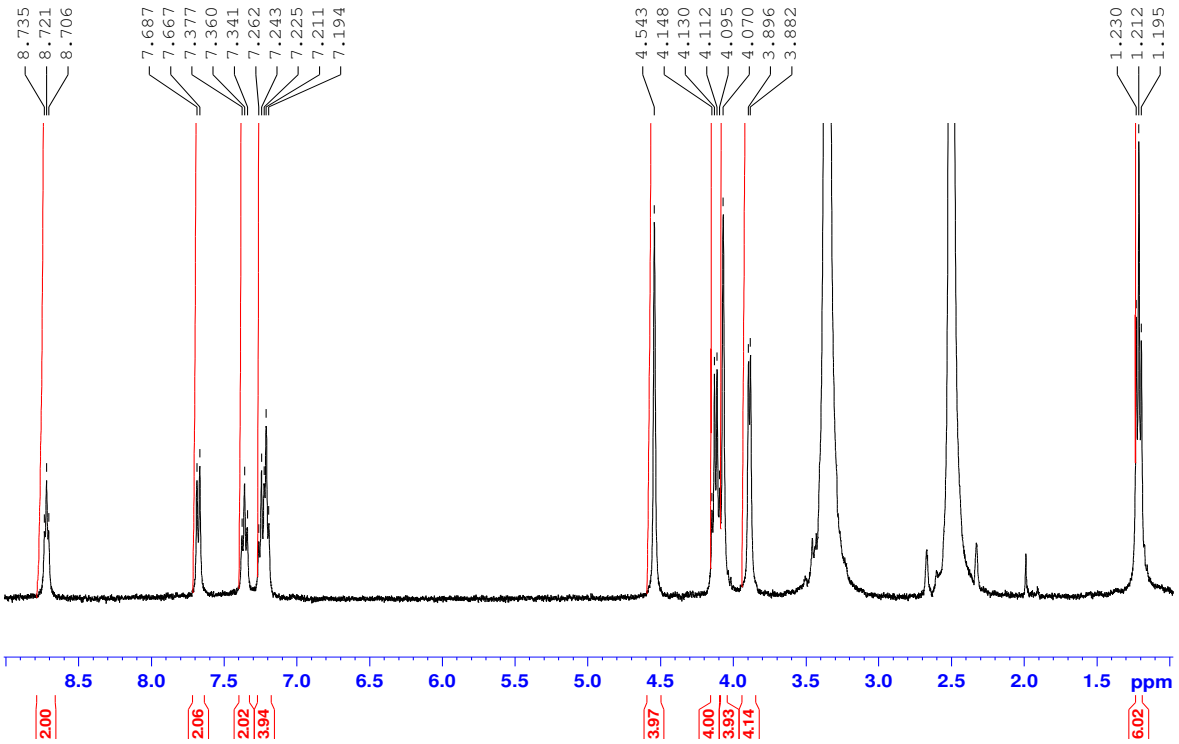

Fig. 2.29 ^{1}H NMR spectrum of 1,1'-*N, N'*{-*ortho*-(ferrocenyl)-bisbenzoyl}-glycine ethyl ester **94**.

2.11.2 ^{13}C and DEPT 135 studies of 1, 1'-*N, N'*-{*ortho*-(ferrocenyl)-bisbenzoyl} amino acid and dipeptide esters.

^{13} C NMR and DEPT 135 spectra were obtained for compounds **94**-**96**. In each case the carbonyl peaks of the amide bonds and the ethyl ester are the most downfield peaks. They appear between δ 172.5 and δ 168.6. As all derivatives are *ortho* disubstituted compounds there are 6 aromatic signals present, as each carbon is non-equivalent. The quaternary carbons were identified by their absence in the DEPT 135 spectra. For a 1,1'-disubstituted ferrocenyl system 3 carbon peaks are present. The *ipso* carbon is observed between δ 84.8 and δ 84.6. The *ortho* and *meta* carbons of the cyclopentadienyl (η^5-C_5H_4) rings appear between δ 70.9 and δ 70.0. For compound **94** the methylene carbon atoms

are observed at δ 60.5 and δ 41.0. These peaks can be identified from their negative resonances in the DEPT 135 spectra. For compounds **95** and **96** the methylene carbons appear at δ 60.4, δ 41.9, δ 40.6 and δ 60.5, δ 41.7 respectively. The α carbon of compound **96** appears at δ 47.6, while the methyl group appears at δ 17.1. The methyl group of the ethyl ester is present at δ 14.0 in each spectra.

2.12 Infra red spectroscopic studies of *N*-(ferrocenyl)benzoyl peptide esters.

Infra red (IR) spectroscopy is a technique by which numerous functional groups may be identified. Following absorption of IR radiation molecular vibrations, for example stretching, bending and rocking, are induced [(13)].

The region of the spectrum above 1500 cm^{-1} gives the most information on the structure of the molecule, while the fingerprint region (less than 1500 cm^{-1}) contains numerous absorption bands and is of less consequence. The IR spectra of *N*-(ferrocenyl)benzoyl peptide esters were obtained in potassium bromide and generally show two bands greater than 3000 cm^{-1} that correspond to the secondary amide groups. The hydrogen bonding ability of amides, Amide II (Figure 2.30), lowers and broadens the N-H stretching frequencies. The carbonyl stretches for Amide I generally observed stretching between 1695 cm^{-1} and 1680 cm^{-1}, while the carbonyl of Amide II occurs around 1540 cm^{-1}.

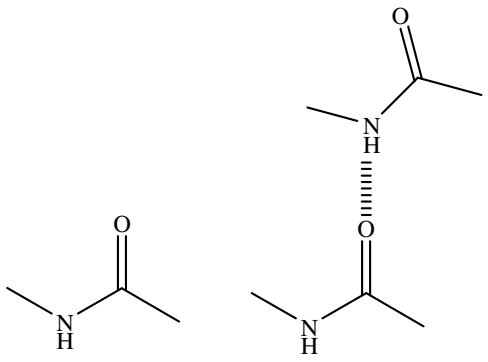

Fig. 2.30 Amide configurations that give rise to two bands in IR spectra.

Aromatic groups can be characterized by weak C-H stretching bands at around 3030 cm^{-1} and by bands between 1600 cm^{-1} and 1500 cm^{-1}. The substitution pattern of disubstituted aromatic systems may be inferred from the strong bands associated with C-H out of plane vibrations less at than 900 cm^{-1}. The frequency of these C-H vibrations is dependent on the number of adjacent hydrogens on the benzene ring, therefore the frequency is a means of predicting the substitution pattern. However, these bands are not always the only or strongest bands in this region therefore assignment based on these factors should be treated with caution [10].

Table 2.5: IR frequencies of *N*-(ferrocenyl)benzoyl peptide esters (cm^{-1}).

Compound	N-H	C=O Amide I and II	C=O Ester	Aryl C-H
75	3356	1680, 1610	1745	1558, 1518
79	3261	1685, 1650	1742	1578, 1542
83	3284, 3235	1655, 1620	1749	1559, 1523
88	3275	1648, 1607	1751	1578, 1519
91	3293	1650, 1609	1739	1560, 1542

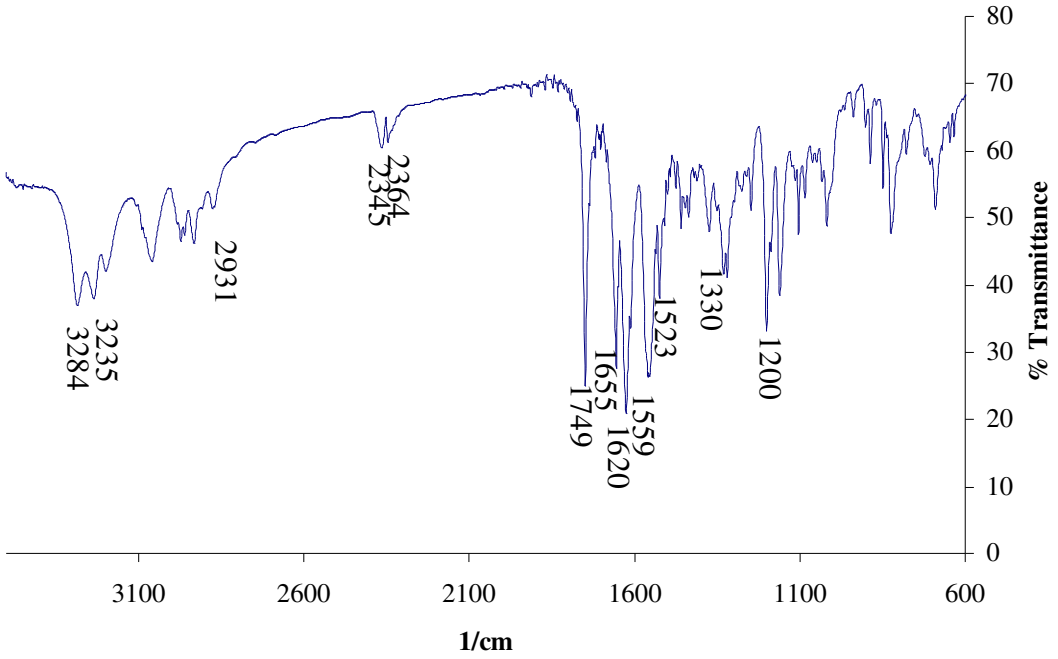

Fig. 2.31 IR spectrum of *N*-{*para*-(ferrocenyl)-benzoyl}-γ-aminobutyric acid-L-2-aminobutyric acid ethyl ester **83**.

2.13 UV-Vis spectroscopic studies of *N*-(ferrocenyl)benzoyl peptide esters.

The ultraviolet and visible (UV-Vis) spectra of organic compounds are as a result of transitions between electronic energy levels. The transitions are usually from bonding or lone pair orbitals to unfilled non-bonding or anti-bonding orbitals.

The wavelength of the absorption is a measure of the separation of energy levels between the two orbitals. Particular attention should be focused on the region above 200 nm where excitation of electrons from p and d orbitals, π orbitals and especially π conjugated systems lead to informative and useful spectra.

The UV-Vis spectra of *N*-(ferrocenyl)benzoyl peptide esters differ significantly. The *para* derivatives give the strongest absorbance bands. This is due to the benzoyl and the (η^5-C_5H_4) rings lying in the same plane as each other creating a larger chromophore. In general larger chromphores lead to stronger absorbances. The *para* derivatives have maxima at approximately 350 nm and 450 nm corresponding to the π and π* transition of the benzoyl moiety and the metal to ligand charge transfer (MLCT) of ferrocene respectively. The absorbances in the region of 350 nm are absent from *N*-ferrocenoyl peptide esters. For the *ortho* and *meta* derivatives the absorbances are not as intense and appear at shorter wavelengths. The *ortho* derivatives have absorbance bands at 325 nm and 440 nm while for the *meta* derivatives absorbance bands are present at 330 nm and 445 nm. These absorbances also yield information about the efficiency of chromophore absorbance. The *para* derivatives have a greater degree of conjugation and therefore have more intense absorbences compared to the *ortho* and *meta* derivatives. Extinction co-efficient (ε) values are calculated using the Beer-Lambert Law, A = ε.C.l., where A is absorbance, C is concentration in mol/L and l is the path length of the cell in centimetres [13].

Table 2.6 UV-Vis data (nm) for *N*-{*ortho, meta* and *para*-(ferrocenyl)-benzoyl}-glycine-glycine-glycine ethyl ester

Compound	$\lambda_{max\ 1}$	ε_1	$\lambda_{max\ 2}$	ε_2
86	439	812	333	1875
87	447	833	335	2242
88	449	1674	359	2400

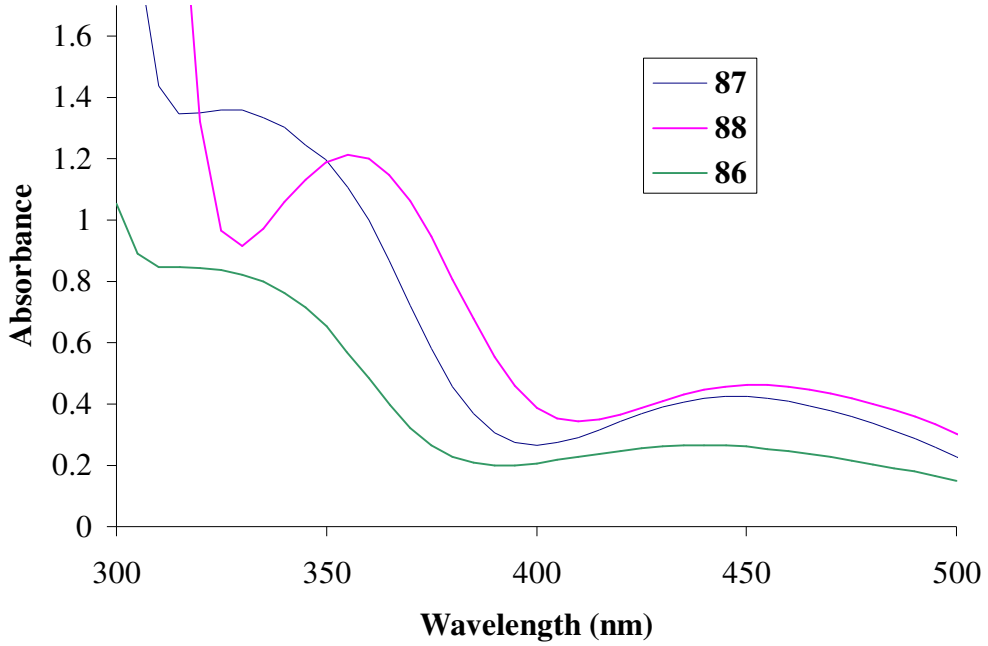

Fig. 2.32 UV-Vis spectra of *N*-{*ortho, meta* and *para*-(ferrocenyl)benzoyl}-glycine-glycine-glycine ethyl ester **86**-**88**.

2.14 Cyclic voltammetry of *N*-(ferrocenyl)benzoyl peptide esters.

All *N*-(ferrocenyl)benzoyl peptide compounds (**20**, **45**-**96**) exhibit one electron, reversible, redox waves similar to ferrocene, under the same conditions. The E°′ values range from 33 mV to 78 mV versus the ferrocene/ferricenium redox couple (Fc/Fc^+). These redox potential values are much lower than those observed for *N*-ferrocenoyl peptide esters, for example *N*-Fc-Ala-Ala-OMe shows a redox potential of 190 mV (vs

Fc/Fc$^+$), while *N*-Fc-Ala-Phe-OMe has a redox potential of 230 mV (vs Fc/Fc$^+$) [14]. The benzoyl moiety is therefore responsible for the lower redox potentials of compounds **20**, **45**-**96**. The extensive conjugation of the benzene ring acts as an electron bridge during the redox process and therefore makes the initial oxidation of the iron centre easier.

Figure 2.33 illustrates the cyclic voltammograms of ferrocene and *N*-{*para*-(ferrocenyl)-benzoyl}-glycine-L-norvaline ethyl ester **76**. The difference of 72 mV is clearly visible.

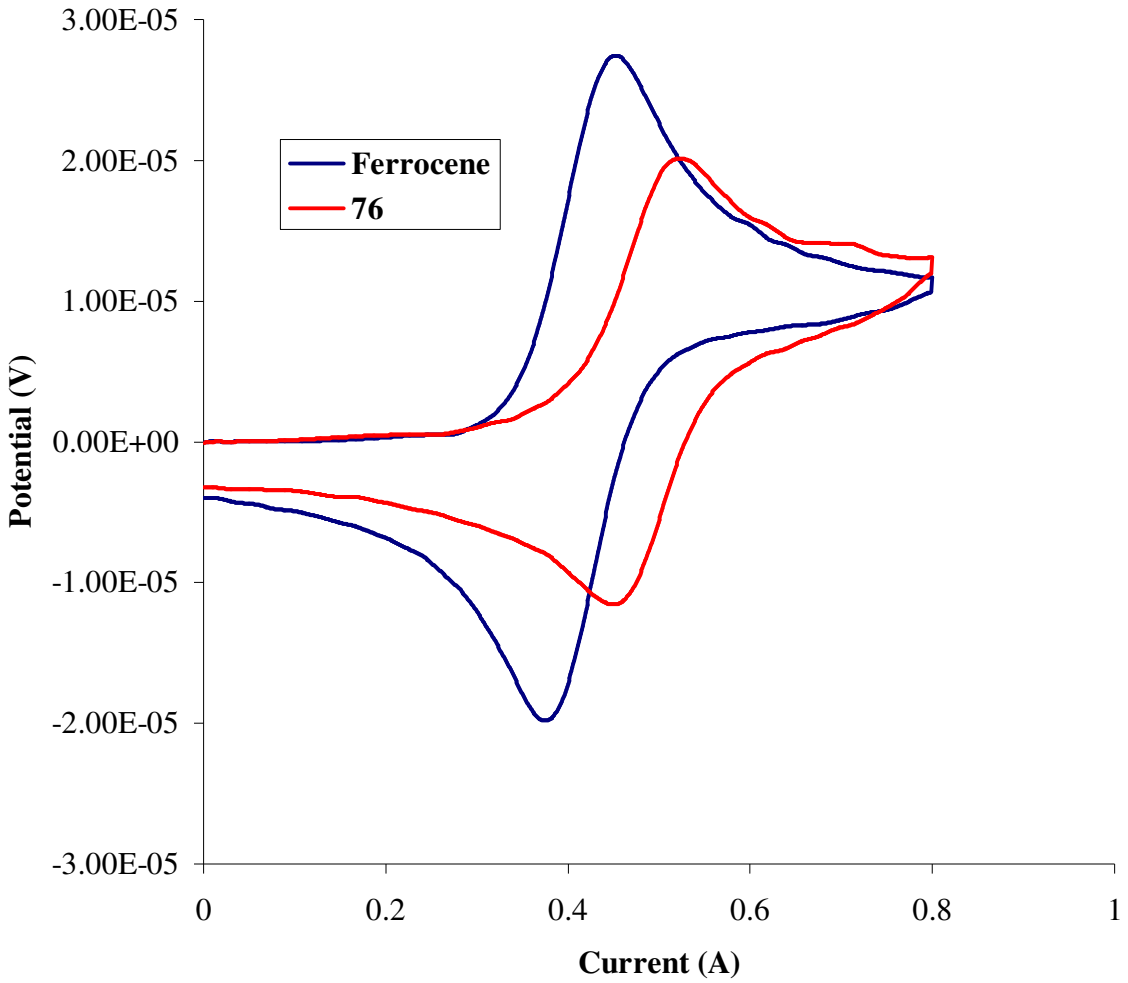

Fig. 2.33 Cyclic voltammograms of ferrocene and compound **76** (0.1M TBAP in ACN, Ag/AgCl, 0.1 V/s).

A notable trend is observed whereby the orientation around the central benzoyl moiety effects the redox potentials in the order *ortho* < *meta* < *para*. Oxidation of the ferrocenyl

unit in the *ortho* derivatives occurs more readily compared to the *meta* and *para* derivatives. It is possible that the *ortho* orientation around the benzoyl moiety imparts electron density to the ferrocene and therefore makes the iron centre more susceptible to oxidation. This electron density is less pronounced in the *meta* and *para* derivatives.

2.15 Mass spectrometric studies of *N*-(ferrocenyl)benzoyl peptide esters.

Mass spectrometry enables the determination of the relative molecular mass of many different classes of compounds [15]. The mass spectrometer can be split into three distinct parts, namely the ion source, the analyser and the detector. After the sample has been introduced into the ion source ionization occurs. The ions are then extracted into the analyser and separated according to their mass to charge ratio (*m/z*). The separated ions are detected and displayed as a mass spectrum.

Electrospray ionization (ESI) mass spectrometry was employed in the analysis of *N*-(ferrocenyl)benzoyl dipeptide esters, compounds **48**-**50**, **63**-**65** and **75**-**77**, and confirmed the correct relative molecular mass for all the compounds. The remaining compounds are currently being analysed. Examination of the mass spectra revealed the presence of both radical-cations, $[M]^{+\bullet}$ as well as $[M+H]^+$ species. Adducts due to sodium were also present 22 Da higher than the protonated molecular ion species. Sequence specific fragment ions were not observed, or were of low intensity in the mass spectra of *N-meta* and *N-para*-(ferrocenyl)benzoyl dipeptide esters. However an important diagnostic fragment ion at *m/z* $[M-65]^+$ was observed in the mass spectra of the *N-ortho*-(ferrocenyl)benzoyl dipeptide esters for example compound **50** at *m/z* 439. This corresponds to the loss of the unsubstituted (η^5-C_5H_5) ring. The formation of this fragment ion is possibly due to steric hindrance between the *ortho* substituted benzoyl substituents and the unsubstituted (η^5-C_5H_5) ring. The ESI mass spectrum of compound **50** is presented in Figure 2.34.

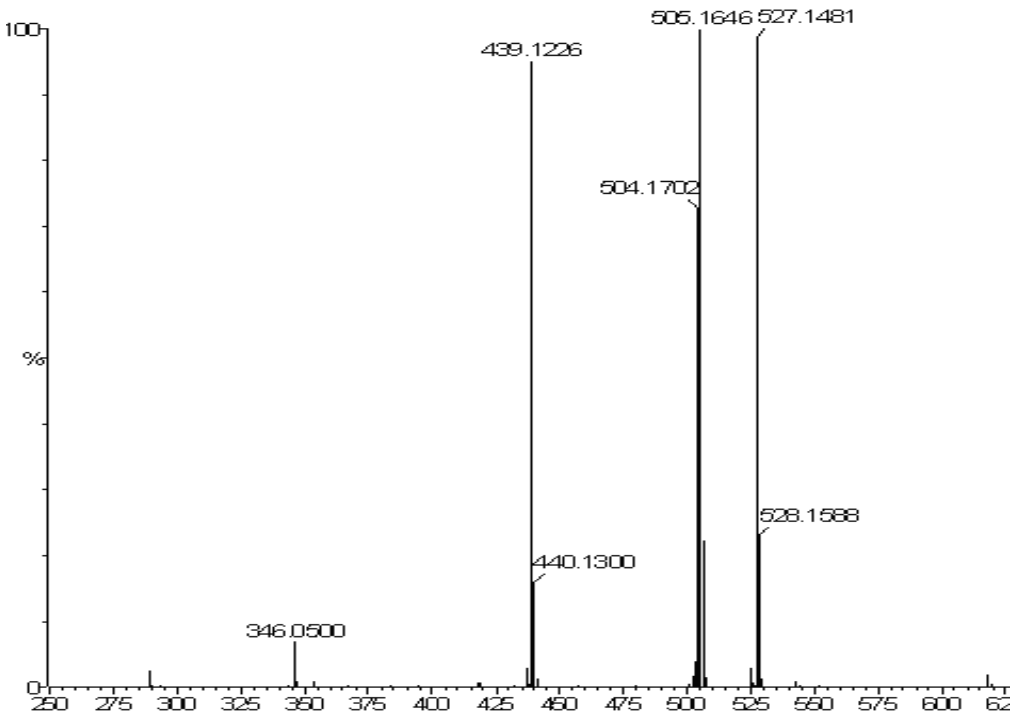

Fig. 2.34 ESI mass spectrum of *N*-{*ortho*-(ferrocenyl)-benzoyl}-glycine-L-norleucine ethyl ester **50**.

2.16 Conclusions.

A series of *ortho*, *meta* and *para* N-(ferrocenyl)benzoyl peptide esters were prepared and structurally characterized. Each novel compound incorporated an electroactive ferrocene core, a conjugated aromatic linker and a di-, tri-, or tetrapeptide chain, with each part exerting a specific effect on biological activity. The ferrocene moiety is required for the possible production of hydroxyl radicals, the benzoyl group facilitates this process by lowering the redox potential of the ferrocene and the peptide fragment can interact with other molecules *via* hydrogen bonding.

These compounds were prepared in good yields, following a number of synthetic steps. These novel compounds were characterized by a range of spectroscopic techniques including ^{1}H NMR, ^{13}C NMR, DEPT 135, HMQC, IR, UV-Vis, MS and CV. All compounds gave data in accordance with their proposed structures.

References

1. Togni, A., Hayashi, T., *Ferrocenes*, **1994**, Wiley, VCH publications.
2. Savage, D., Gallagher, J. F., Ida, Y., Kenny, P. T. M., *Inorg. Chem. Comm.*, **2002**, *5*, 1034.
3. Savage, D. M., *' The Synthesis and Characterization of Novel N-Ferrocenyl Benzoyl Amino Acid and Dipeptide Derivatives'*, DCU, Ph.D, Thesis, **2003**.
4. Hanson, J. R., '*Organic Synthetic Methods'*, **2002**, RSC.
5. White, A., *J. Biochem.*, **1959**, *71*, 217.
6. Marder, O., Alberico, F., *Chemistry Today Peptides,* **2003**, 35.
7. Jones, J., '*Amino Acid and Peptide Synthesis'*, Oxford University Press, **1992**.
8. Rosenblum, M., Glenn-Howells, W., Banerjee, A. K., Bennett, C., *J. Am. Chem. Soc.*, **1962**, *84*, 2726.
9. Breitmaier, E., '*Structure Elucidation by NMR in Organic Chemistry'*, Wiley, **1993**.
10. Williams, D. H., Fleming, I., *'Spectroscopic Methods in Organic Chemistry'*, McGraw-Hill, **1995** 5th edition.
11. Matos, K., Soderquist, J. A., *J. Org. Chem.*, **1998**, *63*, 461.
12. Knapp, R., Rehahn, M., *J. Organomet. Chem.,* **1993**, *452*, 235.
13. McMurry, J., *'Organic Chemistry'*, Brooks/Cole, **2000** 5th edition.
14. van Staveren, D. R., Weyhermuller, T., Metzler Nolte, N., *Dalton Trans*., **2003**, 210.
15. Silverstein, R. M., Webster, F. X., Kiemle, D. J., '*Spectrometric Identification of Organic Compounds*', John Wiley and Sons, **2005**, 7th edition.

Chapter 3

In vitro anti-cancer activity of *N*-(ferrocenyl)benzoyl peptide esters

3.1 Introduction

The term cancer is used to describe diseases characterized by uncontrolled, abnormal cell division and that are capable of spreading to other parts of the body through the blood and lymph systems. It may be found in many forms including solid tissue formations and leukaemias. Cancers result from a reduction or loss of control of the growth of cells [(1)]. In the early stages the cells formed resemble the parent cells but as the cancer advances they lose the appearance and function of the parent cell. If this loss of function is not halted the consequences will be life threatening. Both external (chemicals and radiation) and internal (hormones and inherited genes) forces acting alone or in tandem may be responsible for the initiation and propagation of cancer. In addition, many years can pass between cause and detection and in some types of cancer the early detection of malignant growths is a major problem [(2)].

Lung cancer is the most prevalent cancer worldwide, with 1.5 million cases diagnosed in 2003. This is greater than the diagnoses of breast, colon and prostrate cancer combined. The five year survival rate in the United States is 16.8% while in Great Britain the Figure is half that [(3)]. Lung cancer is the leading cause of cancer mortality in Ireland. It is responsible for approximately 20% of all cancer deaths [(4)]. Smoking is responsible for about 87% of cases, with chemical exposure also a contributory factor. Despite being one of the easier diseases to prevent it remains one of the most difficult to treat. This is primarily due to the late presentation of symptoms, the high level of metastasis and the development of resistance to chemotherapeutic agents. Radiation and chemotherapy treatments are crucial in lung cancer treatment as surgery is only effective in the early stages of lung cancer. 75-85% of all cases of lung cancer are non–small cell lung cancers (NSCLC). The chemotherapy drugs used are dependant on whether the cancer is classified as small cell lung cancer (SCLC) or NSCLC. The primary treatments for SCLC are cisplatin, carboplatin, cyclophosphamide or a combination of cisplatin and etoposide. Current therapy for NSCLC is surgery and adjuvant chemotherapy for early-stage disease

and palliative chemotherapy (and/or radiation therapy) for advanced disease. Cisplatin is frequently used in the treatment of NSCLC as is carboplatin, vindesine or more recently taxol and taxotere. Treatment for NSCLC with cisplatin demonstrated that chemotherapy for treatment of early stage disease improved 5-year survival from 50% to 55% [5, 6]. The development of resistance to a particular or a combination of unrelated cancer drugs is a major impediment in the treatment of cancer. This multiple drug resistance (MDR) is a result of a variety of changes in the cell, for example the increased activity of drug pumps like P-glycoprotein (Pgp) [6].

Within the cell, apoptosis has an important defensive role as it selectively kills abnormal cells, in particular pre-cancerous and cancerous cells. Enhancement of apoptosis in cancer cells may serve as an effective treatment. Ferrocene compounds are the first to exploit the overproduction of hydrogen peroxide in cancer cells to produce hydroxyl radicals (•OH) and enable selective killing of cancer cells by triggering apoptosis. This accumulation of high concentrations of hydrogen peroxide is a characteristic of cancer cells due to the over expression of superoxide dismutase (SOD) that transforms superoxide ions into hydrogen peroxide [7]. This abundance of hydrogen peroxide in cancerous cells has the potential to act as a prodrug, which in turn would decrease the unwanted side effects associated with conventional cancer treatment. The generation of hydroxyl radicals by ferrocene compounds following reaction with hydrogen peroxide is considered to be the main cause of activity. Ferrocene can be repeatedly oxidised by hydrogen peroxide and subsequently reduced, thus maintaining a high level of hydroxyl radicals in the cancer cell [8].

The *N*-(ferrocenyl)benzoyl peptide esters synthesised in this work were screened *in vitro* against the NSCLC cell line H1299, cisplatin and carboplatin resistant variants. This work was undertaken in collaboration with Dermot O'Sullivan and Dr. Norma O'Donovan of the National Institute for Cellular Biotechnology. An acid phosphatase assay was used which is an example of a colorimetric endpoint assay [9]. It is an indirect way of measuring cytotoxicity as it involves the evaluation of enzyme activity following a given treatment period. Acid phosphatase is an enzyme which dephosphorylates *p*-nitrophenol phosphate converting it to *p*-nitrophenol. In the presence of a strong base *p*-nitrophenol can be quantified colorimetrically. Thus cells were treated with the *N*-

(ferrocenyl)benzoyl peptide esters at a range of concentrations and incubated for 5-6 days until cell confluency was reached. Cell survival was determined by measuring acid phosphatase activity.

Table 3.1 displays the preliminary activity of several *N*-(ferrocenyl)benzoyl amino acid peptide esters and also the clinically used platinum derivatives, cisplatin and carboplatin. Compound **20** was identified as a lead compound and the aim was to investigate the change in biological activity after;

a) altering the orientation around the central benzoyl moiety,
b) increasing the number of amino acid residues,
c) increasing the number of methylene groups in the first and second amino acids,
d) preparing a 1,1'-disubstituted derivative of compound **20**.

Table 3.1 IC_{50} values for selected *N*-(ferrocenyl)benzoyl esters and platinum drugs versus H1299 lung cancer cells.

Compound	**IC_{50} value (μM)**
N-{*ortho*-(ferrocenyl)-benzoyl}-Gly-OEt*	48 ± 13%
N-{*ortho*-(ferrocenyl)-benzoyl}-Gly-Gly-OEt **45**	20 ± 10%
N-{*ortho*-(ferrocenyl)-benzoyl}-L-Ala-Gly-OEt **53**	21 ± 15%
N-{*ortho*-(ferrocenyl)-benzoyl}-Gly-L-Ala-OEt **20**	5.3 ± 8%
Carboplatin	10.0 ± 16%
Cisplatin	1.5 ± 7%

*Note: Originally prepared by David Savage [10]

3.2 Effect of redox potential and orientation around the central benzoyl moiety on cell proliferation.

The orientation around the central benzoyl moiety was altered to assess the effects of such a change on the growth of cells. A notable trend is seen where the orientation around the central benzoyl moiety effects the redox potentials in the order *ortho* < *meta* < *para*. Oxidation of the ferrocenyl unit in the *ortho* derivatives occurs more readily

compared to the *meta* and *para* derivatives. If the production of ROS is the primary mechanism of action then the derivative with the lowest redox potential , i.e. the easiest derivative to oxidise, would be the most active. However, no apparent correlation between redox potential and cytotoxicity was observed, Table 3.2.

Table 3.2 IC_{50} values and redox potentials for selected *N*-{ortho-(ferrocenyl)benzoyl} peptide esters.

Compound	IC_{50} value (μM)	Redox potential (mV)
N-{*ortho*-(ferrocenyl)-benzoyl}-Gly-OEt	48 ± 13%	27
20	5.3 ± 8%	50
45	20 ± 10%	49
53	21 ± 15%	49

This lack of correlation between cytotoxicity and a low redox potential does not eliminate the possibility of redox behaviour playing a role in cytotoxicity, conversely it implies a secondary mode of action is involved. The substitution pattern of the *N*-(ferrocenyl)benzoyl peptide esters may have a significant effect on the degree to which hydrogen bonding groups of the peptide chain can interact with nucleotide bases in the centre of the DNA helix [(11)]. Figure 3.1 illustrates the *in vitro* activity of *N*-{*ortho, meta* and *para*-(ferrocenyl)-benzoyl}-glycine-L-alanine ethyl esters **20**, **62**, **74**.

Compounds **20**, **62** and **74** have IC_{50} values of 5.3 μM, 4.0 μM and 6.6 μM (RSD ≈ 10%) respectively. These values are within a narrow range when the relative standard deviation (RSD) is considered. This demonstrates that change of orientation around the central benzoyl moiety does not affect bioactivity significantly. For compounds **20**, **62** and **74** the *ortho* derivative again has the lowest redox potential but was not the most active *in vitro*. This further illustrates that a low redox potential is not crucial for activity. The redox potentials of *N*-(ferrocenyl)benzoyl peptide esters are much lower than those observed for *N*-ferrocenoyl dipeptide esters, for example *N*-Fc-Ala-Ala-OMe shows a redox potential of 190 mV (vs Fc/Fc^+), while *N*-Fc-Ala-Phe-OMe has a redox potential of 230 mV (vs Fc/Fc^+). These *N*-ferrocenoyl derivatives are completely inactive *in vitro*, indicating that the benzoyl group, which is responsible for lowering the redox potential is

also required for activity. It is plausible that hydrogen bonding, lipophilicity and DNA interactions also play a role in the cytotoxicity of *N*-(ferrocenyl)benzoyl peptide esters.

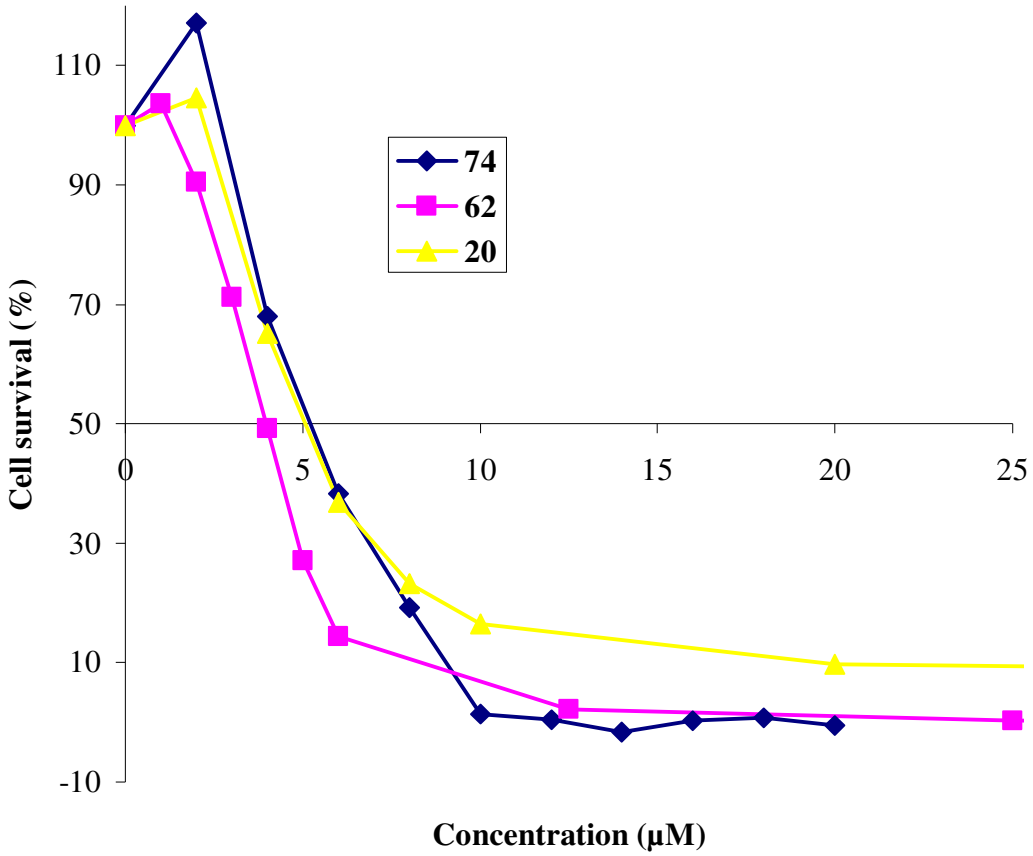

Fig. 3.1 *In vitro* anti-proliferative effect of *N*-{*ortho, meta* and *para*-(ferrocenyl)-benzoyl}-glycine-L-alanine **20**, **62**, **74**.

3.3 Effect of increasing peptide chain length on cell proliferation.

N-{*ortho*-(ferrocenyl)-benzoyl}-glycine ethyl ester was initially tested for its *in vitro* anti-proliferative activity towards lung cancer cells. This compound was found to be cytotoxic and had an IC_{50} value of 48 µM. Therefore other derivatives were evaluated for their anti-cancer activity against lung cancer cell lines. The dipeptide derivative *N*-

{*ortho*-(ferrocenyl)-benzoyl}-glycine-glycine ethyl ester was shown to have an IC_{50} value of 20 μM (RSD 10%). As the dipeptide derivative was more active than the amino acid derivative, a logical extension of this study was the preparation of longer peptide chains. Therefore the peptide moiety was extended by the addition of additional glycine residues.

A plot of cell survival versus compound concentration for the compounds *N*-{*ortho*-(ferrocenyl)-benzoyl}-glycine ethyl ester, **45**, **86** and **89** is presented in Figure 3.2. Compound **48** had an IC_{50} value of 20 μM while compound **86** and **89** both had IC_{50} values greater than 50 μM. Thus increasing the length of the peptide chain from dipeptide to tri- and tetrapeptide has a negative impact on the anti-proliferative effect of the ferrocenyl derivatives. Compound **86** had an IC_{50} value of 63 μM (RSD 8%), whereas compound **89** did not register an IC_{50} value in the concentration range used. The increasing peptide chain length may make the compound too polar and prevent it from permeating the lipophilic cell membrane. It can therefore be concluded that a dipeptide chain is required for optimum activity, Figure 3.2. Derivatives **86** and **89** have very similar redox potentials compared to *N*-(ferrocenyl)benzoyl dipeptide esters which are highly active *in vitro*, this confirms that the peptide chain imparts a secondary mechanism of action to these compounds.

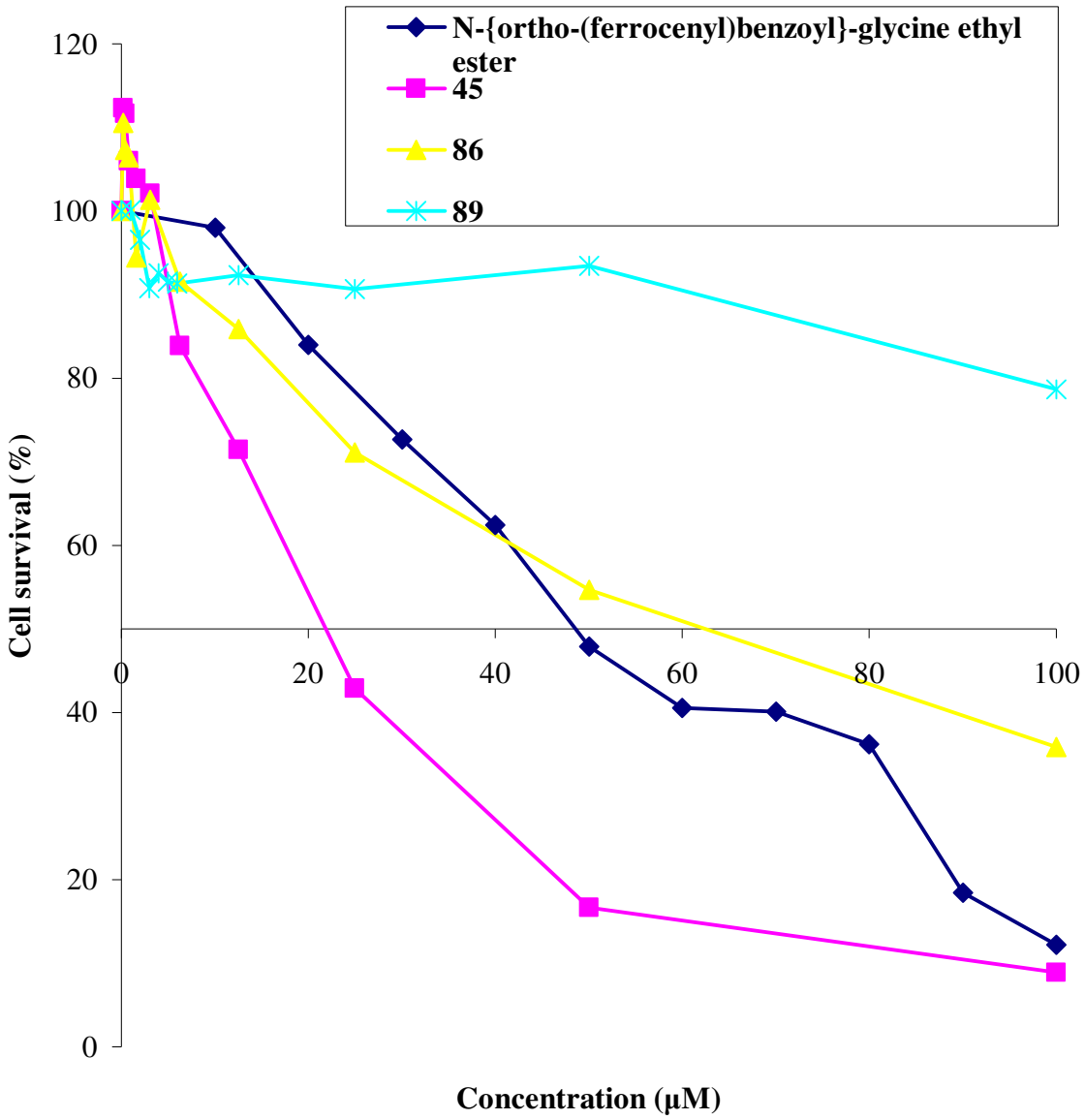

Fig. 3.2 *In vitro* anti-proliferative effect of *N*-{*ortho*-(ferrocenyl)-benzoyl}-glycine ethyl ester, **45**, **86** and **89**.

3.4 Effect of increasing the number of methylene groups in both the first and second amino acids of the dipeptide chain on cell proliferation.

From early biological data it was observed that the glycine-L-alanine derivative **20** was more active than the glycine-glycine derivative **45** and the L-alanine-glycine derivative

53. Hence the glycine residue of the dipeptide that is attached to the benzoyl group is important for activity. The larger amino acid alanine as the second residue also increased activity. To assess the effects of lipophilicity, the alanine residue was replaced with residues that differ by a methylene (CH_2) unit.

Increasing the number of methylene groups in a chain or ring increases the size and also the lipophilicity of the molecule. An improvement in activity following an increase in the number of methyelene groups is due to an increase in lipid solubility leading to better membrane permeability. The opposite effect where an increase in the number of methylene groups leads to a decrease in activity is a result of a reduction in water solubility. This results in poor distribution of the molecule in aqueous media and the trapping of the drug in biological membrane [(1)].

As the *meta* derivative, *N*-{*meta*-(ferrocenyl)-benzoyl}-glycine-L-alanine ethyl ester **62** was the most active compound tested, the *meta* derivatives *N*-{*meta*-(ferrocenyl)-benzoyl}-glycine-L-2-aminobutyric acid ethyl ester **63**, *N*-{*meta*-(ferrocenyl)-benzoyl}-glycine-L-norvaline ethyl ester **64** and *N*-{*meta*-(ferrocenyl)-benzoyl}-glycine-L-norleucine ethyl ester **65** were subsequently tested *in vitro*, Figure 3.3. The IC_{50} values of **63, 64** and **65** versus H1299 lung cancer cells were 10.5 µM, 19.1 µM and 18.9 µM respectively (RSD = 6%, 25% and 7%). It is evident from the data that an increase in alkyl chain length, and hence the lipophilicity, also increases the IC_{50} values. The relatively large degree of error observed for **64** would suggest its true value maybe less than that of **65**, which would indicate a linear increase in IC_{50} value with respect to increasing chain length.

N-{*meta*-(ferrocenyl)-benzoyl}-β-alanine-L-alanine ethyl ester **66** and *N*-{*meta*-(ferrocenyl)-benzoyl}-γ-aminobutyric acid-L-alanine ethyl ester **70** were also tested *in vitro* in order to compare the effect of an increase in the number of methylene groups in the first amino acid of the dipeptide. It is clear that increasing the number of methylene groups in the first amino acid residue has a different effect on activity compared to increasing the length of the alkyl chain of the second amino acid residue, Figure 3.4. Compound **66** and **70** have IC_{50} values of 9.8 µM and 4.6 µM respectively (RSD = 17% and 12%).

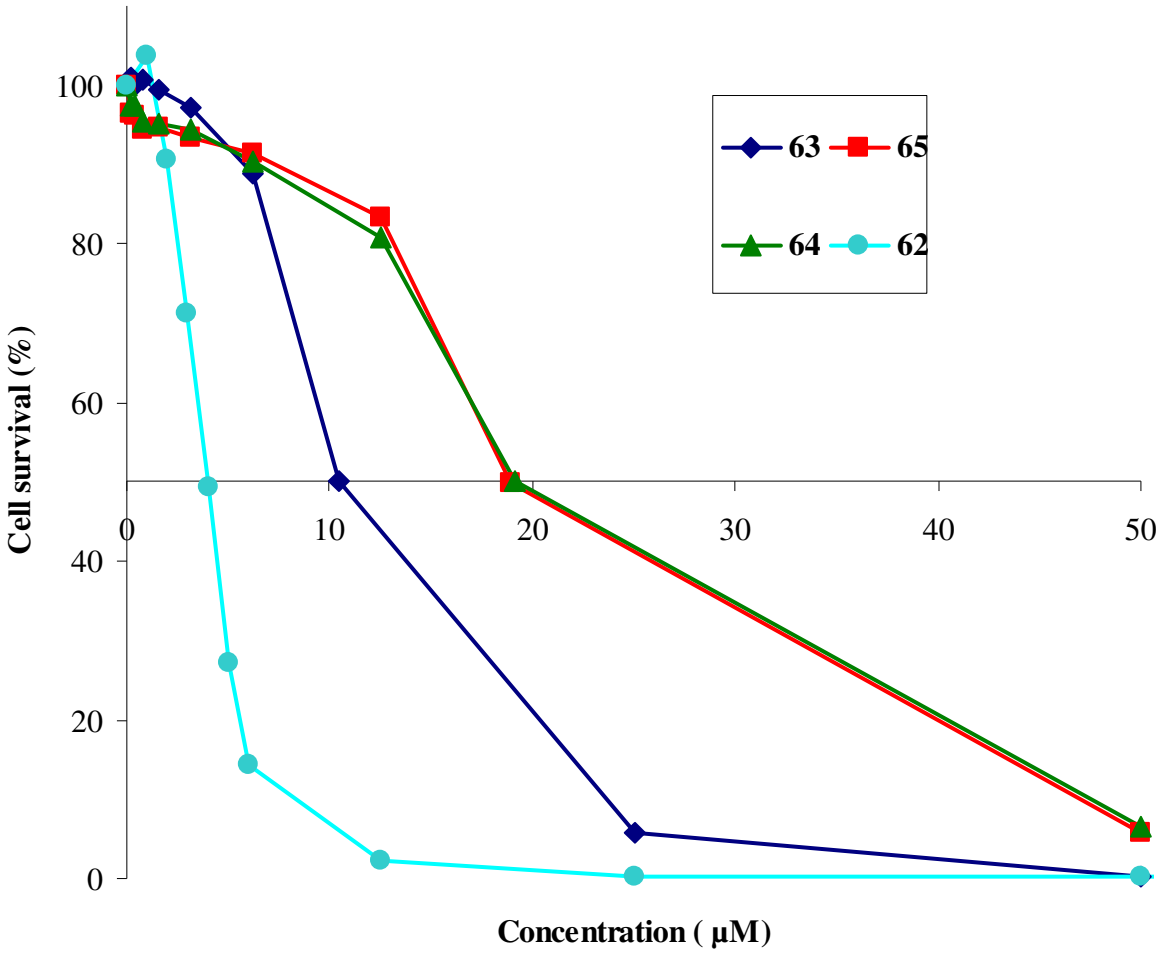

Fig. 3.3 *In vitro* anti-proliferative effect of *N*-{*meta*-(ferrocenyl)-benzoyl} dipeptide esters, **62**, **63**, **64** and **65**.

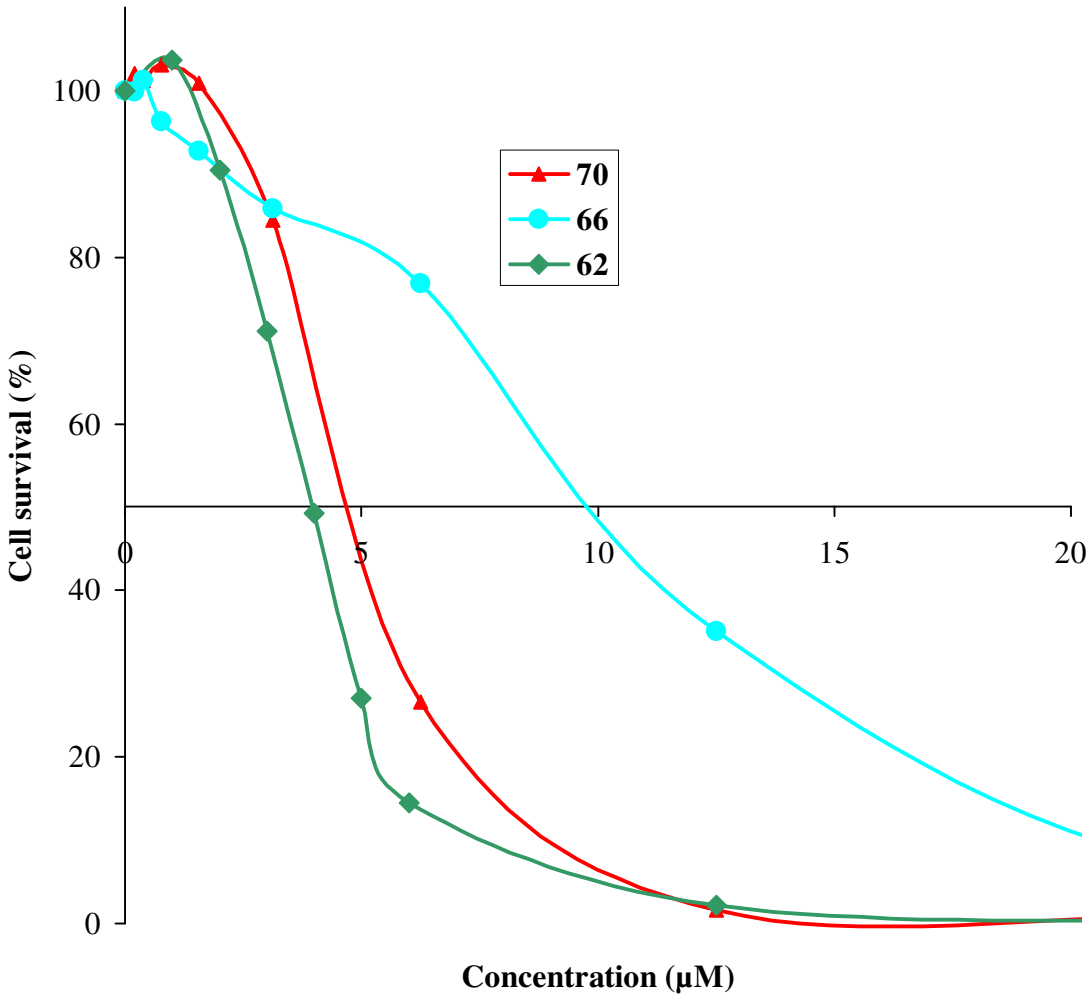

Fig. 3.4 *In vitro* anti-proliferative effect of *N*-{*meta*-(ferrocenyl)-benzoyl} dipeptide esters, **62**, **66,** and **70**.

3.5 Anti-cancer activity of 1,1'-*N*, *N*'-{*ortho*-(ferrocenyl)-bisbenzoyl}-glycine-L-alanine ethyl ester.

The anti-proliferative effect of 1,1'-*N, N'*-{*ortho*-(ferrocenyl)-bisbenzoyl}-glycine-L-alanine ethyl ester **96** was also assayed to investigate the effect of a disubstituted ferrocene group on cell proliferation. It was hoped that the inclusion of an additional aromatic moiety and dipeptide chain would improve activity. The second dipeptide chain

would allow for increased hydrogen bonding with proteins, whereas the extra aromatic group may facilitate intercalation of the compound with DNA. The ferrocene group would maintain its redox behaviour and still produce hydroxyl radicals following reaction with hydrogen peroxide.

The visible loss of activity of compound **96** (IC_{50} = 85 µM, RSD 10%) illustrated in Figure 3.5 indicates the obvious negative effect an additional benzoyl and dipeptide group have on activity. The increased size and molecular weight of compound **96** may hinder its ability to interact with target sites, while the increased polarity of the molecule resulting from an extra peptide chain may prevent it from reaching target sites.

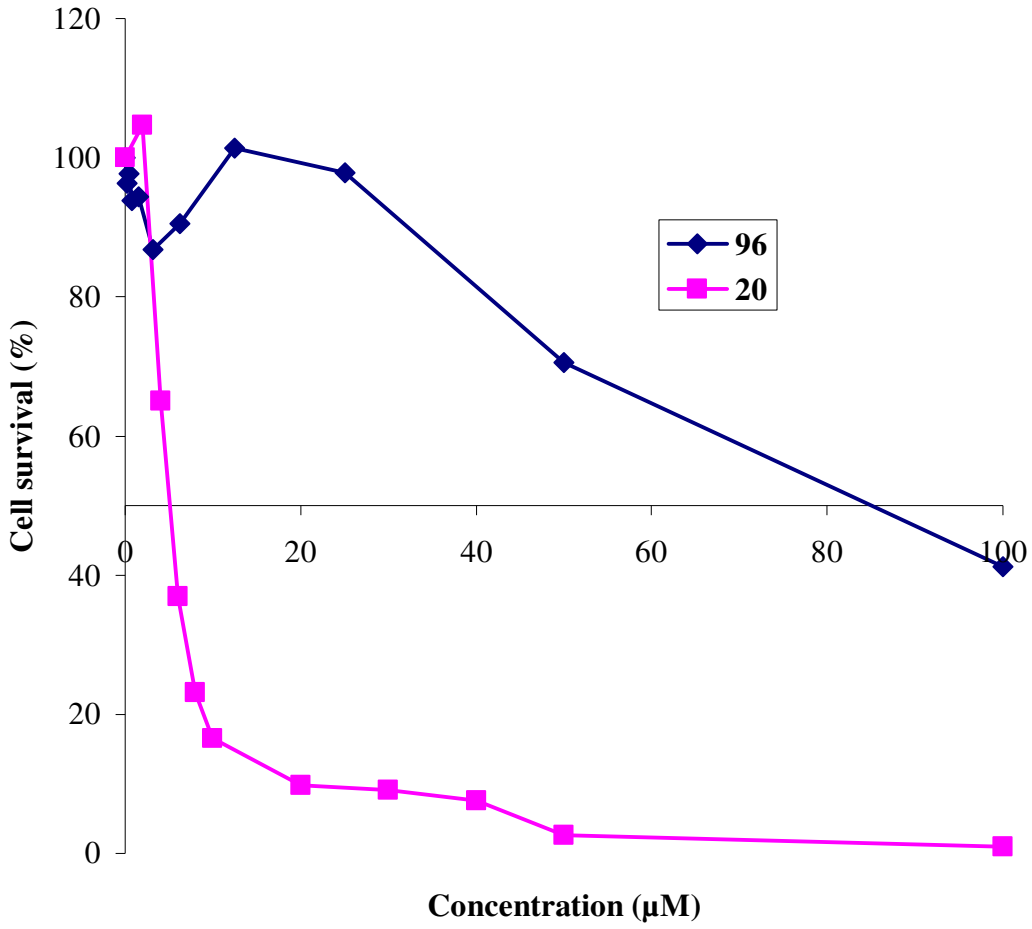

Fig. 3.5 *In vitro* anti-proliferative effect of the disubstituted derivative **96** and the monosubstituted derivative **20**.

3.6 Cell cycle analysis of *N*-{*ortho*-(ferrocenyl)-benzoyl}-glycine-L-alanine ethyl ester.

A large amount of research has been carried out *in vitro* yielding information on the growth and division of cells. The cell cycle is typically divided into synthesis (S), mitosis (M) and gap (sub G0, G1 and G2) phases. Upon reaching the boundary between the G1 and S phases the cell must decide whether to divide into two daughter cells or die, as the cell can only exist in subsequent phases for a short period. It is after this G1/S boundary that the majority of chemotherapeutic agents function by blocking progression resulting in cell death. [(12)].

Cell cycle assays were performed on a control sample and on H1299 lung cancer cells treated with *N*-{*ortho*-(ferrocenyl)-benzoyl}-glycine-L-alanine ethyl ester **20** at concentrations of 5 μM, 10 μM, 20 μM and 40 μM. Figure 3.6 illustrates the percentage of cells in each stage of the cell cycle at varying concentrations of compound **20**. As the concentration of **20** increases, the percentage of cells in the G1 phase of the cell cycle decreases, suggesting a block in the G2/M phase, preventing the cells re-entering the G1 phase. The increase in G2/M population supports this result. Figure 3.7 B shows the effect of treating the cells with **20** at 40 μM compared to a control, Figure 3.7 A. The damaged cells and debris are clearly visible in Figure 3.7 B. This suggests a novel mechanism of action for the *N*-(ferrocenyl)benzoyl dipeptide ester derivatives.

DNA content analysis on A549 and H1299 lung cancer cells confirmed that taxol induced G2/M phase arrest in the cell cycle of both cell lines. This was accompanied by a decrease in the G1 phase population [(13)]. The G2/M phase arrest is caused by taxol binding to the β-subunit of microtubulin. The resulting taxol-microtubulin complex does not have the ability to disassemble, affecting basic cellular function [(14)]. These results were similar to those observed for **20** however the results for taxol were at a much lower concentration, 2 x 10^{-3} μM to 1 μM. The taxol induced G2/M arrest is followed by apoptotic cell death *via* a number of pathways.

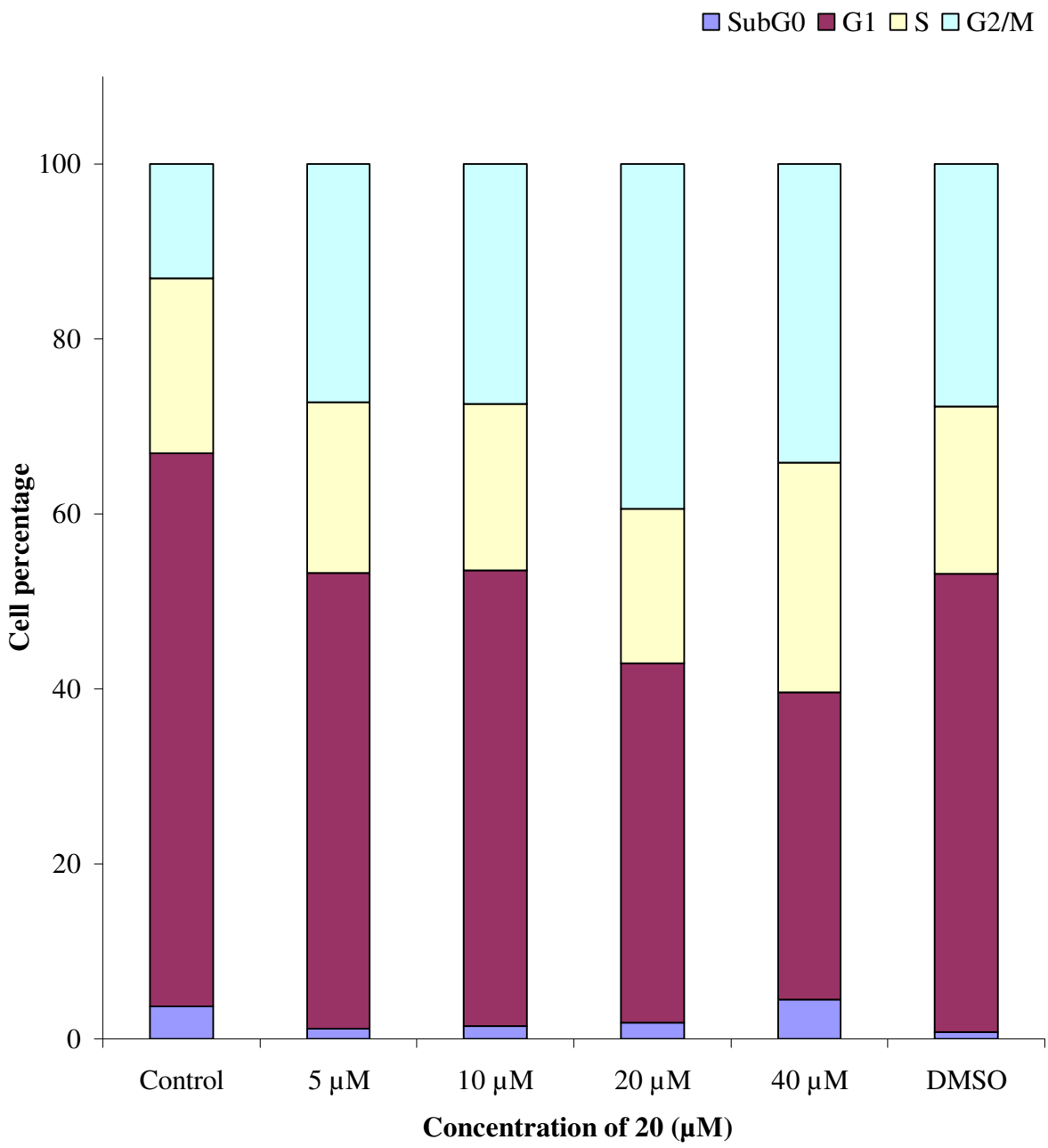

Fig. 3.6 Cell cycle analysis for compound **20** versus H1299 cancer cells.

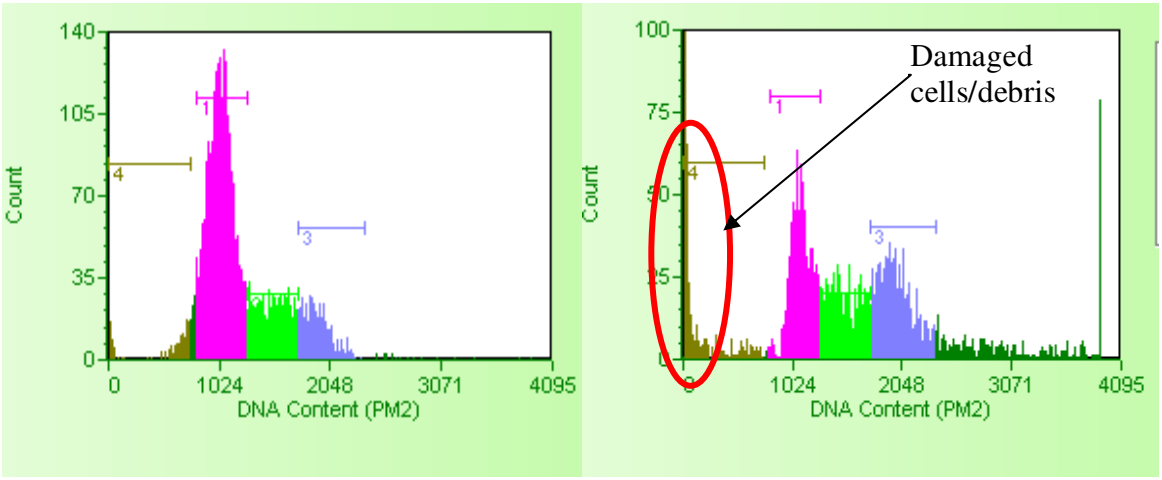

(A) (B)

Fig. 3.7 Cell cycle analysis of compound **20** at 40 µM (B) and a control sample (A) versus H1299 lung cancer cells.

3.7 Conclusions.

In summary, various *N*-(ferrocenyl)benzoyl peptide esters were tested *in vitro* to assess their anti-proliferative effect on the non-small cell lung cancer cell line H1299. Analogues of the lead compound *N*-{*ortho*-(ferrocenyl)-benzoyl}-glycine-L-alanine ethyl ester **20** were prepared with the aim of improving its biological activity.

The derivatives that were tested had various substitution patterns around the central benzoyl group. The derivatives also had varying degrees of lipophilicity and hydrophilicity with respect to the lead compound **20**. The substitution pattern was found not to be critical for activity with the *meta* and *para* derivatives of compound **20** showing comparable activity. *N*-{*meta*-(ferrocenyl)-benzoyl}-glycine-L-alanine ethyl ester **62** was the most active compound in the entire study with an IC_{50} value of 4.0 µM (± 10%). Biological activity decreased when longer peptide chains were added to the ferrocenyl benzoyl group. When additional methylene groups were added to the side chain of the second amino acid residue a loss in activity was observed. This result was not repeated when extra methylene groups were appended to the first amino acid residue of the dipeptide derivatives. The γ-aminobutyric acid derivative displayed comparable activity to the compounds with glycine as the first amino acid. The biological activity of 1,1'-*N,*

N'-{*ortho*-(ferrocenyl)-bisbenzoyl}-glycine-L-alanine ethyl ester **96** was also assayed to investigate the effect of a disubstituted ferrocene group on cell proliferation. A significant decrease in activity was observed for this compound. *N*-{*ortho*-(ferrocenyl)-benzoyl}-glycine-L-alanine ethyl ester **20** was shown to cause arrest in the G2/M phase of the cell cycle. This represents a possible mode of action for *N*-(ferrocenyl)benzoyl dipeptide esters.

References

1. Thomas, G., 'Medicinal Chemistry, An Introduction', John Wiley and Sons, **2000**.
2. Nicolaou, K. C., Montagnon, T., 'Molecules that changed the world', Weinheim, **2008**.
3. Khuri, F. R., Cohen, V., *Clin. Can. Res.*, **2004**, *10*, 4249.
4. http://www.who.int/research/en/.
5. Non-small cell lung cancer collaborative group, Chemotherapy for non-small cell lung cancer, *Cochrane Database of Systematic Reviews*, **2000**, *2*, CD002131.
6. Breen, L., Murphy, L., Keenan, J., Clynes, M., *Toxicology in vitro*, **2008**, *22*, 1234.
7. Kinnula, V. L., Crapo, J. D., *Free Rad. Bio. Med.*, **2004**, *36*, 718.
8. Wlassoff, W. A., Albright, C. D., Sivashinski, S., Ivanova, A., Appelbaum, J. G., Salganik, R. I., *J. Pharma. Pharmacol.*, **2007**, *59*, 1549.
9. Kelly, P. N., Pretre, A., Devoy, S., O'Reilly, J., Devery, R., Goel, A., Gallagher, J. F., Lough, A. J., Kenny, P. T. M., *J. Organomet. Chem.*, **2007**, *692*, 1327.
10. Savage, D. M., *'The Synthesis and Characterization of Novel N-Ferrocenyl Benzoyl Amino Acid and Dipeptide Derivatives'*, DCU, Ph.D, Thesis, **2003**.
11. Mooney, A., Corry, A. J., O'Sullivan, D., Rai, D. K., Kenny, P. T. M., *J. Organomet. Chem.* **2008**, doi:10.1016/j.organchem.2008.09.064.
12. Reddy, M. V. R., Mallireddigari, M. R., Cosenza, S. C., Palella, V. R., Iqbal, N. M., Robell, K. A., Kang, A. D., Reddy, E. P., *J. Med Chem.*, **2008**, *51*, 86.
13. Gas, G. C., Holiday, D., Gallardo, R., Haas, C., *Cancer Letters*, **2001**, *165*, 147.
14. Kumar, N., *J. Biol. Chem*., **1981**, *256*, 10435.

Experimental details

Experimental Note

All chemicals were purchased from Sigma-Aldrich and used as received. Commercial grade reagents were used without further purification. Riedel de Haën silica gel was used for flash and thin layer chromatography. Where necessary solvents were purified prior to use, dichloromethane was distilled from calcium hydride and triethylamine was distilled and stored over potassium hydroxide pellets. Melting points were determined using a Griffin melting point apparatus and are uncorrected. Infrared spectra were recorded on a Nicolet 405 FT-IR spectrometer and UV-Vis spectra on a Hewlett-Packard 8452A diode array UV-Vis spectrophotometer. NMR spectra were obtained on a Bruker AC 400 NMR spectrometer operating at 400 MHz for ^{1}H NMR and 100 MHz for ^{13}C NMR. The ^{1}H and ^{13}C NMR chemical shifts (ppm) are relative to TMS and all coupling constants (*J*) are in Hertz. Electrospray ionization mass spectra were obtained on a Micromass LCT mass spectrometer. Elemental Analysis was carried out by the Microanalytical Laboratory at University College Dublin. Cyclic voltammograms were recorded in acetonitrile (Sigma-Aldrich), with 0.1 M tetrabutylammonium perchlorate (TBAP) as a supporting electrolyte, using a CH Instruments 600a electrochemical analyzer (Pico-Amp Booster and Faraday Cage). The experiments were carried out at room temperature. A three-electrode cell consisting of a glassy carbon working-electrode, a platinum wire counter-electrode and an Ag/AgCl reference electrode was used. The E°´ values obtained for the test samples were referenced relative to the ferrocene/ferricenium redox couple.

General procedures for the synthesis of starting materials for N-(ferrocenyl)benzoyl peptide esters.

***ortho*-Ferrocenyl ethyl benzoate 37.**

Concentrated hydrochloric acid (4 mls) was added to a solution of ethyl-2-aminobenzoate (1.90 g, 11.5 mmol) in 15 mls of deionized water. Sodium nitrite (0.90 g, 13 mmol) in 15 mls of deionized water was then added to this solution with stirring at a temperature of less than 5 ^{o}C. The resulting pale yellow diazonium salt was added to ferrocene (2.14 g, 11.5 mmol) in 50 mls of diethyl ether and allowed to react for 12 hours. The reaction was washed with water and the organic layer was dried over $MgSO_4$. The solvent was removed *in vacuo*. Column chromatography {eluant 3:2 petroleum ether (40-60 ^{o}C) :diethyl ether} yielded the desired product as a red solid (1.69 g, 44%). m.p. 65-67 ^{o}C.

^{1}H NMR (400 MHz) δ (*d*$_6$-DMSO): 7.88 (1H, d, *J* = 8 Hz, ArH), 7.52 (1H, t, *J* = 6 Hz, ArH), 7.41 (1H, d, *J* = 7.6 Hz, ArH), 7.32 (1H, t, *J* = 7.6 Hz, ArH), 4.47 {2H, t, *J* = 1.6 Hz, *ortho* on (η^5-C_5H_4)}, 4.33 {2H, t, *J* = 1.6 Hz, *meta* on (η^5-C_5H_4)}, 4.17 (2H, q, *J* = 7.2 Hz, -OC*H*$_2$CH$_3$), 4.09 {5H, s, (η^5-C_5H_5)}, 1.14 (3H, t, *J* = 7.2 Hz, -OCH$_2$C*H*$_3$).

^{13}C NMR (100 MHz) δ (*d*$_6$-DMSO): 169.0, 137.4, 131.8, 131.0, 130.1, 127.8, 125.9, 85.1, 70.1, 69.5, 68.7, 60.7 (-ve DEPT), 13.8.

***ortho*-Ferrocenyl benzoic acid 38.**

ortho-Ferrocenyl ethyl benzoate (1.0 g, 3 mmol) in 15 mls of methanol was added to 15 mls of a 10% sodium hydroxide solution and refluxed for 3 hours. The solution was cooled in ice and concentrated HCl was added until pH 2 was reached. The product was isolated by filtration as an orange solid (0.51 g, 56%). m.p. 124-126 °C.

^{1}H NMR (400 MHz) δ (*d*$_6$-DMSO: 13.0 (1H, s, -COO*H*), 7.82 (1H, d, *J* = 8 Hz, ArH), 7.44 (1H, t, *J* = 8 Hz, ArH), 7.37 (1H, d, *J* = 8 Hz, ArH), 7.27 (1H, t, *J* = 8 Hz, ArH), 4.55 {2H, s, *ortho* on (η^5-C_5H_4)}, 4.32 {2H, s, *meta* on (η^5-C_5H_4)}, 4.08 {5H, s, (η^5-C_5H_5)}.

^{13}C NMR (100 MHz) δ (*d*$_6$-DMSO): 171.2, 137.0, 133.3, 131.1, 129.8, 127.9, 126.1, 85.5, 69.9, 69.1, 68.5.

***meta*-Ferrocenyl ethyl benzoate 39.**

Concentrated hydrochloric acid (4 mls) was added to a solution of ethyl-3-aminobenzoate (1.90 g, 11.5 mmol) in 15 mls of deionized water. Sodium nitrite (0.90 g, 13 mmol) in 15 mls of deionized water was then added to this solution with stirring at a temperature of less than 5 ^{o}C. The resulting pale yellow diazonium salt was added to ferrocene (2.14 g, 11.5 mmol) in 50 mls of diethyl ether and allowed to react for 12 hours. The reaction was washed with water and the organic layer was dried over $MgSO_4$. The solvent was removed *in vacuo*. Column chromatography {eluant 3:2 petroleum ether (40-60 ^{o}C) :diethyl ether} yielded the desired product as a red solid (1.81 g, 46 %). m.p. 74-76 ^{o}C.

^{1}H NMR (400 MHz) δ (*d*$_6$-DMSO): 8.03 (1H, s, ArH), 7.85 (1H, d, *J* = 8 Hz, ArH), 7.75 (1H, d, *J* = 8 Hz, ArH), 7.45 (1H, t, *J* = 8 Hz, ArH), 4.84 {2H, t, *J* = 2 Hz, *ortho* on (η^5-C_5H_4)}, 4.39 {2H, t, *J* = 2 Hz, *meta* on (η^5-C_5H_4)}, 4.34 (2H, q, *J* = 7.2 Hz, -OC*H*$_2$CH$_3$), 4.03 {5H, s, (η^5-C_5H_5)}, 1.35 (3H, t, *J* = 8 Hz, -OCH$_2$C*H*$_3$).

^{13}C NMR (100 MHz) δ (*d*$_6$-DMSO): 165.8, 139.8, 130.6, 130.0, 129.0, 128.7, 125.8, 83.4, 69.4, 69.3, 66.4, 60.7 (-ve DEPT), 14.2.

***meta*-Ferrocenyl benzoic acid 40.**

meta-Ferrocenyl ethyl benzoate (1.0 g, 3 mmol) in 15 mls of methanol was added to 15 mls of a 10% sodium hydroxide solution and refluxed for 3 hours. The solution was cooled in ice and concentrated HCl was added until pH 2 was reached. The product was isolated by filtration as an orange solid (0.58 g, 63%). m.p. 160-162 ^{o}C.

^{1}H NMR (400 MHz) δ (*d*$_6$-DMSO): 12.9 (1H, s, -COO*H*), 8.03 (1H, s, ArH), 7.85 (1H, d, *J* = 7.2 Hz, ArH), 7.77 (1H, d, *J* = 8 Hz, ArH), 7.50 (1H, t, *J* = 8 Hz, ArH), 4.83 {2H, t, *J* = 1.6 Hz, *ortho* on (η^5-C_5H_4)}, 4.39 {2H, t, *J* = 1.6 Hz, *meta* on (η^5-C_5H_4)}, 4.03 {5H, s, (η^5-C_5H_5)}.

^{13}C NMR (100 MHz) δ (*d*$_6$-DMSO): 168.2, 139.5, 131.2, 130.2, 128.7, 126.6, 126.1, 83.7, 69.4, 69.2, 66.4.

***para*-Ferrocenyl ethyl benzoate 41a.**

Concentrated hydrochloric acid (4 mls) was added to a solution of ethyl-4-aminobenzoate (1.90 g, 11.5 mmol) in 15 mls of deionized water. Sodium nitrite (0.90 g, 13 mmol) in 15 mls of deionized water was then added to this solution with stirring at a temperature of less than 5 ^{o}C. The resulting pale yellow diazonium salt was added to ferrocene (2.14 g, 11.5 mmol) in 50 mls of diethyl ether and allowed to react for 12 hours. The reaction was washed with water and the organic layer was dried over $MgSO_4$. The solvent was removed *in vacuo*. Column chromatography {eluant 3:2 petroleum ether (40-60 ^{o}C) :diethyl ether} yielded the desired product as a red solid (1.91 g, 51 %).

***para*-Ferrocenyl ethyl benzoate *via* cross coupling 41b.**

Ferroceneboronic acid (0.50 g, 2.17 mmol) was dissolved in 40 mls of dimethoxyethane. Ethyl-4-iodobenzoate (0.60 g, 2.17 mmol), {1,1′-bis-(diphenylphosphino) ferrocene}dichloropalladium(II) (0.075 g) and 5 mls of 3 M K_2CO_3 were then added. The reaction was refluxed for 72 hours. Water (30 mls) was added and the reaction was extracted with chloroform (3 x 50 mls). The combined organic layers were then washed with water (3 x 50 mls) and dried over $MgSO_4$. The solvent was removed *in vacuo*. Column chromatography {eluant 3:2 petroleum ether (40-60 ^{o}C):diethyl ether} yielded the desired product as a red solid (0.12 g, 34 %). m.p. 92-94 ^{o}C.

^{1}H NMR (400 MHz) δ (*d_6*-DMSO): 7.86 (2H, d, *J* = 6.8 Hz, ArH), 7.67 (2H, d, *J* = 6.8 Hz, ArH), 4.90 {2H, t, *J* = 2 Hz, *ortho* on (η^5-C_5H_4)}, 4.45 {2H, t, *J* = 2 Hz, *meta* on (η^5-C_5H_4)}, 4.32 (2H, q, *J* = 7.2 Hz, -OC*H_2*CH_3), 4.03 {5H, s, (η^5-C_5H_5)}, 1.33 (3H, t, *J* = 7.2 Hz, -OCH_2C*H_3*).

^{13}C NMR (100 MHz) δ (*d_6*-DMSO): 165.7, 145.1, 130.1 129.2, 125.7, 82.6, 69.8, 69.6, 66.6, 60.5 (-ve DEPT), 14.2.

***para*-Ferrocenyl benzoic acid 42.**

para-Ferrocenyl ethyl benzoate (1.0 g, 3 mmol) in 15 mls of methanol was added to 15 mls of a 10% sodium hydroxide solution and refluxed for 3 hours. The solution was cooled in ice and concentrated HCl was added until pH 2 was reached. The product was isolated by filtration as an orange solid (0.53 g, 58%). m.p. lit (decomp.) at 203 ^{o}C.

^{1}H NMR (400 MHz) δ (d_6-DMSO): 12.7 (1H, s, -COO*H*), 7.87 (2H, d, *J* = 7.2 Hz, ArH), 7.64 (2H, d, *J* = 7.2 Hz, ArH), 4.90 {2H, t, *J* = 1.6 Hz, *ortho* on (η^5-C_5H_4)}, 4.41 {2H, t, *J* = 1.6 Hz, *meta* on (η^5-C_5H_4)}, 4.04 {5H, s, (η^5-C_5H_5)}.

^{13}C NMR (100 MHz) δ (d_6-DMSO): 167.3, 144.6, 129.4, 127.8, 125.6, 82.9, 69.7, 69.5, 66.7.

Glycyl-glycyl-glycine ethyl ester hydrochloride 43.

Glycyl-glycyl-glycine (0.42 g, 2.22 mmol) was added slowly to a solution of ethanol (30 mls) and thionyl chloride (5 mls) at 0 ^{o}C. The solution was stirred at room temperature for 72 hours. Evaporation of solvent furnished the desired product as a white powder (0.51 g, 90%). m.p. (decomp.) at 200 ^{o}C.

^{1}H NMR (400 MHz) δ (d_6-DMSO): 8.96 (1H, t, *J* = 6 Hz, -CON*H*-), 8.68 (1H, t, *J* = 6 Hz, -CON*H*-), 8.46 (3H, br s, -N$H_3^+Cl^-$), 4.17 (2H, q, *J* = 7.2 Hz, -OCH_2CH$_3$), 3.90 (4H, d, *J* = 6.8 Hz, -NHCH_2CO-), 3.68, (2H, s, -NHCH_2CO-), 1.12 (3H, t, *J* = 6.8 Hz, -OCH$_2$CH_3)

^{13}C NMR (100 MHz) δ (d_6-DMSO): 169.6, 168.8, 168.3, 60.4 (-ve DEPT), 41.7 (-ve DEPT), 40.53 (-ve DEPT), 40.1 (-ve DEPT), 14.0.

Glycyl-glycyl-glycyl-glycine ethyl ester hydrochloride 44.

Glycyl-glycyl-glycyl-glycine (0.178 g, 0.72 mmol) was added slowly to a solution of ethanol (30 mls) and thionyl chloride (5 mls) at 0 ^{o}C. The solution was stirred at room temperature for 72 hours. Evaporation of solvent furnished the desired product as a white powder (0.21g, 94%). m.p. (decomp.) at 210 ^{o}C.

^{1}H NMR (400 MHz) δ (d_6-DMSO): 8.72 (1H, t, *J* = 5.6 Hz -CON*H*-), 8.37 (2H, q, *J* = 6 Hz -CON*H*-), 8.13 (3H, br s, -N$H_3^+Cl^-$), 4.09 (2H *J* = 7.2 -OCH_2CH$_3$), 3.84 (4H, t, *J* = 6 Hz, -NHCH_2CO-), 3.76 (2H, d, *J* = 6 Hz -NHCH_2CO-), 3.60 (2H, s, -NHCH_2CO-), 1.19 (3H , t, *J* = 7.2 Hz -OCH$_2$CH_3).

^{13}C NMR (100 MHz) δ (d_6-DMSO): 169.7, 169.2, 168.6, 166.3, 60.4 (-ve DEPT), 41.9 (-ve DEPT), 41.6 (-ve DEPT), 40.6 (-ve DEPT), 40.1 (-ve DEPT), 14.0.

General procedure for the synthesis of N-{ortho-(ferrocenyl)-benzoyl} dipeptide esters.

_N_-{*ortho*-(ferrocenyl)-benzoyl}-glycine-glycine ethyl ester 45.

1-Hydroxybenzotriazole (0.14 g, 1 mmol) was added to a solution of *ortho*-ferrocenyl benzoic acid (0.27 g, 0.9 mmol), *N*-(3-dimethylaminopropyl)-*N*'-ethylcarbodiimide hydrochloride (0.2 g, 1 mmol) and triethylamine (2 mls) in dichloromethane (40 mls) at 0 ^{o}C. After 30 minutes glycyl-glycine ethyl ester (0.2 g, 1 mmol) was added and the reaction was stirred at room temperature for 48 hours. The reaction mixture was washed with water, 10% potassium hydrogen carbonate and 5% citric acid. The organic layer was dried over $MgSO_4$ and the solvent was removed *in vacuo*. The product was purified by column chromatography (eluant 1:1 hexane:ethyl acetate). Recrystallization from hexane: ethyl acetate furnished the title compound as orange needles (0.198 g, 49%). m.p. 69-71 °C; $E°' = 49$ mV (vs Fc/Fc^+).

UV-Vis λ_{max} ACN: 326, 439 nm.

I.R. υ_{max} (KBr): 3397, 2983, 1737, 1657, 1650, 1524, 1379, 1202 cm^{-1}.

^{1}H NMR (400 MHz) δ (*d_6*-DMSO): 8.50 (1H, t, *J* = 6Hz, -CON*H*-), 8.20 (1H, t, *J* = 6 Hz, -CON*H*-), 7.79 (1H, d, *J* = 7.6 Hz, ArH), 7.40 (1H, t, *J* = 7.6 Hz, ArH), 7.29-7.24 (2H, m, ArH), 4.64 {2H, t, *J* = 2 Hz, *ortho* on (η^5-C_5H_4)}, 4.27 {2H, t, *J* = 2 Hz, *meta* on (η^5-C_5H_4)}, 4.22 (2H, q, *J* = 7.2 Hz, -OC*H_2*CH_3), 4.06 {5H, s, (η^5-C_5H_5)}, 3.87 (2H, d, *J* = 5.6 Hz, -NHC*H_2*CO-), 3.83 (2H, d, *J* = 5.6 Hz, -NHC*H_2*CO-), 1.28 (3H, t, *J* = 7.2 Hz, -OCH_2C*H_3*).

^{13}C NMR (100 MHz) δ (*d_6*-DMSO): 170.5, 170.1, 169.7, 136.6, 136.4, 130.4, 129.1, 127.8, 125.8, 84.8, 69.8, 69.1, 68.6, 60.9 (-ve DEPT), 42.3(-ve DEPT), 41.0(-ve DEPT), 14.4.

_N_-{*ortho*-(ferrocenyl)-benzoyl}-glycine-L-alanine methyl ester 46.

For compound **46** glycine-L-alanine methyl ester (0.15 g, 0.75 mmol) was used as a starting material. The product was purified by column chromatography (eluant 1:1 hexane:ethyl acetate) and isolated as an orange oil (0.12 g, 46%). $E°' = 47$ mV (vs Fc/Fc^+); $[\alpha]_D^{20} = -50^o$ (c 2, EtOH).

UV-Vis λ_{max} ACN: 331, 439 nm.

I.R. ν_{max} (KBr): 3550, 2916, 1771, 1650, 1560 cm^{-1}.

^{1}H NMR (400 MHz) δ (*d_6*-DMSO): 8.48 (1H, t, *J* = 6 Hz, -CON*H*-), 8.31 (1H, d, *J* = 6.8 Hz, -CON*H*-), 7.78 (1H, d, *J* = 8 Hz, ArH), 7.42-7.38 (1H, m, ArH), 7.24 (2H, d, *J* = 4.4 Hz, ArH), 4.66 {2H, s, *ortho* on (η^5-C_5H_4)}, 4.33 {1H, quint, *J* = 7.2 Hz, -C*H*(CH_3)}, 4.26 {2H, s, *meta* on (η^5-C_5H_4)}, 4.05 {5H, s, (η^5-C_5H_5)} 3.90-3.75 (2H, m, -NHC*H_2*CO-), 3.64 (3H, s, -OC*H_3*), 1.29 {3H, d, *J* = 7.2 Hz, -CH(C*H_3*)}.

^{13}C NMR (100 MHz) δ (*d_6*-DMSO): 173.0, 170.3, 168.6, 136.3, 136.1, 130.0, 128.7, 127.4, 125.4, 84.3, 69.4, 68.8, 68.2, 51.9, 47.5, 41.7 (-ve DEPT), 17.1.

***N*-{*ortho*-(ferrocenyl)-benzoyl}-glycine-L-alanine ethyl ester 20.**

For compound **20** glycine-L-alanine ethyl ester (0.13 g, 0.75 mmol) was used as a starting material. The product was purified by column chromatography (eluant 1:1 hexane:ethyl acetate) and isolated as an orange oil (0.15 g, 56%). E°´ = 50 mV (vs Fc/Fc^+); $[\alpha]_D^{20}$ = -21° (c 2, EtOH).

UV-Vis λ_{max} ACN: 324, 445 nm.

I.R. ν_{max} (KBr): 3577, 3281, 1793, 1657, 1560, 1293 cm^{-1}.

^{1}H NMR (400 MHz) δ (*d_6*-DMSO): 8.47 (1H, t, *J* = 6 Hz, -CON*H*-), 8.29 (1H, d, *J* = 6.8 Hz, -CON*H*-), 7.78 (1H, d, *J* = 7.6 Hz, ArH), 7.42-7.37 (1H, m, ArH), 7.23 (2H, d, *J* = 4 Hz, ArH), 4.66-4.64 {2H, m, *ortho* on (η^5-C_5H_4)}, 4.32-4.25 {3H, m, *meta* on (η^5-C_5H_4), -C*H*(CH_3)}, 4.10 (2H, q, *J* = 6.8 Hz, -OC*H_2*CH_3), 4.04 {5H, s, (η^5-C_5H_5)}, 3.89-3.75 (2H, m, -NHC*H_2*CO-), 1.28 {3H, d, *J* = 7.2 Hz, -CH(C*H_3*)}, 1.19 (3H, t, *J* = 7.2 Hz, -OCH_2C*H_3*).

^{13}C NMR (100 MHz) δ (*d_6*-DMSO): 172.5, 170.0, 168.6, 138.2, 136.2, 130.0, 128.7, 127.4, 125.4, 84.3, 69.4, 68.8, 68.2, 60.5 (-ve DEPT), 47.6, 41.7 (-ve DEPT), 17.1, 14.0.

***N*-{*ortho*-(ferrocenyl)-benzoyl}-glycine-L-alanine propyl ester 47.**

For compound **47** glycine-L-alanine propyl ester (0.21 g, 0.95 mmol) was used as a starting material. The product was purified by column chromatography (eluant 1:1 hexane:ethyl acetate) and isolated as an orange oil (0.14 g, 36%). E°´ = 48 mV (vs Fc/Fc^+); $[\alpha]_D^{20}$ = -39° (c 2, EtOH).

UV-Vis λ_{max} ACN: 331, 442 nm.

I.R. ν_{max} (KBr): 3560, 2920, 1789, 1661, 1556 cm^{-1}.

^{1}H NMR (400 MHz) δ (*d_6*-DMSO): 8.77 (1H, t, *J* = 5.6 Hz, -CON*H*-), 8.29 (1H, d, *J* = 6.8 Hz, -CON*H*-), 7.78 (1H, d, *J* = 7.6 Hz, ArH), 7.42-7.38 (1H, m, ArH), 7.23 (2H, d, *J* = 4.4 Hz, ArH), 4.65 {2H, s, *ortho* on (η^5-C_5H_4)}, 4.32-4.26 {3H, m, *meta* on (η^5-C_5H_4), -C*H*(CH_3)}, 4.05-4.01 {7H, m, (η^5-C_5H_5), -OC*H*$_2$$CH_2CH_3$}, 3.89-3.75 (2H, m, -NHC*H*$_2$CO-), 1.61 (2H, sx, *J* = 7.2 Hz, -OCH_2C*H*$_2$$CH_3$), 1.29 {3H, d, *J* = 7.2 Hz, -CH(C*H*$_3$)}, 0.89 (3H, t, *J* = 7.2 Hz, -OCH_2CH_2C*H*$_3$).

^{13}C NMR (100 MHz) δ (*d_6*-DMSO): 172.6, 169.9, 168.6, 136.2, 136.1, 130.0, 128.9, 127.4, 125.4, 84.3, 69.4, 68.7, 68.2, 65.9 (-ve DEPT), 47.7, 41.7 (-ve DEPT), 21.5 (-ve DEPT), 17.1, 10.2.

***N*-{*ortho*-(ferrocenyl)-benzoyl}-glycine-L-2-aminobutyric acid ethyl ester 48.**

For compound **48** glycine-L-2-aminobutyric acid ethyl ester (0.14 g, 0.75 mmol) was used as a starting material. The product was purified by column chromatography (eluant 1:1 hexane:ethyl acetate) and isolated as an orange oil (0.07 g, 25%). E°´ = 38 mV (vs Fc/Fc^+); $[\alpha]_D^{20}$ = +4° (c 2, MeOH).

UV-Vis λ_{max} ACN: 330, 440 nm.

I.R. ν_{max} (KBr): 3568, 2927, 1793, 1654, 1560, 1420, 1120 cm^{-1}.

^{1}H NMR (400 MHz) δ (*d_6*-DMSO): 8.47 (1H, t, *J* = 6 Hz, -CON*H*-), 8.22 (1H, d, *J* = 7.2 Hz, -CON*H*-), 7.80 (1H, d, *J* = 8 Hz, ArH), 7.42-7.37 (1H, m, ArH), 7.24 (2H, d, *J* = 4 Hz, ArH), 4.66 {2H, s, *ortho* on (η^5-C_5H_4)}, 4.26-4.19 {3H, m, *meta* on (η^5-C_5H_4), -C*H*(C_2H_5)}, 4.15-4.07 (2H, m, -OC*H*$_2$$CH_3$), 4.04 {5H, s, ($\eta^5$-$C_5H_5$)}, 3.92-3.78 (2H, m, -NHC*H*$_2$CO-), 1.79-1.60 {2H, m, -CH(C*H*$_2$$CH_3$)}, 1.20 (3H, t, *J* = 7.2 Hz, -OCH_2C*H*$_3$), 0.89 {3H, t, *J* = 7.2 Hz, -CH(CH_2C*H*$_3$)}.

^{13}C NMR (100 MHz) δ (*d_6*-DMSO): 171.9, 169.9, 168.9, 136.3, 136.0, 130.0, 128.7, 127.4, 125.4, 84.3, 69.4, 68.7, 68.2, 60.4 (-ve DEPT), 53.3, 41.8 (-ve DEPT), 24.5 (-ve DEPT), 14.1, 10.1.

Analysis: found: C, 62.60; H, 5.95; N, 5.80,

$C_{25}H_{28}FeN_2O_4$ requires: C, 63.04; H, 5.92; N, 5.88.

Mass spectrum: found: $[M]^{+\bullet}$ 476.1413,

$C_{25}H_{28}FeN_2O_4$ requires: 476.1398.

***N*-{*ortho*-(ferrocenyl)-benzoyl}-glycine-L-norvaline ethyl ester 49.**

For compound **49** glycine-L-norvaline ethyl ester (0.15 g, 0.75 mmol) was used as a starting material. The product was purified by column chromatography (eluant 1:1 hexane:ethyl acetate) and isolated as an orange oil (0.09 g, 31%). E°´ = 43 mV (vs Fc/Fc^+); $[\alpha]_D^{20} = +19^o$ (c 2, MeOH).

UV-Vis λ_{max} ACN: 329, 445 nm.

I.R. ν_{max} (KBr): 3569, 3423, 2963, 1735, 1560, 1261, 1105 cm^{-1}.

^1H NMR (400 MHz) δ (d_6-DMSO): 8.46 (1H, t, *J* = 6 Hz, -CON*H*-), 8.20 (1H, d, *J* = 7.6 Hz, -CON*H*-), 7.80 (1H, d, *J* = 7.6 Hz, ArH), 7.40-7.37 (1H, m, ArH), 7.24 (2H, d, *J* = 4 Hz, ArH), 4.66-4.64 {2H, m, *ortho* on (η^5-C_5H_4)}, 4.27-4.20 {3H, m, *meta* on (η^5-C_5H_4), -C*H*(C_3H_7)}, 4.14-4.06 (2H, m, -OC*H*$_2$$CH_3$), 4.02 {5H, s, ($\eta^5$-$C_5H_5$)}, 3.91- 3.77 (2H, m, -NHC*H*$_2$CO-), 1.72-1.55 {4H, m, -CH(C*H*$_2$C*H*$_2$$CH_3$)}, 1.21 (3H, t, *J* = 6.8 Hz, -OCH_2C*H*$_3$), 0.90 {3H, t, *J* = 7.2 Hz, -CH(CH_2CH_2C*H*$_3$)}.

^{13}C NMR (100 MHz) δ (d_6-DMSO): 172.1, 170.0, 168.8, 136.0, 130.0, 129.9, 128.7, 127.4, 125.4, 84.3, 69.4, 68.7, 68.2, 60.4 (-ve DEPT), 51.7, 41.8 (-ve DEPT), 33.2 (-ve DEPT), 18.5 (-ve DEPT), 14.1, 13.5.

Analysis: found: C, 64.16; H, 6.35; N, 5.80,

$C_{26}H_{30}FeN_2O_4$ requires: C, 63.68; H, 6.17; N, 5.71.

Mass spectrum: found: $[M]^{+\bullet}$ 490.1575,

$C_{26}H_{30}FeN_2O_4$ requires: 490.1555.

***N*-{*ortho*-(ferrocenyl)-benzoyl}-glycine-L-norleucine ethyl ester 50.**

For compound **50** glycine-L-norleucine ethyl ester (0.16 g, 0.75 mmol) was used as a starting material. The product was purified by column chromatography (eluant 1:1 hexane:ethyl acetate) and isolated as an orange oil (0.10 g, 34%). E°´ = 38 mV (vs Fc/Fc^+); $[\alpha]_D^{20} = +14^o$ (c 2, MeOH).

UV-Vis λ_{max} ACN: 329, 440 nm.

I.R. ν_{max} (KBr): 3314, 2961, 1840, 1735, 1560 1261, 1105 cm^{-1}.

^{1}H NMR (400 MHz) δ (d_6-DMSO): 8.46 (1H, t, *J* = 6 Hz, -CON*H*-), 8.20 (1H, d, *J* = 7.6 Hz, -CON*H*-), 7.80 (1H, d, *J* = 7.6 Hz, ArH), 7.42-7.37 (1H, m, ArH), 7.24 (2H, d, *J* = 4 Hz, ArH), 4.65 {2H, q, *J* = 1.6 Hz, *ortho* on (η^5-C_5H_4)}, 4.28-4.23 {3H, m, *meta* on (η^5-C_5H_4), -C*H*(C_4H_9)}, 4.13-4.06 (2H, m, -OC$H_2$$CH_3$), 4.06 {5H, s, ($\eta^5$-$C_5H_5$)}, 3.91-3.77 (2H, m, -NHCH_2CO-), 1.73-1.58 {2H, m, -CH(C$H_2$$CH_2CH_2CH_3$)}, 1.32-1.25 {4H, m, -CH(CH_2CH_2C$H_2$$CH_3$)}, 1.20 (3H, t, *J* = 6.8 Hz, -OCH_2CH_3), 0.87 {3H, t, *J* = 7.6 Hz -CH($CH_2CH_2CH_2$CH_3}.

^{13}C NMR (100 MHz) δ (d_6-DMSO): 172.1, 169.9, 168.9, 136.2, 136.1, 130.0, 128.7, 127.4, 125.4, 84.3, 69.4, 68.7, 68.2, 60.4 (-ve DEPT), 51.9, 41.8 (-ve DEPT), 30.8 (-ve DEPT), 27.3 (-ve DEPT), 21.7 (-ve DEPT) 14.1 13.7.

Analysis:	found:	C, 63.81; H, 6.45; N, 5.32,
$C_{26}H_{30}FeN_2O_4$	requires:	C, 64.29; H, 6.39; N, 5.55.
Mass spectrum:	found: $[M]^{+\bullet}$	504.1702,
$C_{27}H_{32}FeN_2O_4$	requires:	504.1711.

***N*-{*ortho*-(ferrocenyl)-benzoyl}-glycine-L-leucine ethyl ester 51.**

For compound **51** glycine-L-leucine ethyl ester hydrochloride (0.25 g, 1 mmol) was used as a starting material. The product was purified by column chromatography (eluant 1:1 hexane:ethyl acetate) and isolated as an orange oil (0.19 g, 67%). E°´ = 40 mV (vs Fc/Fc^+); $[\alpha]_D^{20}$ = -47° (c 2, EtOH).

^{1}H NMR (400 MHz) δ (d_6-DMSO): 8.47 (1H, t, *J* = 6 Hz, -CON*H*-), 8.24 (1H, d, *J* = 8 Hz, -CON*H*-), 7.78 (1H, d, *J* = 7.6 Hz, ArH), 7.42-7.37 (1H, m, ArH), 7.23 (2H, d, *J* = 4 Hz, ArH), 4.66-4.64 {2H, m, *ortho* on (η^5-C_5H_4)}, 4.35-4.26 {1H, m, -C*H*($CH_2CH(CH_3)_2$)}, 4.25 {2H, t, *J* = 2 Hz, *meta* on (η^5-C_5H_4)}, 4.11 (2H, q, *J* = 7.2 Hz, -OC$H_2$$CH_3$), 4.05 {5H, s, ($\eta^5$-$C_5H_5$)}, 3.90-3.77 (2H, m, -NHCH_2CO-), 1.63-1.46 {3H, m, -CH(CH_2C*H*(CH_3)$_2$)}, 1.20 (3H, t, *J* = 6.8 Hz, -OCH_2CH_3), 0.90 {3H, d, *J* = 6.4 Hz, -CH_2CH(CH_3)$_2$}, 0.86 {3H, d, *J* = 6.4 Hz, -CH_2CH(CH_3)$_2$}.

^{13}C NMR (100 MHz) δ (d_6-DMSO): 172.3, 169.9, 168.9, 136.3, 136.0, 130.0, 128.7, 127.4, 125.4, 84.3, 69.4, 68.7, 68.2, 60.5 (-ve DEPT), 50.3, 41.7 (-ve DEPT), 39.7 (-ve DEPT), 24.1, 22.7, 21.4, 14.0.

***N*-{*ortho*-(ferrocenyl)-benzoyl}-glycine-L-phenylalanine ethyl ester 52.**

For compound **52** glycine-L-phenylalanine ethyl ester hydrochloride (0.2 g, 0.7 mmol) was used as a starting material. The product was purified by column chromatography (eluant 1:1 hexane:ethyl acetate) and isolated as an orange solid (0.11 g, 28%). m.p. 51-53 °C; E°′ = 51 mV (vs Fc/Fc^+); $[\alpha]_D^{20}$= +2° (c 2.1, EtOH).

UV-Vis λ_{max} ACN: 323, 440 nm.

I.R. υ_{max} (KBr): 3331, 2933, 1735, 1654, 1648, 1523, 1376, 1216 cm^{-1}.

^{1}H NMR (400 MHz) δ (d_6-DMSO): 8.45 (1H, t, *J* = 6 Hz, -CON*H*-), 8.34 (1H, d, *J* = 7.6 Hz, -CON*H*-), 7.77 (1H, d, *J* = 8 Hz, ArH), 7.40 (1H, t, *J* = 8 Hz, ArH), 7.31-7.18 (7H, m, ArH), 4.65 {2H, s, *ortho* on (η^5-C_5H_4)}, 4.52-4.46 {1H, m, *J* = 6.4 Hz, -C*H*(CH_2Ph)}, 4.25 {2H, s, *meta* on (η^5-C_5H_4)}, 4.08-4.02 {7H, m, (η^5-C_5H_5), -O$CH_2$$CH_3$}, 3.80 (2H, t, *J* = 5.2 Hz, -NHCH_2CO-), 3.04-2.92 {2H, m, -CH(CH_2Ph)}, 1.11 (3H, t, *J* = 7.2 Hz, -OCH_2CH_3).

^{13}C NMR (100 MHz) δ (d_6-DMSO): 171.7, 170.3, 169.2, 137.3, 136.6, 136.4, 130.7, 129.5, 129.1, 128.6, 127.7, 127.0, 125.7, 84.3, 69.4, 68.7, 68.2, 60.9 (-ve DEPT), 54.1, 42.2 (-ve DEPT), 37.3 (-ve DEPT), 14.3.

***N*-{*ortho*-(ferrocenyl)-benzoyl}-L-alanine-glycine ethyl ester 53.**

For compound **53** L-alanine-glycine ethyl ester hydrochloride (0.2 g, 1.0 mmol) was used as a starting material. The product was purified by column chromatography (eluant 1:1 hexane:ethyl acetate). Recrystallization from hexane:ethyl acetate furnished the title compound as orange needles (0.181 g, 39%). m.p 55-57 °C; E°′ = 49 mV (vs Fc/Fc^+); $[\alpha]_D^{20}$= +0.3° (c 2.05, EtOH).

UV-Vis λ_{max} ACN: 321, 441 nm.

I.R. υ_{max} (KBr): 3326, 2933, 1752, 1655, 1638, 1509, 1200 cm^{-1}.

^{1}H NMR (400 MHz) δ (d_6-DMSO): 8.35 (1H, d, *J* = 7.2 Hz, -CON*H*-), 8.18 (1H, t, *J* = 7.2 Hz, -CON*H*-), 7.80 (1H, d, *J* = 8 Hz, ArH), 7.41 (1H, t, *J* = 8 Hz, ArH), 7.26-7.24 (2H, m, ArH), 4.59-4.57 {2H, m, *ortho* on (η^5-C_5H_4)}, 4.41 {1H, quint, *J* = 7.6 Hz, -C*H*(CH_3)}, 4.29-4.25 {2H, m, *meta* on (η^5-C_5H_4)}, 4.13-4.01 {7H, m, -OC*H*$_2$$CH_3$, ($\eta^5$-$C_5H_5$)}, 3.93-3.78 (2H, m, -NHC*H*$_2$CO-), 1.25 {3H, d, *J* = 7.6 Hz, -CH(C*H*$_3$)}, 1.17 (3H, t, *J* = 7.2 Hz, -OCH$_2$C*H*$_3$)

^{13}C NMR (100 MHz) δ (d_6-DMSO):173.0, 170.1, 169.7, 136.6, 136.5, 130.5, 129.0, 127.8, 125.8, 84.6, 69.4, 69.1, 68.4, 60.8 (-ve DEPT), 48.7, 41.1 (-ve DEPT), 18.0, 14.4.

***N*-{*ortho*-(ferrocenyl)-benzoyl}-β-alanine-L-alanine ethyl ester 54.**

For compound **54** β-alanine-L-alanine ethyl ester (0.26 g, 0.95 mmol) was used as a starting material. The product was purified by column chromatography (eluant 1:1 hexane:ethyl acetate) and isolated as an orange solid (0.14 g, 36%). m.p. 99-101 ^{o}C; E$^{o\prime}$ = 33 mV (vs Fc/Fc$^+$); $[\alpha]_D^{20}$ = -21^o (c 2, EtOH).

UV-Vis λ_{max} ACN: 328, 445 nm.

I.R. ν_{max} (KBr): 3276, 3081, 2346, 1736, 1542, 1449, 1307, 1195, 1048, 822 cm^{-1}.

^{1}H NMR (400 MHz) δ (d_6-DMSO): 8.42 (1H, d, *J* = 6.8 Hz, -CON*H*-), 8.23 (1H, t, *J* = 5.6 Hz, -CON*H*-), 7.84 (1H, d, *J* = 8 Hz, ArH), 7.45 (1H, t, *J* = 8 Hz, ArH), 7.29 (1H, t, *J* = 7.6 Hz, ArH), 7.21 (1H, d, *J* = 6.8 Hz, ArH), 4.68 {2H, s, *ortho* on (η^5-C_5H_4)}, 4.36 {2H, t, *J* = 1.6 Hz, *meta* on (η^5-C_5H_4)}, 4.27 {1H, quint, *J* = 7.2 Hz, -C*H*(CH_3)}, 4.18-4.08 {7H, m, (η^5-C_5H_5), -OC*H*$_2$$CH_3$}, 3.34-3.32 (2H, m, -NHC*H*$_2$CH$_2$CO-), 2.40 (2H, t, *J* = 6.8 Hz, -NHCH$_2$C*H*$_2$CO-), 1.32 {3H, d, *J* = 7.2 Hz, -CH(C*H*$_3$)}, 1.24 (3H, t, *J* = 7.6 Hz, -OCH$_2$C*H*$_3$).

^{13}C NMR (100 MHz) δ (d_6-DMSO): 172.7, 170.2, 170.0, 136.7, 135.8, 129.9, 128.5, 127.1, 125.4, 84.4, 69.4, 68.6, 68.2, 60.3 (-ve DEPT), 47.6, 35.6 (-ve DEPT), 34.5 (-ve DEPT), 16.9, 14.0.

***N*-{*ortho*-(ferrocenyl)-benzoyl}-β-alanine-L-2-aminobutyric acid ethyl ester 55.**

For compound **55** β-alanine-L-2-aminobutyric acid ethyl ester (0.32 g, 1.3 mmol) was used as a starting material. The product was purified by column chromatography (eluant

1:1 hexane:ethyl acetate), and isolated as an orange solid (0.20 g, 50%). m.p. 132-134 ^{o}C; E$^{o\prime}$ = 52 mV (vs Fc/Fc^{+}); $[\alpha]_D^{20}$ = -20^{o} (c 2, EtOH).

UV-Vis λ_{max} ACN: 326, 445 nm.

I.R. ν_{max} (KBr): 3255, 3082, 2346, 1741, 1542, 1432, 1311, 1206, 1151, 1074, 891 cm^{-1}.

^{1}H NMR (400 MHz) δ (*d*$_6$-DMSO): 8.28 (1H, d, *J* = 7.6 Hz, -CON*H*-), 8.15 (1H, t, *J* = 5.6 Hz, -CON*H*-), 7.78 (1H, d, *J* = 7.2 Hz, ArH), 7.37 (1H, t, *J* = 7.6 Hz, ArH), 7.22 (1H, t, *J* = 7.6 Hz, ArH), 7.14 (1H, d, *J* = 7.6 Hz, ArH), 4.64 {2H, t, *J* = 1.2 Hz, *ortho* on (η^5-C_5H_4)}, 4.36 {2H, t, *J* = 1.6 Hz, *meta* on (η^5-C_5H_4)}, 4.14-4.02 {8H, m, (η^5-C_5H_5), -OC*H*$_2$CH$_3$, -C*H*(C_2H_5)}, 3.38-3.35 (2H, m, -NHC*H*$_2$CH$_2$CO-), 2.43 (2H, t, *J* = 7.6 Hz, -NHCH$_2$C*H*$_2$CO-), 1.80-1.63 {2H, m, -CH(C*H*$_2$CH$_3$)}, 1.25 (3H, t, *J* = 6.8 Hz, -OCH$_2$C*H*$_3$), 0.96 {3H, t, *J* = 7.6 Hz, -CH(CH$_2$C*H*$_3$)}.

^{13}C NMR (100 MHz) δ (*d*$_6$-DMSO): 172.1, 170.5, 169.7, 136.7, 135.8, 129.9, 128.5, 127.1, 125.4, 84.4, 69.4, 68.6, 68.2, 60.3 (-ve DEPT), 53.4, 35.7 (-ve DEPT), 34.5 (-ve DEPT), 24.2 (-ve DEPT), 14.1, 10.3.

***N*-{*ortho*-(ferrocenyl)-benzoyl}-β-alanine-L-norvaline ethyl ester 56.**

For compound **56** β-alanine-L-norvaline ethyl ester (0.33 g, 1.3 mmol) was used as a starting material. The product was purified by column chromatography (eluant 1:1 hexane:ethyl acetate) and isolated as an orange solid (0.21 g, 51%). m.p. 116-118 ^{o}C; E$^{o\prime}$ = 49 mV (vs Fc/Fc^{+}); $[\alpha]_D^{20}$ = -16^{o} (c 2, EtOH).

UV-Vis λ_{max} ACN: 326, 445 nm.

I.R. ν_{max} (KBr): 3260, 3083, 2876, 1743, 1663, 1542, 1389, 1310, 1268, 1196, 1069 cm^{-1}.

^{1}H NMR (400 MHz) δ (*d*$_6$-DMSO): 8.28 (1H, d, *J* = 7.2 Hz, -CON*H*-), 8.15 (1H, t, *J* = 5.6 Hz, -CON*H*-), 7.80 (1H, d, *J* = 7.2 Hz, ArH), 7.38 (1H, t, *J* = 7.4 Hz, ArH), 7.22 (1H, t, *J* = 6.6 Hz, ArH), 7.14 (1H, d, *J* = 7.6 Hz, ArH), 4.57 {2H, t, *J* = 1.6 Hz, *ortho* on (η^5-C_5H_4)}, 4.29 {2H, t, *J* = 1.6 Hz, *meta* on (η^5-C_5H_4)}, 4.22-4.17 {1H, m, -C*H*(C_3H_7)}, 4.12-4.06 {7H, m, (η^5-C_5H_5), -OC*H*$_2$CH$_3$}, 3.31-3.29 (2H, m, -NHC*H*$_2$CH$_2$CO-), 2.36 (2H, t, *J* = 7.6 Hz, -NHCH$_2$C*H*$_2$CO-), 1.67-1.53 {2H, m, -CH(C*H*$_2$CH$_2$CH$_3$)}, 1.38-1.28 {2H, m, -CH(CH$_2$C*H*$_2$CH$_3$)}, 1.18 (3H, t, *J* = 7.2 Hz, -OCH$_2$C*H*$_3$), 0.87 {3H, t, *J* = 7.2 Hz, -CH(CH$_2$CH$_2$C*H*$_3$)}.

^{13}C NMR (100 MHz) δ (d_6-DMSO): 172.3, 170.5, 169.7, 136.7, 135.8, 129.9, 128.5, 127.1, 125.4, 84.4, 69.4, 68.6, 68.2, 60.3 (-ve DEPT), 51.7, 35.7 (-ve DEPT), 34.5 (-ve DEPT), 32.9 (-ve DEPT), 18.6 (-ve DEPT), 14.1, 13.5.

***N*-{*ortho*-(ferrocenyl)-benzoyl}-β-alanine-L-norleucine ethyl ester 57.**

For compound **57** β-alanine-L-norleucine ethyl ester (0.33 g, 1.2 mmol) was used as a starting material. The product was purified by column chromatography (eluant 1:1 hexane:ethyl acetate) and isolated as an orange solid (0.21 g, 49%). m.p. 93-95 ^{o}C; E$^{o\prime}$ = 51 mV (vs Fc/Fc^{+}); $[\alpha]_D^{20}$ = -51^{o} (c 2, EtOH).

UV-Vis λ_{max} ACN: 329, 445 nm.

I.R. ν_{max} (KBr): 3270, 2930, 2346, 1794, 1654, 1459, 1376, 1192, 1026 cm^{-1}.

^{1}H NMR (400 MHz) δ (d_6-DMSO): 8.27 (1H, d, *J* = 7.2 Hz, -CON*H*-), 8.14 (1H, t, *J* = 5.6 Hz, -CON*H*-), 7.77 (1H, d, *J* = 7.2 Hz, ArH), 7.38 (1H, t, *J* = 7.8 Hz, ArH), 7.22 (1H, t, *J* = 7.4 Hz, ArH), 7.14 (1H, d, *J* = 7.6 Hz, ArH), 4.57 {2H, t, *J* = 1.6 Hz, *ortho* on (η^5-C_5H_4)}, 4.29 {2H, t, *J* = 1.6 Hz, *meta* on (η^5-C_5H_4)}, 4.20-4.15 {1H, m, -C*H*(C_4H_9)}, 4.12-4.08 {7H, m, (η^5-C_5H_5), -OC$H_2$$CH_3$}, 3.32-3.29 (2H, m, -NHC$H_2$$CH_2$CO-), 2.36 (2H, t, *J* = 7.6 Hz, -NHCH_2CH_2CO-), 1.69-1.56 {2H, m, -CH(C$H_2$$CH_2$$CH_2$$CH_3$)}, 1.32-1.24 {4H, m, -CH(CH_2CH_2C$H_2$$CH_3$)}, 1.18 (3H, t, *J* = 6.8 Hz, -OCH_2CH_3), 0.86 {3H, t, *J* = 7.2 Hz, -CH($CH_2$$CH_2$$CH_2CH_3$)}.

^{13}C NMR (100 MHz) δ (d_6-DMSO): 172.2, 170.4, 169.6, 136.6, 135.7, 129.8, 128.4, 127.0, 125.3, 84.4, 69.3, 68.5, 68.1, 60.2 (-ve DEPT), 51.9, 35.7 (-ve DEPT), 34.5 (-ve DEPT), 30.5 (-ve DEPT), 27.5 (-ve DEPT), 21.7 (-ve DEPT), 14.1, 13.7.

***N*-{*ortho*-(ferrocenyl)-benzoyl}-γ-aminobutyric acid-L-alanine ethyl ester 58.**

For compound **58** γ-aminobutyric acid-L-alanine ethyl ester (0.19 g, 0.95 mmol) was used as a starting material. The product was purified by column chromatography (eluant 1:1 hexane:ethyl acetate) and isolated as an orange oil (0.13g, 32%). E$^{o\prime}$ = 46 mV (vs Fc/Fc^{+}); $[\alpha]_D^{20}$ = -41^{o} (c 2, EtOH).

UV-Vis λ_{max} ACN: 327, 445 nm.

I.R. ν_{max} (KBr): 3284, 3081, 2935, 1548, 1458, 1376, 1304, 1266, 1157, 1005, 890 cm^{-1}.

^{1}H NMR (400 MHz) δ (d_6-DMSO): 8.22 (1H, d, *J* = 7.2 Hz, -CON*H*-), 8.16 (1H, t, *J* = 5.6 Hz, -CON*H*-), 7.80 (1H, d, *J* = 8 Hz, -ArH), 7.39 (1H, t, *J* = 7.2 Hz, ArH), 7.23 (1H, t, *J* = 7.2 Hz, ArH), 7.17 (1H, d, *J* = 7.6 Hz, ArH), 4.58 {2H, t, *J* = 2 Hz, *ortho* on (η^5-C_5H_4)}, 4.28 {2H, t, *J* = 2 Hz, *meta* on (η^5-C_5H_4)}, 4.22 {1H, quint, *J* = 7.6 Hz, -C*H*(CH_3)}, 4.10-4.02 {7H, m, (η^5-C_5H_5), -OC*H*$_2$$CH_3$}, 3.14 (2H, q, *J* = 6.8 Hz, -NHC*H*$_2$$CH_2CH_2CO$-), 2.11 (2H, t, *J* = 7.2 Hz, -$NHCH_2CH_2C$*H*$_2$CO-), 1.66 (2H, quint, *J* = 7.2 Hz, -$NHCH_2C$*H*$_2$$CH_2CO$-), 1.25 {3H, d, *J* = 7.2 Hz, -CH(C*H*$_3$)}, 1.18 (3H, t, *J* = 7.2 Hz, -OCH_2C*H*$_3$).

^{13}C NMR (100 MHz) δ (d_6-DMSO): 172.7, 171.8, 169.7, 137.0, 135.7, 129.9, 128.4, 127.0, 125.5, 84.5, 69.4, 68.6, 68.2, 60.3 (-ve DEPT), 47.6, 38.5 (-ve DEPT), 32.5 (-ve DEPT), 25.0 (-ve DEPT), 16.9, 14.0.

***N*-{*ortho*-(ferrocenyl)-benzoyl}-γ-aminobutyric acid-L-2-aminobutyric acid ethyl ester 59.**

For compound **59** γ-aminobutyric acid-L-2-aminobutyric acid ethyl ester (0.22 g, 1 mmol) was used as a starting material. The product was purified by column chromatography (eluant 1:1 hexane:ethyl acetate) and isolated as an orange oil (0.19 g, 46%). E°´ = 45 mV (vs Fc/Fc^+); $[\alpha]_D^{20}$ = -19° (c 2, EtOH).

UV-Vis λ_{max} ACN: 328, 445 nm.

I.R. ν_{max} (KBr): 3284, 3082, 2876, 1736, 1528, 1459, 1375, 1299, 1105, 1026 cm^{-1}.

^{1}H NMR (400 MHz) δ (d_6-DMSO): 8.23-8.20 (2H, m, 2-CON*H*-), 7.86 (1H, d, *J* = 8 Hz, ArH), 7.45 (1H, t, *J* = 7.2 Hz, ArH), 7.29 (1H, t, *J* = 7.6 Hz, ArH) 7.23 (1H, d, *J* = 7.6 Hz, ArH), 4.64 {2H, t, *J* = 2 Hz, *ortho* on (η^5-C_5H_4)}, 4.31 {2H, t, *J* = 2 Hz, *meta* on (η^5-C_5H_4)}, 4.22-4.08 {8H, m, (η^5-C_5H_5), -OC*H*$_2$$CH_3$, -C*H*($C_2H_5$)}, 3.21-3.16 (2H, m, -NHC*H*$_2$$CH_2CH_2CO$-), 2.20 (2H, t, *J* = 7.2 Hz, -$NHCH_2CH_2C$*H*$_2$CO-), 1.80-1.61 {4H, m, -$NHCH_2C$*H*$_2$$CH_2CO$-, -CH(C*H*$_2$$CH_3$)}, 1.24 (3H, t, *J* = 7.2 Hz, -OCH_2C*H*$_3$), 0.95 {3H, t, *J* = 7.6 Hz, -CH(CH_2C*H*$_3$)}.

^{13}C NMR (100 MHz) δ (d_6-DMSO): 172.2, 172.1, 169.7, 137.0, 135.7, 129.9, 128.4, 127.0, 125.5, 84.5, 69.4, 68.6, 68.2, 60.3 (-ve DEPT), 53.3, 38.4 (-ve DEPT), 32.6 (-ve DEPT), 25.1 (-ve DEPT), 24.2 (-ve DEPT), 14.1, 10.3.

***N*-{*ortho*-(ferrocenyl)-benzoyl}- γ -aminobutyric acid-L-norvaline ethyl ester 60.**

For compound **60** γ -aminobutyric acid-L-norvaline ethyl ester (0.25 g, 1 mmol) was used as a starting material. The product was purified by column chromatography (eluant 1:1 hexane:ethyl acetate) and isolated as an orange oil (0.20 g, 47%). E°´ = 43 mV (vs Fc/Fc^+); $[\alpha]_D^{20} = -25^o$ (c 2, EtOH).

UV-Vis λ_{max} ACN: 327, 440 nm.

I.R. ν_{max} (KBr): 3280, 2928, 2364, 1719, 1637, 1560, 1542, 1262, 1213, 1107, 1032 cm^{-1}.

^1H NMR (400 MHz) δ (d_6-DMSO): 8.17-8.13 (2H, m, 2-CON*H*-), 7.79 (1H, d, *J* = 7.2 Hz, ArH), 7.38 (1H, t, *J* = 7.4 Hz, ArH), 7.23 (1H, t, *J* = 7.4 Hz, ArH), 7.15 (1H, d, *J* = 7.4 Hz, ArH), 4.57 {2H, t, *J* = 2 Hz, *ortho* on (η^5-C_5H_4)}, 4.28 {2H, t, *J* = 2 Hz, *meta* on (η^5-C_5H_4)}, 4.22-4.16 {1H, m, -C*H*(C_3H_7)}, 4.11-4.07 {7H, m, (η^5-C_5H_5), -O*CH*$_2$$CH_3$)}, 3.13-3.11 (2H, m, -NHC*H*$_2$$CH_2CH_2CO$-), 2.12 (2H, t, *J* = 7.6 Hz, -$NHCH_2CH_2CH_2CO$-), 1.67-1.58 {4H, m, -$NHCH_2CH_2CH_2CO$-, -CH(C*H*$_2$$CH_2CH_3$)}, 1.34-1.30 {2H, m, -CH($CH_2CH_2CH_3$)}, 1.17 (3H, t, *J* = 7.2 Hz, -OCH_2CH_3), 0.87 {3H, t, *J* = 7.6 Hz, -CH($CH_2CH_2CH_3$)}.

^{13}C NMR (100 MHz) δ (d_6-DMSO): 172.4, 170.0, 169.7, 137.0, 135.7, 129.9, 128.4, 127.0, 125.5, 84.5, 69.4, 68.6, 68.1, 60.3 (-ve DEPT), 51.6, 38.5 (-ve DEPT), 32.9 (-ve DEPT), 32.6 (-ve DEPT), 25.1 (-ve DEPT), 18.6 (-ve DEPT), 14.1, 13.4.

***N*-{*ortho*-(ferrocenyl)-benzoyl}-γ-aminobutyric acid-L-norleucine ethyl ester 61.**

For compound **61** γ-aminobutyric acid-L-norleucine ethyl ester (0.23 g, 1 mmol) was used as a starting material. The product was purified by column chromatography (eluant 1:1 hexane:ethyl acetate) and isolated as an orange oil (0.14 g, 32%). E°´ = 48 mV (vs Fc/Fc^+); $[\alpha]_D^{20} = -44^o$ (c 2, EtOH).

UV-Vis λ_{max} ACN: 327, 445 nm.

I.R. ν_{max} (KBr): 3293, 3082, 2957, 1735, 1542, 1375, 1268, 1190, 1105, 1029 cm^{-1}.

^1H NMR (400 MHz) δ (d_6-DMSO): 8.17-8.13 (2H, m, 2-CON*H*-), 7.78 (1H, d, *J* = 8 Hz, ArH), 7.38 (1H, t, *J* = 7.6 Hz, ArH), 7.23 (1H, t, *J* = 7.6 Hz, ArH), 7.16 (1H, d, *J* = 7.6 Hz, ArH) 4.57 {2H, t, *J* = 1.6 Hz, *ortho* on (η^5-C_5H_4)}, 4.28 {2H, t, *J* = 1.6 Hz, *meta* on

(η^5-C_5H_4)}, 4.20-4.15 {1H, m, -C*H*(C_4H_9)}, 4.12-4.04 {7H, m, (η^5-C_5H_5), -O*C*$H_2$$CH_3$)}, 3.13-3.09 (2H, m -NHC$H_2$$CH_2$$CH_2$CO-), 2.12 (2H, t, *J* = 7.2 Hz, -NHCH$_2$CH$_2$CH_2CO-), 1.68-1.54 {4H, m, -NHCH$_2$CH_2CH$_2$CO-, -CH(CH_2CH$_2$CH$_2$CH$_3$)}, 1.28-1.20 {4H, m, -CH(CH$_2$CH_2CH_2CH$_3$)}, 1.18 (3H, t, *J* = 7.2 Hz, -OCH$_2$CH_3), 0.86 {3H, t, *J* = 6.8 Hz, -CH(CH$_2$CH$_2$CH$_2$CH_3)}.

^{13}C NMR (100 MHz) δ (*d*$_6$-DMSO): 172.3, 172.0, 169.7, 137.0, 135.7, 129.9, 128.4, 127.0, 125.4, 84.5, 69.4, 68.6, 68.1, 60.3 (-ve DEPT), 51.8, 38.5 (-ve DEPT), 32.6 (-ve DEPT), 30.5 (-ve DEPT), 27.5 (-ve DEPT), 25.1 (-ve DEPT), 21.6 (-ve DEPT), 14.1, 13.7.

General procedure for the preparation of N-{meta-(ferrocenyl)-benzoyl} dipeptide esters.

***N*-{*meta*-(ferrocenyl)-benzoyl}-glycine-L-alanine ethyl ester 62.**

1-Hydroxybenzotriazole (0.11 g, 0.83 mmol) was added to a solution of *meta*-ferrocenyl benzoic acid (0.20 g, 0.65 mmol), *N*-(3-dimethylaminopropyl)-*N'*-ethylcarbodiimide hydrochloride (0.16 g 0.83 mmol) and triethylamine (2 mls) in dichloromethane (40 mls) at 0 ^{o}C. After 30 minutes glycine-L-alanine ethyl ester (0.16 g, 0.83 mmol) was added and the reaction was stirred at room temperature for 48 hours. The reaction mixture was washed with water, 10% potassium hydrogen carbonate and 5% citric acid. The organic layer was dried over $MgSO_4$ and the solvent was removed *in vacuo*. The product was purified by column chromatography (eluant 1:1 hexane:ethyl acetate). Recrystallization from ethyl acetate furnished the product as an orange solid (0.14 g, 30%). m.p. 94-96 ^{o}C; $E^{o\prime}$ = 66 mV (vs Fc/Fc^+); $[\alpha]_D^{20}$ = -22^{o} (c 2, EtOH).

UV-Vis λ_{max} ACN: 326, 443 nm.

I.R. ν_{max} (KBr): 3550, 2917, 1792, 1651, 1563 cm^{-1}.

^{1}H NMR (400 MHz) δ (*d*$_6$-DMSO): 8.79 (1H, t, *J* = 5.6 Hz, -CON*H*-), 8.41 (1H, d, *J* = 7.2 Hz, -CON*H*-), 8.00 (1H, s, ArH), 7.73-7.68 (2H, m, ArH), 7.40 (1H, t, *J* = 7.6 Hz, ArH), 4.85 {2H, t, *J* = 1.6 Hz, *ortho* on (η^5-C_5H_4)}, 4.39 {2H, t, *J* = 2 Hz, *meta* on (η^5-C_5H_4)}, 4.28 {1H, quint, *J* = 7.2 Hz, -C*H*(CH_3)}, 4.09 (2H, q, *J* = 7.2 Hz, -O*C*$H_2$$CH_3$),

4.03-3.87 {7 H, m, (η^5-C_5H_5), -NHC*H*$_2$CO-}, 1.29 {3H, d, *J* = 7.2 Hz, -CH(C*H*$_3$)}, 1.18 (3H, t, *J* = 7.2 Hz, -OCH$_2$C*H*$_3$).

^{13}C NMR (100 MHz) δ (*d*$_6$-DMSO): 172.6, 169.0, 166.4, 139.2, 134.0, 128.7, 128.4, 124.9, 124.2, 84.0, 69.4, 69.1, 66.3, 60.5 (-ve DEPT), 47.7, 42.1 (-ve DEPT), 17.0, 14.0.

***N*-{*meta*-(ferrocenyl)-benzoyl}-glycine-L-2-aminobutyric acid ethyl ester 63.**

For compound **63** glycine-L-2-aminobutyric acid ethyl ester (0.14 g, 0.83 mmol) was used as a starting material. The product was purified by column chromatography (eluant 1:1 hexane:ethyl acetate). Recrystallization from ethyl acetate furnished the product as an orange solid (0.11 g, 39%). m.p. 124-126 ^{o}C; E$^{o\prime}$ = 58 mV (vs Fc/Fc$^+$); $[\alpha]_D^{20}$ = +1^{o} (c 2, MeOH).

UV-Vis λ_{max} ACN: 328, 445 nm.

I.R. ν_{max} (KBr): 3569, 2965, 1735, 1560, 1261, 1105 cm^{-1}.

^{1}H NMR (400 MHz) δ (*d*$_6$-DMSO): 8.77 (1H, t, *J* = 6 Hz, -CON*H*-), 8.31 (1H, d, *J* = 7.6 Hz, -CON*H*-), 8.00 (1H, s, ArH), 7.74-7.69 (2H, m, ArH), 7.40 (1H, t, *J* = 7.6 Hz, ArH), 4.86 {2H, t, *J* = 2 Hz, *ortho* on (η^5-C_5H_4)}, 4.39 {2H, t, *J* = 2 Hz, *meta* on (η^5-C_5H_4)}, 4.23-4.17 {1H, m, -C*H*(C_2H_5)}, 4.12-4.08 (2H, m, -OC*H*$_2$CH$_3$), 4.03-3.90 {7H, m, (η^5-C_5H_5), -NHC*H*$_2$CO-), 1.78-1.62 {2H, m, -CH(C*H*$_2$CH$_3$)}, 1.19 (3H, t, *J* = 7.2 Hz, -OCH$_2$C*H*$_3$), 0.90 {3H, t, *J* = 7.2 Hz, -CH(CH$_2$C*H*$_3$)}.

^{13}C NMR (100 MHz) δ (*d*$_6$-DMSO): 171.9, 169.2, 166.3, 139.2, 134.0, 128.7, 128.4, 124.9, 124.2, 84.0, 69.4, 69.1, 66.4, 60.4 (-ve DEPT), 53.4, 42.1 (-ve DEPT), 24.3 (-ve DEPT), 14.1, 10.2.

Analysis:	found:	C, 62.54; H, 5.95; N, 5.73,
$C_{25}H_{28}FeN_2O_4$	requires:	C, 63.04; H, 5.92; N, 5.88.
Mass spectrum:	found: $[M]^{+\bullet}$	476.1380,
$C_{25}H_{28}FeN_2O_4$	requires:	476.1398.

***N*-{*meta*-(ferrocenyl)-benzoyl}-glycine-L-norvaline ethyl ester 64.**

For compound **64** glycine-L-norvaline ethyl ester (0.15 g, 0.75 mmol) was used as a starting material. The product was purified by column chromatography (eluant 1:1

hexane:ethyl acetate). Recrystallization from ethyl acetate furnished the product as an orange solid (0.10 g, 31%). m.p. 138-140 ^{o}C; E$^{o\prime}$ = 52 mV (vs Fc/Fc^{+}); $[\alpha]_D^{20}$ = -9^{o} (c 2, MeOH).

UV-Vis λ_{max} ACN: 330, 445 nm.

I.R. ν_{max} (KBr): 3651, 2961, 1840, 1735, 1560, 1261, 1105 cm^{-1}.

^{1}H NMR (400 MHz) δ (*d*$_6$-DMSO): 8.75 (1H, t, *J* = 6 Hz, -CON*H*-), 8.30 (1H, d, *J* = 7.6 Hz, -CON*H*-), 8.00 (1H, s, ArH), 7.73-7.68 (2H, m, ArH), 7.40 (1H, t, *J* = 7.6 Hz, ArH), 4.85 {2H, t, *J* = 1.6 Hz, *ortho* on (η^5-C_5H_4)}, 4.40 {2H, t, *J* = 1.6 Hz, *meta* on (η^5-C_5H_4)}, 4.29-4.23 {1H, m, -C*H*(C_3H_7)}, 4.12-4.08 (2H, m, -OC*H*$_2$$CH_3$), 4.06-3.84 {7H, m, ($\eta^5$-$C_5H_5$), -NHC*H*$_2$CO-}, 1.71-1.57 {2H, m, -CH(C*H*$_2$$CH_2CH_3$)}, 1.38-1.36 {2H, m, -$CH(CH_2CH_2CH_3)$}, 1.19 (3H, t, *J* = 7.2 Hz, -OCH_2CH_3), 0.88 {3H, t, *J* = 7.6 Hz, -$CH(CH_2CH_2CH_3)$}.

^{13}C NMR (100 MHz) δ (*d*$_6$-DMSO): 172.2, 169.2, 166.3, 139.2, 134.0, 128.7, 128.4, 124.9, 124.2, 84.0, 69.4, 69.0, 66.4, 60.4 (-ve DEPT), 51.7, 42.0 (-ve DEPT), 33.0 (-ve DEPT), 18.5 (-ve DEPT), 14.0, 13.5.

Analysis:	found:	C, 64.11; H, 6.47; N, 5.89,
$C_{26}H_{30}FeN_2O_4$	requires:	C, 63.68; H, 6.17; N, 5.71.
Mass spectrum:	found: $[M]^{+\bullet}$	490.1573,
$C_{26}H_{30}FeN_2O_4$	requires:	490.1555.

***N*-{*meta*-(ferrocenyl)-benzoyl}-glycine-L-norleucine ethyl ester 65.**

For compound **65** glycine-L-norleucine ethyl ester (0.19 g, 0.86 mmol) was used as a starting material. The product was purified by column chromatography (eluant 1:1 hexane:ethyl acetate). Recrystallization from ethyl acetate furnished the product as an orange solid (0.14 g, 34%). m.p. 141-143 ^{o}C; E$^{o\prime}$ = 54 mV (vs Fc/Fc^{+}); $[\alpha]_D^{20}$ = +19^{o} (c 2, MeOH).

UV-Vis λ_{max} ACN: 328, 445 nm.

I.R. ν_{max} (KBr): 3558, 2958, 1774, 1605, 1206, 1151 cm^{-1}.

^{1}H NMR (400 MHz) δ (*d*$_6$-DMSO): 8.84 (1H, t, *J* = 5.6 Hz, -CON*H*-), 8.39 (1H, d, *J* = 7.6 Hz, -CON*H*-), 8.07 (1H, s, ArH), 7.80-7.75 (2H, m, ArH), 7.46 (1H, t, *J* = 7.6 Hz,

ArH), 4.92 {2H, t, *J* = 1.6 Hz, *ortho* on (η^5-C_5H_4)}, 4.45 {2H, t, *J* = 1.6 Hz, *meta* on (η^5-C_5H_4)}, 4.33-4.28 {1H, m, -C*H*(C_4H_9)}, 4.19-4.12 (2H, m, -OC*H*$_2$$CH_3$), 4.09-3.95 {7H, m, ($\eta^5$-$C_5H_5$), -NHC*H*$_2$CO-), 1.79-1.64 {2H, m, -CH(C*H*$_2$$CH_2CH_2CH_3$)}, 1.36-1.33 {4H, m, -CH(CH_2C*H*$_2$C*H*$_2$$CH_3$)}, 1.25 (3H, t, *J* = 7.2 Hz, -OCH_2C*H*$_3$), 0.93 {3H, t, *J* = 7.2 Hz, -CH($CH_2CH_2CH_2$C*H*$_3$)}.

^{13}C NMR (100 MHz) δ (*d*$_6$-DMSO): 172.1, 169.2, 166.3, 139.2, 134.0, 128.7, 128.4, 124.9, 124.2, 84.0, 69.4, 69.1, 66.3, 60.4 (-ve DEPT), 51.9, 42.1 (-ve DEPT), 30.7 (-ve DEPT), 27.4 (-ve DEPT), 21.7 (-ve DEPT), 14.0, 13.8.

Analysis:	found:	C, 64.01; H, 6.36; N, 5.26,
$C_{26}H_{30}FeN_2O_4$	requires:	C, 64.29; H, 6.39; N, 5.55.
Mass spectrum:	found: $[M]^{+\bullet}$	504.1704,
$C_{27}H_{32}FeN_2O_4$	requires:	504.1711.

***N*-{*meta*-(ferrocenyl)-benzoyl}-β-alanine-L-alanine ethyl ester 66.**

For compound **66** β-alanine-L-alanine ethyl ester (0.18 g, 1 mmol) was used as a starting material. The product was purified by column chromatography (eluant 1:1 hexane:ethyl acetate). Recrystallization from ethyl acetate furnished the product as an orange solid (0.11 g, 28%). m.p. 108-110 ^{o}C; E$^{o\prime}$ = 52 mV (vs Fc/Fc^+); $[\alpha]_D^{20}$ = +21^{o} (c 2, EtOH).

UV-Vis λ_{max} ACN: 328, 445 nm.

I.R. ν_{max} (KBr): 3276, 3079, 2345, 1736, 1579, 1364, 1323, 1154, 1104, 1054 cm^{-1}.

^{1}H NMR (400 MHz) δ (*d*$_6$-DMSO): 8.53 (1H, t, *J* = 5.2 Hz, -CON*H*-), 8.38 (1H, d, *J* = 6.8 Hz, -CON*H*-), 7.94 (1H, s, ArH), 7.69 (1H, d, *J* = 7.6 Hz, ArH), 7.64 (1H, d, *J* = 8.0 Hz, ArH), 7.38 (1H, t, *J* = 8.0 Hz, ArH), 4.85 {2H, t, *J* = 1.6 Hz, *ortho* on (η^5-C_5H_4)}, 4.39 {2H, t, *J* = 1.6 Hz, *meta* on (η^5-C_5H_4)}, 4.23 {1H, quint, *J* = 7.2 Hz, -C*H*(CH_3)}, 4.19-4.03 {7H, m, (η^5-C_5H_5), -OC*H*$_2$$CH_3$}, 3.49 (2H, q, *J* = 6.8 Hz, -NHC*H*$_2$$CH_2$CO-), 2.44 (2H, t, *J* = 7.2 Hz, -$NHCH_2$C*H*$_2$CO-), 1.26 {3H, d, *J* = 7.6 Hz, -CH(C*H*$_3$)}, 1.16 (3H, t, *J* = 6.8 Hz, -OCH_2C*H*$_3$).

^{13}C NMR (100 MHz) δ (*d*$_6$-DMSO): 172.7, 170.4, 166.1, 139.2, 134.5, 128.5, 128.3, 124.7, 124.1, 84.0, 69.4, 69.1, 66.4, 60.3 (-ve DEPT), 47.6, 36.0 (-ve DEPT), 34.9 (-ve DEPT), 16.9, 14.0.

***N*-{*meta*-(ferrocenyl)-benzoyl}-β-alanine-L-2-aminobutyric acid ethyl ester 67.**

For compound **67** β-alanine-L-2-aminobutyric acid ethyl ester (0.19 g, 0.95 mmol) was used as a starting material. The product was purified by column chromatography (eluant 1:1 hexane:ethyl acetate). Recrystallization from ethyl acetate furnished the product as an orange solid (0.22 g, 55%). m.p. 126-128 ^{o}C; $E^{o\prime}$ = 65 mV (vs Fc/Fc^{+}); $[\alpha]_D^{20}$ = -31^{o} (c 2, EtOH).

UV-Vis λ_{max} ACN: 329, 445 nm.

I.R. ν_{max} (KBr): 3261, 3081, 2345, 1712, 1685, 1578, 1376, 1189, 1031 cm^{-1}.

^{1}H NMR (400 MHz) δ (*d_6*-DMSO): 8.52 (1H, t, *J* = 5.6 Hz, -CON*H*-), 8.30 (1H, d, *J* = 7.6 Hz, -CON*H*-), 7.94 (1H, s, ArH), 7.71-7.64 (2H, m, ArH), 7.38 (1H, t, *J* = 7.6 Hz, ArH), 4.84 {2H, t, *J* = 1.6 Hz, *ortho* on (η^5-C_5H_4)}, 4.39 {2H, t, *J* = 2 Hz, *meta* on (η^5-C_5H_4)}, 4.19-4.14 {1H, m, -C*H*(C_2H_5)}, 4.12-4.08 {7H, m, (η^5-C_5H_5), -OC*H*$_2$$CH_3$}, 3.49 (2H, q, *J* = 6.8 Hz, -NHC*H*$_2$$CH_2$CO-), 2.48-2.46 (2H, m, -NHCH_2C*H*$_2$CO-), 1.74-1.57 {2H, m, -CH(C*H*$_2$$CH_3$)}, 1.16 (3H, t, *J* = 7.2 Hz, -OCH_2C*H*$_3$), 0.87 {3H, t, *J* = 7.2 Hz, -CH(CH_2C*H*$_3$)}.

^{13}C NMR (100 MHz) δ (*d_6*-DMSO): 172.1, 170.7, 166.1, 139.2, 134.5, 128.4, 128.3, 124.7, 124.1, 84.0, 69.4, 69.0, 66.4, 60.3 (-ve DEPT), 53.4, 36.0 (-ve DEPT), 34.9 (-ve DEPT), 24.2 (-ve DEPT), 14.0, 10.3.

***N*-{*meta*-(ferrocenyl)-benzoyl}-β-alanine-L-norvaline ethyl ester 68.**

For compound **68** β-alanine-L-norvaline ethyl ester (0.20 g, 0.95 mmol) was used as a starting material. The product was purified by column chromatography (eluant 1:1 hexane:ethyl acetate). Recrystallization from ethyl acetate furnished the product as an orange powder (0.18 g, 44%). m.p. 146-148 ^{o}C; $E^{o\prime}$ = 58 mV (vs Fc/Fc^{+}); $[\alpha]_D^{20}$ = -20^{o} (c 2, EtOH).

UV-Vis λ_{max} ACN: 329, 445 nm.

I.R. ν_{max} (KBr): 3267, 2930, 1741, 1685, 1579, 1459, 1321, 1188, 1104, 1032 cm^{-1}.

^{1}H NMR (400 MHz) δ (*d_6*-DMSO): 8.51 (1H, t, *J* = 5.6 Hz, -CON*H*-), 8.30 (1H, d, *J* = 7.6 Hz, -CON*H*-), 7.94 (1H, s, ArH), 7.71-7.64 (2H, m, ArH), 7.38 (1H, t, *J* = 7.6 Hz,

ArH), 4.85 {2H, t, *J* = 1.6 Hz, *ortho* on (η^5-C_5H_4)}, 4.39 {2H, t, *J* = 1.6 Hz, *meta* on (η^5-C_5H_4)}, 4.22-4.18 {1H, m, -C*H*(C_3H_7)} 4.11-4.02 {7H, m, (η^5-C_5H_5), -OC*H*$_2$$CH_3$}, 3.49 (2H, q, *J* = 7.2 Hz, -NHC*H*$_2$$CH_2CO$-), 2.47-2.40 (2H, m, -NHCH$_2$C*H*$_2$CO-), 1.68-1.52 {2H, m, -CH(C*H*$_2$$CH_2CH_3$)}, 1.35-1.24 {2H, m, -CH(CH_2C*H*$_2$$CH_3$)}, 1.16 (3H, t, *J* = 7.2 Hz, -OCH$_2$C*H*$_3$), 0.82 {3H, t, *J* = 7.2 Hz, -CH(CH_2CH_2C*H*$_3$)}.

^{13}C NMR (100 MHz) δ (*d*$_6$-DMSO): 172.3, 170.7, 166.1, 139.2, 134.5, 128.5, 128.3, 124.7, 124.1, 84.0, 69.4, 69.0, 66.4, 60.3 (-ve DEPT), 51.7, 36.0 (-ve DEPT), 35.0 (-ve DEPT), 32.9 (-ve DEPT), 18.6 (-ve DEPT), 14.0, 13.4.

***N*-{*meta*-(ferrocenyl)-benzoyl}-β-alanine-L-norleucine ethyl ester 69.**

For compound **69** β-alanine-L-norleucine ethyl ester (0.22 g, 0.95 mmol) was used as a starting material. The product was purified by column chromatography (eluant 1:1 hexane:ethyl acetate). Recrystallization from ethyl acetate furnished the product as an orange powder (0.18 g, 42%). m.p. 142-144 ^{o}C; E$^{o\prime}$ = 68 mV (vs Fc/Fc$^+$); $[\alpha]_D^{20}$ = -65^{o} (c 2, EtOH).

UV-Vis λ_{max} ACN: 328, 445 nm.

I.R. ν_{max} (KBr): 3261, 2933, 2860, 2346, 1741, 1605, 1542, 1377, 1271, 1184 cm^{-1}.

^{1}H NMR (400 MHz) δ (*d*$_6$-DMSO): 8.51 (1H, t, *J* = 5.6 Hz, -CON*H*-), 8.30 (1H, d, *J* = 7.6 Hz, -CON*H*-), 7.94 (1H, s, ArH), 7.71-7.64 (2H, m, ArH), 7.37 (1H, t, *J* = 8 Hz, ArH), 4.84 {2H, t, *J* = 1.6 Hz, *ortho* on (η^5-C_5H_4)}, 4.38 {2H, t, *J* = 2 Hz, *meta* on (η^5-C_5H_4)}, 4.22-4.18 {1H, m, -C*H*(C_4H_9)}, 4.13-4.01 {7H, m, (η^5-C_5H_5), -OC*H*$_2$$CH_3$}, 3.49 (2H, q, *J* = 7.2 Hz, -NHC*H*$_2$$CH_2CO$-), 2.47-2.45 (2H, m, -NHCH$_2$C*H*$_2$CO-), 1.69-1.54 {2H, m, -CH(C*H*$_2$$CH_2CH_2CH_3$)}, 1.25-1.20 {4H, m, -CH(CH_2C*H*$_2$C*H*$_2$$CH_3$)}, 1.16 (3H, t, *J* = 6.8 Hz, -OCH$_2$C*H*$_3$), 0.80 {3H, t, *J* = 7.2 Hz, -CH($CH_2CH_2CH_2$C*H*$_3$)}.

^{13}C NMR (100 MHz) δ (*d*$_6$-DMSO): 172.3, 170.7, 166.1, 139.2, 134.5, 128.5, 128.3, 124.7, 124.1, 84.0, 69.4, 69.0, 66.4, 60.3 (-ve DEPT), 51.9, 36.0 (-ve DEPT), 34.9 (-ve DEPT), 30.5 (-ve DEPT), 27.4 (-ve DEPT), 21.6 (-ve DEPT), 14.0, 13.7.

***N*-{*meta*-(ferrocenyl)-benzoyl}-γ-aminobutyric acid-L-alanine ethyl ester 70.**

For compound **70** γ-aminobutyric acid-L-alanine ethyl ester (0.19 g, 0.95 mmol) was used as a starting material. The product was purified by column chromatography (eluant 1:1 hexane:ethyl acetate). Recrystallization from ethyl acetate furnished the product as an orange powder (0.13 g, 32%). m.p. 128-130 ^{o}C; E$^{o\prime}$ = 62 mV (vs Fc/Fc^{+}); $[\alpha]_D^{20}$ = -71^{o} (c 2, EtOH).

UV-Vis λ_{max} ACN: 330, 439 nm.

I.R. ν_{max} (KBr): 3331, 2929, 2346, 1629, 1459, 1376, 1199, 1104, 1055 cm^{-1}.

^{1}H NMR (400 MHz) δ (*d*$_6$-DMSO): 8.51 (1H, t, *J* = 5.6 Hz, -CON*H*-), 8.29 (1H, d, *J* = 6.8 Hz, -CON*H*-), 7.95 (1H, s, ArH), 7.71-7.65 (2H, m, ArH), 7.38 (1H, t, *J* = 8 Hz, ArH), 4.85 {2H, t, *J* = 2 Hz, *ortho* on (η^5-C_5H_4)}, 4.39 {2H, t, *J* = 2 Hz, *meta* on (η^5-C_5H_4)}, 4.22 {1H, quint, *J* = 7.2 Hz, -C*H*(CH_3)}, 4.10-4.02 {7H, m, (η^5-C_5H_5), -OCH_2*H*$_2$$CH_3$}, 3.32-3.26 (2H, m -NHC$H_2$$CH_2$$CH_2$CO-), 2.20 (2H, t, *J* = 7.2 Hz, -NHC$H_2$$CH_2CH_2$CO-), 1.81-1.74 (2H, m, -NHCH_2C$H_2$$CH_2$CO-), 1.25 {3H, d, *J* = 7.2 Hz, -CH(C*H*$_3$)}, 1.18 (3H, t, *J* = 6.8 Hz, -OCH_2C*H*$_3$).

^{13}C NMR (100 MHz) δ (*d*$_6$-DMSO): 172.7, 172.9, 166.1, 139.2, 134.6, 128.5, 128.3, 124.7, 124.1, 84.1, 69.4, 69.1, 66.4, 60.3 (-ve DEPT), 47.6, 38.9 (-ve DEPT), 32.6 (-ve DEPT), 25.3 (-ve DEPT), 16.9, 14.0.

***N*-{*meta*-(ferrocenyl)-benzoyl}-γ-aminobutyric acid-L-2-aminobutyric acid ethyl ester 71.**

For compound **71** γ-aminobutyric acid-L-2-aminobutyric acid ethyl ester (0.20 g, 0.95 mmol) was used as a starting material. The product was purified by column chromatography (eluant 1:1 hexane:ethyl acetate). Recrystallization from ethyl acetate furnished the product as an orange powder (0.15 g, 36%). m.p. 97-99 ^{o}C; E$^{o\prime}$ = 56 mV (vs Fc/Fc^{+}); $[\alpha]_D^{20}$ = +16^{o} (c 2, EtOH).

UV-Vis λ_{max} ACN: 327, 445 nm.

I.R. ν_{max} (KBr): 3278, 3080, 2988, 2345 1740, 1604, 1368, 1206, 1104, 1031 cm^{-1}.

^{1}H NMR (400 MHz) δ (*d*$_6$-DMSO): 8.51 (1H, t, *J* = 5.6 Hz, -CON*H*-), 8.23 (1H, d, *J* = 7.2 Hz, -CON*H*-), 7.94 (1H, s, ArH), 7.71-7.65 (2H, m, ArH), 7.38 (1H, t, *J* = 8 Hz, ArH), 4.85 {2H, t, *J* = 1.6 Hz, *ortho* on (η^5-C_5H_4)}, 4.39 {2H, t, *J* = 1.6 Hz, *meta* on

(η^5-C_5H_4)}, 4.17-4.05 {8H, m, (η^5-C_5H_5), -OC*H*$_2$CH$_3$, -C*H*(C_2H_5)}, 3.32-3.28 (2H, m, -NHC*H*$_2$CH$_2$CH$_2$CO-), 2.24 (2H, t, *J* = 7.6 Hz, -NHCH$_2$CH$_2$C*H*$_2$CO-), 1.82-1.57 {4H, m, -NHCH$_2$C*H*$_2$CH$_2$CO-, -CH(C*H*$_2$CH$_3$)}, 1.18 (3H, t, *J* = 7.2 Hz, -OCH$_2$C*H*$_3$), 0.88 {3H, t, *J* = 7.6 Hz, -CH(CH$_2$C*H*$_3$)}.

^{13}C NMR (100 MHz) δ (*d*$_6$-DMSO): 172.3, 172.1, 166.1, 139.2, 134.6, 128.5, 128.3, 124.7, 124.1, 84.1, 69.4, 69.0, 66.4, 60.3 (-ve DEPT), 53.4, 38.9 (-ve DEPT), 32.6 (-ve DEPT), 25.4 (-ve DEPT), 24.7 (-ve DEPT), 14.1, 10.3.

***N*-{*meta*-(ferrocenyl)-benzoyl}-γ-aminobutyric acid-L-norvaline ethyl ester 72.**

For compound **72** γ-aminobutyric acid-L-norvaline ethyl ester (0.22 g, 0.95 mmol) was used as a starting material. The product was purified by column chromatography (eluant 1:1 hexane:ethyl acetate). Recrystallization from ethyl acetate furnished the product as an orange powder (0.25 g, 59%). m.p. 102-104 ^{o}C; E$^{o\prime}$ = 64 mV (vs Fc/Fc$^+$); $[\alpha]_D^{20}$ = -51^{o} (c 2, EtOH).

UV-Vis λ_{max} ACN: 331, 445 nm.

I.R. ν_{max} (KBr): 3301, 3104, 2345, 1794, 1606, 1458, 1375, 1203, 1146, 1020 cm^{-1}.

^{1}H NMR (400 MHz) δ (*d*$_6$-DMSO): 8.51 (1H, t, *J* = 5.6 Hz, -CON*H*-), 8.23 (1H, d, *J* = 7.6 Hz, -CON*H*-), 7.95 (1H, s, ArH), 7.71-7.65 (2H, m, ArH), 7.38 (1H, t, *J* = 8 Hz, ArH), 4.85 {2H, t, *J* = 2 Hz, *ortho* on (η^5-C_5H_4)}, 4.39 {2H, t, *J* = 2 Hz, *meta* on (η^5-C_5H_4)}, 4.23-4.18 {1H, m, -C*H*(CH$_3$)}, 4.14-4.07 {7H, m, (η^5-C_5H_5), -OC*H*$_2$CH$_3$}, 3.31-3.26 (2H, m, -NHC*H*$_2$CH$_2$CH$_2$CO-), 2.22 (2H, t, *J* = 7.6 Hz, -NHCH$_2$CH$_2$C*H*$_2$CO-), 1.80 (2H, quint, *J* = 5.6 Hz, -NHCH$_2$C*H*$_2$CH$_2$CO-), 1.65-1.57 {2H, m, -CH(C*H*$_2$CH$_2$CH$_3$)}, 1.34-1.30 {2H, m, -CH(CH$_2$C*H*$_2$CH$_3$)}, 1.18 (3H, t, *J* = 6.8 Hz, -OCH$_2$C*H*$_3$), 0.86 {3H, t, *J* = 7.2 Hz, -CH(CH$_2$CH$_2$C*H*$_3$)}.

^{13}C NMR (100 MHz) δ (*d*$_6$-DMSO): 172.4, 172.2, 166.1, 139.2, 134.6, 128.5, 128.3, 124.7, 124.1, 84.1, 69.4, 69.1, 66.4, 60.3 (-ve DEPT), 51.7, 38.9 (-ve DEPT), 32.9 (-ve DEPT), 32.6 (-ve DEPT), 25.4 (-ve DEPT), 18.6 (-ve DEPT), 14.0, 13.4.

***N*-{*meta*-(ferrocenyl)-benzoyl}-γ-aminobutyric acid-L-norleucine ethyl ester 73.**

For compound **73** γ-aminobutyric acid-L-norleucine ethyl ester (0.23 g, 0.95 mmol) was used as a starting material. The product was purified by column chromatography (eluant 1:1 hexane:ethyl acetate). Recrystallization from ethyl acetate furnished the product as an orange powder (0.24 g, 55%). m.p. 112-114 ^{o}C; $E^{o\prime}$ = 61 mV (vs Fc/Fc^{+}); $[\alpha]_D^{20}$ = +29^{o} (c 2, EtOH).

UV-Vis λ_{max} ACN: 330, 445 nm.

I.R. ν_{max} (KBr): 3312, 2924, 1751, 1604, 1541, 1458, 1319, 1104, 1000 cm^{-1}.

^{1}H NMR (400 MHz) δ (*d*$_6$-DMSO): 8.51 (1H, t, *J* = 5.6 Hz, -CON*H*-), 8.23 (1H, d, *J* = 7.6 Hz, -CON*H*-), 7.95 (1H, s, ArH), 7.71-7.65 (2H, m, ArH), 7.38 (1H, t, *J* = 7.6 Hz, ArH), 4.85 {2H, t, *J* = 2 Hz, *ortho* on (η^5-C_5H_4)}, 4.39 {2H, t, *J* = 2 Hz, *meta* on (η^5-C_5H_4)}, 4.22-4.16 {1H, m, -C*H*(C_4H_9)}, 4.12-4.03 {7H, m, (η^5-C_5H_5), -OC*H*$_2$$CH_3$)}, 3.32-3.26 (2H, m, -NHC*H*$_2$$CH_2CH_2CO$-), 2.22 (2H, t, *J* = 7.2 Hz, -$NHCH_2CH_2CH_2CO$-), 1.78 (2H, quint, *J* = 7.2 Hz, -$NHCH_2CH_2CH_2CO$-), 1.66-1.57 {2H, m, -CH(C*H*$_2$$CH_2CH_2CH_3$)}, 1.30-1.27 {4H, m, -CH(CH_2C*H*$_2$C*H*$_2$$CH_3$)}, 1.17 (3H, t, *J* = 7.2 Hz, -OCH_2C*H*$_3$), 0.85 {3H, t, *J* = 7.2 Hz, -CH($CH_2CH_2CH_2$C*H*$_3$)}.

^{13}C NMR (100 MHz) δ (*d*$_6$-DMSO): 172.3, 172.2, 166.1, 139.2, 134.6, 128.5, 128.3, 124.7, 124.1, 84.1, 69.4, 69.0, 66.4, 60.3 (-ve DEPT), 51.9, 38.9 (-ve DEPT), 32.6 (-ve DEPT), 30.5 (-ve DEPT), 27.5 (-ve DEPT), 25.4 (-ve DEPT), 21.7 (-ve DEPT), 14.0, 13.7.

General procedure for the preparation of N-{para-(ferrocenyl)-benzoyl} dipeptide esters.

N-{*para*-(ferrocenyl)-benzoyl}-glycine-L-alanine ethyl ester 74.

1-Hydroxybenzotriazole (0.11 g, 0.83 mmol) was added to a solution of *para*-ferrocenyl benzoic acid (0.20 g, 0.65 mmol), *N*-(3-dimethylaminopropyl)-*N*'-ethylcarbodiimide hydrochloride (0.16 g 0.83 mmol) and triethylamine (2 mls) in dichloromethane (40 mls) at 0 ^{o}C. After 30 minutes glycine-L-alanine ethyl ester (0.14 g, 0.83 mmol) was added and the reaction was stirred at room temperature for 48 hours. The reaction mixture was washed with water, 10% potassium hydrogen carbonate and 5% citric acid. The organic layer was dried over $MgSO_4$ and the solvent was removed *in vacuo*. The product was

purified by column chromatography (eluant 1:1 hexane:ethyl acetate). Recrystallization from ethyl acetate furnished the product as an orange solid (0.16 g, 33%). m.p. 170-172 ^{o}C; E$^{o\prime}$ = 73 mV (vs Fc/Fc^{+}); $[\alpha]_D^{20}$ = +9^{o} (c 2, EtOH).

UV-Vis λ_{max} ACN: 350, 452 nm.

I.R. ν_{max} (KBr): 3569, 2925, 1780, 1650, 1555 cm^{-1}.

^{1}H NMR (400 MHz) δ (*d*$_6$-DMSO): 8.68 (1H, t, *J* = 5.6 Hz, -CON*H*-), 8.38 (1H, d, *J* = 6.8 Hz, -CONH-), 7.79 (2H, d, *J* = 8.4 Hz, ArH), 7.61 (2H, d, *J* = 8.4 Hz, ArH), 4.89 {2H, t, *J* = 1.6 Hz, *ortho* on (η^5-C_5H_4)}, 4.41 {2H, t, *J* = 1.6 Hz, *meta* on (η^5-C_5H_4)}, 4.27 {1H, quint, *J* = 7.2 Hz, -C*H*(CH_3)}, 4.09 (2H, q, *J* = 6.4 Hz, -OC*H*$_2$$CH_3$), 4.02 {5H, s, ($\eta^5$-$C_5H_5$)}, 3.98-3.84 (2H, m, -NHC*H*$_2$CO-), 1.30 (3H, d, *J* = 7.2 Hz, -CH(C*H*$_3$)}, 1.18 (3H, t, *J* = 7.2 Hz, -OCH$_2$C*H*$_3$).

^{13}C NMR (100 MHz) δ (*d*$_6$-DMSO): 172.5, 169.4, 168.0, 143.2, 131.2, 127.5, 125.3, 82.5, 69.4, 66.5, 66.2, 60.5 (-ve DEPT), 47.6, 42.0 (-ve DEPT), 17.0, 14.0

***N*-{*para*-(ferrocenyl)-benzoyl}-glycine-L-2-aminobutyric acid ethyl ester 75.**

For compound **75** glycine-L-2-aminobutyric acid ethyl ester (0.16 g, 0.83 mmol) was used as a starting material. The product was purified by column chromatography (eluant 1:1 hexane:ethyl acetate). Recrystallization from ethyl acetate furnished the product as an orange powder (0.14 g, 45%). m.p. 110-112 ^{o}C; E$^{o\prime}$ = 77 mV (vs Fc/Fc^{+}); $[\alpha]_D^{20}$ = +10^{o} (c 2, MeOH).

UV-Vis λ_{max} ACN: 355, 450 nm.

I.R. ν_{max} (KBr): 3569, 2957, 1639, 1605, 1506, 1401, 1104 cm^{-1}.

^{1}H NMR (400 MHz) δ (*d*$_6$-DMSO): 8.66 (1H, t, *J* = 6 Hz, -CON*H*-), 8.27 (1H, d, *J* = 7.6 Hz, -CON*H*-), 7.81 (2H, d, *J* = 8.4 Hz, ArH), 7.64 (2H, d, *J* = 8.4 Hz, ArH), 4.89 {2H, t, *J* = 2 Hz, *ortho* on (η^5-C_5H_4)}, 4.41 {2H, t, *J* = 2 Hz, *meta* on (η^5-C_5H_4)}, 4.22-4.17 {1H, m, -C*H*(C_2H_5)}, 4.17-4.07 (2H, m, -OC*H*$_2$$CH_3$), 4.04-3.87 {7H, m, ($\eta^5$-$C_5H_5$), -NHC*H*$_2$CO-}, 1.78-1.61 {2H, m, -CH(C*H*$_2$$CH_3$)}, 1.19 (3H, t, *J* = 7.2 Hz, -OCH$_2$C*H*$_3$), 0.90 {3H, t, *J* = 7.6 Hz, -CH(CH$_2$C*H*$_3$)}.

^{13}C NMR (100 MHz) δ (d_6-DMSO): 171.9, 169.2, 166.2, 142.7, 131.1, 127.4, 125.3, 83.2, 69.5, 66.5, 66.4, 60.4 (-ve DEPT), 53.3, 42.2 (-ve DEPT), 24.4 (-ve DEPT), 14.1, 10.2.

Analysis:	found:	C, 62.55; H, 5.95; N, 5.76,
$C_{25}H_{28}FeN_2O_4$	requires:	C, 63.04; H, 5.92; N, 5.88.
Mass spectrum:	found: $[M]^{+\bullet}$	476.1391,
$C_{25}H_{28}FeN_2O_4$	requires:	476.1398.

***N*-{*para*-(ferrocenyl)-benzoyl}-glycine-L-norvaline ethyl ester 76.**

For compound **76** glycine-L-norvaline ethyl ester (0.15 g, 0.75 mmol) was used as a starting material. The product was purified by column chromatography (eluant 1:1 hexane:ethyl acetate). Recrystallization from ethyl acetate furnished the product as an orange solid (0.21 g, 73%). m.p. 122-124 ^{o}C; E$^{o\prime}$ = 72 mV (vs Fc/Fc^{+}); $[\alpha]_D^{20}$ = -5^{o} (c 2, MeOH).

UV-Vis λ_{max} ACN: 355, 450 nm.

I.R. ν_{max} (KBr): 3355, 2957, 1639, 1543, 1198, 1104 cm^{-1}.

^{1}H NMR (400 MHz) δ (d_6-DMSO): 8.67 (1H, t, *J* = 6 Hz, -CON*H*-), 8.30 (1H, d, *J* = 7.6 Hz, -CON*H*-), 7.81 (2H, d, *J* = 8.4 Hz, ArH), 7.64 (2H, d, *J* = 8.4 Hz, ArH), 4.90 {2H, t, *J* = 2 Hz, *ortho* on (η^5-C_5H_4)}, 4.51 {2H, t, *J* = 2 Hz, *meta* on (η^5-C_5H_4)}, 4.28-4.23 {1H, m, -C*H*(C_3H_7)}, 4.13-4.05 (2H, m, -OC*H*$_2$CH$_3$), 4.02 {5H, s, (η^5-C_5H_5)}, 3.99-3.86 (2H, m, -NHC*H*$_2$CO-), 1.71-1.56 {2H, m, -CH(C*H*$_2$CH$_2$CH$_3$)}, 1.39-1.28 {2H, m, -CH(CH$_2$C*H*$_2$CH$_3$)}, 1.20 (3H, t, *J* = 7.2 Hz, -OCH$_2$C*H*$_3$), 0.90 {3H, t, *J* = 7.2 Hz, -CH(CH$_2$CH$_2$C*H*$_3$)}.

^{13}C NMR (100 MHz) δ (d_6-DMSO): 172.2, 169.2, 166.2, 142.7, 131.1, 127.4, 125.3, 83.2, 69.5, 66.6, 66.5, 60.4 (-ve DEPT), 51.7, 42.1 (-ve DEPT), 33.0 (-ve DEPT), 18.5 (-ve DEPT), 14.0, 13.5.

Analysis:	found:	C, 64.06; H, 6.39; N, 5.90,
$C_{26}H_{30}FeN_2O_4$	requires:	C, 63.68; H, 6.17; N, 5.71.
Mass spectrum:	found: $[M]^{+\bullet}$	490.1551,
$C_{26}H_{30}FeN_2O_4$	requires:	490.1555.

***N*-{*para*-(ferrocenyl)-benzoyl}-glycine-L-norleucine ethyl ester 77.**

For compound **77** glycine-L-norleucine ethyl ester (0.18 g, 0.86 mmol) was used as a starting material. The product was purified by column chromatography (eluant 1:1 hexane:ethyl acetate). Recrystallization from ethyl acetate furnished the product as an orange solid (0.13 g, 40%). m.p. 135-137 ^{o}C; E$^{o\prime}$ = 69 mV (vs Fc/Fc^{+}); $[\alpha]_D^{20}$ = -6^{o} (c 2, MeOH).

UV-Vis λ_{max} ACN: 355, 450 nm.

I.R. ν_{max} (KBr): 3413, 2974, 1745, 1680, 1413, 1149 cm^{-1}.

^{1}H NMR (400 MHz) δ (*d_6*-DMSO): 8.66 (1H, t, *J* = 6 Hz, -CON*H*-), 8.27 (1H, d, *J* = 7.6 Hz, -CON*H*-), 7.80 (2H, d, *J* = 8.4 Hz, ArH), 7.62 (2H, d, *J* = 8.8 Hz, ArH), 4.89 {2H, t, *J* = 2 Hz, *ortho* on (η^5-C_5H_4)}, 4.41 {2H, t, *J* = 2 Hz, *meta* on (η^5-C_5H_4)}, 4.27-4.21 {1H, m, -C*H*(C_4H_9)}, 4.11-4.07 (2H, m, -OC*H_2*CH_3), 4.02 {5H, s, (η^5-C_5H_5)}, 3.99-3.90 (2H, m, -NHC*H_2*CO-), 1.73-1.61 {2H, m, -CH(C*H_2*$CH_2CH_2CH_3$)}, 1.32-1.24 {4H, m, -CH(CH_2C*H_2*C*H_2*CH_3)}, 1.18 (3H, t, *J* = 7.2 Hz, -OCH_2C*H_3*), 0.86 {3H, t, *J* = 6.4 Hz, -CH($CH_2CH_2CH_2$C*H_3*)}.

^{13}C NMR (100 MHz) δ (*d_6*-DMSO): 172.1, 169.2, 166.5, 142.7, 131.1, 127.4, 125.3, 83.2, 69.5, 66.6, 66.5, 60.4 (-ve DEPT), 51.9, 42.1 (-ve DEPT), 30.7 (-ve DEPT), 27.4 (-ve DEPT), 21.7 (-ve DEPT), 14.0, 13.7.

Analysis:	found:	C, 63.96; H, 6.50; N, 5.41;
$C_{26}H_{30}FeN_2O_4$	requires:	C, 64.29; H, 6.39; N, 5.55;
Mass spectrum:	found: $[M]^{+\bullet}$	504.1702
$C_{27}H_{32}FeN_2O_4$	requires:	504.1711

***N*-{*para*-(ferrocenyl)-benzoyl}-β-alanine-L-alanine ethyl ester 78.**

For compound **78** β-alanine-L-alanine ethyl ester (0.18 g, 0.95 mmol) was used as a starting material. The product was purified by column chromatography (eluant 1:1 hexane:ethyl acetate). Recrystallization from ethyl acetate furnished the product as an orange powder (0.19 g, 52%). m.p. 167-169 ^{o}C; E$^{o\prime}$ = 70 mV (vs Fc/Fc^{+}); $[\alpha]_D^{20}$ = -23^{o} (c 2, EtOH).

UV-Vis λ_{max} ACN: 349, 450 nm.

I.R. ν_{max} (KBr): 3255, 3080, 2980, 2869, 1655, 1518, 1428, 1197, 885 cm^{-1}.

^{1}H NMR (400 MHz) δ (*d*$_6$-DMSO): 8.44 (1H, t, *J* = 5.6 Hz, -CON*H*-), 8.36 (1H, d, *J* = 6.8 Hz, -CON*H*-), 7.71 (2H, d, *J* = 8.4 Hz, ArH), 7.59 (2H, d, *J* = 8.4 Hz, ArH), 4.88 {2H, t, *J* = 1.6 Hz, *ortho* on (η^5-C_5H_4)}, 4.41 {2H, t, *J* = 2 Hz, *meta* on (η^5-C_5H_4)}, 4.24 {1H, quint, *J* = 7.2 Hz, -C*H*(CH_3)}, 4.13-4.04 (2H, m, -OC*H*$_2$$CH_3$), 4.02 {5H, s, ($\eta^5$-$C_5H_5$)}, 3.46 (2H, q, *J* = 7.2 Hz, -NHC*H*$_2$$CH_2$CO-), 2.43 (2H, t, *J* = 7.6 Hz, -NHCH$_2$C*H*$_2$CO-), 1.26 {3H, d, *J* = 7.2 Hz, -CH(C*H*$_3$)}, 1.16 (3H, t, *J* = 6.8 Hz, -OCH$_2$C*H*$_3$).

^{13}C NMR (100 MHz) δ (*d*$_6$-DMSO): 172.7, 170.4, 166.0, 142.5, 131.5, 127.3, 125.3, 83.2, 69.5, 69.4, 66.6, 60.4 (-ve DEPT), 47.6, 35.9 (-ve DEPT), 34.9 (-ve DEPT), 16.9, 14.0.

***N*-{*para*-(ferrocenyl)-benzoyl}-β-alanine- L-2-aminobutyric acid ethyl ester 79.**

For compound **79** β-alanine- L-2-aminobutyric acid ethyl ester (0.20 g, 1 mmol) was used as a starting material. The product was purified by column chromatography (eluant 1:1 hexane:ethyl acetate). Recrystallization from ethyl acetate furnished the product as an orange powder (0.19 g, 50%). m.p. 156-158 ^oC; $E^{o\prime}$ = 71 mV (vs Fc/Fc^+); $[\alpha]_D^{20}$ = -42^o (c 2, EtOH).

UV-Vis λ_{max} ACN: 349, 450 nm.

I.R. ν_{max} (KBr): 3261, 3081, 2971, 1742, 1578, 1376, 1322, 1189, 1104, 914 cm^{-1}.

^{1}H NMR (400 MHz) δ (*d*$_6$-DMSO): 8.52 (1H, t, *J* = 5.2 Hz, -CON*H*-), 8.36 (1H, d, *J* = 7.6 Hz, -CON*H*-), 7.81 (2H, d, *J* = 8.4 Hz, ArH), 7.66 (2H, d, *J* = 8.4 Hz, ArH), 4.95 {2H, t, *J* = 1.6 Hz, *ortho* on (η^5-C_5H_4)}, 4.47 {2H, t, *J* = 1.6 Hz, *meta* on (η^5-C_5H_4)}, 4.24 {1H, m, -C*H*(C_2H_5)}, 4.17-4.09 (2H, m, -OC*H*$_2$$CH_3$), 4.08 {5H, s, ($\eta^5$-$C_5H_5$)}, 3.53 (2H, q, *J* = 7.2 Hz, -NHC*H*$_2$$CH_2$CO-), 2.52 (2H, t, *J* = 7.2 Hz, -NHCH$_2$C*H*$_2$CO-), 1.79-1.65 {2H, m, -CH(C*H*$_2$$CH_3$)}, 1.23 (3H, t, *J* = 7.2 Hz, -OC*H*$_2$C*H*$_3$), 0.94 {3H, t, *J* = 7.2 Hz, -CH(CH$_2$C*H*$_3$)}.

^{13}C NMR (100 MHz) δ (d_6-DMSO): 172.1, 170.7, 166.0, 142.5, 131.5, 127.3, 125.3, 83.2, 69.5, 69.4, 66.6, 60.2 (-ve DEPT), 53.4, 35.9 (-ve DEPT), 34.9 (-ve DEPT), 24.2 (-ve DEPT), 14.0, 10.3.

***N*-{*para*-(ferrocenyl)-benzoyl}-β-alanine- L-norvaline ethyl ester 80.**

For compound **80** β-alanine-L-norvaline ethyl ester (0.21 g, 0.95 mmol) was used as a starting material. The product was purified by column chromatography (eluant 1:1 hexane:ethyl acetate). Recrystallization from ethyl acetate furnished the product as an orange powder (0.20 g, 51%). m.p. 137-139 ^{o}C; E°´ = 73 mV (vs Fc/Fc^{+}); $[\alpha]_D^{20}$ = +23^{o} (c 2, EtOH).

UV-Vis λ_{max} ACN: 349, 450 nm.

I.R. ν_{max} (KBr): 3310, 3254, 3078, 1741, 1655, 1521, 1389, 1303, 1106 cm^{-1}.

^{1}H NMR (400 MHz) δ (d_6-DMSO): 8.50 (1H, t, *J* = 5.6 Hz, -CON*H*-), 8.36 (1H, d, *J* = 7.6 Hz, -CON*H*-), 7.84 (2H, d, *J* = 8.4 Hz, ArH), 7.65 (2H, d, *J* = 8.4 Hz, ArH), 4.94 {2H, t, *J* = 2 Hz, *ortho* on (η^5-C_5H_4)}, 4.47 {2H, t, *J* = 1.6 Hz, *meta* on (η^5-C_5H_4)}, 4.31-4.08 {8H, m, -C*H*(C_3H_7), -O$CH_2$$CH_3$, ($\eta^5$-$C_5H_5$)}, 3.52 (2H, q, *J* = 7.2 Hz, -NHC$H_2$$CH_2$CO-), 2.53-2.49 (2H, m, -NHCH_2CH_2CO-), 1.72-1.59 (2H, m, -CH(C$H_2$$CH_2$$CH_3$)}, 1.39-1.31 {2H, m, -CH(CH_2C$H_2$$CH_3$)}, 1.23 (3H, t, *J* = 6.8 Hz, -OCH_2CH_3), 0.93 (3H, t, *J* = 7.2 Hz, -CH($CH_2$$CH_2CH_3$)}.

^{13}C NMR (100 MHz) δ (d_6-DMSO): 172.3, 170.7, 166.0, 142.5, 131.5, 127.3, 125.3, 83.2, 69.5, 69.4, 66.0, 60.3 (-ve DEPT), 51.7, 36.0 (-ve DEPT), 34.9 (-ve DEPT), 32.9 (-ve DEPT), 18.6 (-ve DEPT), 14.0, 13.4.

***N*-{*para*-(ferrocenyl)-benzoyl}-β-alanine-L-norleucine ethyl ester 81.**

For compound **81** β-alanine-L-norleucine ethyl ester (0.22 g, 0.95 mmol) was used as a starting material. The product was purified by column chromatography (eluant 1:1 hexane:ethyl acetate). Recrystallization from ethyl acetate furnished the product as an orange powder (0.24 g, 54%). m.p. 142-144 ^{o}C; E°´ = 78 mV (vs Fc/Fc^{+}); $[\alpha]_D^{20}$ = +17^{o} (c 2, EtOH).

UV-Vis λ_{max} ACN: 349, 450 nm.

I.R. ν_{max} (KBr): 3260, 2759, 2345, 1648, 1542, 1300, 1104, 1032 cm^{-1}.

^{1}H NMR (400 MHz) δ (*d*$_6$-DMSO): 8.50 (1H, t, *J* = 5.6 Hz, -CON*H*-), 8.36 (1H, d, *J* = 7.6 Hz, -CON*H*-), 7.81 (2H, d, *J* = 8.4 Hz, ArH), 7.65 (2H, d, *J* = 8.4 Hz, ArH), 4.94 {2H, t, *J* = 1.6 Hz, *ortho* on (η^5-C_5H_4)}, 4.47 {2H, t, *J* = 1.6 Hz, *meta* on (η^5-C_5H_4)}, 4.29-4.24 {1H, m, -C*H*(C_4H_9)}, 4.18-4.10 (2H, m, -OC*H*$_2$$CH_3$), 4.08 {5H, s, ($\eta^5$-$C_5H_5$)}, 3.53 (2H, q, *J* = 7.2 Hz, -NHC*H*$_2$$CH_2CO$-), 2.53-2.49 (2H, m, -$NHCH_2$C*H*$_2$CO-), 1.73-1.61 {2H, m, -CH(C*H*$_2$$CH_2CH_2CH3$)}, 1.35-1.27 {4H, m, -CH(CH_2C*H*$_2$C*H*$_2$$CH_3$)}, 1.23 (3H, t, *J* = 7.2 Hz, -OCH_2C*H*$_3$), 0.89 {3H, t, *J* = 7.2 Hz, -CH($CH_2CH_2CH_2$C*H*$_3$)}.

^{13}C NMR (100 MHz) δ (*d*$_6$-DMSO): 172.3, 170.7, 166.0, 142.5, 131.5, 127.2, 125.3, 83.2, 69.5, 69.4, 66.6, 60.3 (-ve DEPT), 51.9, 36.0 (-ve DEPT), 35.0 (-ve DEPT), 30.5 (-ve DEPT), 27.5(-ve DEPT), 21.7 (-ve DEPT), 14.0, 13.7.

***N*-{*para*-(ferrocenyl)-benzoyl}-γ-aminobutyric acid-L-alanine ethyl ester 82.**

For compound **82** γ-aminobutyric acid-L-alanine ethyl ester (0.19 g, 0.95 mmol) was used as a starting material. The product was purified by column chromatography (eluant 1:1 hexane:ethyl acetate). Recrystallization from ethyl acetate furnished the product as an orange powder (0.19 g, 47%). m.p. 144-146 ^oC; $E^{o\prime}$ = 74 mV (vs Fc/Fc^+); $[\alpha]_D^{20}$ = -39^o (c 2, EtOH).

UV-Vis λ_{max} ACN: 349, 450 nm.

I.R. ν_{max} (KBr): 3292, 3058, 1746, 1559, 1458, 1320, 1206, 1103 cm^{-1}.

^{1}H NMR (400 MHz) δ (*d*$_6$-DMSO): 8.43 (1H, t, *J* = 5.2 Hz, -CON*H*-), 8.28 (1H, d, *J* = 6.8 Hz, -CON*H*-), 7.76 (2H, d, *J* = 8.4 Hz, ArH), 7.60 (2H, d, *J* = 8.4 Hz, ArH), 4.88 {2H, t, *J* = 2 Hz, *ortho* on (η^5-C_5H_4)}, 4.41 {2H, t, *J* = 2 Hz, *meta* on (η^5-C_5H_4)}, 4.23 {1H, quint, *J* = 7.2 Hz, -C*H*(CH_3)}, 4.10-4.00 {7H, m, (η^5-C_5H_5), -OC*H*$_2$$CH_3$}, 3.30-3.26 (2H, m, -NHC*H*$_2$$CH_2CH_2CO$-), 2.18 (2H, t, *J* = 7.2 Hz, -$NHCH_2CH_2$C*H*$_2$CO-), 1.75 (2H, quint, *J* = 7.2 Hz, $NHCH_2$C*H*$_2$$CH_2$CO-), 1.25 {3H, d, *J* = 7.2 Hz, -C*H*(CH_3)}, 1.18 (3H, t, *J* = 6.8 Hz, -OCH_2C*H*$_3$).

^{13}C NMR (100 MHz) δ (*d*$_6$-DMSO): 172.7, 171.9, 166.1, 142.5, 131.7, 127.3, 125.3, 83.3, 69.5, 69.4, 66.6, 60.3 (-ve DEPT), 47.6, 38.8 (-ve DEPT), 32.6 (-ve DEPT), 25.3 (-ve DEPT), 16.9, 14.0.

***N*-{*para*-(ferrocenyl)-benzoyl}-γ-aminobutyric acid-L-2-aminobutyric acid ethyl ester 83.**

For compound **83** γ-aminobutyric acid-L-2-aminobutyric acid ethyl ester (0.20 g, 1mmol) was used as a starting material. The product was purified by column chromatography (eluant 1:1 hexane:ethyl acetate). Recrystallization from ethyl acetate furnished the product as an orange powder (0.16 g, 39%). m.p. 171-173 ^{o}C; E$^{o\prime}$ = 71 mV (vs Fc/Fc^{+}); $[\alpha]_D^{20}$ = -12^{o} (c 2, EtOH).

UV-Vis λ_{max} ACN: 349, 450 nm.

I.R. ν_{max} (KBr): 3284, 3058, 2345, 1749, 1655, 1655, 1559, 1330, 1160, 1018 cm^{-1}.

^{1}H NMR (400 MHz) δ (*d*$_6$-DMSO): 8.50 (1H, t, *J* = 5.6 Hz, -CON*H*-), 8.29 (1H, d, *J* = 7.6 Hz, -CON*H*-), 7.82 (2H, d, *J* = 8.4 Hz, ArH), 7.64 (2H, d, *J* = 8.4 Hz, ArH), 4.94 {2H, t, *J* = 1.6 Hz, *ortho* on (η^5-C_5H_4)}, 4.47 {2H, t, *J* = 2 Hz, *meta* on (η^5-C_5H_4)}, 4.22-4.08 {8H, m, (η^5-C_5H_5), -OC*H*$_2$CH$_3$, -C*H*(C_2H_5)}, 3.35-3.32 (2H, m, -NHC*H*$_2$CH$_2$CH$_2$CO-), 2.27 (2H, t, *J* = 7.2 Hz, -NHCH$_2$CH$_2$C*H*$_2$CO-), 1.85-1.63 {4H, m, -NHCH$_2$C*H*$_2$CH$_2$CO-, -CH(C*H*$_2$CH$_3$)}, 1.24 (3H, t, *J* = 7.2 Hz, -OCH$_2$C*H*$_3$), 0.95 {3H, t, *J* = 7.2 Hz, -CH(CH$_2$C*H*$_3$)}.

^{13}C NMR (100 MHz) δ (*d*$_6$-DMSO): 172.2, 169.4, 166.0, 142.4, 131.6, 127.3, 125.3, 83.3, 69.5, 69.4, 66.6, 60.3 (-ve DEPT), 53.4, 38.8 (-ve DEPT), 32.6 (-ve DEPT), 25.4 (-ve DEPT), 24.2 (-ve DEPT), 14.1 10.3.

***N*-{*para*-(ferrocenyl)-benzoyl}-γ-aminobutyric acid-L-norvaline ethyl ester 84.**

For compound **84** γ-aminobutyric acid-L-norvaline ethyl ester (0.20g, 0.95 mmol) was used as a starting material. The product was purified by column chromatography (eluant 1:1 hexane:ethyl acetate). Recrystallization from ethyl acetate furnished the product as an orange powder (0.20 g, 47%). m.p. 188-190 ^{o}C; E$^{o\prime}$ = 69 mV (vs Fc/Fc^{+}); $[\alpha]_D^{20}$ = +14^{o} (c 2, EtOH).

UV-Vis λ_{max} ACN: 349, 450 nm.

I.R. ν_{max} (KBr): 3293, 3065, 2870, 1910, 1663, 1380, 1199, 1161, 1103 cm^{-1}.

^{1}H NMR (400 MHz) δ (*d*$_6$-DMSO): 8.50 (1H, t, *J* = 5.6 Hz, -CON*H*-), 8.29 (1H, d, *J* = 7.6 Hz, -CON*H*-), 7.82 (2H, d, *J* = 8.4 Hz, ArH), 7.66 (2H, d, *J* = 8.4 Hz, ArH), 4.94

{2H, t, *J* = 2 Hz, *ortho* on (η^5-C_5H_4)}, 4.47 {2H, t, *J* = 2 Hz, *meta* on (η^5-C_5H_4)}, 4.28-4.23 {1H, m, -C*H*(C_3H_7)}, 4.18-4.08 {7H, m, (η^5-C_5H_5), -OC*H*$_2$$CH_3$}, 3.37-3.30 (2H, m, -NHC*H*$_2$$CH_2CH_2CO$-), 2.26 (2H, t, *J* = 7.6 Hz, -$NHCH_2CH_2CH_2$CO-), 1.82 (2H, quint, *J* = 6.8 Hz, $NHCH_2CH_2CH_2$CO-), 1.73-1.59 {2H, m, -CH(C*H*$_2$$CH_2CH_3$)}, 1.44-1.33 {2H, m, -CH(CH_2C*H*$_2$$CH_3$)}, 1.24 (3H, t, *J* = 7.2 Hz, -OCH_2C*H*$_3$), 0.93 {3H, t, *J* = 7.2 Hz, -CH(CH_2CH_2C*H*$_3$)}.

^{13}C NMR (100 MHz) δ (*d*$_6$-DMSO): 172.4, 169.5, 166.0, 142.4, 131.7, 127.3, 125.3, 83.3, 69.5, 69.4, 66.6, 60.3 (-ve DEPT), 51.7, 38.8 (-ve DEPT), 32.9 (-ve DEPT), 32.6 (-ve DEPT), 25.4 (-ve DEPT), 18.6 (-ve DEPT), 14.1, 13.4.

***N*-{*para*-(ferrocenyl)-benzoyl}-γ-aminobutyric acid-L-norleucine ethyl ester 85.**

For compound **85** γ-aminobutyric acid-L-norleucine ethyl ester (0.22 g, 0.95 mmol) was used as a starting material. The product was purified by column chromatography (eluant 1:1 hexane:ethyl acetate). Recrystallization from ethyl acetate furnished the product as an orange powder (0.21 g, 48%). m.p. 166-168 ^{o}C; E$^{o\prime}$ = 70 mV (vs Fc/Fc^+); $[\alpha]_D^{20}$ = -11^{o} (c 2, EtOH).

UV-Vis λ_{max} ACN: 349, 451 nm.

I.R. ν_{max} (KBr): 3315, 2931, 1751, 1522, 1509, 1376, 1220, 1191, 1018 cm^{-1}.

^{1}H NMR (400 MHz) δ (*d*$_6$-DMSO): 8.49 (1H, t, *J* = 5.6 Hz, -CON*H*-), 8.30 (1H, d, *J* = 7.6 Hz, -CON*H*-), 7.82 (2H, d, *J* = 8.4 Hz, ArH), 7.66 (2H, d, *J* = 8.8 Hz, ArH), 4.94 {2H, t, *J* = 2 Hz, *ortho* on (η^5-C_5H_4)}, 4.47 {2H, t, *J* = 2 Hz, *meta* on (η^5-C_5H_4)}, 4.26-4.21 {1H, m, -C*H*(C_4H_9)}, 4.18-4.11 (2H, m, -OC*H*$_2$$CH_3$), 4.08 {5H, s, ($\eta^5$-$C_5H_5$)}, 3.36-3.30 (2H, m, -NHC*H*$_2$$CH_2CH_2CO$-), 2.26 (2H, t, *J* = 7.2 Hz, -$NHCH_2CH_2CH_2$CO-), 1.80 (2H, quint, *J* = 7.2 Hz, -$NHCH_2CH_2CH_2$CO-), 1.75-1.60 {2H, m, -CH(C*H*$_2$$CH_2CH_2CH_3$)}, 1.39-1.30 {4H, m, -CH(CH_2C*H*$_2$C*H*$_2$$CH_3$)}, 1.24 (3H, t, *J* = 7.2 Hz, -OCH_2C*H*$_3$), 0.92 {3H, t, *J* = 6.8 Hz, -CH($CH_2CH_2CH_2$C*H*$_3$)}.

^{13}C NMR (100 MHz) δ (*d*$_6$-DMSO): 172.4, 169.5, 166.0, 142.2, 131.7, 127.3, 125.3, 83.3, 69.5, 69.4, 66.6, 60.3 (-ve DEPT), 51.9, 38.8 (-ve DEPT), 32.6 (-ve DEPT), 30.5 (-ve DEPT), 27.5 (-ve DEPT), 25.4 (-ve DEPT), 21.7 (-ve DEPT), 14.1, 13.7.

General procedure for the preparation of N-(ferrocenyl)benzoyl tri- and tetrapeptide esters.

***N*-{*ortho*-(ferrocenyl)-benzoyl}-glycyl-glycyl-glycine ethyl ester 86.**

1-Hydroxybenzotriazole (0.189 g, 1.4 mmol) was added to a solution of *ortho*-ferrocenyl benzoic acid (0.245 g, 0.8 mmol), *N*-(3-dimethylaminopropyl)-*N*'-ethylcarbodiimide hydrochloride (0.267 g 1.4 mmol) and triethylamine (2 mls) in dichloromethane (40 mls) at 0 ^{o}C. After 30 minutes glycyl-glycyl-glycine ethyl ester hydrochloride (0.23 g, 0.9 mmol) was added and the reaction was stirred at room temperature for 48 hours. The reaction mixture was washed with water, 10% potassium hydrogen carbonate and 5% citric acid. The organic layer was dried over $MgSO_4$ and the solvent was removed *in vacuo*. The product was purified by column chromatography (eluant: ethyl acetate). Recrystallization from ethyl acetate furnished the product as an orange solid (0.24 g, 59%). m.p. 138-140 ^{o}C; $E^{o\prime}$ = 39 mV (vs Fc/Fc^{+}).

UV-Vis λ_{max} ACN: 335, 450 nm.

I.R. ν_{max} (KBr): 3293, 2927, 2851, 1737, 1691, 1516, 1426, 1277, 1104 cm^{-1}.

^{1}H NMR (400 MHz) δ (*d*$_6$-DMSO): 8.54 (1H, t, *J* = 6 Hz, -CON*H*-), 8.32 (1H, t, *J* = 5.6 Hz, -CON*H*-), 8.13 (1H, t, *J* = 6 Hz, -CON*H*-), 7.85 (1H, d, *J* = 7.6 Hz, ArH), 7.42 (1H, t, *J* = 4.8 Hz, ArH), 7.38-7.22 (2H, m, ArH), 4.65 {2H, t, *J* = 1.6 Hz, *ortho* on (η^5-C_5H_4)}, 4.26 {2H, t, *J* = 1.6 Hz, *meta* on (η^5-C_5H_4)}, 4.05 {7H, m, (η^5-C_5H_5), -OC*H*$_2$CH$_3$}, 3.83-3.78 (6H, m, -NHC*H*$_2$CO-), 1.17 (3H, t, *J* = 7.2 Hz, -OCH$_2$C*H*$_3$)

^{13}C NMR (100 MHz) δ (*d*$_6$-DMSO): 170.1, 169.6, 169.3, 169.1, 136.2, 136.0, 130.6, 128.7, 127.4, 125.4, 84.4, 69.4, 68.8, 68.2, 60.4 (-ve DEPT), 42.3 (-ve DEPT), 41.7 (-ve DEPT), 40.6 (-ve DEPT), 14.0.

Analysis:	found:	C, 59.72; H, 5.56; N, 8.75,
$C_{25}H_{27}FeN_3O_5$	requires:	C, 59.42; H, 5.39; N, 8.32.
Mass spectrum:	found: $[M+Na]^{+}$	528.20,
$C_{25}H_{27}N_3O_5FeNa$	requires:	528.12.

***N*-{*meta*-(ferrocenyl)-benzoyl}-glycyl-glycyl-glycine ethyl ester 87.**

For compound **87** *meta*-ferrocenyl benzoic acid (0.24 g, 0.8 mmol) was used as a starting material. Recrystallization from ethyl acetate furnished the product as a yellow solid (0.26 g, 64%). m.p. 166-168 ^{o}C; $E^{o\prime}$ = 55 mV (vs Fc/Fc^{+}).

UV-Vis λ_{max} ACN: 325, 450 nm.

I.R. ν_{max} (KBr): 3229, 3079, 1831, 1725, 1740, 1603, 1335, 1118, 1105 cm^{-1}.

^{1}H NMR (400 MHz) δ (*d_6*-DMSO): 8.89 (1H, t, *J* = 6 Hz, -CON*H*-), 8.32-8.29 (2H, m, -CON*H*-), 8.01 (1H, s, ArH), 7.75-7.70 (2H, m, ArH), 7.43 (1H, t, *J* = 8 Hz, ArH), 4.86 {2H, t, *J* = 2 Hz, *ortho* on (η^5-C_5H_4)}, 4.40, {2H, t, *J* = 1.6 Hz, *meta* on (η^5-C_5H_4)}, 4.12, (2H, q, *J* = 7.2 Hz, -OC*H_2*CH_3), 4.04 {5H, s, (η^5-C_5H_5)}, 3.95 (2H, d, *J* = 6 Hz, -NHC*H_2*CO-), 3.86 (2H, d, *J* = 6 Hz, -NHC*H_2*CO-), 3.77 (2H, d, *J* = 6 Hz, -NHC*H_2*CO-), 1.20 (3H, t, *J* = 7.2 Hz -OCH_2C*H_3*).

^{13}C NMR (100 MHz) δ (*d_6*-DMSO): 170.0, 169.7, 169.4, 166.6, 139.2, 133.9, 128.8, 128.4, 124.9, 124.3, 83.9, 69.4, 69.1, 66.4, 60.4 (-ve DEPT), 42.8 (-ve DEPT), 41.7 (-ve DEPT), 40.6 (-ve DEPT), 14.0.

Analysis:	found:	C, 59.08; H, 5.22; N, 8.64;
$C_{25}H_{27}FeN_3O_5$	requires:	C, 59.42; H, 5.39; N, 8.32;
Mass spectrum:	found: $[M+Na]^{+}$	528.20
$C_{25}H_{27}N_3O_5FeNa$	requires:	528.12

***N*-{*para*-(ferrocenyl)-benzoyl}-glycyl-glycyl-glycine ethyl ester 88.**

For compound **88** *para*-ferrocenyl benzoic acid (0.21g, 0.7 mmol) was used as a starting material. Recrystallization from ethyl acetate furnished the product as an orange solid. (0.22 g, 62%). m.p. 206-208 ^{o}C; $E^{o\prime}$ = 73 mV (vs Fc/Fc^{+}).

UV-Vis λ_{max} ACN: 355, 450 nm.

I.R. ν_{max} (KBr): 3275, 3090, 2987, 2345, 1751, 1607, 1519, 1378, 1249, 1028, 993 cm^{-1}.

^{1}H NMR (400 MHz) δ (*d_6*-DMSO): 8.79 (1H, t, *J* = 6 Hz, -CON*H*-), 8.30 (2H, t, *J* = 6.4 Hz, -CON*H*-), 7.83 (2H, d, *J* = 8.4 Hz, ArH), 7.65 (2H, d, *J* = 8.4 Hz, ArH), 4.90 {2H, t, *J* = 2 Hz, *ortho* on (η^5-C_5H_4)}, 4.41 {2H, t, *J* = 1.6 Hz, *meta* on (η^5-C_5H_4)}, 4.10 (2H, q, *J* = 7.2 Hz, -OC*H_2*CH_3), 4.02 {5H, s, (η^5-C_5H_5)}, 3.92 (2H, d, *J* = 5.6 Hz, -NHC*H_2*CO-),

3.86 (2H, d, *J* = 6 Hz, -NHC*H*$_2$CO-), 3.76 (2H, d, *J* = 6 Hz, -NHC*H*$_2$CO-), 1.19 (3H, t, *J* = 6.8 Hz -OCH$_2$C*H*$_3$).

^{13}C NMR (100 MHz) δ (*d*$_6$-DMSO): 169.7, 169.5, 169.4, 166.5, 142.8, 130.9, 127.5, 125.3, 83.1, 69.5, 66.6, 66.4, 60.4 (-ve DEPT), 42.7 (-ve DEPT), 41.7 (-ve DEPT), 40.6 (-ve DEPT), 14.0.

Analysis:	found:	C, 59.32; H, 5.47; N, 7.91,
$C_{25}H_{27}FeN_3O_5$	requires:	C, 59.42; H, 5.39; N, 8.32.
Mass spectrum:	found: $[M+Na]^+$	528.20,
$C_{25}H_{27}N_3O_5FeNa$	requires:	528.12.

***N*-{*ortho*-(ferrocenyl)-benzoyl}-glycyl-glycyl-glycyl-glycine ethyl ester 89.**

For compound **89** *ortho*-ferrocenyl benzoic acid (0.18 g, 0.6 mmol) and glycyl-glycyl-glycyl-glycine ethyl ester hydrochloride (0.18 g, 0.6 mmol) were used as starting materials. The product was purified by column chromatography (eluant 9:1 ethyl acetate:methanol). Recrystallization from ethyl acetate furnished the product as an orange solid (0.10 g, 30%). m.p. 168-170 ^{o}C; E$^{o\prime}$ = 44 mV (vs Fc/Fc$^+$).

UV-Vis λ_{max} ACN: 332, 445 nm.

I.R. ν_{max} (KBr): 3293, 3083, 2346, 1522, 1430, 1407, 1211, 1105, 1011 cm^{-1}.

^{1}H NMR (400 MHz) δ (*d*$_6$-DMSO): 8.50 (1H, t, *J* = 6 Hz, -CON*H*-), 8.35-8.29 (2H, m, -CON*H*-), 8.17 (1H, t, *J* = 5.6 Hz, -CON*H*-), 7.87 (1H, d, *J* = 7.6 Hz, ArH), 7.47 (1H, t, *J* = 4.8 Hz, ArH), 7.35-7.31 (2H, m, ArH), 4.71 {2H, *J* = 2 Hz, *ortho* on (η^5-C$_5$H$_4$)}, 4.33 {2H, t, *J* = 2 Hz, *meta* on (η^5-C$_5$H$_4$)}, 4.17-4.11 {7H, m, (η^5-C$_5$H$_5$), -OC*H*$_2$CH$_3$}, 3.91 (4H, t, *J* = 4.8 Hz, -NHC*H*$_2$CO-), 3.86 (2H, d, *J* = 5.6 Hz, -NHC*H*$_2$CO-), 3.81 (2H, d, *J* = 6 Hz, -NHC*H*$_2$CO-), 1.25 (3H, t, *J* = 7.2 Hz, -OCH$_2$C*H*$_3$).

^{13}C NMR (100 MHz) δ (*d*$_6$-DMSO): 170.1, 169.6, 169.3, 169.2, 169.1, 136.2, 136.0, 130.0, 128.7, 127.4, 125.4, 84.4, 69.4, 68.7, 68.2, 60.4 (-ve DEPT), 42.3 (-ve DEPT), 42.1 (-ve DEPT), 41.7 (-ve DEPT), 40.6 (-ve DEPT), 14.0.

Analysis:	found:	C, 57.18; H, 5.53; N, 9.75,
$C_{27}H_{30}FeN_4O_6$	requires:	C, 57.66; H, 5.38; N, 9.96.
Mass spectrum:	found: $[M+Na]^+$	585.20,

$C_{27}H_{30}N_4O_6FeNa$ requires: 585.12.

***N*-{*meta*-(ferrocenyl)-benzoyl}-glycyl-glycyl-glycyl-glycine ethyl ester 90.**

For compound **90** *meta*-ferrocenyl benzoic acid (0.18 g, 0.6 mmol) was used as a starting material. Recrystallization from ethyl acetate furnished the product as a yellow solid (0.09 g, 27%). m.p. 171-173 ^{o}C; E°´ = 58 mV (vs Fc/Fc^{+}).

UV-Vis λ_{max} ACN: 330, 450 nm.

I.R. ν_{max} (KBr): 3280, 3084, 2366, 1735, 1559, 1458, 1376, 1283, 1204, 1148 cm^{-1}.

^{1}H NMR (400 MHz) δ (d_6-DMSO): 8.95 (1H, t, *J* = 4.4 Hz, -CON*H*-), 8.34 (2H, q, *J* = 3.2 Hz, -CON*H*-), 8.29 (2H, t, *J* = 6 Hz, -CON*H*-), 8.01 (1H, s, ArH), 7.87-7.79 (2H, m, ArH), 7.47 (1H, t, *J* = 7.6 Hz, ArH), 4.93 {2H, t, *J* = 1.6 Hz, *ortho* on (η^5-C_5H_4)}, 4.46 {2H, t, *J* = 1.6 Hz, *meta* on (η^5-C_5H_4)}, 4.15 (2H, q, *J* = 7.2 Hz, -OC$H_2$$CH_3$), 4.10 {5H, s, ($\eta^5$-$C_5H_5$)}, 4.02 (2H, d, *J* = 5.6 Hz, -NHCH_2CO-), 3.89-3.82 (6H, m, -NHCH_2CO-), 1.25 (3H, t, *J* = 7.2 Hz, -OCH$_2$CH_3).

^{13}C NMR (100 MHz) δ (d_6-DMSO): 169.6, 169.5, 169.3, 169.1, 166.6, 139.2, 133.9, 128.8, 128.4, 124.9, 124.3, 84.0, 69.4, 69.1, 66.4, 60.4 (-ve DEPT), 42.8 (-ve DEPT), 42.1 (-ve DEPT), 41.7 (-ve DEPT), 40.6 (-ve DEPT), 14.0.

Analysis: found: C, 57.57; H, 5.74; N, 10.09,

$C_{27}H_{30}FeN_4O_6$ requires: C, 57.66; H, 5.38; N, 9.96.

Mass spectrum: found: $[M+Na]^{+}$ 585.20,

$C_{27}H_{30}N_4O_6FeNa$ requires: 585.12.

***N*-{*para*-(ferrocenyl)benzoyl}-glycyl-glycyl-glycyl-glycine ethyl ester 91.**

For compound **91** *para*-ferrocenyl benzoic acid (0.18g, 0.6 mmol) was used as a starting material. Recrystallization from ethyl acetate furnished the product as an orange solid (0.10 g, 30%). m.p. 160-162 ^{o}C; E°´ = 75 mV (vs Fc/Fc^{+}).

UV-Vis λ_{max} ACN: 349, 450 nm.

I.R. ν_{max} (KBr): 3270, 2937, 2739, 2345, 1719, 1542, 1474, 1283, 1120, 1035 cm^{-1}.

^{1}H NMR (400 MHz) δ (d_6-DMSO): 8.83 (1H, t, *J* = 5.6 Hz, -CON*H*-), 8.29-8.21 (3H, m, -CON*H*-), 7.83 (2H, d, *J* = 8.4 Hz ArH), 7.64 (2H, d, *J* = 8.4 Hz ArH), 4.90 {2H, t, *J* =

1.6 Hz, *ortho* on (η^5-C_5H_4)}, 4.41 {2H, t, *J* = 1.6 Hz, *meta* on (η^5-C_5H_4)}, 4.01 (2H, q, *J* = 6.8 Hz, -OC*H*$_2$CH$_3$), 3.93 (2H, d, *J* = 5.6 Hz -NHC*H*$_2$CO-), 3.82 (2H, d, *J* = 6 Hz, -NHC*H*$_2$CO-), 3.76 (4H, t, *J* = 6.4 Hz, -NHC*H*$_2$CO-), 1.18 (3H, t, *J* = 7.2 Hz, -OCH$_2$C*H*$_3$).

^{13}C NMR (100 MHz) δ (*d*$_6$-DMSO): 169.60, 169.57, 169.3, 169.2, 166.5, 142.8, 131.1, 127.6, 125.3, 83.2, 69.53, 69.47, 66.6, 60.4 (-ve DEPT), 42.8 (-ve DEPT), 42.1 (-ve DEPT), 41.7 (-ve DEPT), 41.2 (-ve DEPT), 14.0.

Analysis:	found:	C, 57.96; H, 5.77; N, 10.18,
$C_{27}H_{30}FeN_4O_6$	requires:	C, 57.66; H, 5.38; N, 9.96.
Mass spectrum:	found: $[M+Na]^+$	585.20,
$C_{27}H_{30}N_4O_6FeNa$	requires:	585.12.

General procedure for the preparation of starting materials for 1,1'-N,N'-{ortho-(ferrocenyl)-bisbenzoyl} amino acid and dipeptide esters.

1,1'-*N,N'-ortho*-(ferrocenyl)bisethyl benzoate 92.

Concentrated hydrochloric acid (5 mls) was added to a solution of ethyl-2-aminobenzoate (3.90 g, 23.6 mmol) in 15 mls of deionized water. Sodium nitrite (1.78 g, 25.8 mmol) in 15 mls of deionized water was then added to this solution with stirring at a temperature of less than 5 ^{o}C. The resulting pale yellow diazonium salt was added to ferrocene (2.0 g, 10.8 mmol) in 50 mls of diethyl ether and allowed to react for 36 hours. The reaction was then washed with water and the organic layer was dried over $MgSO_4$. The solvent was removed *in vacuo*. Column chromatography {eluant 3:2 petroleum ether (40-60 ^{o}C) :diethyl ether} yielded the desired product as a red solid. (0.84 g, 16%).

UV-Vis λ_{max} ACN: 338, 445 nm.

^{1}H NMR (400 MHz) δ (*d*$_6$-DMSO): 7.68 (2H, d, *J* = 4.8 Hz, ArH), 7.41-7.39 (4H, m, ArH), 7.30 (2H, t, *J* = 7.8 Hz, ArH) 4.33 {4H, t, *J* = 2 Hz, *ortho* on (η^5-C_5H_4)}, 4.27 {4H, t, *J* = 2 Hz, *meta* on (η^5-C_5H_4)}, 4.12 (4H, q, *J* = 7.2 Hz, -OC*H*$_2$CH$_3$), 1.10 (6H, t, *J* = 7.2 Hz, -OCH$_2$C*H*$_3$).

^{13}C NMR (100 MHz) δ (d_6-DMSO): 169.0, 136.5, 131.8, 130.8, 130.1, 127.8, 125.9, 85.7, 71.5, 70.5, 60.9 (-ve DEPT), 13.7.

1,1'-*N,N'-ortho*-(ferrocenyl)bisbenzoic acid 93.

1,1'-*N,N'-ortho*-(ferrocenyl)bisethyl benzoate (0.5 g, 1.17 mmol) in 15 mls of methanol was added to 15 mls of a 10% sodium hydroxide solution and refluxed for 3 hours. The solution was cooled in ice and concentrated HCl was added until pH 2 was reached. The product was isolated by filtration as an orange solid (0.24 g, 48%).

UV-Vis λ_{max} ACN: 339, 440 nm.

^{1}H NMR (400 MHz) δ (d_6-DMSO): 12.84 (2H, br s, -COO*H*), 7.68 (2H, d, *J* = 7.6 ArH), 7.38-7.33 (4H, m, ArH), 7.29 (2H, t, *J* = 6.4 Hz, ArH), 4.41 {4H, t, *J* = 2 Hz, *ortho* on (η^5-C_5H_4)}, 4.20 {4H, t, *J* = 2 Hz, *meta* on (η^5-C_5H_4).

^{13}C NMR (100 MHz) δ (d_6-DMSO): 170.7, 136.0, 133.0, 130.7, 129.5, 127.5, 125.8, 85.6, 70.6, 70.5.

General procedure for preparation of 1,1'-N,N'-{ortho-(ferrocenyl)-bisbenzoyl} amino acid and dipeptide esters.

1,1'-*N,N'*{-*ortho*-(ferrocenyl)-bisbenzoyl}-glycine ethyl ester 94.

1-Hydroxybenzotriazole (0.05 g, 0.37 mmol) was added to a solution of 1,1'-*N,N'-ortho*-(ferrocenyl) benzoic acid (0.08 g, 0.18 mmol), *N*-(3-dimethylaminopropyl)-*N*'-ethylcarbodiimide hydrochloride (0.07 g 0.36 mmol) and triethylamine (2 mls) in dichloromethane (40 mls) at 0 ^{o}C. After 30 minutes glycine ethyl ester hydrochloride (0.05 g, 0.4 mmol) was added and the reaction was stirred at room temperature for 48 hours. The reaction mixture was washed with water, 10% potassium hydrogen carbonate and 5% citric acid. The organic layer was dried over $MgSO_4$ and the solvent was removed *in vacuo*. The product was purified by column chromatography {eluant 1:1 petroleum ether (40-60 ^{o}C):ethyl acetate} and isolated as an orange oil (0.015 g, 14%).

$E^{o'}$ = 59 mV (vs Fc/Fc^+).

UV-Vis λ_{max} ACN: 330, 442 nm.

I.R. ν_{max} (KBr): 3568, 2921, 1790, 1658, 1568 cm^{-1}.

^{1}H NMR (400 MHz) δ (*d_6*-DMSO): 8.72 (2H, t, *J* = 5.6 Hz, -CON*H*-), 7.69 (2H, d, *J* = 8 Hz, ArH), 7.37 (2H, t, *J* = 6.8 Hz ArH), 7.26-7.19 (4H, m, ArH), 4.54 {4H, s, *ortho* on (η^5-C_5H_4)}, 4.13 (4H, q, *J* = 7.2 Hz, -OC*H_2*CH_3), 4.07 {4H, s, *meta* on (η^5-C_5H_4)}, 3.89 (4H, d, *J* = 5.6 Hz -NHC*H_2*CO-), 1.21 (6H, t, *J* = 7.2 Hz -OCH_2C*H_3*).

^{13}C NMR (100 MHz) δ (*d_6*-DMSO): 170.2, 169.7, 136.2, 135.7, 130.1, 128.9, 127.3, 125.4, 84.6, 70.9, 70.0, 60.5 (-ve DEPT), 41.0 (-ve DEPT), 14.0

1,1'-*N,N'*-{*ortho*-(ferrocenyl)-bisbenzoyl}-glycyl-glycine ethyl ester 95.

For compound **95** glycyl-glycine ethyl ester hydrochloride (0.09 g, 0.46 mmol) was used as a starting material. The product was purified by column chromatography {eluant 1:1 petroleum ether (40-60 ^oC):ethyl acetate}and isolated as an orange oil (0.05 g, 31%). E°´ = 61 mV (vs Fc/Fc^+).

UV-Vis λ_{max} ACN: 328, 440 nm.

I.R. ν_{max} (KBr): 3565, 2925, 1790, 1651, 1560 cm^{-1}.

^{1}H NMR (400 MHz) δ (*d_6*-DMSO): 8.50 (2H, t, *J* = 6 Hz, -CON*H*-), 8.22 (2H, t, *J* = 6 Hz, -CON*H*-), 7.68 (2H, d, *J* = 8 Hz, ArH), 7.36 (2H, t, *J* = 7.2 Hz, ArH), 7.28-7.21 (4H, m, ArH), 4.53 {4H, t, *J* = 2 Hz, *ortho* on (η^5-C_5H_4)}, 4.13-4.07 {8H, m, *meta* on (η^5-C_5H_4), -OC*H_2*CH_3}, 3.88 (4H, d, *J* = 5.6 Hz, -NHC*H_2*CO-), 3.81 (4H, d, *J* = 5.6 Hz, -NHC*H_2*CO-), 1.22 (6H, t, *J* = 7.2 Hz, -OCH_2C*H_3*).

^{13}C NMR (100 MHz) δ (*d_6*-DMSO): 170.3, 169.7, 169.3, 136.0, 135.5, 130.0, 128.7, 127.3, 125.3, 84.8, 70.9, 70.0, 60.4 (-ve DEPT), 41.9 (-ve DEPT), 40.6 (-ve DEPT), 14.0.

1,1'-*N,N'*-{*ortho*-(ferrocenyl)-bisbenzoyl}-glycyl-L-alanine ethyl ester 96.

For compound **96** glycyl-L-alanine ethyl ester hydrochloride (0.09 g, 0.46 mmol) was used as a starting material. The product was purified by column chromatography {eluant 1:1 petroleum ether (40-60 ^oC):ethyl acetate} and isolated as an orange oil (0.06 g, 35%). E°´ = 59 mV (vs Fc/Fc^+); $[\alpha]_D^{20}$ = -23^o (c 2, EtOH).

UV-Vis λ_{max} ACN: 338, 440 nm.

I.R. ν_{max} (KBr): 3566, 2920, 1790, 1660, 1562 cm^{-1}.

^{1}H NMR (400 MHz) δ (*d*$_6$-DMSO): 8.52 (2H, t, *J* = 6 Hz, -CON*H*-), 8.36 (2H, d, *J* = 7.2 Hz, -CON*H*-), 7.75 (2H, d, *J* = 7.6 Hz, ArH), 7.43-7.39 (2H, m, ArH), 7.30 (4H, d, *J* = 4 Hz, ArH), 4.62-4.59 {4H, m, *ortho* on (η^5-C_5H_4)}, 4.35 {2H, quint, *J* = 7.2 Hz, -C*H*(CH_3)}, 4.19-4.10 {8H, m, *meta* on (η^5-C_5H_4), -OC*H*$_2$$CH_3$}, 3.94-3.83 (4H, m, -NHC*H*$_2$CO-), 1.36 {6H, d, *J* = 7.2 Hz, -CH(C*H*$_3$)}, 1.26 (6H, t, *J* = 7.2 Hz, -OCH$_2$C*H*$_3$). ^{13}C NMR (100 MHz) δ (*d*$_6$-DMSO): 172.5, 170.0, 168.6, 136.1, 135.6, 130.0, 128.7, 127.3, 125.4, 84.8 70.9, 70.0, 60.5 (-ve DEPT), 47.8, 41.8 (-ve DEPT), 17.1, 14.0.

General in vitro anti-proliferation assay procedure.

The compound was dissolved in 100 µl of DMSO and dilutions at two times their final concentrations were prepared in cell culture media. 100 µl of these compound dilutions were added to plates containing cells that had been incubated for 24 hours in a 37 ^{o}C, 5% CO_2 incubator. The plates were then incubated in the same conditions for 6-7 days or until cell confluency reached 80-90%. The assessment of cell survival in the presence of the drug was then measured using an acid phosphatase assay. Media was removed from the plates and each well on the plate was washed with 100 µl PBS. This was removed and 100 µl of freshly prepared phosphatase substrate in 0.1 M sodium acetate was added to each well. The plates were then incubated in the dark for 2 hours at 37 ^{o}C. Colour development was monitored during this time then the enzymatic reaction was stopped by adding 50 µl of 1N NaOH. The fluorescence of the plate was measured at 405 nm with a reference wavelength of 620 nm. The IC_{50} value was determined by plotting cell survival percentage (relative to control cells) against drug concentration.

General cell cycle analysis procedure.

2.5 x 10^4 cells were plated in wells of 24-well plates, in RPMI 1640 media (Gibco) containing 10% foetal calf serum (Harlan). After 24 hours, the cells were treated with compound **20**. Dimethyl sulfoxide (DMSO) control wells were included in each assay. After 72 hours the media was collected into microcentrifuge tubes and the wells were washed with PBS, which was also collected. Cells were trypsinised and added to the media collected for each sample. The tubes were centrifuged at 300 x g for 5 minutes and the media was aspirated. The cell pellets were re-suspended in PBS, and each cell

suspension was transferred to a well of a round bottomed 96 well plate. The plate was centrifuged at 450 x g for 5 minutes and the supernatant aspirated leaving approximately 15 µl in each well. The remaining volume was used to re-suspend the cells and 200 µl of ice cold 70 % ethanol was added gradually to each well. The plates were then stored at 4 ^{o}C overnight. After fixing, the cells were stained according to the protocol for the Guava PCA-96 cell cycle assay and analysed on the Guava EasyCyte (Guava Technologies).

Section 2

Ferrocenoyl self assembled monolayers as anion sensors

Chapter 4

Anion sensors

4.1 Introduction.

The design of molecular and ionic receptors and the study of their potential sensing abilities have been subject to increased scrutiny in recent years [(1)]. This interest stems from the importance of ionic species in biological and chemical processes. The overall goal of this research is the creation of responsive or intelligent materials and new sensory devices. In due course it is hoped this will lead to an improved understanding of the intermolecular forces that govern the binding process [(2)]. Photochemical, chemical and electrical measurements are all reasonable methods to impart control on a host-guest system. Electrochemistry is the most attractive of these methods as electron transfer represents the most basic form of chemical reaction. Although electron transfer is relatively simple, the gain or loss of electrons in the host or guest can lead to large changes in the magnitude of intermolecular interactions. Three methods have been applied to the electrochemical detection of host-guest interactions [(3)].

1) Ion selective electrodes (ISE's), involve the extraction of a charged guest species into a membrane by an electro-inactive host and the subsequent measurement of the membrane potential.
2) Measurement of potential changes of a redox active host molecule upon formation of a complex using, for example, cyclic voltammetry.
3) Production of an electropolymerizable monomer that contains an ion binding site and polymerization of this monomer onto an electrode surface to yield an ion-selective chemically modified electrode (CME).

Considerable attention has focused on a new generation of molecules that contain signalling or responsive functional groups as a central part of the host framework. The incorporation of such functional groups in close proximity to a binding site enables the host to be used as a model sensor for a target guest species. Binding of a guest species will alter the electrochemical behaviour of the host molecule [(4)].

The detection of anions is of particular importance as anions have been implicated in the metabolic processes of all living organisms, while phosphates and nitrates are known to cause pollution in waterways leading to eutrophication [5]. The design of anion receptors is particularly difficult, with a number of factors responsible for this. Anions are larger than isoelectronic cations resulting in a lower charge to radius ratio and therefore less effective electrostatic interactions. In addition, anions may be sensitive to pH, becoming protonated at low pH and therefore losing their negative charge. Solvent effects also play a crucial role in anion sensing. Hydrogen bonding can occur between the solvent and the anion so that the receptor must effectively compete with the solvent environment. Additionally, anions display a wide range of geometries. Therefore a high degree of optimization may be required to ensure the receptor is complementary to the anion. For example, anions may be spherical (halides), linear (azide), trigonal planar (nitrate) or tetrahedral (phosphate) [3].

4.2 Ferrocenoyl and ferrocenyl based anion receptors.

Metallocenes, such as ferrocene, and other transition metal complexes have been employed in a variety of applications ranging from molecular sensors to peptide mimetic models [6]. The majority of organometallic based sensors contain a ferrocenyl or ferrocenoyl moiety with a macrocyclic group attached, with both moieties employed in the recognition event.

Beer *et al* were the first to explore the potential of ferrocene as a possible anion sensing agent. During cyclic voltammetry experiments compound **97** displayed a cathodic shift in the redox couple of both the cobaltocene and ferrocene redox centres after addition of various anions [7]. As ferrocene is a neutral molecule there are no electrostatic interactions between the receptor and the anion until the ferrocene has been oxidised to the ferricenium cation. This indicates that electrostatic interactions of the receptor can effectively be turned on by electrochemical oxidation, resulting in ferrocene based receptors becoming attractive candidates for anion sensing [8].

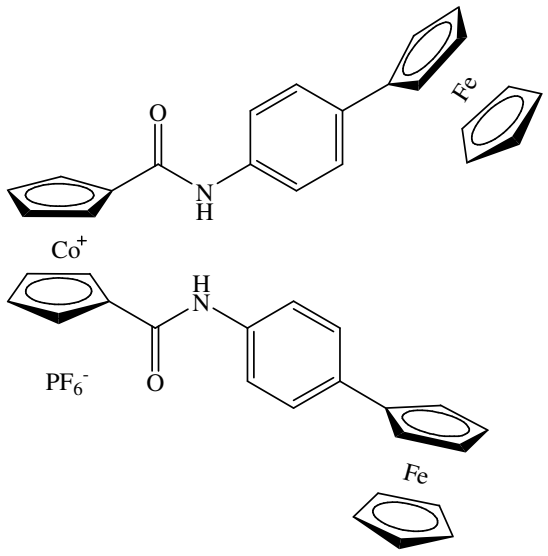

97

Gallagher prepared novel *N*-ferrocenoyl and *N*-ferrocenyl benzoyl amino acid and peptide derivatives as innovative electrochemical anion sensory agents. ^{1}H NMR titration and electrochemical experiments were used to investigate the behaviour of the ferrocenoyl derivatives [9]. *N*-ferrocenoyl glycine-glycine methyl ester **98** was shown to sense halides and dihydrogen phosphate anions with a preference for dihydrogen phosphate. There was an appreciable cathodic shift of 110 mV with respect to the ferrocene/ferricenium redox couple on addition of dihydrogen phosphate.

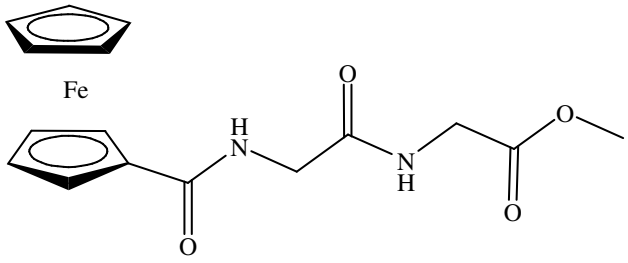

98

There was also a considerable downfield shift in the amide protons upon addition of anions during ^{1}H NMR titration experiments. The anions used were hydrogen sulphate, bromide, chloride and dihydrogen phosphate. The change in ppm ranged from 0.25 to 2.0 ppm with dihydrogen phosphate again showing the greatest shift. When a titration curve of compound **98** was plotted a 1:2 receptor:anion stoichiometry was observed. Other

dipeptide derivatives showed smaller cathodic perturbations of the ferrocene/ferricenium redox couple and smaller changes in chemical shift of the amide protons. Compound **98** was the most effective anion sensor in this study as it was the least sterically hindered derivative compared to, for example, the Leu-Leu-OEt dipeptide derivative. The particular anions were able to interact more closely with the amide groups in compound **98** than in the bulkier dipeptide derivatives. The electrochemical results for **98** are similar to those of *N*-ferrocenoyl glycine methyl, ethyl and benzyl esters **99** which showed cathodic shifts of 120 mV, 95 mV and 110 mV in the presence of dihydrogen phosphate [10].

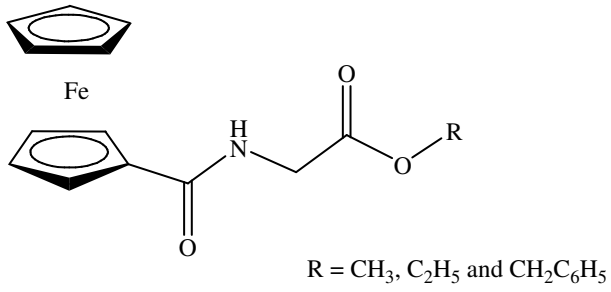

99

Goel and Savage prepared a series of novel *N*-(ferrocenyl)benzoyl amino acid and dipeptide esters. With the inclusion of the benzoyl spacer group three different cavities are possible [11,12,13]. The amide group may be *ortho*, *meta* or *para* to the ferrocene (Figure 4.1).

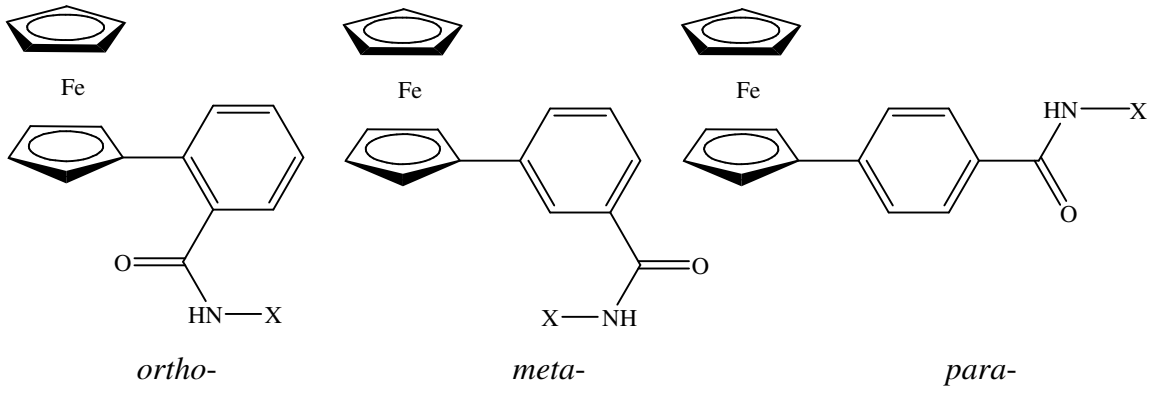

Fig. 4.1 *N*-(ferrocenyl)benzoyl derivatives where X = amino acid/peptide esters.

It was anticipated that by varying the distance between the redox centre and the hydrogen bonding groups of the amino acid or peptide moiety it would be possible to bind anions selectively and also to bind larger anions. Cyclic voltammetry and ^{1}H NMR titration studies suggested that there was little or no interaction between these *N*-(ferrocenyl)benzoyl compounds and the anions with which they were tested. From this it can be concluded that the benzoyl group had a negative effect on complexation. The ferrocene group no longer takes part in the complexation process as there was no electrochemical response upon anion addition [14].

Receptors **100-102** are ferrocene based receptors prepared by Beer *et al* that incorporate secondary amides with hydrogen bonding ability. These receptors showed dihydrogen phosphate induced cathodic perturbations (240 mV in acetonitrile) in the presence of ten fold excesses of chloride and hydrogen sulphate [7, 15].

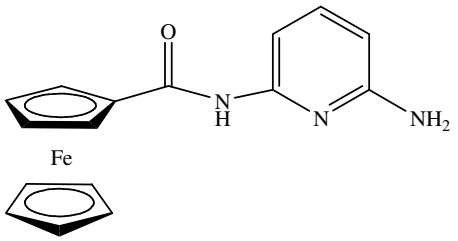

100

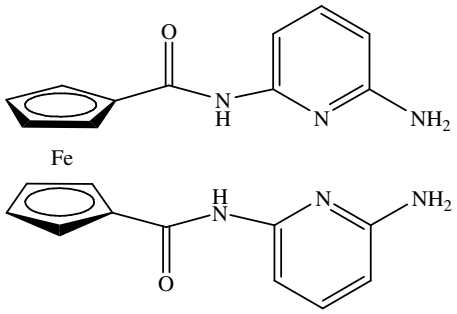

101

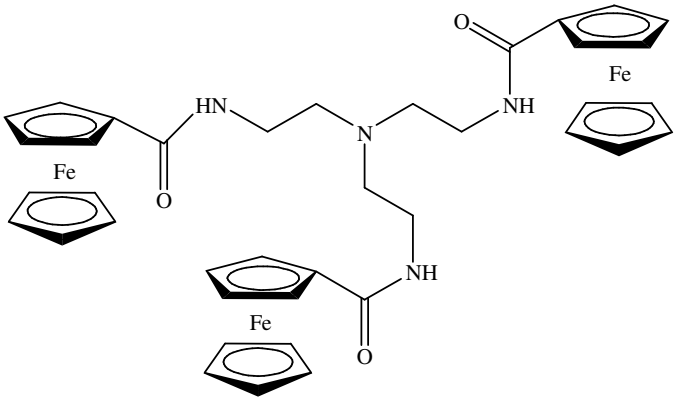

102

A range of ferrocenoyl receptors with amide functionalities, **103-105** were prepared by Reynes *et al* [8]. These receptors displayed cathodic shifts of up to 260 mV for adenosine triphosphate and dihydrogen phosphate. The electrochemical investigations showed that the formation of an anion-receptor complex was occurring. A gradual negative shift of the ferrocene/ferricenium redox couple was observed and a new redox wave also appeared at a less positive potential. A shift of 2 ppm was evident for the amide protons of these receptors on addition of dihydrogen phosphate following ^{1}H NMR titration experiments.

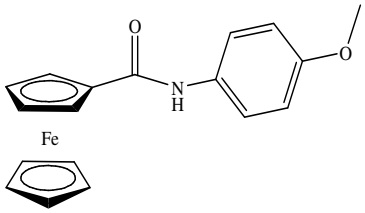

103

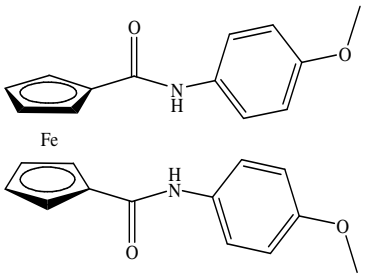

104

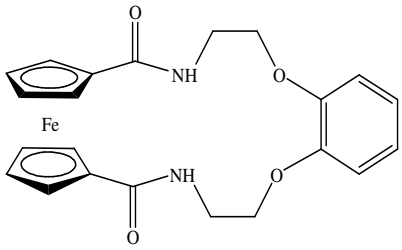

105

Kingston *et al* have also synthesised a range of neutral and charged transition metal co-ordinated ferrocene phosphine amide receptors **106-109**. Mo, Cr, Rh and Ru ligands were used and all were shown to electrochemically sense halides, hydrogen sulphate and dihydrogen phosphate [15]. Receptor **106**, the ferrocene appended phosphine amide ligand, was used as the starting material for the synthesis of the transition metal complexes **107-109**. The incorporation of phosphine into receptors enhances the strength of anion binding due to coordination of the phosphine to the transition metals. The Lewis acid metal centre withdraws electron density from the ferrocene. The positively charged ferricenium or the oxidised transition metal centres are stabilised by the bound anion, thus facilitating the redox process. There was a significant cathodic perturbation observed in the ferrocene and metal centre oxidation potentials following the addition of chloride, bromide and hydrogen sulphate anions. The magnitude of the cathodic perturbation is proportional to the stability of the complex. The chloride ion showed a larger cathodic shift than the bromide ion. This may be due to the higher charge to radius ratio of chloride. The chloride ion also shows larger cathodic shifts than hydrogen sulphate for the macrocyclic receptors, **107-108**, containing Rh, Mo and Cr Lewis acids. This is due to

the complementary size of the chloride ion to the specific receptor compared to the hydrogen sulphate anion [16]. The positively charged Ru receptor **109** exhibited the greatest anion binding ability. From this it may assumed that electrostatic forces are important in anion binding when a Lewis acid centre is involved.

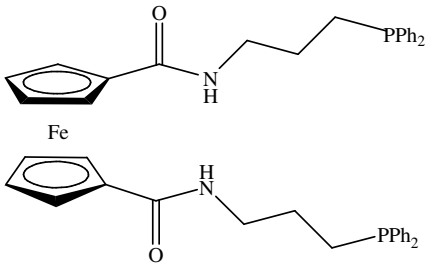

106

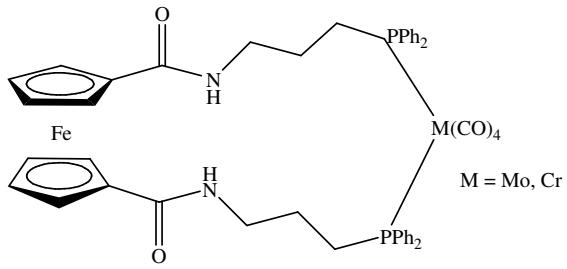

107

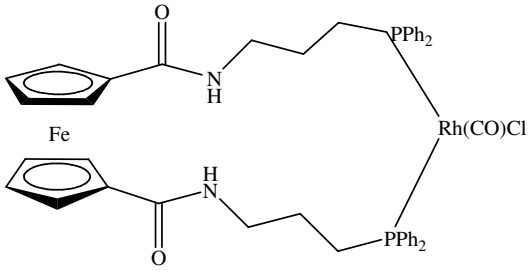

108

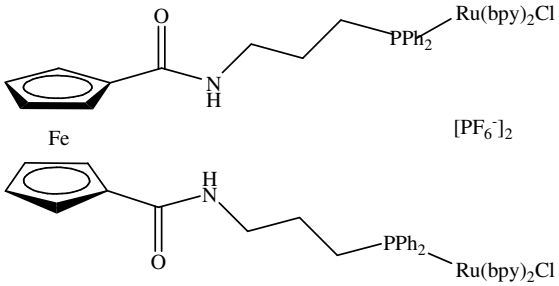

109

The synthesis of a novel ferrocene based thiacalix[4]arenes with notable selectivity for dihydrogen phosphate anions and europium cations has been reported [17]. The ferrocene/ferricenium redox couple of compound **110** showed a single quasi-reversible oxidation wave. Upon the addition of dihydrogen phosphate, a cathodic shift of 275 mV was observed. This cathodic perturbation was attributed to hydrogen bonding between the anion and the amide protons of compound **110**.

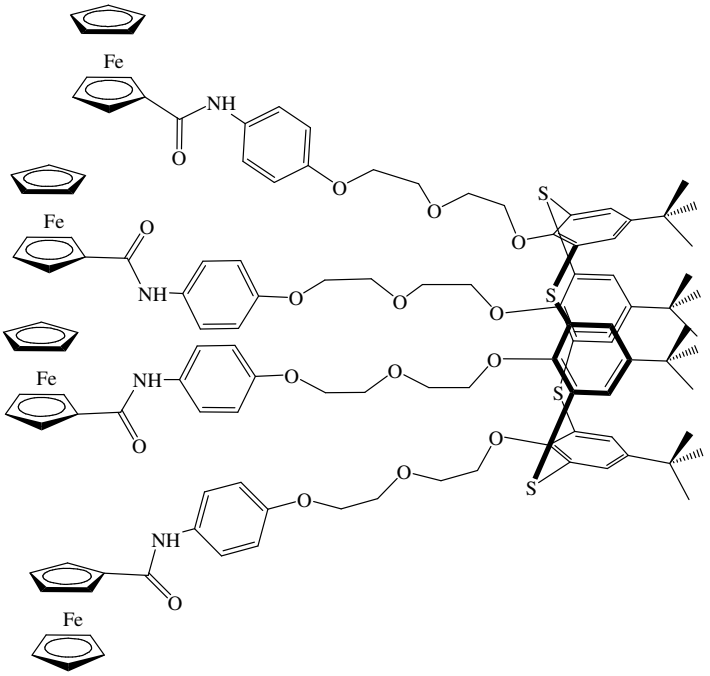

110

In general, upon the addition of cations to a ferrocene based receptor an anodic shift in redox potential is observed. This is a result of the ferrocene becoming harder to oxidise. However, in the case of compound **110** a significant cathodic shift of 130 mV is observed. This would suggest that the europium cation is somehow increasing the electron density at the ferrocene centre. In ^{1}H NMR titration experiments of **110** with europium cations the methylene and aromatic protons showed upfield changes in chemical shift. This indicates that the europium cation is entrapped by the polyether linkage and the disulfide bonds. The amide protons show a downfield shift implying they are also involved in the complexation process.

A series of cyclic and acyclic ferrocene-amine receptors, such as receptors **111** and **112** can electrochemically sense and selectively bind dihydrogen phosphate and hydrogen sulphate in aqueous solutions [(18)]. The binding is pH dependant and at pH 6.5 a 1:1 complex of anion to receptor is observed for **111**. Cathodic perturbations of 60 mV were observed in the presence of phosphate anions. Calibration curves of the change in potential versus [Anion]/[**111**] were constructed. These curves demonstrated that dihydrogen phosphate and hydrogen sulphate anions, in competition solutions, could be quantitatively sensed. Ferrocenyl receptors **112**, exhibits selective binding and redox

recognition of anionic guests in competitive aqueous solvent mixtures [19]. During competition ^{1}H NMR experiments dihydrogen phosphate was still bound to the receptor even in the presence of hydrogen sulphate. However in ^{1}H NMR titration experiments receptor **112** also displayed affinity for the diphosphate anion in preference to dihydrogen phosphate. A 2:1 receptor:anion model was observed with an overall stability constant of 4600 M^{-2}. The detection of diphosphate was also observed during electrochemical experiments, with a 70 mV cathodic shift observed for the ferrocene/ferricenium redox couple.

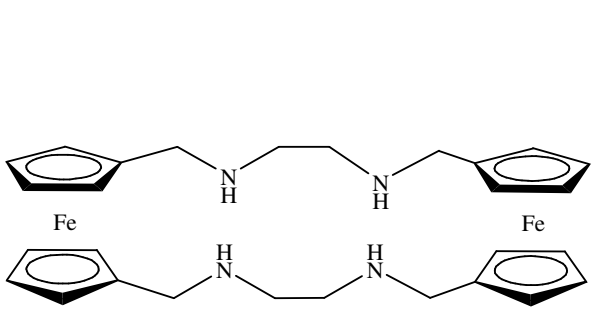

111

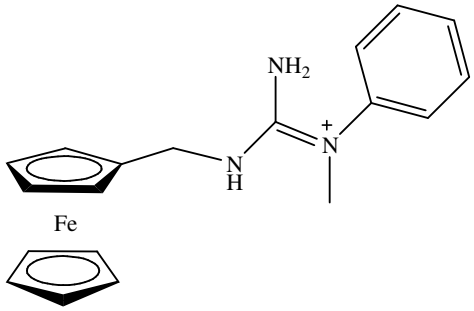

112

Szymanska *et al* used a ferrocene functionalized calix[4]pyrrole **113** in a modified carbon paste electrode for sensing anions in water. This application is intended for use in medicine, food analysis and environmental monitoring [20]. Carbon paste electrodes modified with **113** displayed decreases in the redox current of the ferrocene upon titration with halides and dihydrogen phosphate. There were also cathodic shifts in the ferrocene/ferricenium redox couple of between 10 mV and 22 mV in the presence of these anions, with dihydrogen phosphate showing the largest cathodic shift.

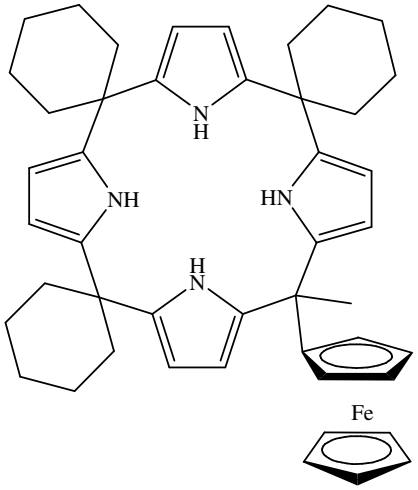

113

Goel *et al* have reported the anion sensing capabilities of a series of 1,1'-*N*, *N*'-ferrocenoylbisamino acid esters [21]. The receptors, for example **114**, contain an electroactive ferrocene core and two parallel amino acid strands. Interaction between the host and guest can either be electrostatic, when the ferrocene is in the oxidized form, or *via* hydrogen bonding through the amide groups. Each receptor exhibited an electrochemical response to environmentally important ions such as acetate, chloride, nitrate, dihydrogen phosphate and hydrogen sulphate. Receptor **114** also displays binding towards the biologically important anions, pyruvate and glutamate. However the results were not entirely quantifiable due to poor solubilities of the ion pairs formed between the host and guest.

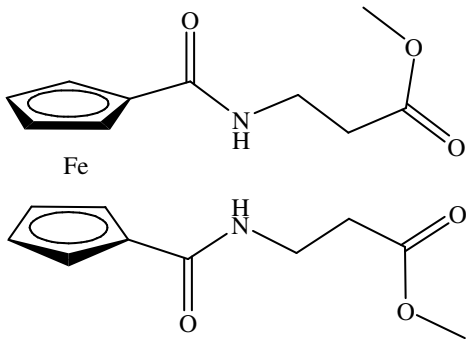

114

4.3 Ion recognition by self assembled monolayers (SAMs).

It is quarter of a century since Nuzzo and Allara published the first paper in this field when they showed how dialkyldisulfides (R-S-S-R) form ordered monolayers on gold surfaces [22]. Sulphur compounds absorb spontaneously onto the surface of metals, for example gold and platinum. Gold is the most frequently used metal as it has no stable oxide at ambient temperatures [23]. The sulphur groups are chemisorbed onto the gold surface forming a gold-sulphur bond that results in a densely packed, ordered monolayer surface. In electrochemistry the efficacy of thiol and sulphide based SAMs arises from their ability to survive electrochemical experiments. The sulphur atoms are resistant to oxidation, reduction and desorption and are stable over a wide range of potentials and to various electrolytes [24]. The structural order and the diversity of terminal functionalities that may be included have lead to SAMs being employed in a wide range of applications in science and technology [1].

Within the field of electrochemical sensing, the majority of investigations have been carried out in solution using soluble redox active sensors. These molecules must be incorporated onto solid surfaces to produce a sensory device. Attention is currently focused on developing different thin film receptors on platforms. Various surfaces have been used for example, glass slides, metals and polymeric supports. The advantages of SAM receptors are the ease of preparation, reproducibility of results and a fast response to the sensing event. Sensors using SAMs have been successfully applied in the monitoring of inorganic species, pH and also as biosensors [25].

4.3.1 Inorganic Sensors

There have been numerous examples of electrodes modified with SAMs capable of detecting redox active and redox inactive inorganic species. The ability to sense metal ions is of major importance due to their durability and toxicity to the environment. Initial studies in this area included a simple carboxylic acid terminated SAM capable of detecting cadmium (II) and a 4-alkylthio pyridine SAM as a chromium (VI) sensor. Detection limits of 10^{-10} M were observed for these SAMs [26, 27]. The selectivity relies as much on the potential window of the metal ion as it does on the affinity of the ligand for

the metal. A mixed monolayer containing 1-decanethiol and 3,3'-thiodipropionic acid, **115** and **116**, was prepared by Nagaoka and was shown to selectively sense copper (II) and silver (I) in aqueous conditions [28].

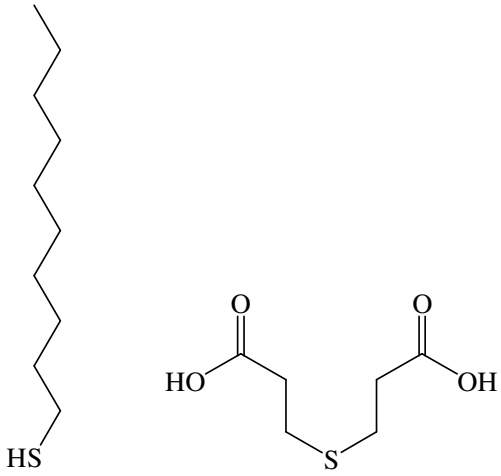

115 **116**

In a mixed monolayer of this kind the 3,3'-thiodipropionic acid allowed the close approach of the metal to the electrode surface with the 1-decanethiol preventing direct access of the metal to the electrode. This prevented electrode fouling and hence the loss of reproducibility.

The use of simple amino acids and short peptides has proven to be very important in the detection of redox active metals. Liu has demonstrated the ability of cysteine monolayers to sense copper (II) in aqueous media with a detection limit of 3.9×10^{-10} M [29]. The performance of the SAM is greatly influenced by the pH of the solution. Optimum binding occurs at pH 5, this also corresponds to the isoelectric point of the amino acid, suggesting that the zwitterion is the binding moiety. As the pH was decreased, the carboxyl group becomes protonated and is therefore unable to take part in the ion binding process.

The tripeptide Gly-Gly-His was modified with a thiol group to generate receptor **117** which was then shown to sense copper (II) ions in sub parts per billion detection limits in aqueous media [30]. No change in the redox wave of the complex was observed with repeated scanning, demonstrating the stability of the complex. This stability has been attributed to the complexation of the copper (II) ion by arrangement of four of the five nitrogen atoms in a tetragonal shape. This arrangement was confirmed by electrospray

ionization Fourier transform ion cyclotron resonance mass spectrometry (FT-ICR MS) in the negative ion mode. In the absence of the copper the dominant fragment ion of the tripeptide is present at m/z 156.04 Da, which arises from the cleavage of the histidine residue leaving Gly-Gly. In the presence of copper the cleavage of histidine is prevented by its role in the complexation event. The pseudo-parent ion, [**117** + Cu^{2+}-3H]$^-$, is observed at 331.02 Da with the dominant fragment ion at 287.03 Da equating to the decarboxylation of the histidine. Thus in solution the binding of copper is through the deprotonated nitrogen atoms of the peptide bonds.

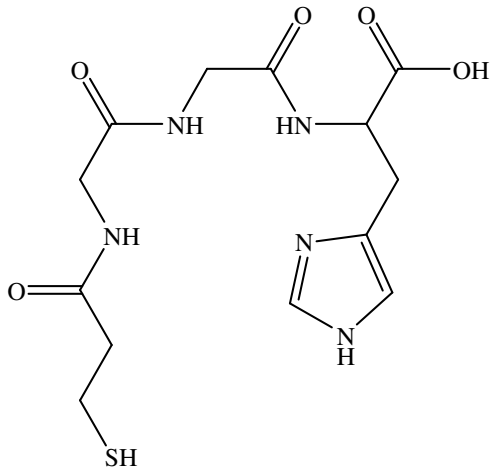

117

4.3.2 Recognition of anions by ferrocene containing SAMs.

The binding and sensing of anions in solution and at the surface solution interface is a considerable challenge. However, monolayers designed as anion sensors have recently been reported and this field has emerged as a promising research area [(1)].

Astruc employed a SAM of receptor **118** on a gold electrode to recognise dihydrogen phosphate in DCM [(31)]. A negative shift of 0.29 V was observed in the redox potential of the SAM upon addition of the anion. The large shift in redox potential suggests a significant structural rearrangement of the binding site. This is due to the anion having a greater affinity for the amidoferricenium alkylthiolate form compared to the unoxidised form of the SAM. The probable double hydrogen bonding interaction between the amidoferrocene group and the dihydrogen phosphate anion works in conjunction with the electrostatic interaction of the amidoferricenium form. When other anions, for example

hydrogen sulphate, nitrate, chloride and bromide, were investigated much smaller changes in redox response were observed.

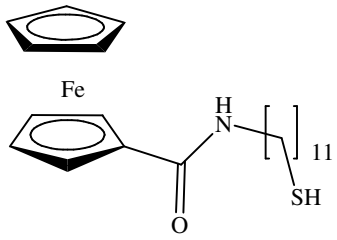

118

Beer observed that directly linking amide functionalities to the ferrocene molecule led to significant cathodic shifts in the ferrocene redox couple upon addition of anions. The redox response of the ferrocene in these 1,1'-bis(alkyl-*N*-amido)ferrocene SAMs is greatly increased by the surface pre-organisation of the host on the electrode surface [(32)]. A SAM of receptor **119** was shown to sense dihydrogen phosphate with a cathodic shift of 210 mV in the presence of a 100 fold excess of halide ions. In this work a 'surface induced amplification' phenomena was evident. The assembly of the host molecule acts as a pseudo-macrocycle on the electrode surface and gives larger cathodic shifts than the same molecule in solution. These SAMs also gave reproducible cathodic shifts of 20-25 mV for perrhennate anions in water, a model anion species for the pertechnetate anionic pollutant from the nuclear industry.

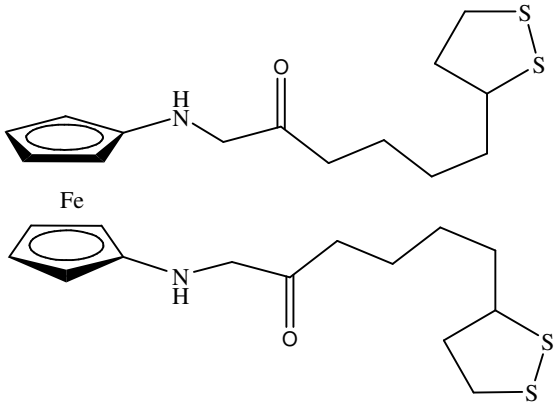

119

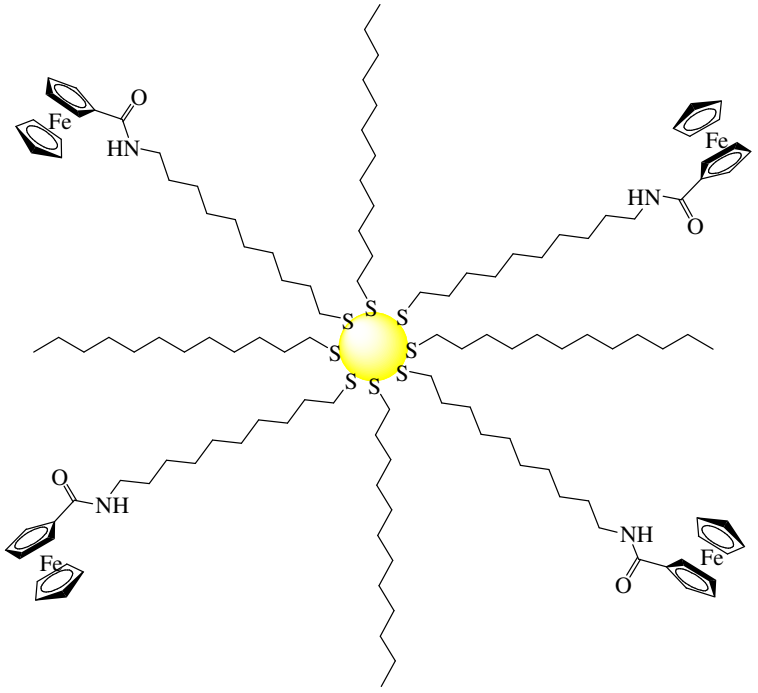

120

Anion receptors have also been immobilized on gold nanoparticles, creating a 3-dimensional anion sensor. Gold nanoparticles were treated with dodecanethiol and amido(ferrocenyl)alkanethiol ligands to produce a 3-dimensional mixed monolayer **120**. These gold nanoparticles have been shown to sense oxoanions such as dihydrogen phosphate and hydrogen sulphate in DCM [33].

After addition of dihydrogen phosphate to solutions of the gold nanoparticles a new redox wave appeared cathodically shifted 220 mV from the initial redox wave. After the addition of 1 equivalent of dihydrogen phosphate anions the initial wave had completely disappeared. This indicates a 1:1 interaction between the anion and the amidoferricenium group. This interaction is shown in Figure 4.2 and was initially proposed by Alonso for receptor **118** [31].

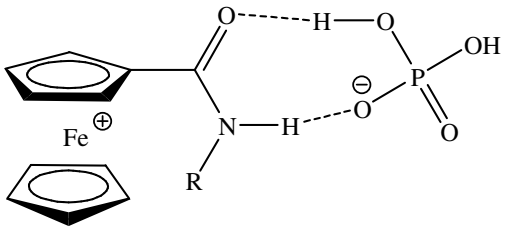

Fig. 4.2 Hydrogen bonding ability of amide groups appended to ferrocene.

When monolayers of receptor **120** were titrated with hydrogen sulphate anions a less pronounced cathodic shift of 30 mV is observed. This indicates a much weaker binding interaction. This is possibly due to the delocalization of the negative charge of the anion over 3 oxygen atoms for hydrogen sulphate compared to 2 for dihydrogen phosphate. Another feature of hydrogen sulphate binding is the disappearance of the original redox wave after approximately 0.5 equivalents of anion. This indicates a 2:1 receptor-anion complex.

The effective electrochemical sensing of dihydrogen phosphate and adenosine triphospate was achieved by Reynes using gold electrodes with ferrocenylalkylammonium thiol derivatives in organic electrolytes [34]. It was evident that the electrochemical response of these monolayers was comparable to that of the receptor in solution. There was no enhanced electrochemical response when the receptor was immobilized onto a gold surface as Beer had observed [32]. From this it can be concluded that the recognition properties of the cationic receptor **121** do not change when absorbed onto a surface.

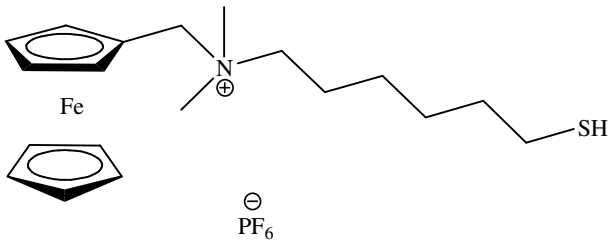

121

The strong ion pairing interactions between the anion and receptor **121** are responsible for the redox response of the receptor. This effect is further increased by the oxidation of the ferrocene to the ferricenium ion. Upon addition of anions to ACN there was a negative shift in the ferrocene/ferricenium redox couple corresponding to a more easily oxidised redox centre. Oxidation of the ferrocene also leads to electrostatic interactions between the ferricenium ion and the anion.

Electrochemical impedance spectroscopy has recently been applied to investigate the anion sensing abilities of cyclotriveratrylene SAMs **122** in aqueous media [35]. This technique is based on measuring the response of an electrochemical system to alternating

potentials. The binding of charged species to receptors on the electrode surface can affect the electron transfer process between the electrodes and a redox probe. The effect is a result of electrostatic attraction or repulsion between the monolayer surface and the redox probe. Charge transfer resistance (R_{et}) will be affected by the changes across the system and therefore be used to detect binding events at the surface solution interface. This technique is an effective and convenient method for detecting anions in aqueous media. In such experiments a redox probe is required, in the case of monolayers of **122** $Fe(CN)_6^{3-/4-}$ was used. The addition of acetate resulted in an increase in the R_{et} from 162 kΩ to a maximum of 329 kΩ at which time the acetate concentration was 15 mM, whereas 25 mM of dihydrogen phosphate increased the R_{et} to 183 kΩ. The increase in R_{et} is due to the electrostatic repulsion between the redox probe and the monolayer surface. When the redox probe was changed to the positively charged $Ru(NH_3)_6^{3+/2+}$, the R_{et} value decreased from 33.9 kΩ in the absence of acetate to a minimum of 10.9 kΩ after addition of 20 mM of acetate ions. Dihydrogen phosphate had a smaller effect on the system as the R_{et} decreases from 33.9 kΩ to 31.2 kΩ. This result confirms the build up of a negative surface charge after anion binding. In titration with chloride, bromide, nitrate and hydrogen sulphate, there was no response observed in experiments in solution or on a monolayer.

^1H NMR titration experiments were also carried out using the tetrabutylammonium salts of chloride, bromide, nitrate, hydrogen sulphate and dihydrogen phosphate. The chemical shifts of the -NH protons of the amide groups were monitored. Dihydrogen phosphate and acetate were the only anions to change the chemical shift of the amide protons. The binding constants for these two anions were 14 and 57 M^{-1} respectively.

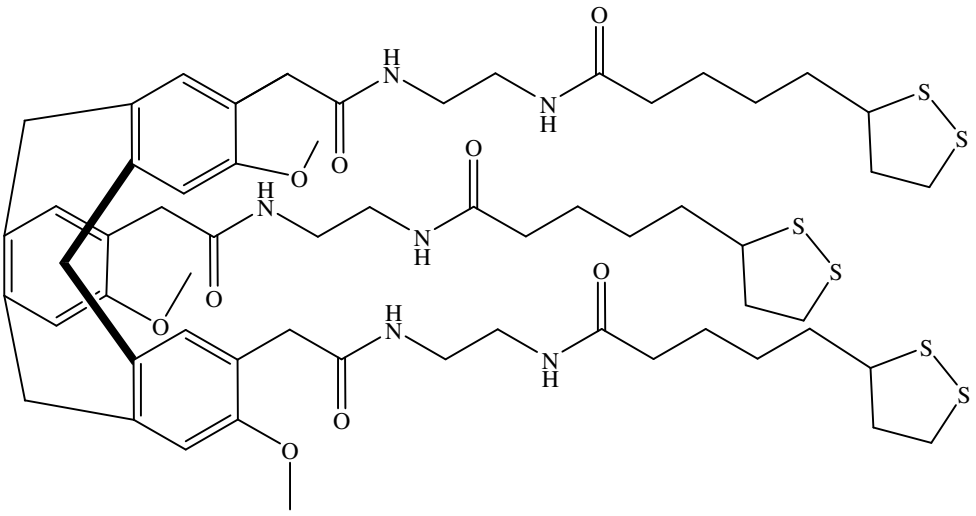

122

Subsequently, UV-Vis spectroscopic experiments in the presence of anions also gave comparable results for compound **122**. There was a slight decrease in the absorbance of compound **122** caused by dihydrogen phosphate, while acetate gave a much larger decrease in absorbance.

A calix[6]crown-4 SAM **123**, with thioctic ester groups, bound fluoride ions in aqueous media. This was confirmed by ^{1}H NMR titration experiments and impedance spectroscopy [(36)]. Upon addition of bromide, nitrate and hydrogen sulphate anions there was no change in the chemical shift of the amide protons of compound **123**. Chloride, acetate and dihydrogen phosphate gave small changes in chemical shift, while titration with fluoride ions resulted in significant downfield shifts of the amide protons and gave a binding constant of 326 M^{-1}. The degree of binding for fluoride ions is not surprising due to the strength of fluorine as a hydrogen bond acceptor. In impedance spectroscopy measurements, with $Fe(CN)_6^{3-/4-}$ as the redox probe, fluoride ions also gave the largest change in R_{et} (ΔR_{et} = 104.1 kΩ). The increase in R_{et} is due to complexation of fluoride ions at the electrode surface causing an increase in the negative surface charge which electrostatically repels the approach of $Fe(CN)_6^{3-/4-}$. The binding affinity for **123** is much weaker in the presence of the other anions.

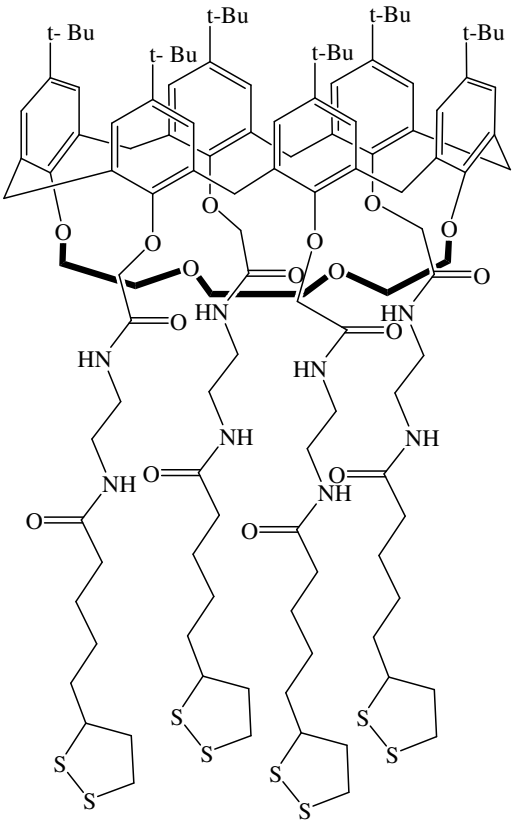

123

4.4 Binding of biomolecules in water.

The binding of small biomolecules is important for the potential development of chemosensors. An increase in solvent polarity dramatically decreases the strength of hydrogen bonding between host and guest. This makes the sensing of biomolecules in aqueous solutions very challenging [37]. Schmuck is currently exploring the use of additional ionic interactions and hydrogen bonding groups to improve binding. Receptor **124** was prepared in an attempt to bind dipeptides with a free carboxylate group.

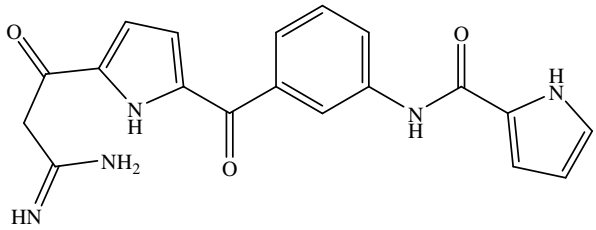

124

The guanidiniocarbonyl pyrrole part of the molecule is predicted to form ion pairs with the carboxylate group of the peptide. The additional hydrogen bonding interactions between the peptide backbone and the receptor further stabilises the complex. During ^{1}H NMR titration experiments with compound **124** and dipeptide salts in aqueous DMSO, significant changes in the chemical shift of the -NH protons of both the receptor and the dipeptide were observed. This indicates that all the -NH groups are involved in binding.

Schmuck has also used a similar guanidinium based receptor **125** to bind anionic sugar molecules in aqueous solutions using ion pair formation and hydrogen bond interactions [38]. ^{1}H NMR titration experiments with the sodium salts of the carbohydrates in question resulted in changes in the chemical shift of the receptor and the -OH protons of the carbohydrate.

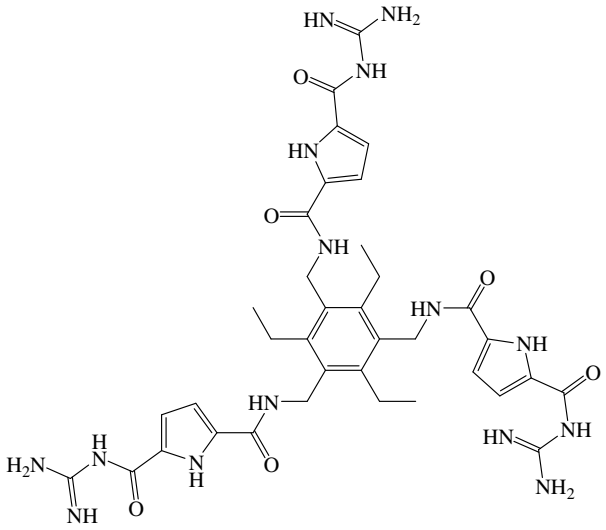

125

4.5 Conclusions.

The majority of research in the field of anion sensing has been performed in organic media. Anion recognition in aqueous media remains a challenging task due to competitive binding from the solvent. Considerable attention has focused on the incorporation of redox active probes onto molecular receptors with the intention of converting molecular level interactions into measurable electrochemical signals. Transferring these molecular recognition properties to SAMs offers a possible solution to

these issues. With the presence of anion sensing groups on the surface of the electrode the recognition process can be measured at the interface between electrode and aqueous solution [35]. A major advantage of this technique is that hydrogen bonding, which is a major factor in anion binding, is enhanced at the monolayer solution interface compared to in bulk solution [36].

Impedance spectroscopy has recently become popular as a means for detecting recognition events at the electrode surface as it provides detailed information on resistance and capacitance changes upon interactions between host and guest molecules. However cyclic voltammetry remains the technique of choice for the investigation of interactions at the monolayer solution interface

It has also been shown that by increasing the number of hydrogen bonding groups in a receptor, binding in aqueous solvents is possible [37]. The use of SAMs as anion sensors is still very much in its infancy but it is envisaged that preparing a monolayer with a redox active site and additional hydrogen bonding groups, sensitive and selective anion sensors for aqueous systems can be developed. A series of compounds that contain ferrocene as a redox active site and peptide residues have therefore been prepared and immobilized onto gold surfaces as SAMs. Anion titration experiments in organic and aqueous media will evaluate their potential as anion sensors.

References.

1. Zhang, S., Cordana, C. M., Echegoyen, L., *Chem. Comm.*, **2006**, 4461.
2. Kaifer, A. E., *Acc. Chem. Res.*, **1999**, *32*, 62.
3. Beer, P. D., Gale, P. A., *Angew. Chem. Int. Ed.*, **2001**, *40*, 486.
4. Padilla-Tosta, M. E., Martinez-Manez, R., Pardo, T., Soto, J., Tendero, M. J. L., *Chem. Comm.*, **1997**, 887.
5. Staffilani, M., Hancock, K. S. B., Steed, J. W., Holman, K. T., Atwood, J. L., Juneja, R. K., Burkhalter, R. S., *J. Am. Chem. Soc.*, **1997**, *119*, 6324.
6. Sheehy, M. J., Gallagher, J. F., Yamashita, M., Ida, Y., White-Colangelo, J., Johnson, J., Orlando, R., Kenny, P. T. M., *J. Organomet. Chem.*, **2004**, *689*, 1511.
7. Beer, P. D., Chen, Z., Goulden, A. J., Graydon, A., Stokes, S. E., Wear, T., *Chem. Comm.*, **1993**, 1834.
8. Reynes, O., Maillaird, F., Moutet, J-C., Royal, G., Saint-Aman, E., Stanciu, G., Dutasta, J-P., Gosse, I., Mulatier, J-C., *J. Organomet. Chem*, **2001**, *637-639*, 356.
9. Gallagher, J. F., Kenny, P. T. M., Sheehy, M. J., *Inorg. Chem. Comm.*, **1999**, 2, 327.
10. Gallagher, J. F., Kenny, P. T. M., Sheehy, M. J., *Inorg. Chem. Comm.*, **1999**, 2, 200.
11. Goel, A., Savage, D., Alley, S. R., Hogan, T., Kelly, P. N., Draper, S. M., Fitchett, C. M., Kenny, P. T. M., *J. Organomet. Chem.*, **2006**, *22*, 4686.
12. Savage, D., Alley, S. R., Gallagher, J. F., Goel, A., Kelly, P. N., Kenny, P. T. M., Inorg. Chem Comm, **2006**, *2*, 152.
13. Savage, D., Malone, G., Alley, S. R., Gallagher, J. F., Goel, A., Kelly, P. N., Mueller-Bunz, H., Kenny, P. T. M., *J. Organomet. Chem.*, **2006**, *3*, 463.
14. Savage, D. M., *'The Synthesis and Characterization of Novel N-Ferrocenyl Bonzoyl Amino Acid and Dipeptide Derivatives'*, DCU, Ph.D, Thesis, **2003**.
15. Beer, P. D., Graydon, A. R., Johnson, A. O. M., Smith, D. K., *Inorg. Chem.*, **1997**, *36*, 2112.
16. Kingston, J. E., Ashford, L., Beer, P. D., Drew, M. G. B., *J. Chem. Soc. Dalton Trans.*, **1999**, 251.

17. Guo, D. S., Liu, Z. P., Ma, J. P., Huang, R. Q., *Tett. Lett.*, **2007**, *48*, 1221.
18. Beer, P. D., Cadman, J., Lloris, J. M., Martinez-Manez, R., Padilla, M. E., Pardo, T., Smith, D. K., Soto, J., *Dalton Trans.*, **1999**, 127.
19. Beer, P.D., Drew, M. G. B., Smith, D. K., *J. Organomet. Chem.*, **1997**, *543*, 259.
20. Szymanska, I., Radecka, H., Radecki, J., Gale, P. A., Warriner, C. N., *J. Electroanal. Chem*, **2006**, *591*, 223.
21. Goel, A., Brennan, N., Brady, N., Kenny, P. T. M., *Biosens. Bioelectron.*, **2007**, *22*, 2047.
22. Nuzzo, R. G., Allara, D. L., *J. Am. Chem. Soc*., **1983**, *105*, 4481.
23. Gooding, J. J., Mearns, F., Yang, W., Liu, J., *Electroanalysis*, **2003**, *15*, 81.
24. Finklea, H. O., '*Self-assembled Monolayers on Electrodes*', Encyclopedia of Analytical Chemistry, John Wiley and Sons.
25. Shervedani, R. K., Babadi, M. K., *Talanta*, **2006**, *69*, 741.
26. Turyan, I., Mandler, D., *Anal. Chem.*, **1994**, *66*, 58.
27. Shen, S., Mark, J. E., Seliskar, C. J., Mark, H. B., Heineman, W. R., *J. Solid State Electrochem.*, **1997**, *1*, 148.
28. Nagaoka, T., Chen, Z., Okuno, H., Nakayama, N., Ogura, K., *Anal. Sci*., **1999**, *15*, 857.
29. Liu, A. C., Chen, D. C., Lin, C. C., Chou, H. H., Chen, C. H., *Anal. Chem.*, **1999**, *71*, 1549.
30. Yang, W., Jaramillo, D., Gooding, J. J., Hibbert, D. B., Zhang, R., Willett, G. D., Kisher, K. J., *Chem. Comm.*, **2001**, 1982.
31. Alonso, E., Labande, A., Raehm, L., Kern, J. M., Astruc, D., *C. R. Acad. Sci.*, **1999**, 209.
32. Beer, P. D., Davis, J. J., Drillsma-Milgrom, D. A., Szemes, F., *Chem. Comm.*, **2002**, 1716.
33. Labande, A., Ruiz, J., Astruc, D., *J. Am Chem. Soc.*, **2002**, *124*, 1782.
34. Reynes, O., Bucher, C., Moutet, J-C., Royal, G., Saint-Aman, E., *Inorg. Chim. Acta*, **2008**, *361*, 1784.
35. Zhang, S., Echegoyen, L., *J. Am Chem. Soc.*, **2005**, *127*, 2006.
36. Zhang, S., Palkar, A., Echegoyen, L., *Langmuir*, **2006**, *22*, 10732.

37. Schmuck, C., Schwegmann, M., *Org. Lett.*, **2005**, *7*, 3517.

38. Schmuck, C., Geiger, L., *J. Am Chem. Soc.*, **2004**, *126*, 8898.

Chapter 5

Results and Discussion II

5.1 Introduction.

The development of electrodes modified with monolayers for ion sensing has led to the successful detection of ionic species at the solution electrode interface. The detection of redox active and inactive metal ions was freely achieved with monolayers of redox active and inactive molecules, for example, pyridines and crown ethers [(1)].

Anion recognition in aqueous media remains a challenging task due to competitive binding from the solvent. The use of cationic anion sensors which employ electrostatic interactions can overcome the problem of solvent competition. However their counter ions have been known to interfere with the recognition process [(2)].

Transferring these molecular recognition properties to SAMs offers a possible solution to these issues. With the presence of anion sensing groups on the surface of the electrode the recognition process can be measured at the interface between electrode and aqueous solution. A major advantage of this technique is that hydrogen bonding, which is a key factor in anion binding, is enhanced at the monolayer solution interface compared to in bulk solution [(3)].

The primary aim of this project is the preparation of self assembled monolayers (SAMs) on gold electrodes that incorporate three main structural components.

a) An electroactive ferrocene core.
b) An amino acid or peptide moiety with hydrogen bonding groups.
c) Sulphur atoms that would facilitate covalent bonding to gold.

An example of such a SAM is illustrated in Figure 5.1.

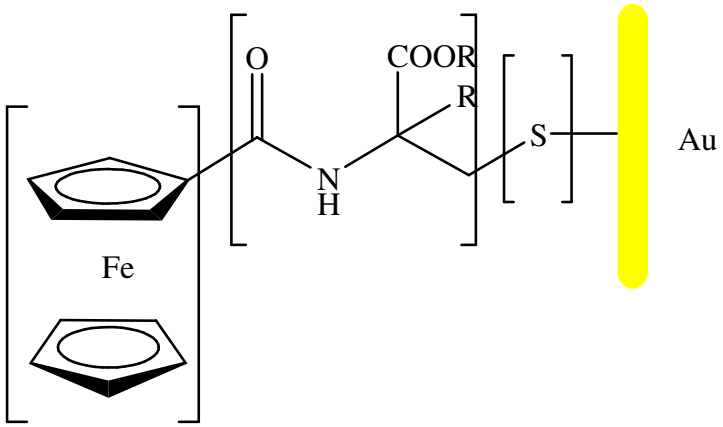

Fig. 5.1 Components of a ferrocene-peptide based monolayer.

The monolayers of the ferrocene derivatives may be characterized by a range of cyclic voltammetry techniques. Valuable information on the coverage and properties of the receptor on the surface of the electrode may be obtained. When the receptors are immobilized on the surface of the electrode, they can be used to detect anions in solution. The oxidised form of the ferrocene can interact with anions electrostatically, while the hydrogen bonding ability of the amide groups is also important for anion binding. The interactions between the receptor and the anions can be easily monitored using cyclic voltammetry. Complexation of anions by the ferrocene receptor would be expected to induce changes in the redox potential and current of the ferrocene/ferricenium redox couple.

5.2 The preparation of *N*-(ferrocenyl)$_2$ and *N*-(ferrocenoyl)$_2$ cystine dimethyl esters derivatives.

Standard peptide coupling reactions were used to prepare the *N*-(ferrocenyl)$_2$ and *N*-(ferrocenoyl)$_2$ cystine dimethyl esters derivatives. Ferrocene carboxylic acids were treated with 1-hydroxybenzotriazole (HOBt), *N*-(3-dimethylaminopropyl)-*N*′-ethylcarbodiimide hydrochloride (EDC), cystine methyl ester hydrochloride and triethylamine (TEA) in dichloromethane at 0 ^{o}C. The *N*-(ferrocenyl)$_2$ and *N*-

(ferrocenoyl)$_2$ cystine dimethyl esters derivatives were purified using column chromatography. Purification of these derivatives proved to be a difficult undertaking. Several columns were required to separate the pure product from the ferrocene carboxylic acid starting materials. This resulted in loss of overall yield. The synthetic route employed in the synthesis of compound **129** and its subsequent immobilization onto a gold electrode is described in Figure 5.2.

The overall yields for compounds **129**-**136** ranged from 11 to 33%. The largest yield was obtained for compound **129**, while the poorest yield was in the preparation of compound **130**. This is not surprising when the structures of the final products are considered. Preparation of **130** requires a large degree of manipulation of the L-cystine dimethyl ester. The reasons for the overall moderate yields can be rationalized by considering the relative approaches of the carboxylic acid groups to each end of the central peptide unit and the need for reaction between two ferrocene carboxylic acid groups and the two amines of the peptide. The size and overall polarity of the final products, in particular **135** and **136** also contributed to low overall yields.

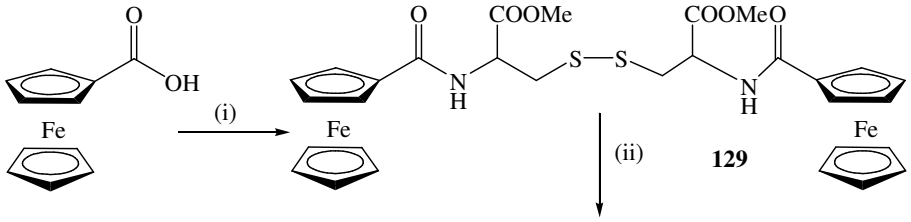

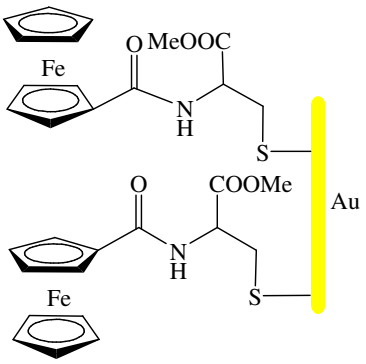

(i) EDC, HOBt, TEA, cystine methyl ester hydrochloride, (ii) immersion of clean gold electrode into ethanolic solution of **129**.

Fig. 5.2 Preparation of monolayers of {*N*-(ferrocenoyl)}$_2$-L-cystine dimethyl ester **129.**

Additional amide groups were incorporated into the SAMs by coupling cystine methyl ester hydrochloride to tert-butoxycarbonyl (BOC) protected glycine and β-alanine (Figure 5.3). All compounds were subsequently characterized using a variety of NMR and spectroscopic techniques. As they were intermediates in the synthesis of *N*-(ferrocenyl)$_2$ and *N*-(ferrocenoyl)$_2$ cystine dimethyl esters they will not be included in the experimental section. Subsequent deprotection of the BOC group enabled the peptide to be coupled to various ferrocene carboxylic acids [4].

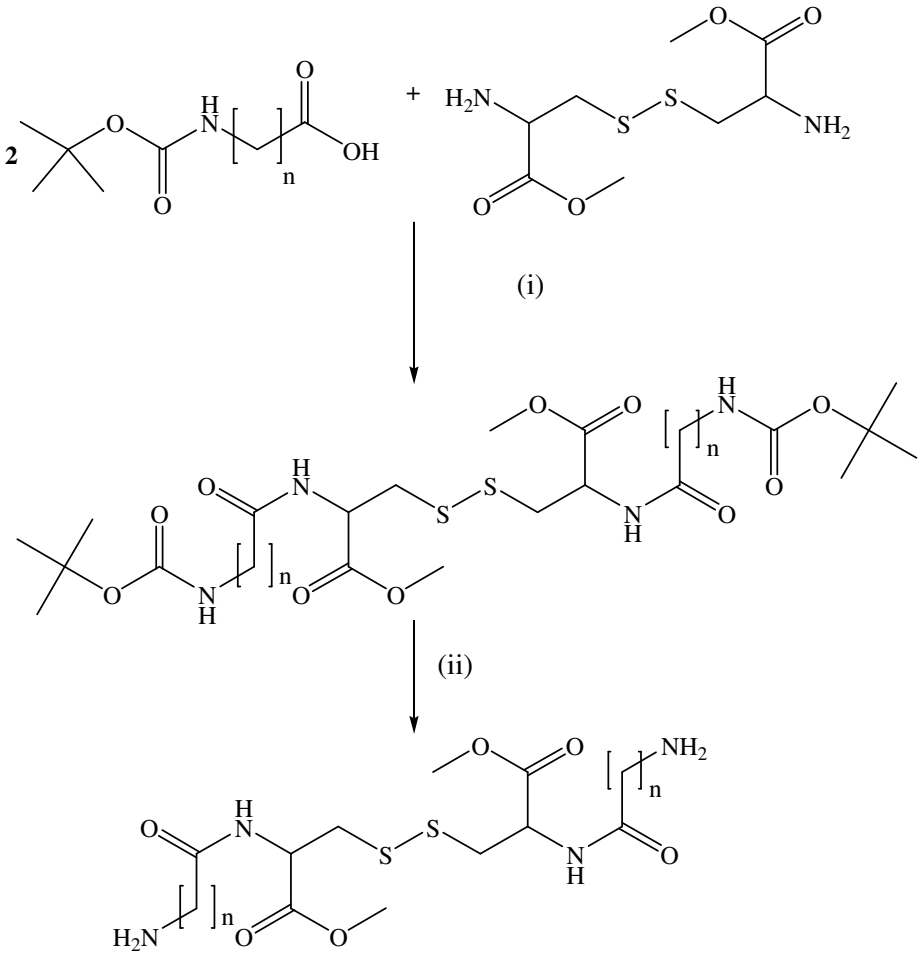

(i) EDC, HOBt, TEA, (ii) trifluoroacetic acid.

Fig. 5.3 Synthesis of cystine residues with additional amide groups.

Aromatic spacers were also added to receptors in order to investigate the effect of a conjugated linker moiety on electrochemical properties and anion sensing ability. The inclusion of aromatic spacers was necessary to assess the degree of cooperative interaction between the redox centre and the hydrogen bonding groups. A similar procedure to that outlined in Figure 5.2 was used, whereby *N*-(ferrocenyl)benzoyl and *N*-(ferrocenyl)naphthoyl carboxylic acids were used as starting materials. The structures of *N*-(ferrocenyl)$_2$ and *N*-(ferrocenoyl)$_2$ cystine dimethyl esters derivatives **129**-**136** are illustrated in Figure 5.4.

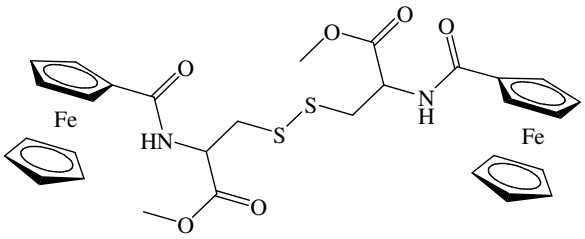

129

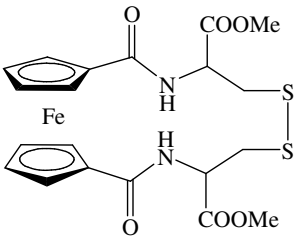

130

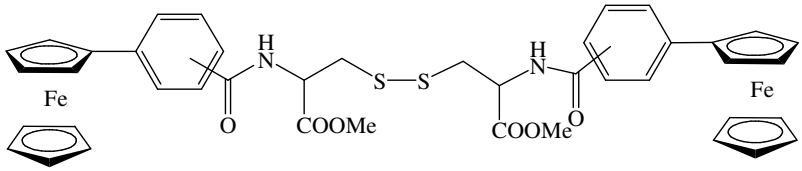

131-133

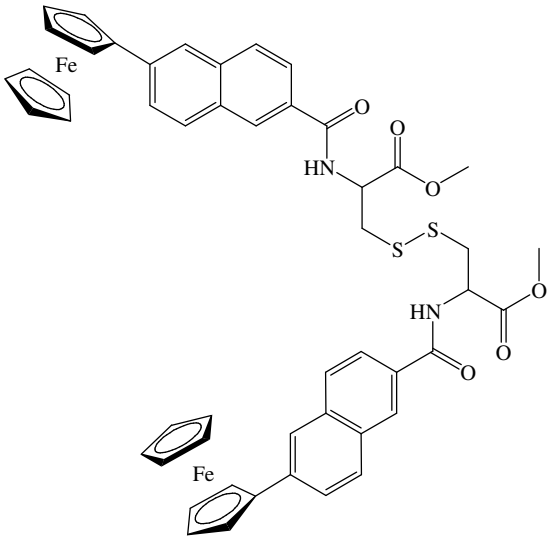

134

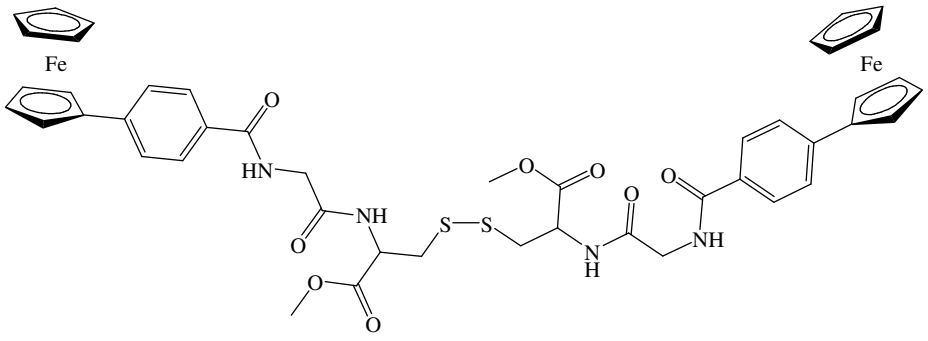

135

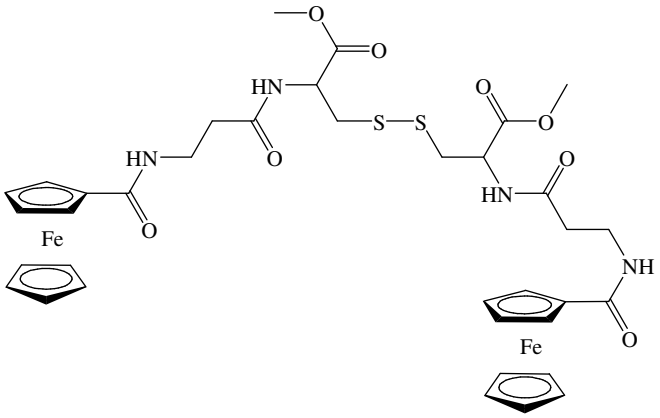

136

Fig. 5.4 *N*-(ferrocenyl)$_2$ and *N*-(ferrocenoyl)$_2$ cystine dimethyl esters derivatives **129**-**136**.

5.3 ^{1}H NMR studies of *N*-(ferrocenyl)$_2$ and *N*-(ferrocenoyl)$_2$ cystine dimethyl esters.

The ^{1}H NMR spectra were obtained in d_6-DMSO. For compounds **131**-**135** peaks were present between δ 8.03 and δ 7.46 which corresponded to the aromatic protons. The splitting pattern was dependent on whether the benzoyl or naphthoyl aromatic spacers were used. The amide protons typically appeared between δ 9.06 and δ 8.19. The mono-substituted ferrocene derivatives gave the archetypal splitting pattern with three peaks between δ 4.97 and δ 3.99 corresponding to the *ortho* (η^5-C_5H_4), *meta* (η^5-C_5H_4) and the (η^5-C_5H_5) protons respectively. For compound **130** four ferrocenyl peaks are observed, representing each of the (η^5-C_5H_4) protons.

Table 5.1 Selected ^{1}H NMR data for *N*-(ferrocenyl)$_2$ and *N*-(ferrocenoyl)$_2$ cystine dimethyl esters derivatives **129**-**136** (δ).

Compound	**Cystine -N*H*-**	***ortho* (η^5-C_5H_4)**	***meta* (η^5-C_5H_4)**	**(η^5-C_5H_5)**
129	8.19	4.85	4.39	4.23
131	9.01	4.73	4.39	4.11
132	9.04	4.95-4.90	4.52	4.09
133	8.90	4.85	4.40	4.00
134	9.06	4.97	4.46	4.06
135	8.56	4.85	4.39	3.99
136	8.54	4.76	4.33	4.16

5.3.1 ^{1}H NMR spectroscopic study of {*N-para*-(ferrocenyl)benzoyl}$_2$-L-cystine dimethyl ester 133.

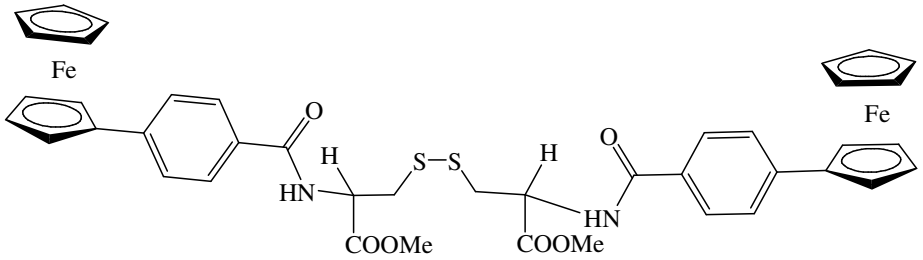

133

The ^{1}H NMR spectrum of **133** has one peak for each proton of the dimeric molecule. This indicates that the corresponding protons on each side of the disulphide bond are in identical chemical environments. The amide protons appear at δ 8.90 as doublets due to coupling with the α-hydrogen of the cystine residue. The typical *para* disubstituted splitting pattern is observed with doublets at δ 7.74 and δ 7.57 respectively, with a coupling constant of 8.4 Hz. The *ortho* and *meta* (η^5-C_5H_4) protons appear as singlets at δ 4.85 and δ 4.40 respectively. The characteristic singlets representing the (η^5-C_5H_5) ring and the methyl ester occur at δ 4.00 and δ 3.79. The α-hydrogen appears as a multiplet between δ 4.80 and δ 4.74. The methylene protons of the L-cystine side chain appear as a multiplet in the broad range of δ 3.27-3.14. This complex splitting pattern is due to the diasterotopic nature of the protons.

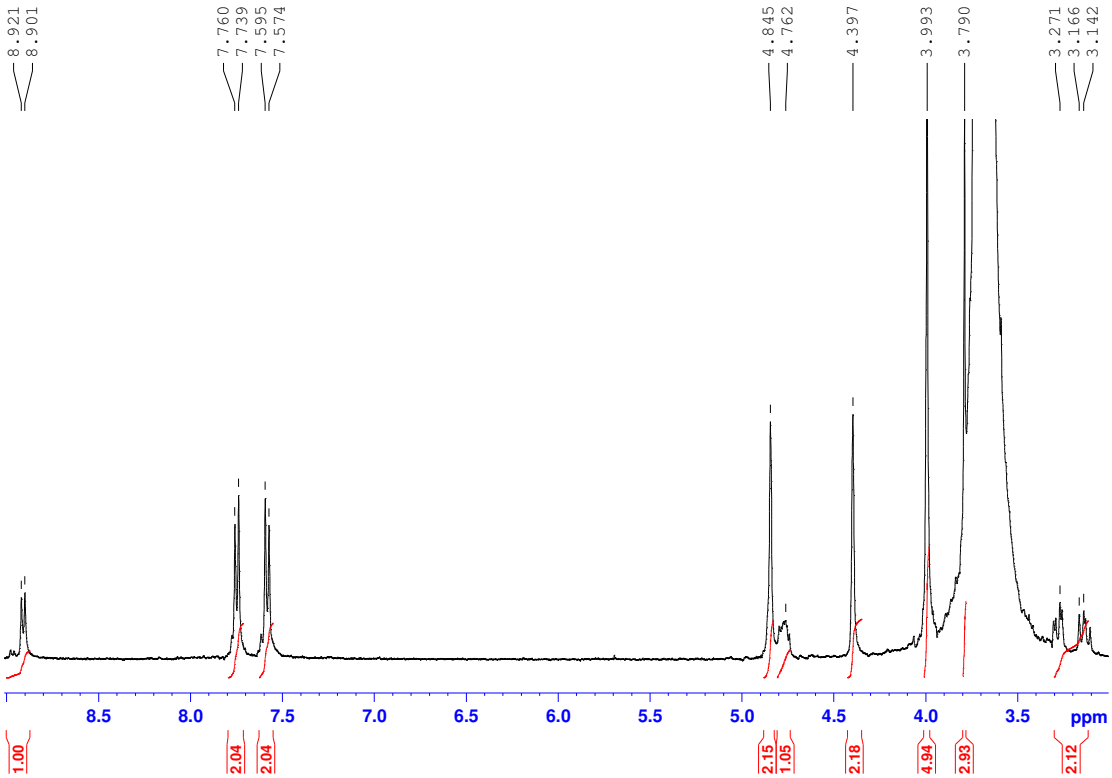

Fig. 5.5 ^{1}H NMR of *N*-{*para*-(ferrocenyl)-benzoyl}$_2$-L-cystine dimethyl ester **133**.

5.4 ^{13}C NMR and DEPT 135 spectroscopic studies of *N*-(ferrocenyl)$_2$ and *N*-(ferrocenoyl)$_2$ cystine dimethyl esters.

^{13}C NMR and DEPT 135 studies were also carried out on each of the compounds prepared. One peak was observed for each carbon on either side of the disulphide bond. The quaternary carbonyl, aromatic and *ipso* ferrocenyl carbons were easily identified by their absence from the DEPT 135 spectrum. The ferrocene quaternary carbon appears between δ 75.5 and δ 84.0 for the mono-substituted derivatives, with the remaining ferrocene carbons appearing between δ 70.2 and δ 66.4. The methylene carbons are easily identified from their negative resonance in the DEPT 135 spectra and are observed between δ 39.0 and δ 37.7 in all spectra.

Table 5.2 Selected ^{13}C NMR data for compounds **129**-**136**.

Compound	*ipso*-(η^5-C_5H_4)	(η^5-C_5H_5)	α *C*	-*C*H_2S-
129	75.5	70.2	51.7	38.8
131	84.0	69.5	51.2	38.1
132	83.9	69.1	52.3	38.8
133	82.9	69.6	52.3	38.4
134	83.9	69.4	51.8	37.7
135	83.0	69.6	52.3	38.9
136	82.7	69.3	52.7	39.0

5.4.1 ^{13}C NMR and DEPT 135 spectroscopic studies of *N*-{*para*-(ferrocenyl)-benzoyl-glycine}$_2$-L-cystine dimethyl ester 135.

The ^{13}C NMR spectrum of {*N*-*para*-(ferrocenyl)-benzoyl-glycine}$_2$-L-cystine dimethyl ester **135** showed peaks at δ 170.8 and δ 169.5 representing the ester and amide carbonyl carbons respectively. The peaks at δ 143.0 and δ 130.7 are the quaternary carbons of the aromatic spacer as these peaks are not present in the DEPT 135 spectrum, while the peaks at δ 127.5 and δ 125.4 represent the two sets of equivalent aromatic carbons. The *ipso* carbon of the (η^5-C_5H_4) is present at δ 83.0 with the remaining ferrocene carbons occurring between δ 69.6 and δ 66.3. The methylene carbons of the glycine and L-cystine moieties appear at δ 42.1 and δ 38.9 respectively and show a negative resonance in the DEPT 135 spectrum.

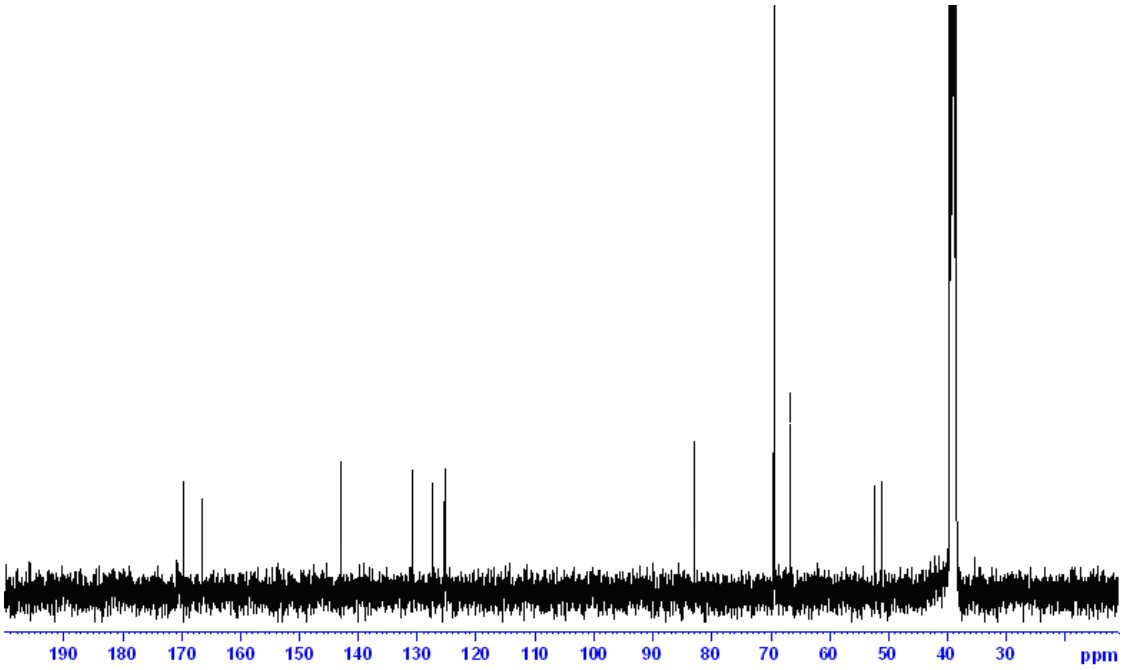

Fig. 5.6 ^{13}C NMR spectrum of {*N-para*-(ferrocenyl)-benzoyl-glycine}$_2$-L-cystine dimethyl ester **135**.

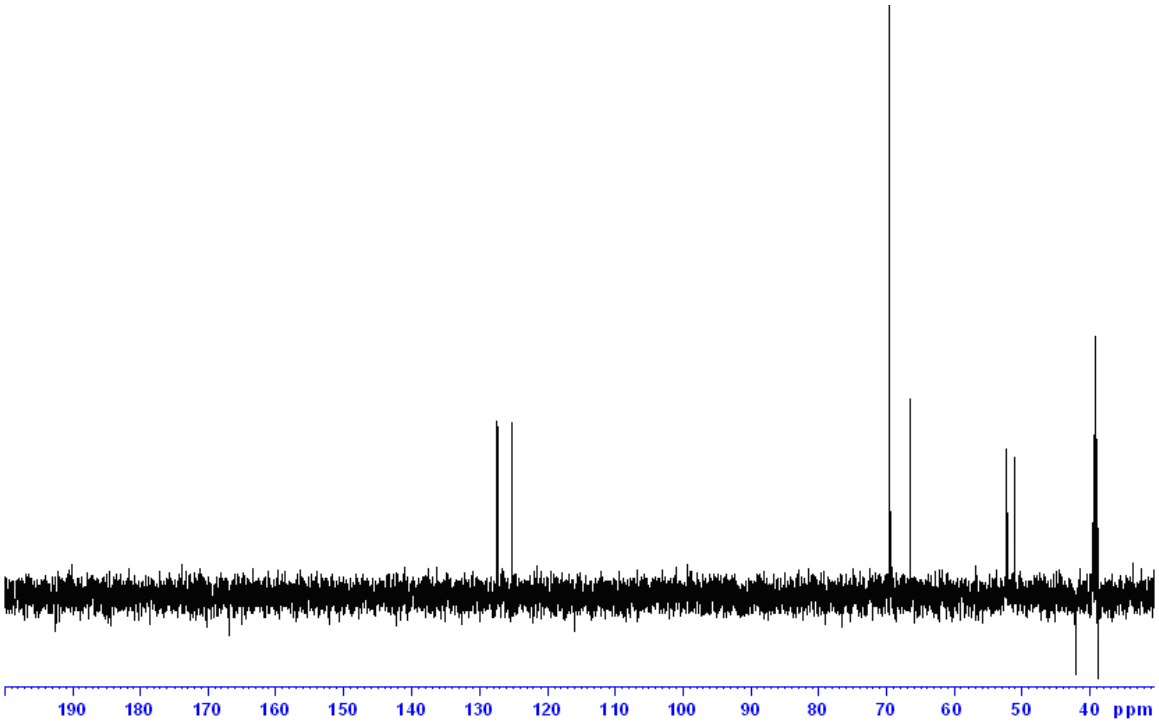

Fig. 5.7 DEPT 135 spectrum of {*N-para*-(ferrocenyl)-benzoyl-glycine}$_2$-L-cystine dimethyl ester **135**.

5.5 COSY and HMQC studies of *N*-(ferrocenyl)$_2$ and *N*-(ferrocenoyl)$_2$ cystine dimethyl esters.

^{1}H-^{1}H and ^{1}H-^{13}C correlation techniques were used to fully assign the proton and carbon chemical shifts for *N*-(ferrocenyl) and *N*-(ferrocenoyl) cystine dimethyl esters. In the COSY spectrum of {*N-ortho*-(ferrocenyl)-benzoyl}$_2$-L-cystine dimethyl ester **131** the amide proton of the L-cystine is coupled with the methine proton at the chiral centre of L-cystine. This methine proton subsequently couples with each of the diastereotopic protons of the L-cystine side chain. These diasterotopic protons also couple with each other. In the aromatic region of the spectrum coupling is observed between the doublet at δ 7.88 and the triplet at δ 7.49, in turn this triplet couples with the multiplet between δ 7.34 and δ 7.28. The *ortho* and *meta* protons of the (η^5-C_5H_4) ring show coupling with each other while the (η^5-C_5H_5) and the methyl ester group protons do not couple with any other protons.

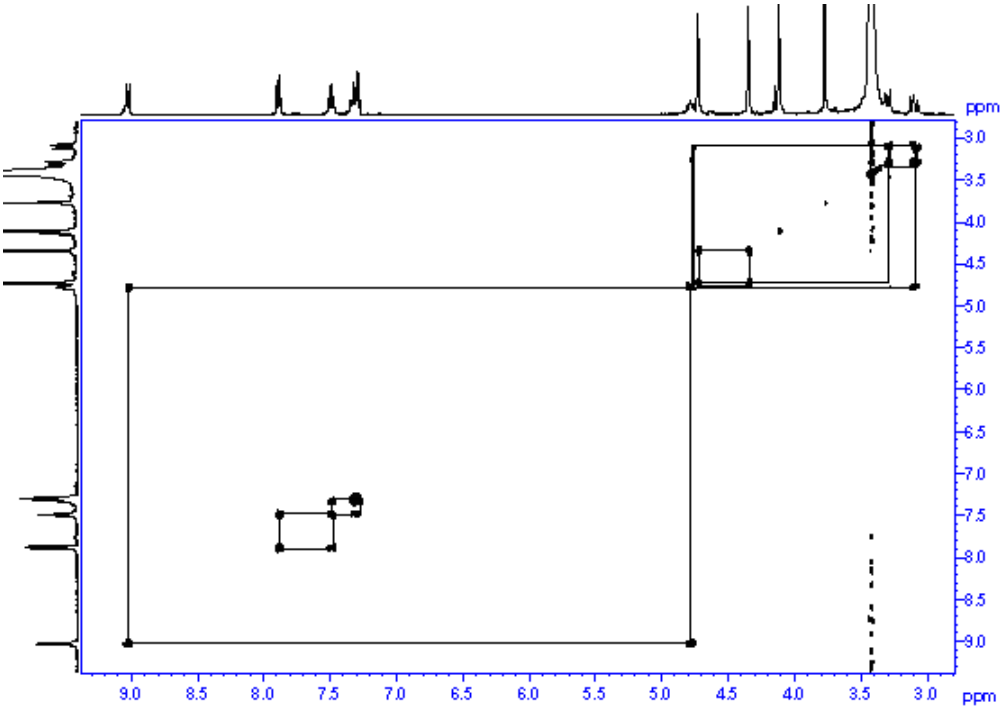

Fig. 5.8 COSY spectrum of {*N-ortho*-(ferrocenyl)-benzoyl}$_2$-L-cystine dimethyl ester **131**.

A HMQC study was also undertaken for *N*-(ferrocenyl)$_2$ and *N*-(ferrocenoyl)$_2$ cystine dimethyl esters, enabling the proton and carbon signals to be unambiguously assigned. The results of the HMQC study of {*N-ortho*-(ferrocenyl)-benzoyl}$_2$-L-cystine dimethyl ester **131** (Figure 5.9) are summarized in Table 5.3.

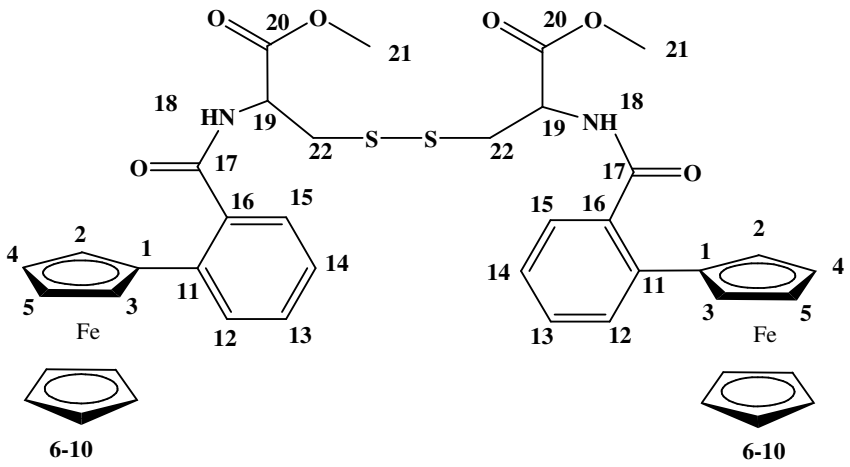

Fig. 5.9 Numbering pattern for {*N-ortho*-(ferrocenyl)-benzoyl}$_2$-L-cystine dimethyl ester **131.**

Table 5.3 ^{1}H and ^{13}C spectroscopic data for **131**.

Site	^{1}H NMR	^{13}C NMR	HMQC
1		84.0	
2 and 3	4.73		68.3
4 and 5	4.39		68.8
6 to 10	4.11		69.5
11		136.6	
12*	7.34-7.28		127.4
13*	7.34-7.28		125.4
14	7.49		129.0
15	7.88		130.1
16		136.2	
17		169.8	

18	9.01		
19	4.81-4.76		51.2
20		171.0	
21	3.77		52.3
22	3.31		38.1

* Signals 12 and 13 may be reversed.

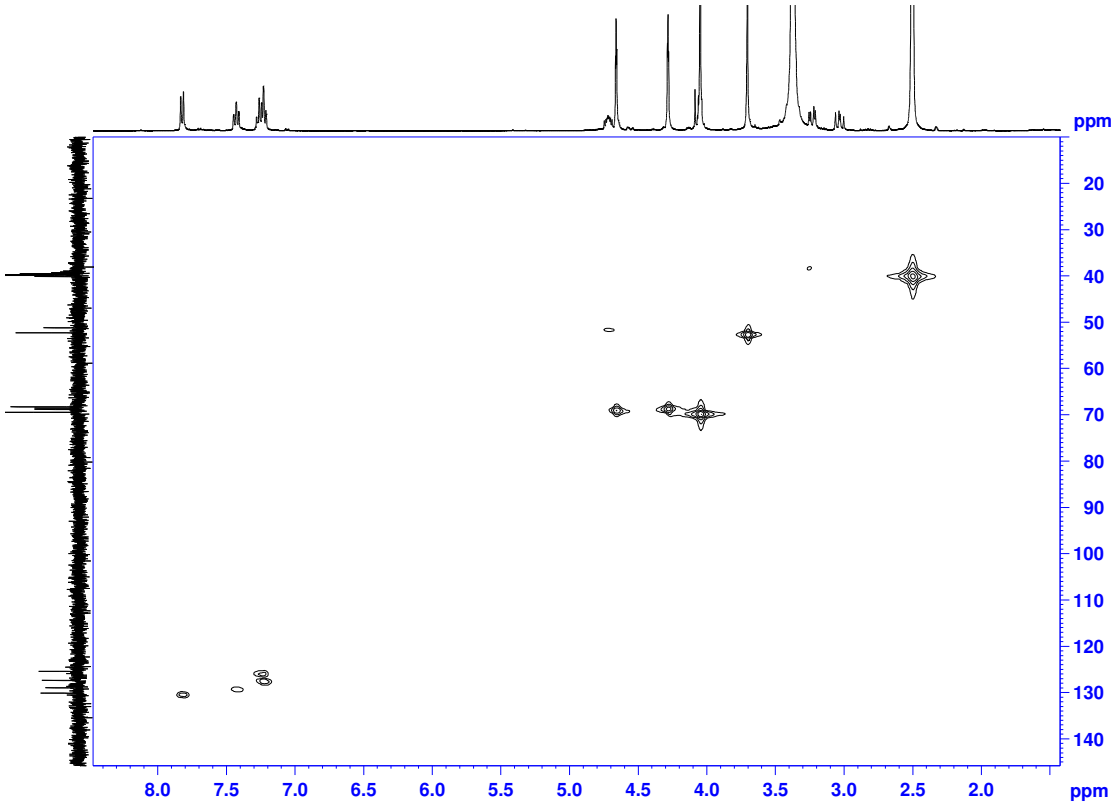

Fig. 5.10 HMQC spectrum of {*N-ortho*-(ferrocenyl)-benzoyl}$_2$-L-cystine dimethyl ester **131**

5.6 Infrared spectroscopic studies of *N*-(ferrocenyl)$_2$ and *N*-(ferrocenoyl)$_2$ cystine dimethyl esters.

The presence of certain functional groups can be confirmed using IR spectroscopy with molecular vibrations of particular functional groups induced at certain wavelengths following infrared radiation. The IR spectrum of {*N-meta*-(ferrocenyl)-benzoyl}$_2$-L-cystine dimethyl ester **132** was obtained as a KBr disk. A peak at 3444 cm^{-1} corresponding to the amide of the L-cystine group is observed, while the ester carbonyl group results in a intense peak at 1734 cm^{-1}. The amide carbonyl group is observed at 1638 cm^{-1} while the bands due to the aromatic ring are present at 1568, 1547 and 1494 cm^{-1} respectively.

Table 5.4 Selected IR data for *N*-(ferrocenyl)$_2$ and *N*-(ferrocenoyl)$_2$ cystine dimethyl esters (cm^{-1}).

Compound	N-H	C=O $_{\text{Amide I}}$	C=O $_{\text{Ester}}$
129	3446	1635	1740
132	3444	1638	1734
133	3445	1609	1740
135	3442, 3260	1699, 1607	1747

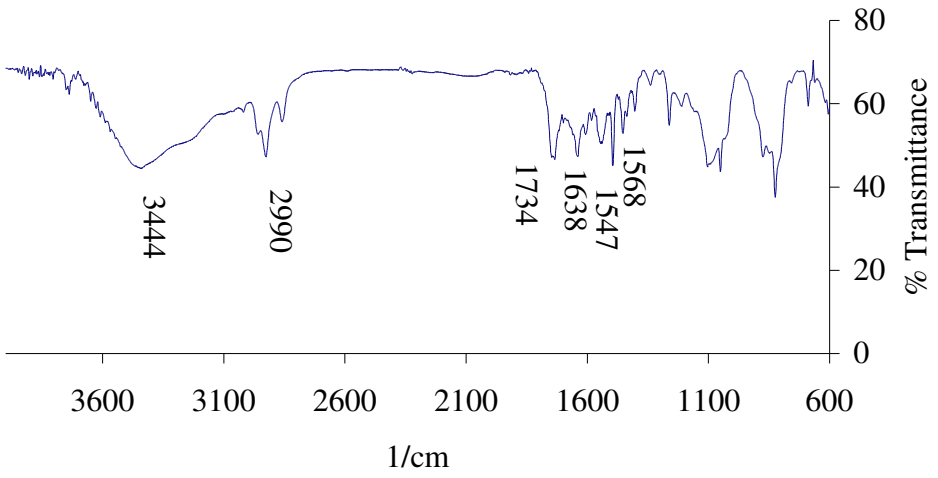

Fig. 5.11 IR spectrum of {*N-meta*-(ferrocenyl)-benzoyl}$_2$-L-cystine dimethyl ester **132**.

5.7 UV-Vis spectroscopic studies of {*N*-*para*-(ferrocenyl)-benzoyl}$_2$-L-cystine dimethyl ester and {*N*-(ferrocenoyl)-β-alanine}$_2$-L-cystine dimethyl ester.

The UV-Vis spectrum of {*N*-*para*-(ferrocenyl)-benzoyl}$_2$-L-cystine dimethyl ester **133** shows absorbance maxima at 350 nm and 450 nm respectively. The strong absorbance at 350 nm is a result of the *para* substituted aromatic spacer and the high degree of conjugation associated with such a system. The spectrum of {*N*-(ferrocenoyl)-β-alanine}$_2$-L-cystine dimethyl ester **136** shows only one absorbance at 440 nm corresponding to the *N*-ferrcenoyl group. The difference between the two spectra is noteworthy and is evident from Figure 5.12.

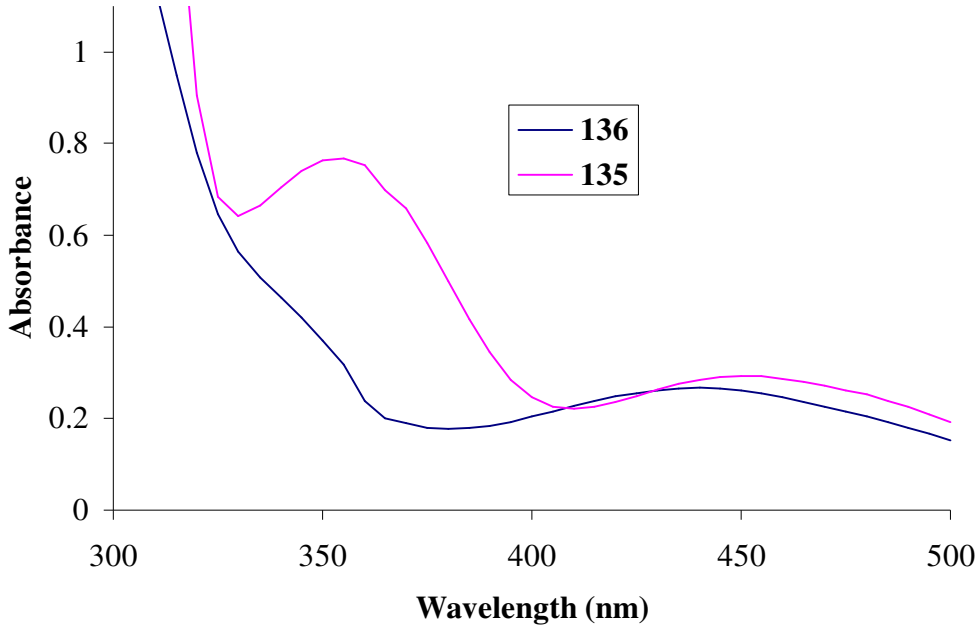

Fig. 5.12 Comparison between UV-Vis spectra of **135** and **136**.

5.8 Cyclic voltammetry.

Cyclic Voltammetry (CV) is a versatile electroanalytical technique for studying electroactive molecules [(5)]. It has been extensively used to evaluate the redox properties

of organometallic species, including ferrocene [6]. In a CV experiment, the voltage applied to the working electrode is scanned from an initial position, A, to a predetermined endpoint, D (Figure 5.13), the scan is then reversed. This forward and reverse scanning can be repeated as many times as is necessary. The potential of the working electrode is controlled versus a reference electrode. For the electrochemistry experiments reported Ag/AgCl is used as the reference electrode. This reference is used in preference to other reference electrodes namely the normal hydrogen electrode (NHE) and the saturated calomel electrode (SCE). The Ag/AgCl electrode is more robust and is easier to maintain. It also does not have the toxicity and safety problems associated with the SCE and NHE [7].

A cyclic voltammogram, is obtained by measuring the current at the working electrode during a potential scan. The voltammogram, such as that in Figure 5.13, is a plot of current versus potential.

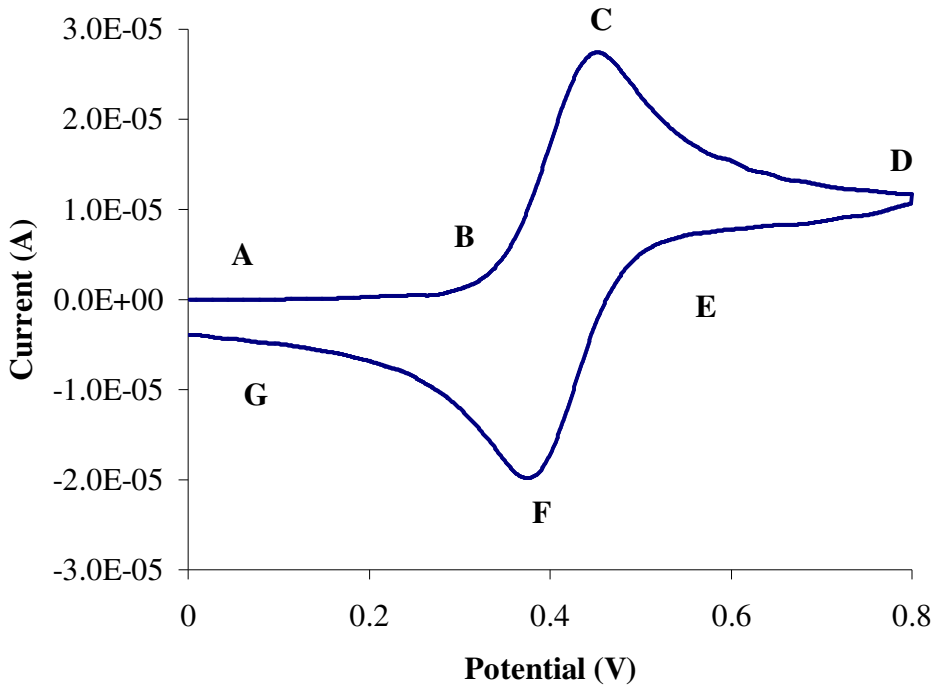

Fig. 5.13 CV of ferrocene in ACN with carbon working electrode, platinum counter electrode and Ag/AgCl reference electrode.

A. The initial potential is applied at 0 V. The potential is then scanned in a positive direction.

B. When the potential is sufficiently positive, the ferrocenyl compound is oxidised to the ferricenium compound, $Fc \rightarrow Fc^{+}$. The anodic current then begins to increase.

C. The anodic current continues to increase until the system surrounding the electrode is depleted of ferrocenyl compound due to its conversion to ferricenium species.

D-G. At this stage the ferricenium species begins to get reduced back to the ferrocenyl species, thus the cathodic current begins. As is the case with a redox system that behaves in an ideal fashion, the reverse scan roughly mirrors the forward scan. The reverse scan ends when the current reaches the start point, 0 V.

5.9 Preparation of the self assembled monolayers on gold.

Gold is the substrate of choice for sulphur containing SAMs, as gold electrodes can be handled in air without oxide formation and they can also tolerate harsh chemical procedures for the removal of organic contaminants [8].

Cleaning protocols form an important part of monolayer preparation. Polishing with 0.05 μm alumina and subsequent electrochemical cycling in 0.5 M H_2SO_4 acts as both a cleaning and an annealing process. Cyclic voltammograms resulting from redox cycling in the gold oxidation region evaluates the cleanliness and the crystallinity of the gold surface and also gives a true value of the gold surface area [9].

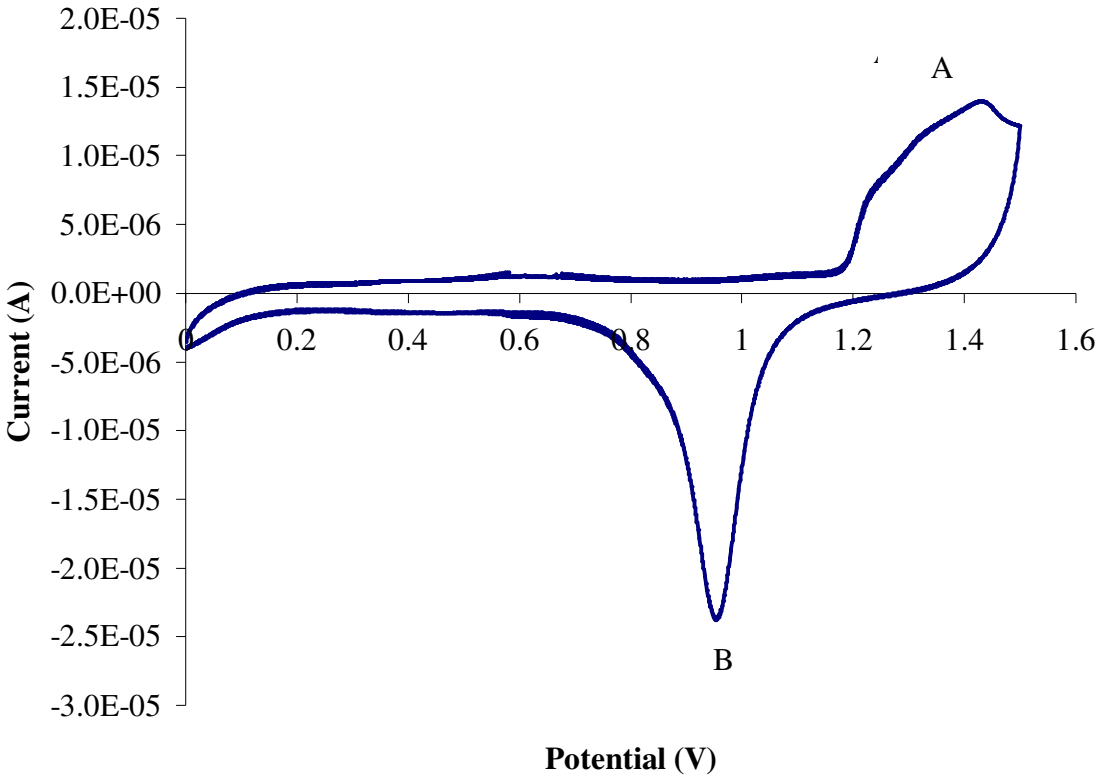

Fig. 5.14 CV of gold electrode during cleaning (0.1 V/s, 0.5 M H_2SO_4).

The potential limits selected in Figure 5.14 are the range within which the gold surface is oxidised and reduced. Oxide formation starts at 1.2 V with the current reaching a maximum at 1.4 V, point A. The area under the gold oxide reduction peak, point B, is used to determine the microscopic surface area of the electrode, equation 1.

$$\text{Area of gold reduction peak (C)} / 390\ (\mu C\ cm^{-2}) \qquad (1)$$

390 $\mu C\ cm^{-2}$ is the value used for the charge density of polycrystalline gold electrodes [10]. The area of the electrode cleaned in Figure 5.14 is 8.77×10^{-2} ($\pm 1.8 \times 10^{-3}$) cm^2.

Soaking the substrate in a solution of the self assembling compound at room temperature followed by rinsing is the most common method of SAM formation. Ethanol is the preferred solvent though any solvent that dissolves the compound can be used. Low

concentrations, in the micromolar range, are favoured for formation of monolayers with a large surface coverage, although quality is not always guaranteed. With higher concentrations a disordered monolayer is formed immediately, evolving into a highly orientated densely packed monolayer over a period of hours [11].

5.10 Electrochemical characterization of self assembled monolayers.

An ideal CV of an electroactive monolayer displays matching anodic and cathodic current peaks. Deviations from ideal CVs are common and reveal elements about the redox centre of the monolayer. A nonzero peak difference between the cathodic and anodic peaks is as a result of changes in the monolayer structure with respect to the redox active site. For example, it is possible for the redox centre in the oxidised form to precipitate with a counter ion. The formal potential (E°′) of the redox centre is also informative as it is common for the monolayer redox centre to have an E°′ value within 100 mV of the E°′ of the compound in solution, suggesting that the dielectric constant is similar to that found at the bare electrode [8].

The cyclic voltammograms of monolayers of **129** were recorded using a platinum wire as a counter electrode and Ag/AgCl as a reference electrode in 0.1 M $LiClO_4$ as supporting electrolyte. The SAM of compound **129** showed a one electron reversible redox wave at an oxidation potential of 0.554 V and a reduction potential of 0.503 V. When the CV of a monolayer of **129** is overlaid with the CV of a blank gold electrode the presence of the ferrocene/ferricenium redox couple is confirmed. This is outlined in Figure 5.15. Redox waves of the ferrocene/ferricenium redox couple are also observed in CV's of SAMs of **130**-**136**.

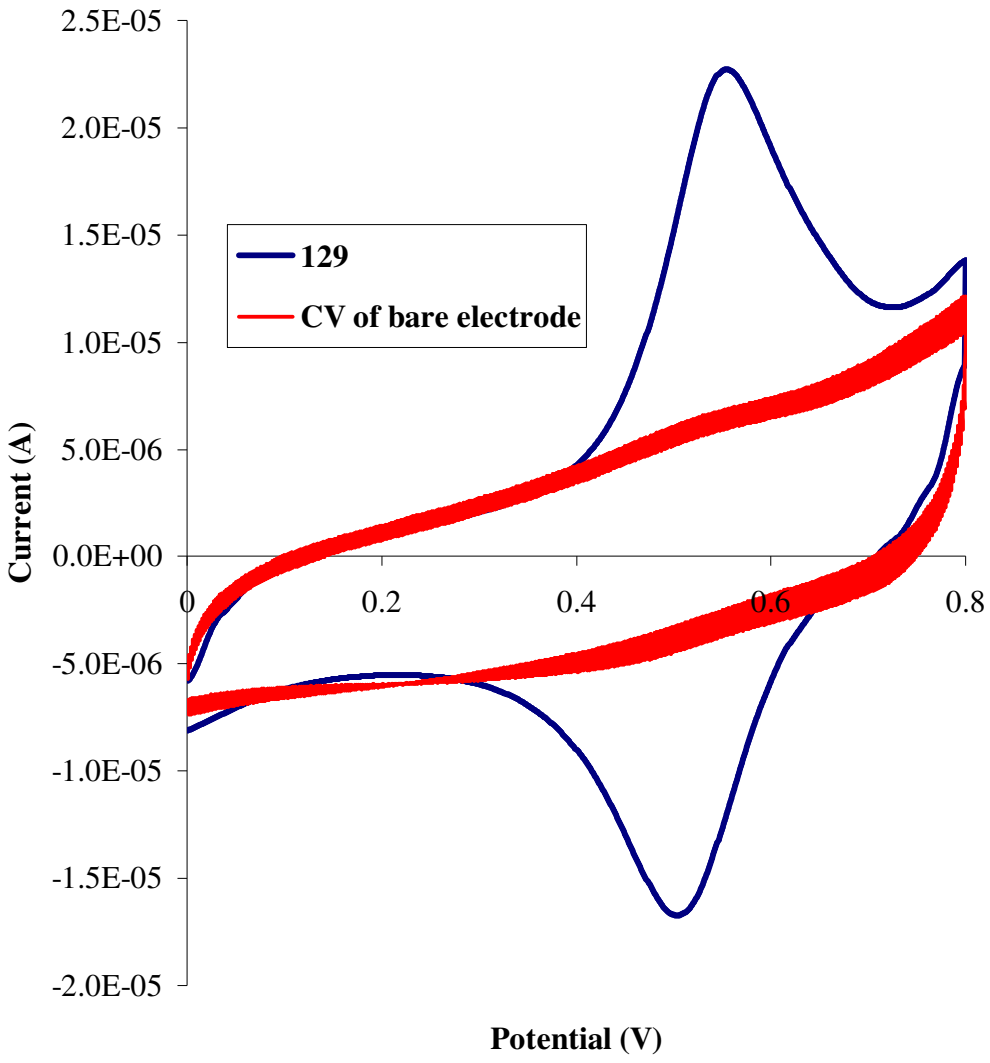

Fig. 5.15 CV of monolayer of compound **129** versus CV of bare gold electrode. (0.1 M $LiClO_4$, 0.1 V/s)

The coverage of the monolayer (Γ) on the electrode surface is calculated by integrating the oxidation peak current and inserting this value into equation 2 [8].

$$\Gamma = Q/ n FA \qquad (2)$$

Where Γ represents the surface coverage (mol/cm^2), Q is the area of peak (C), n is the number of electrons, F is the Faraday constant and A is the area of the electrode (cm^2) calculated from equation 1. A summary of surface coverage for the prepared monolayers in aqueous media are presented in Table 5.5.

Monolayers of thiols, sulphides and disulphides are stable over a wide range of potentials but at very negative potentials in strongly basic electrolytes they are desorbed quantitatively. The half reaction is outlined in equation 3 [12].

$$AuS\text{-}R + e^- \rightarrow Au\ (0) + {}^-S\text{-}R \qquad (3)$$

During desorption experiments electrodes were immersed in 0.5 M KOH and the potential was scanned cathodically from 0 to -1.20 V at a scan rate of 0.1 V/s. Figure 5.16 was recorded for a gold electrode with a monolayer of **136** and shows a desorption wave at -0.90 V versus Ag/AgCl which is due to reductive desorption of the cystine derivatives attached to the surface.

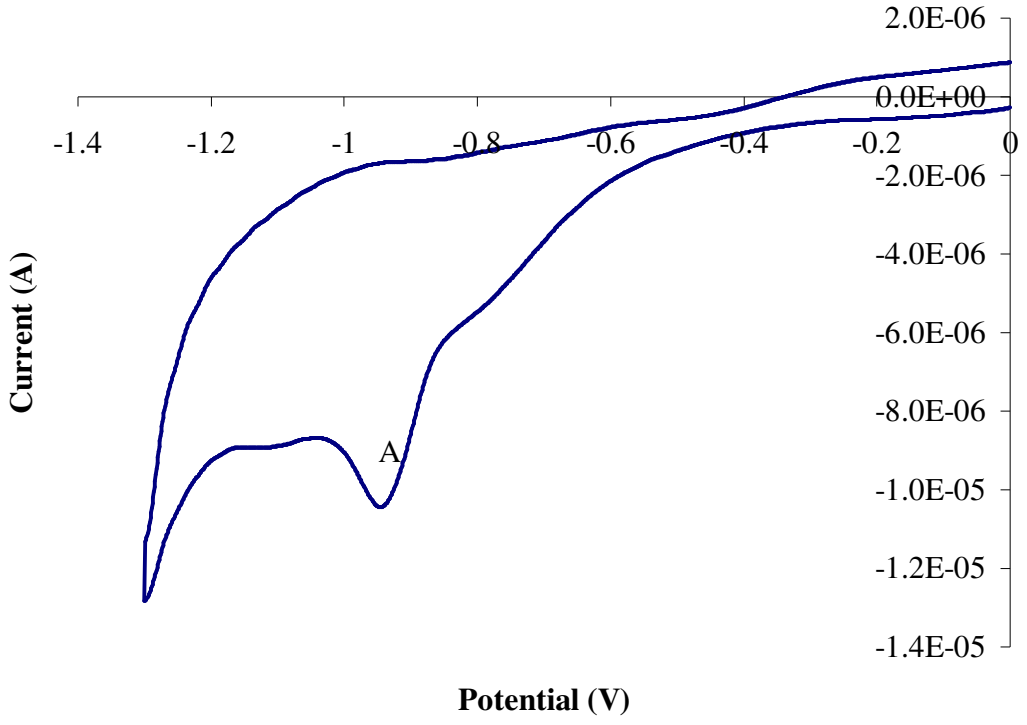

Fig. 5.16 Reductive desorption of a monolayer of **136**.

The shape and position of the desorption peak is indicative of similar monolayers [13]. By integrating the current under the cathodic wave, point A, an estimated surface coverage of $1.44 \times 10^{-10} \pm 1.4 \times 10^{-11}$ mol/cm^2 was obtained for monolayers of **136**.

When calculating surface coverage for monolayers with redox centres, it is usual however to use the peak current under the oxidation or reduction peak. This gives a truer reflection of the coverage of the electroactive species on the surface of the electrode. The results of the electrochemical measurements are summarized in Table 5.5.

From this data it is possible to appreciate the effects an aromatic spacer has on the redox potential of each monolayer. Monolayers of compounds **131**, **132**, **133**, **134** and **135** all have lower redox potentials than monolayers of compounds **129**, **130** and **136**. There is a 200 mV difference between the monolayers with an aromatic spacer and **130**. The large difference in the redox potential of **130** and the other monolayers is possibly explained by the orientation of the ferrocene ring [14] and its disubstituted nature, making the removal of an electron in the oxidation step difficult.

As the monolayers that contain aromatic spacers possess lower redox potentials it is possible that the conjugation of these spacers facilitates the electron transfer process to and from the ferrocene centre. In other words the conjugation acts as an electron bridge and therefore makes electron transfer easier compared to the monolayers with no aromatic spacer.

Table 5.5 Electrochemical characteristics and adsorption values of Au electrodes modified with **129**-**136**.

Compound	**E*pa* (V)**	**E*pc* (V)**	**E°′ (V)**	**Coverage (mol/cm^2)**
129	0.551	0.506	0.529	$1.29 \times 10^{-10} \pm 4.5 \times 10^{-12}$
130	0.783	0.725	0.754	$1.06 \times 10^{-10} \pm 8.1 \times 10^{-12}$
131	0.386	0.336	0.361	$3.33 \times 10^{-10} \pm 4.2 \times 10^{-12}$
132	0.413	0.334	0.374	$1.44 \times 10^{-10} \pm 3.9 \times 10^{-12}$
133	0.472	0.402	0.436	$2.68 \times 10^{-10} \pm 9.3 \times 10^{-12}$
134	0.504	0.347	0.426	$3.48 \times 10^{-10} \pm 1.6 \times 10^{-11}$
135	0.416	0.338	0.377	$6.18 \times 10^{-10} \pm 6.2 \times 10^{-12}$
136	0.515	0.473	0.494	$1.20 \times 10^{-10} \pm 8.3 \times 10^{-12}$

A linear relationship between scan rate υ and oxidation peak current i_p was also found for **129-136**. This relationship is evident from equation 4 [7], therefore a plot of current (A) versus scan rate (V/s) will be linear. Figure 5.17 shows a scan rate dependence plot of **132**.

$$i_p = n^2F^2A\Gamma\upsilon / 4RT \qquad (4)$$

The linear relationship between current and scan rate is illustrated by Figure 5.17. With an R^2 value of 0.99 it can be said that the monolayer of **132** exhibits standard monolayer behaviour. This relationship between scan rate and current is schematically represented in Figure 5.18.

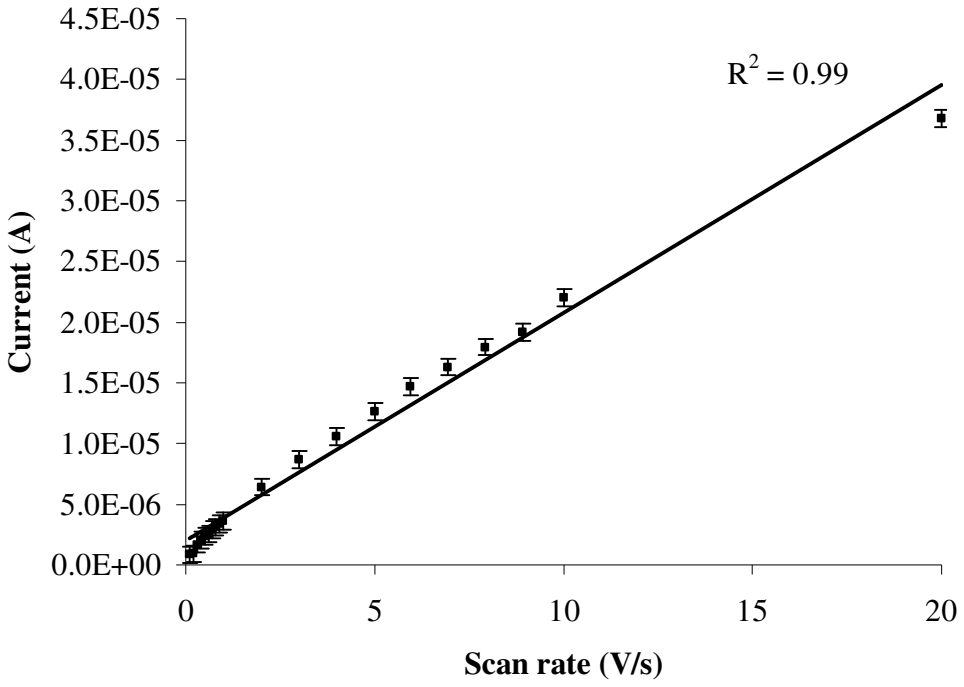

Fig.5.17 Scan rate dependence plot of a monolayer of **132** (0.1 M, $LiClO_4$)

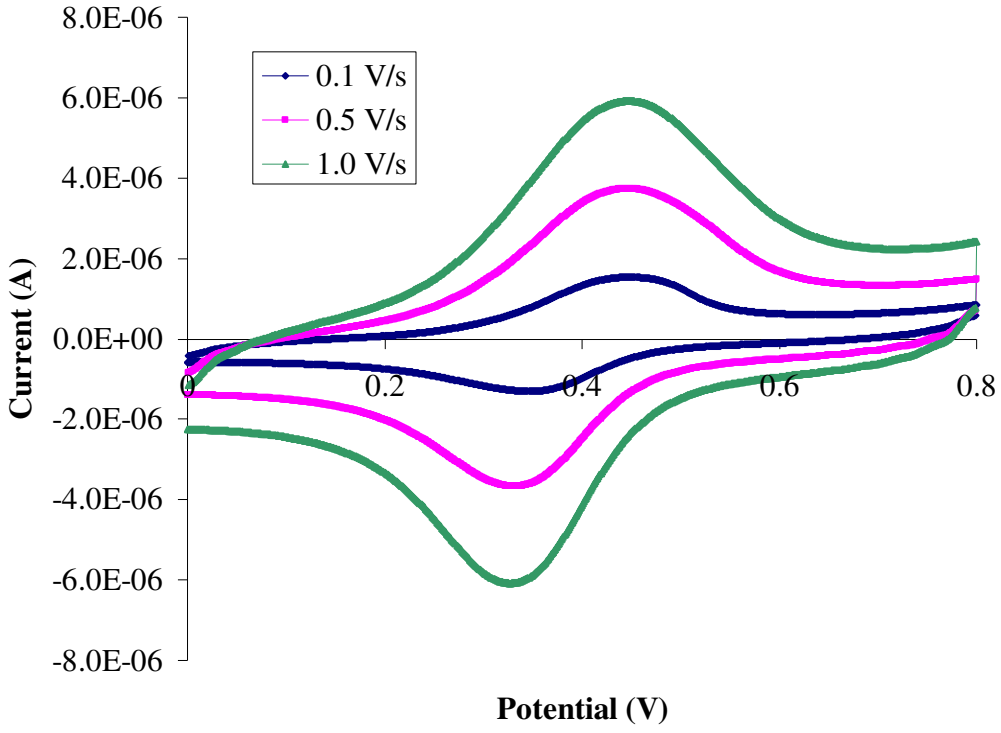

Fig. 5.18 Relationship between scan rate and peak current.

5.11 Conclusions.

N-(ferrocenyl)$_2$ and *N*-(ferrocenoyl)$_2$ cystine dimethyl esters were prepared *via* conventional peptide chemistry and characterized *via* a range of spectroscopic techniques for example, ^{1}H NMR, ^{13}C NMR, DEPT 135, HMQC, IR, UV-Vis, MS and CV.

These compounds were then successfully immobilized onto gold electrodes for the purposes of anion sensing in aqueous media. The immobilization event is aided by the affinity of sulphur atoms for coinage metals such as gold. The monolayers were characterized using a series of electrochemical procedures. Monolayers of each compound exhibited standard monolayer behaviour as the relationship between scan rate and oxidation peak current was linear with a high degree of correlation in each case. In order to improve yields and simplify purification a modified procedure may be used. S-benzyl cysteine, in place of L-cystine methyl ester, would make the coupling of more amino acid residues to the sulphur bearing group more straightforward. Subsequent

removal of the benzyl group would allow for the immobilization of the receptor on gold surfaces. Such an approach may result in an easier synthetic route for the receptor molecules. With the judicious choice of starting materials cavities of varying sizes would result, increasing the selectivity of these receptors.

References

1. Zhang, S., Cardona, C. M., Echegoyen, L., *Chem. Comm.*, **2006**, 4461.
2. Beer, P. D., Gale, P. A., *Angew. Chem. Int. Ed.*, **2001**, *40*, 486.
3. Zhang, S., Palkar, A., Echegoyen, L., *Langmuir*, **2006**, *22*, 10732.
4. Bodanzsky, M., '*Principles of Peptide Synthesis*', Oxford Science Publications, **1992**.
5. Chen, Z., Graydon, A. R., Beer, P. D., *J. Chem. Soc., Faraday Trans.*, **1996**, *92*, 97.
6. Mabbott, G. A., *J. Chem. Ed.*, **1983**, *60*, 697.
7. Bagotsky, V. S., *'Fundamentals of Electrochemistry'*, John Wiley and Sons, **2006**.
8. Finklea, H. O., '*Self-assembled Monolayers on Electrodes*', Encyclopedia of Analytical Chemistry, John Wiley and Sons.
9. Hoogvliet, J. C., Dijksma, M., Kamp, B., van Bennekom, W. P., *Anal. Chem.*, **2000**, *72*, 2016.
10. Trasatti, S., Petrii, O. A., *Pure & Appl. Chem.*, **1991**, *63*, 711.
11. Bain, C. D., Troughton, E. B., Tao, Y-T., Evall, J., Whitesides, G. M., Nuzzo, R. G., *J. Am. Chem. Soc*., **1989**, *111*, 321.
12. Walczak, M. M., Popenoe, D. D., Deinhammer, R. S., Lamp, B. D.,Chung, C., Porter, M. D., *Langmuir*, **1991**, *7*, 2687.
13. Zhang, S., Echegoyen, L., *J. Am. Chem. Soc*., **2005**, *127*, 2006.
14. Kondo, T., Takechi, M., Sato, Y., Uosaki, K., *J. Electroanal. Chem.*, **1995**, *381*, 203.

Chapter 6

Anion Binding Studies of *N*-(ferrocenyl)$_2$ and *N*-(ferrocenoyl)$_2$ cystine dimethyl esters.

6.1 Introduction.

Redox active receptors have great potential as chemical sensors for the detection of non-electroactive ionic species. It is possible to convert molecular level interactions into electrochemically detectable signals. Particular attention has therefore focussed on the immobilization of redox active groups onto receptors to facilitate the measurement of host-guest interactions [(1)]. Receptors that contain ferrocene are of particular interest as ion pairing interactions, an important sensing mode, can be switched on by ferrocene oxidation. Ion-pairing interactions are of particular importance in sensing negatively charged species. The detection and quantitation of anions is of crucial importance due to their roles in every day life. They are implicated in various biological processes, the eutrophication of waterways and the pollution of seas and oceans by pertechnetate following the reprocessing of nuclear fuel [(2)]. Anion receptor design is a particular challenge as they are larger than cations and therefore have a lower charge to radius ratio meaning electrostatic interactions are less effective. Anions are also sensitive to pH, therefore the receptor must act within the pH range of the anion. They also display a wide range of geometries making receptor design more challenging.

The majority of results in the field of anion sensing have been reported in bulk organic solvent. It is important to transfer these recognition events to solid surfaces as the recognition event is greatly enhanced at the surface solution interface. This will therefore aid the sensing of anions in aqueous media. This laboratory has recently published the anion sensing ability of ferrocenyl receptors in organic solvent [(3, 4)]. It was anticipated that by confining the receptor molecules to the electrode surface it would facilitate the binding of various anions in aqueous media. The peptide residues would utilise the hydrogen bonding ability of the amide bond, while the ferrocene moiety would impart

electrostatic interactions to the systems following oxidation. This is illustrated in Figure 6.1.

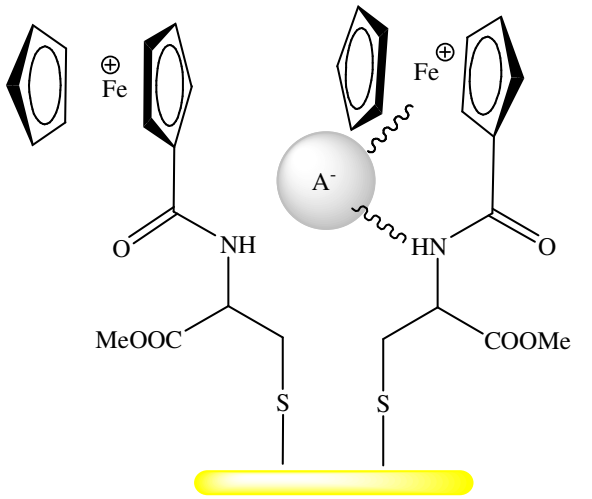

Fig. 6.1: Potential anion binding sites of monolayers of *N*-ferrocenyl and *N*-ferrocenoyl peptide esters, for example **129**.

Each of the synthesised receptors were titrated against three anions, namely chloride, nitrate and dihydrogen phosphate. These anions were selected for their role in water pollution and eutrophication effects. A body of water can be defined as eutrophic if it has an accelerated growth of algae and other higher forms of plant life caused by nutrient enrichment, especially nitrogen and/or phosphorus compounds [(5)]. This leads to an undesirable disturbance to the quality of the water and to the balance of organisms present. Care must be taken when using the term eutrophication, it is essential that the disturbance to the aquatic environment is a consequence of nutrient enrichment, as other factors e.g. climate change can lead to similar changes in the aquatic environment. Anthropogenic eutrophication in coastal areas is a world wide problem of increasing severity where there has been an increase in the occurrence of opportunistic seaweed, Harmful Algal Blooms (HAB), Toxin Producing Algae (TPA), as well as loss of seagrass meadows and harm to fisheries [(6)]. There is a particular concern for landlocked water basins and the Irish Sea would appear to be vulnerable to eutrophication due to it being

an inner sea and it receiving large quantities of anthropogenic nutrients from river discharges.

Eutrophication is therefore the major threat to water quality in Ireland [7]. Nutrient losses from agricultural practices have been implicated directly and indirectly for the eutrophication of surface water in Ireland and the UK. The main point source pollution from agriculture is inappropriately managed farmyard dirty water. This generally consists of farmyard run off, parlour washings, silage and farmyard manure effluents. Land spreading is the most common practice for managing dairy farm dirty water, however, this can lead to the degradation of surface and ground water.

The over fertilisation of grassland has also been identified as a common problem in Ireland. It has recently been reported that 70% of the anthropogenic load of phosphorus in Irish freshwater is from agricultural sources. Nitrogen is also an important contributory factor to eutrophication and has human health implications when present in high concentrations [8]. Therefore, the development of novel sensory devices for the detection of nitrates, phosphates and other anionic pollutants is of considerable importance to the environment and the future of our waterways. These anions were also selected as they display an array or geometries namely, spherical, trigonal planar and tetrahedral.

6.2 Electrochemical anion coordination studies of monolayers of *N*-(ferrocenyl)$_2$ and *N*-(ferrocenoyl)$_2$ cystine dimethyl esters in aqueous media.

The anion sensing ability of monolayers of *N*-ferrocenyl and *N*-ferrocenoyl peptide esters were investigated by cyclic voltammetry experiments. All the electrochemistry experiments were carried out on equipment kindly supplied by Dr. Mary Pryce. A standard three-electrode setup, Figure 6.2, was employed in all experiments where gold was the working electrode, platinum wire was the counter electrode and Ag/AgCl was the reference electrode. The CVs were measured in deionized water with lithium perchlorate ($LiClO_4$) as supporting electrolyte. The measurements were carried out at room temperature and at a scan rate of 0.1 V/s.

Important features of CVs include the position of the anodic peak potential (E_{pa}) and the cathodic peak potential (E_{pc}) [9]. The formal oxidation potential ($E°'$) for an

electrochemically reversible couple, in which electrons are rapidly exchanged, is centred between E_{pa} and E_{pc} and given by equation 1.

$$E^{\circ\prime} = \frac{E_{pa} + E_{pc}}{2} \qquad (1)$$

The magnitude of oxidation and reduction peak current should also be noted as changes in the peak current provide information on the surface coverage of redox molecules on the electrode surface.

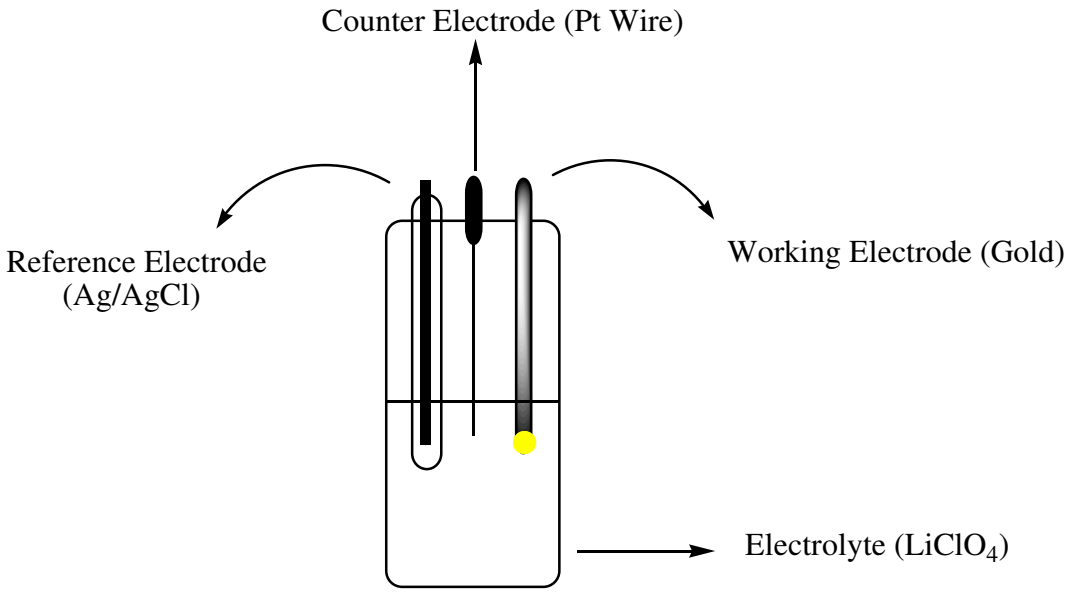

Fig. 6.2 Schematic diagram of an electrochemical cell as used in anion titration experiments.

The monolayers of each compound **129-136** were preliminarily titrated with 2 ml of a 0.01 M solution of chloride, nitrate and dihydrogen phosphate anions, as their tetrabutylammonium salts. It was anticipated that the CVs would display a negative shift in the Fc/Fc^+ redox couple. This is due to the redox centre becoming more easily oxidised following an increase in electron density upon anion binding. However in each case the change in redox potential was minimal but a noticeable change in the peak current of the oxidation and reduction peaks was observed. It is reasonable to suggest that this decrease in peak current is as a result of irreversible binding between the receptor and the anion.

The formerly redox active centre is no longer able to participate in electron transfer resulting in a loss of redox active compounds on the surface of the electrode [1].

The percentage changes in current of the oxidation and reduction peaks of each monolayer are displayed in Table 6.1.

Table 6.1 Percentage decrease in oxidation (Oxn) and reduction (Red) peak current.

Monolayer of:	**Chloride**	**Dihydrogen phosphate**	**Nitrate**
	Oxn (± %), Red (± %)	Oxn (± %), Red (± %)	Oxn (± %), Red (± %)
129	36 (2), 26 (1)	61 (3), 47 (2)	55 (2), 62 (1)
130	N/A*	N/A*	N/A*
131	74 (1), 70 (1)	50 (1), 48 (2)	43 (2), 70 (2)
132	41 (2), 33 (2)	54 (2), 59 (2)	27 (1), 24 (1)
133	26 (2), 31 (2)	54 (3), 59 (2)	27 (3), 24 (1)
134	22 (<1), 8 (1)	1 (<1), 23 (2)	4 (<1), 10 (2)
135	68 (5), 60 (2)	28 (3), 51 (2)	23 (<1), 40 (2)
136	45 (1), 30 (2)	77 (1), 57 (1)	70 (1), 54 (3)

*Note: During titration of monolayers of **130** with anions there was a complete loss of redox activity. The recognition efficiency could therefore not be measured (Figure 6.3).

This acute sensitivity of monolayers of **130** upon titration with various anions is possibly a result of complete complexation of the redox active molecules on the electrode surface. The vast majority of ferrocene molecules are involved in a receptor-anion complex, resulting in complete loss of a redox process in the potential range used.

The sensitivity of **136** towards dihydrogen phosphate is illustrated in Figure 6.4. This is a consequence of the interaction between the anion and the binding sites of the receptor. The formation of a new host-guest complex would generally be expected to yield a new reversible redox wave. However this is not observed in the potential range used. The decrease in peak current of the oxidation and reduction peaks is clearly visible.

The relative insensitivity of **134** towards anions is also illustrated in Figure 6.5. It is possible that the relatively small change in peak current is due to the distance between the two potential binding sites, namely the electrostatic interactions of the ferrocene moiety

and the H-bonding capabilities of the amide bond. This emphasises the importance of electrostatic and hydrogen bonding cooperative interaction to the sensing event.

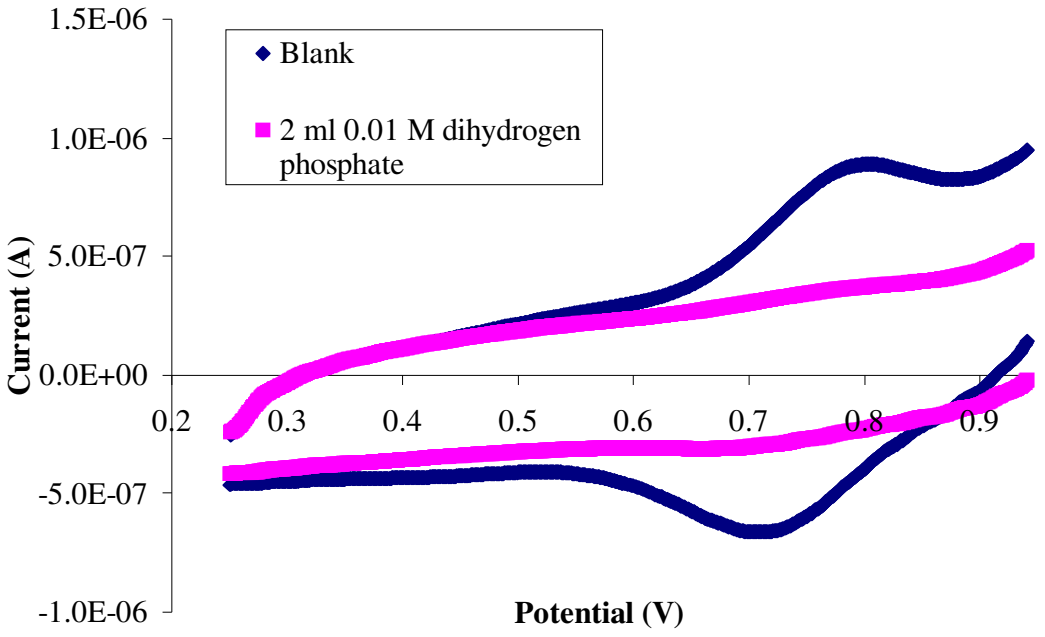

Fig. 6.3 Sensitivity of monolayers of **130** towards dihydrogen phosphate

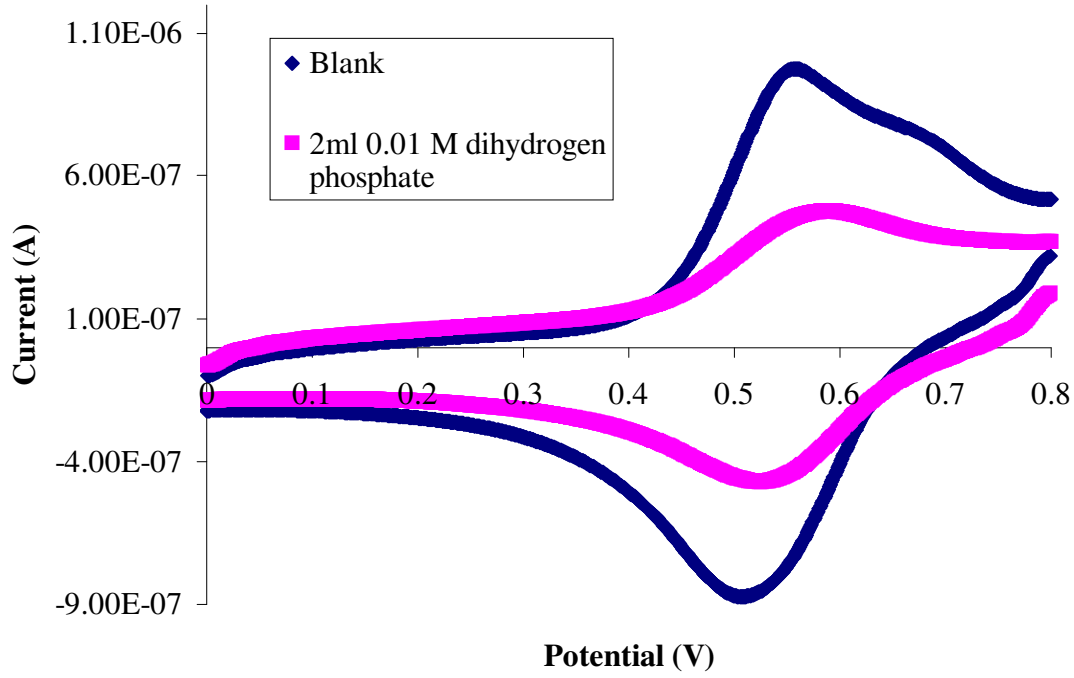

Fig. 6.4 The sensitivity of monolayers of **136** towards dihydrogen phosphate.

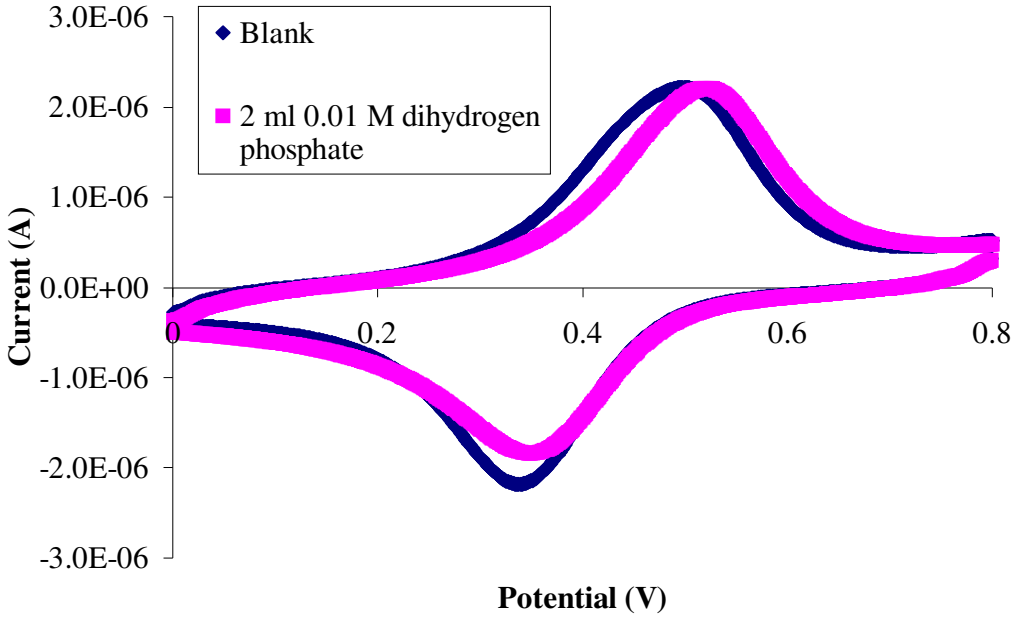

Fig. 6.5 Relative insensitivity of monolayers of **134** towards dihydrogen phosphate.

The affinity of **131** for chloride is of particular interest as *N*-(ferrocenyl)benzoyl peptide esters were found to have little or no affinity for anions during CV titration experiments in bulk solution [(10)]. When the orientation of the molecule on the electrode surface is considered it is possible that a favourable binding cavity for the spherical chloride ion is formed. The close proximity of the amide group and the ferrocene would allow for cooperative interaction between the binding sites and the target anion. The potential binding cavity is illustrated in Figure 6.6. As the orientation of the amide bond around the benzene ring changes to *meta* and *para* the sensitivity of the molecules towards chloride ions decreases, possibly due to the increasing size of the binding cavity and the loss of cooperative interaction between the amide group and the ferrocene. This once again underlines the significance of both the ferrocene and the peptide moieties in the sensing process.

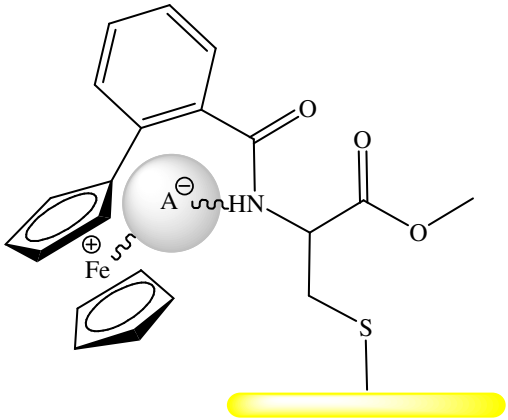

Fig. 6.6 Potential binding cavity of a monolayer of **131**.

Monolayers of **136** display remarkable affinity for nitrate and dihydrogen phosphate anions showing a large decrease in oxidation and reduction peak current in each case. It is possible that the additional amide groups and their proximity to ferrocene enhance the cooperative interaction and the subsequent binding between the receptor and the trigonal planar nitrate and the tetrahedral dihydrogen phosphate anion, Figure 6.7.

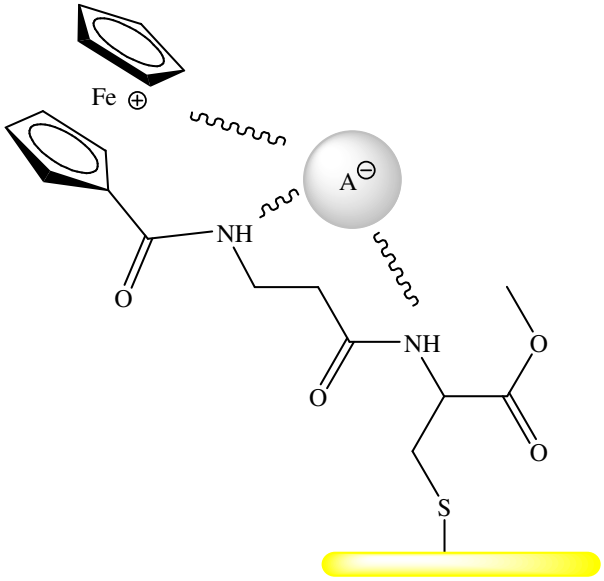

Fig. 6.7 Cooperative interactions involved in binding by monolayers of **136**.

6.3 Monolayer response to changing anion concentration in aqueous media.

In order to further evaluate the sensitivity of monolayers of **131** and **136** to chloride, nitrate and dihydrogen phosphate, a series of solutions of each anion ranging from 10^{-5} M to 10^{-1} M were prepared in deionized water with $LiClO_4$ as supporting electrolyte.
It was anticipated that as anionic concentration increased the decrease in oxidation and reduction peak current would be linear. A plot of change in current of the oxidation and reduction peaks versus anion concentration (1×10^{-5} to 1×10^{-1}) was obtained for each anion. Triplicate measurements were taken for electrodes modified with **131** and **136** in solutions of anions as their tetrabutylammonium salts.

6.3.1 Response of monolayers of 131 to chloride

The plot of change in current for a monolayer of **131** versus concentration of chloride anions is described in Figure 6.8. A high degree of linearity is observed in Figure 6.8. with R^2 values of 0.9952 and 0.9959 for plots of concentration versus changes in oxidation and reduction peak current respectively. The original oxidation and reduction peak currents in blank electrolyte were 1.5^{-6} A and 1.2^{-6} A respectively. Figure 6.9 represents the obvious change in oxidation and reduction peak current as the concentration of chloride anions is increased. Upon titration with the least concentrated solution (1×10^{-5} M) the oxidation peak current decreases by 1^{-6} A, while the reduction peak decreases by around 4^{-7} A. When titrated against the most concentrated solution the overall decrease is approximately 90% of the original oxidation and reduction peak currents. Despite this large decrease the reversible redox activity is maintained.

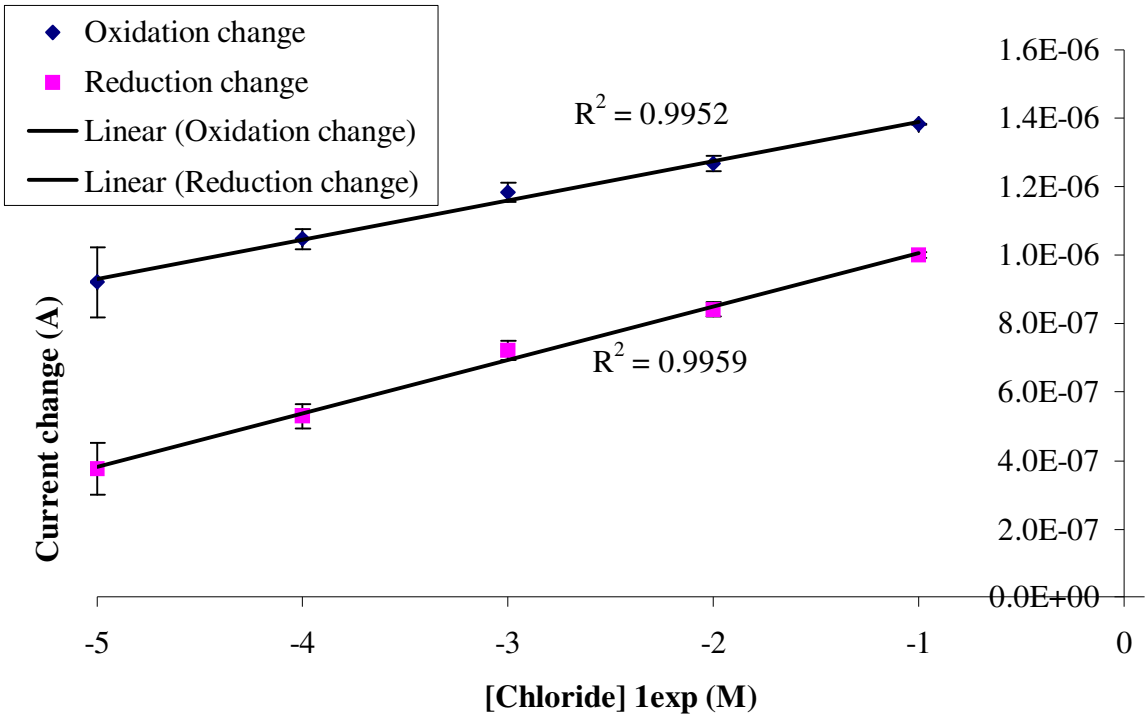

Fig. 6.8 Linear response of monolayers of **131** to changing chloride concentration.

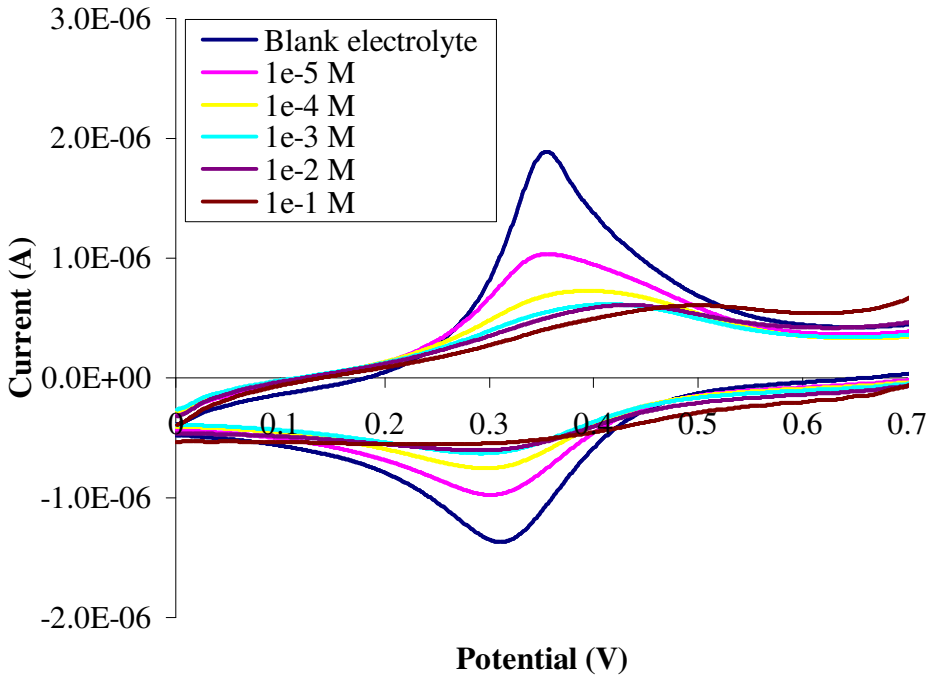

Fig. 6.9 Amperometric response of **131** to changing chloride concentration.

6.3.2 Response of monolayers of 136 to dihydrogen phosphate

The amperometric response of monolayers of **136** to increasing concentrations of dihydrogen phosphate is also linear. The change in current of the oxidation and reduction peaks correlates well with increasing concentration as evidenced by R^2 values of 0.9901 and 0.9904 respectively, Figure 6.10. The peak current values for the ferrocene/ferricenium redox couple in blank electrolyte were 8.3^{-7} A and 8^{-7} A respectively. This linear relationship is clearly illustrated in Figure 6.11. The overall changes in peak currents is comparable with those observed in Figure 6.9, 87% and 75% respectively, even though the initial current values in blank electrolyte were less than in Figure 6.9.

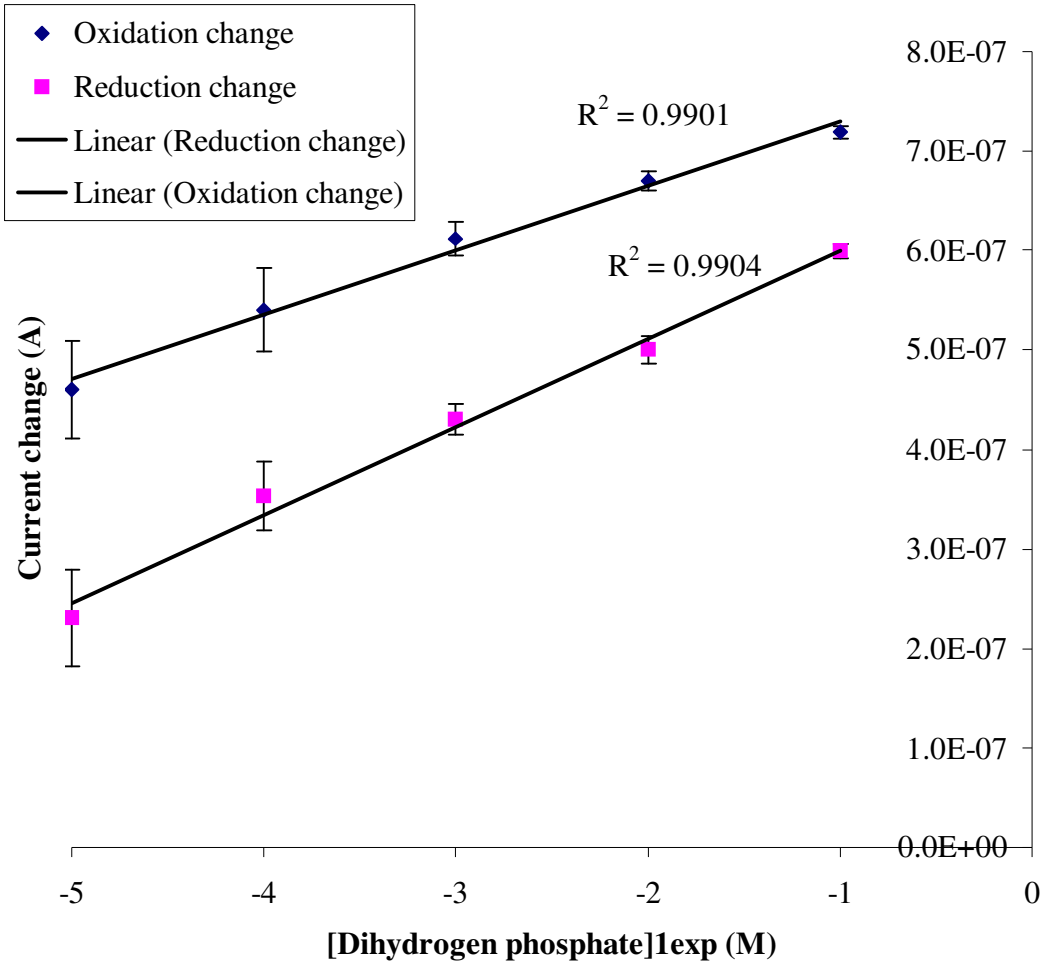

Fig. 6.10 Response of monolayers of **136** to dihydrogen phosphate.

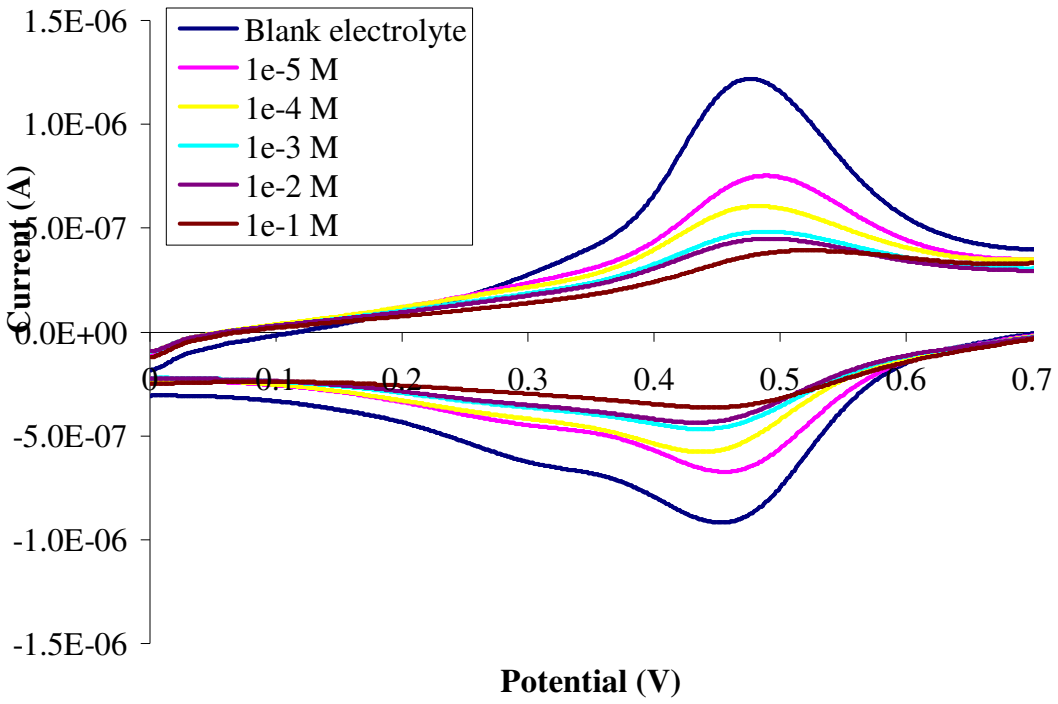

Fig. 6.11 Amperometric response of monolayers of **136** to dihydrogen phosphate.

6.3.3 Response of monolayers of 136 to nitrate

The amperometric response of monolayers of **136** to increasing concentrations of nitrate is also linear with a slightly lower degree of correlation between the data points, Figure 6.12, with R^2 values of 0.9811 and 0.9824 respectively. The initial oxidation and reduction peak currents were 1.3^{-6} A and 1.1^{-6} A in blank electrolyte. The gradual decrease in oxidation and reduction peak currents for monolayers of **136** are clearly illustrated in Figure 6.13. The decrease in peak current is consistent with those observed for chloride and dihydrogen phosphate anions, Figure 6.8 and Figure 6.10, with decreases of 86% and 73% for the oxidation and reduction peak currents.

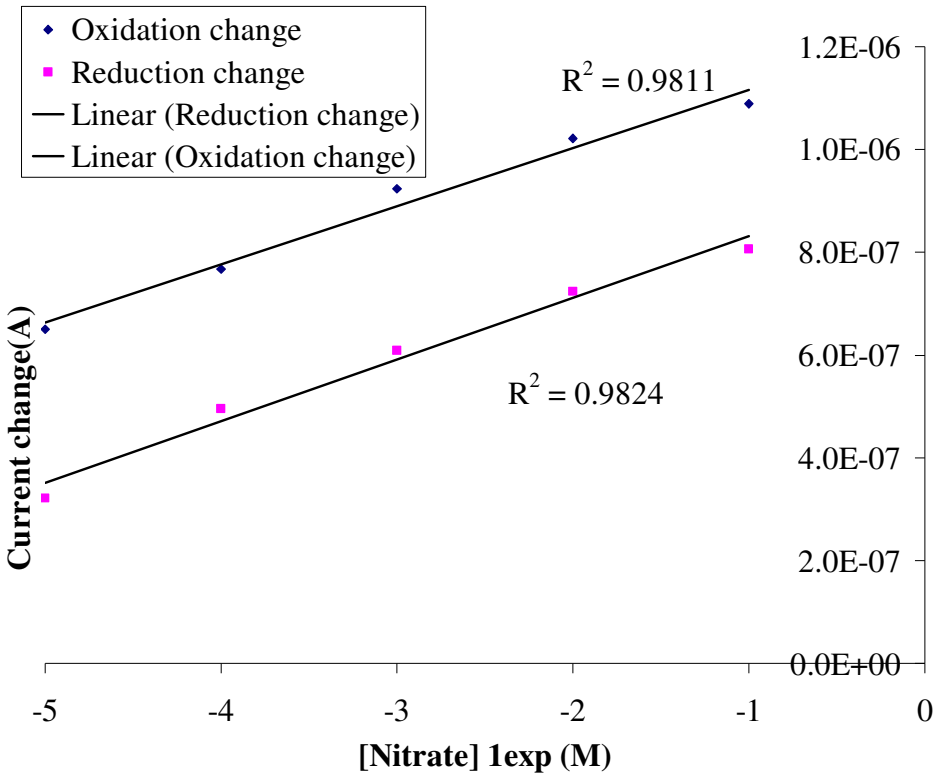

Fig. 6.12 Response of monolayers of **136** to nitrate.

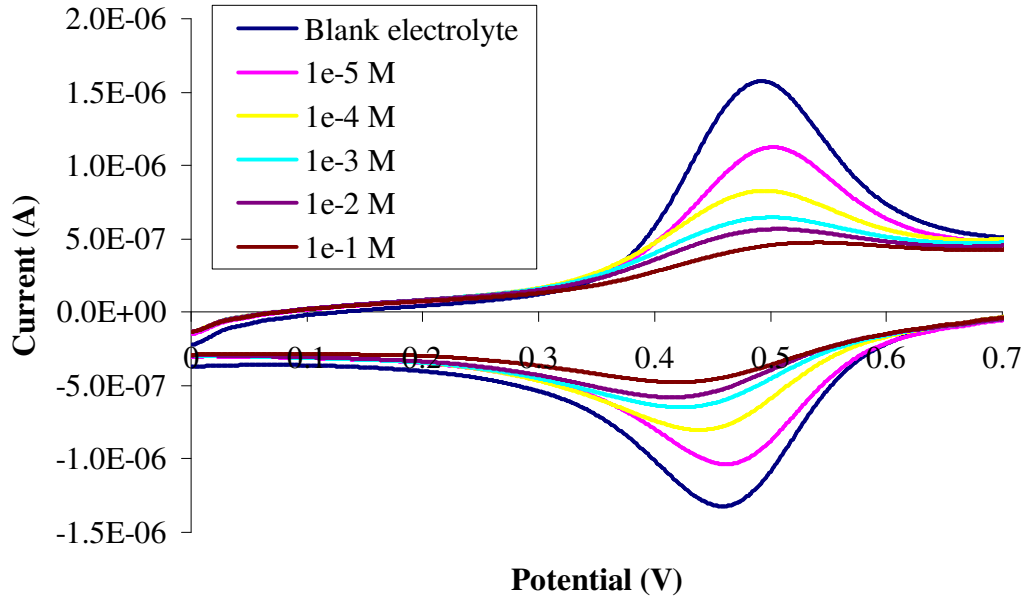

Fig. 6.13 Amperometric response of monolayers of **136** to nitrate

6.4 Determination of adenosine nucleotides in aqueous media.

Monolayers of **136** displayed notable linear response to dihydrogen phosphate anions (Figure 6.10), therefore it was of interest to investigate the response of monolayers of **136** to the biologically important adenosine nucleotide anions, namely adenosine triphosphate **137** (ATP), adenosine diphosphate (ADP) and adenosine phosphate (AMP).

Adenosine nucleotides play crucial roles in cellular metabolism and biochemical pathways. The primary function of ATP is as a medium for intracellular energy transfer. ADP and AMP are also heavily involved in various biochemical processes therefore the accurate measurement of nucleotides is essential, especially when investigating conditions such as cardiac ischemia. As ATP is present in all living cells and disappears rapidly upon cell death it is often used as a gauge of microbial activity in soils, the freshness of fish and as a quality control marker for blood prior to transfusion [(11)].

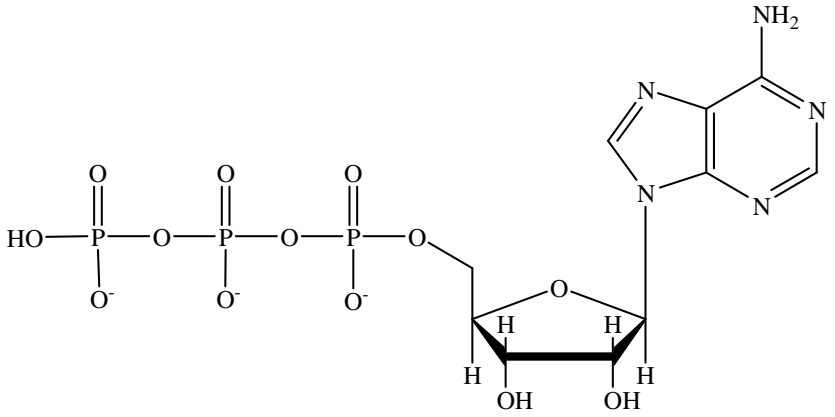

137

CV experiments were performed in aqueous solution of each adenosine nucleotide in concentrations ranging from 1 x 10^{-9} M to 1 x 10^{-1} M with 0.1 M $LiClO_4$ as supporting electrolyte. The changes in oxidation and reduction potential of the ferrocene redox couple, relative to the potentials in anion-free electrolyte, were subsequently plotted versus increasing anion concentration. In the case of each nucleotide the response of both the oxidation and reduction peaks was linear with R^2 values *circa* 0.99 in each case (Figures 6.14, 6.15 and 6.16). Figure 6.17 displays the amperometric response of monolayers of **136** to ATP. These results indicate the sensitivity of monolayers of **136** to

adenosine nucleotides in aqueous media. Sensitivity in the nanomolar range was observed with the electroactivity of the ferrocene/ferricenium redox couple maintained throughout. There were minimal cathodic or anodic shifts in the position of the redox couple. No new reversible redox couples corresponding to a **136**-anion complex was observed in the potential range used.

In titration with AMP the overall decrease in the current of the oxidation and reduction peaks was 96% and 90% respectively. When monolayers of **136** were titrated against ADP, the overall response was similar to that of AMP titrations with a decrease of 89% and 93% in the oxidation and reduction peaks of the ferrocene/ferricenium redox couple compared to in blank electrolyte. Similarly during experiments with ATP the overall decreases were 84% and 79% for the oxidation and reduction peaks respectively. These large decreases in peak currents demonstrate the sensitivity of such monolayers to adenosine nucleotides, however redox activity was maintained throughout, thus facilitating the accurate measurement of changes in redox activity.

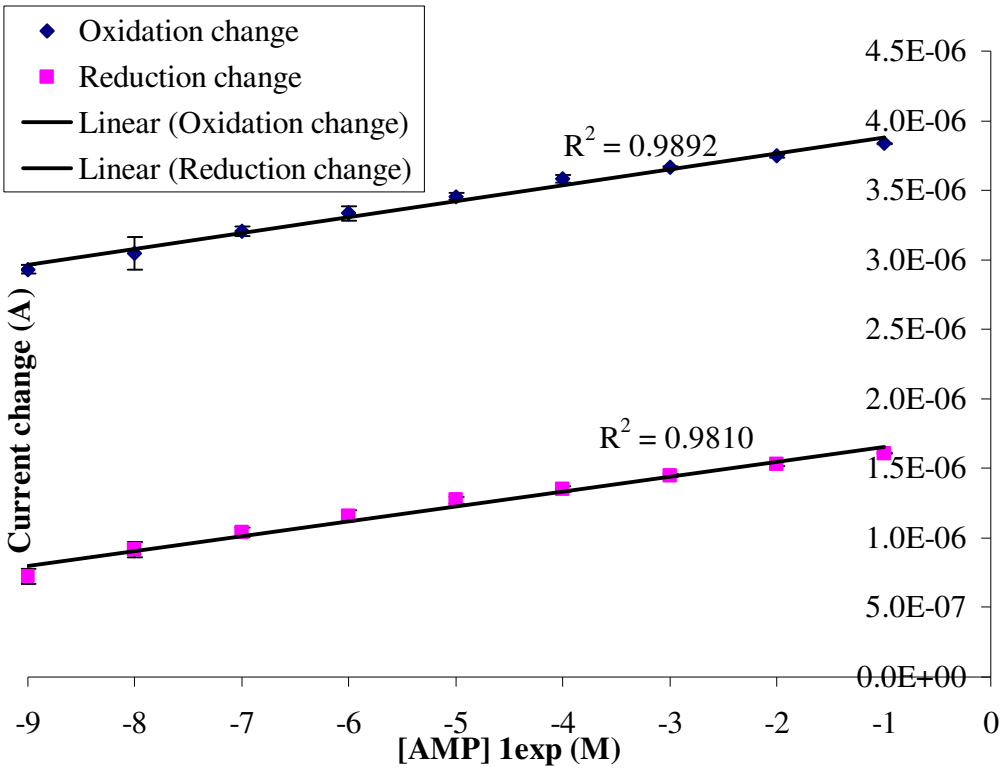

Fig. 6.14 Response of monolayers of **136** to AMP.

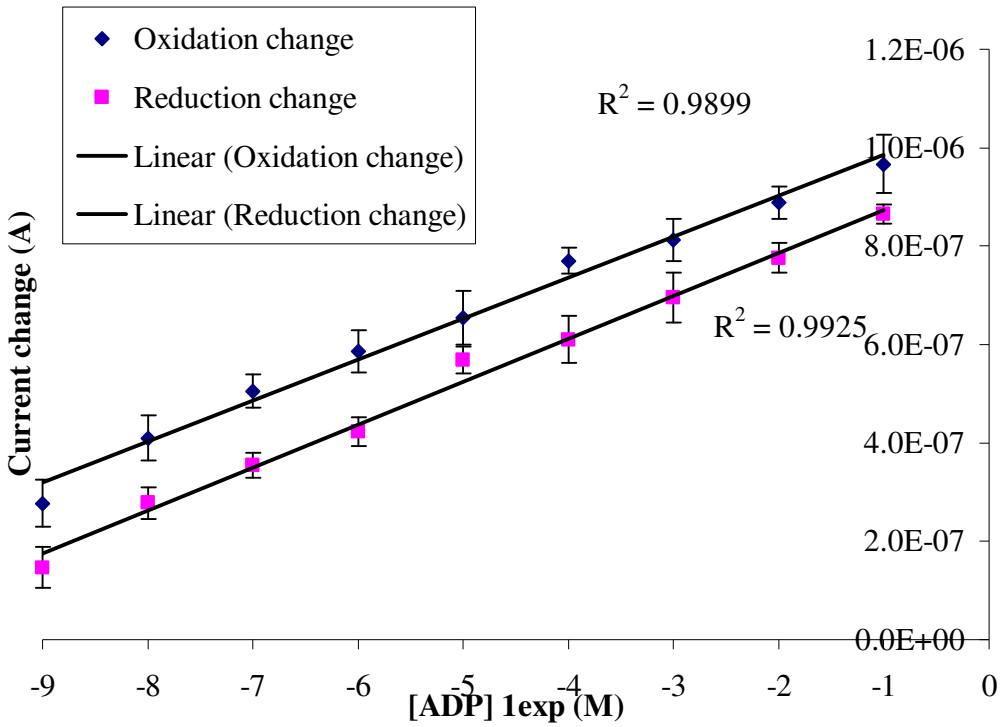

Fig. 6.15 Response of monolayers of **136** to ADP.

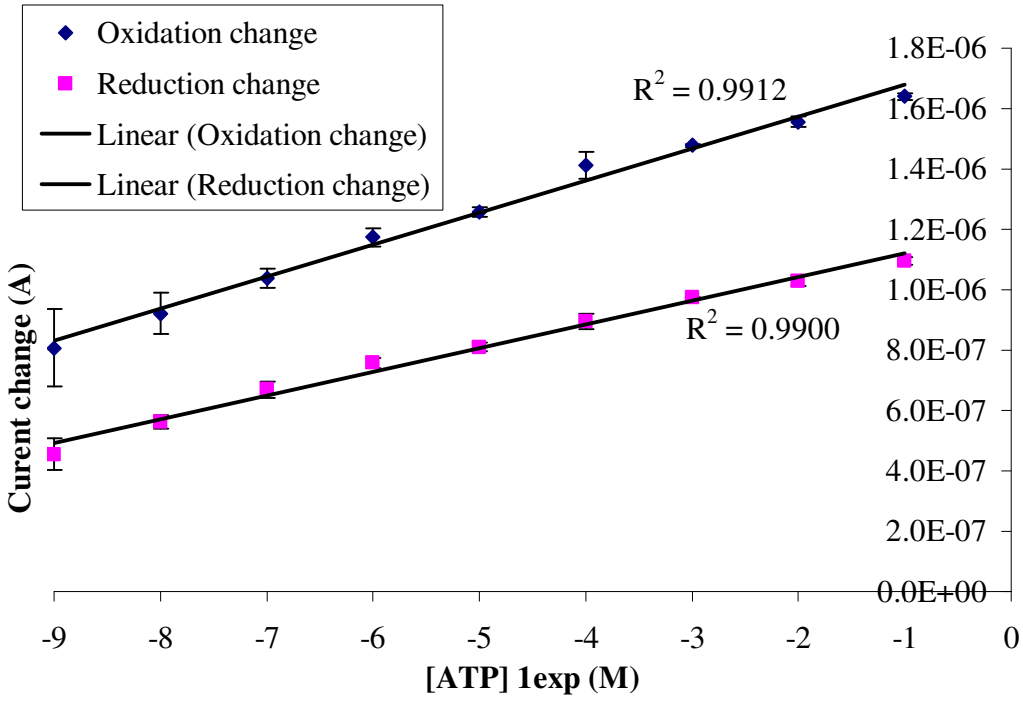

Fig. 6.16 Response of monolayers of **136** to ATP.

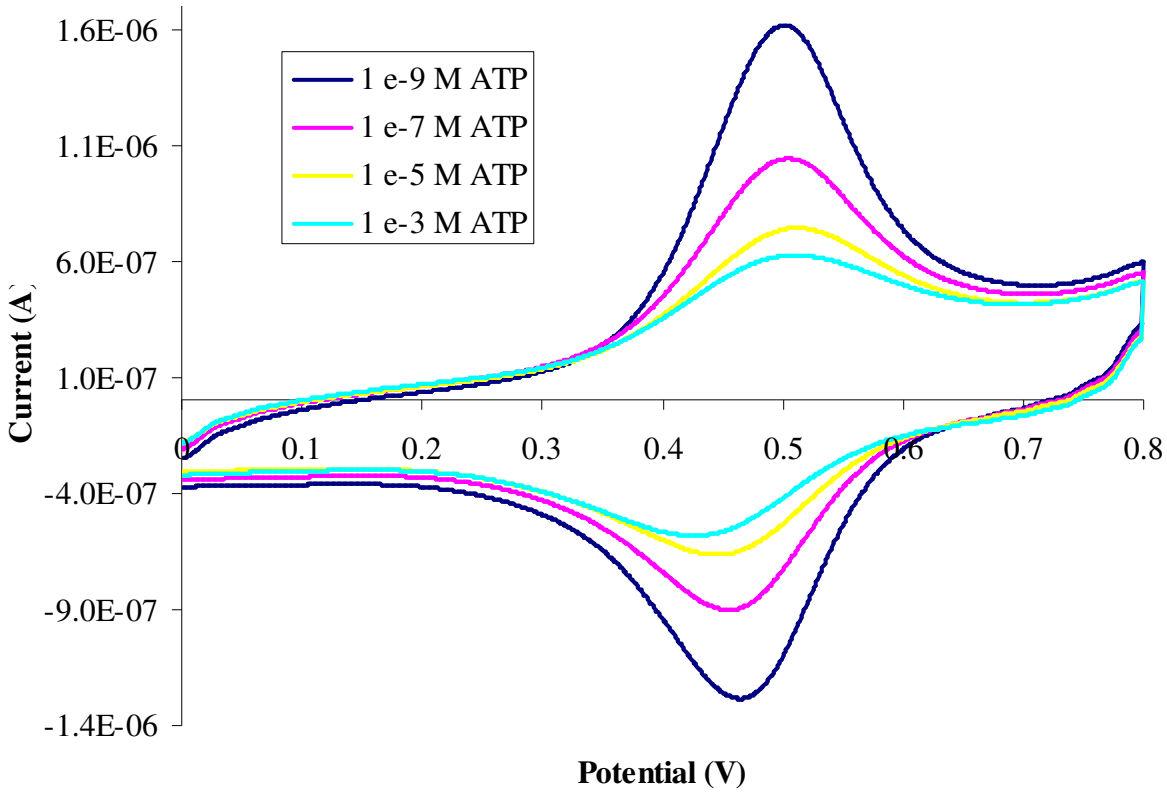

Fig. 6.17 Amperometric response of monolayers of **136** to ATP.

6.5 Monolayer response to changing anion concentration in organic media.

Cyclic voltammetry was also used to investigate the anion sensing ability of monolayers of **131** and **136** versus chloride, dihydrogen phosphate and nitrate anions in organic solvent, namely ACN, with $LiClO_4$ as supporting electrolyte. Monolayers of a (ferrocenylmethyl)trialkylammonium-thiol derivative were recently shown to amperometrically sense dihydrogen phosphate anions in ACN [(1)]. Monolayers of **131** and **136** were again prepared and titrated versus increasing concentrations of anions. In theory, the sensing of anions in organic solvent should be more favourable than in aqueous solution as there is no competitive binding from the solvent [(2)]. However the degree of linear correlation for the change in peak currents versus concentration was less than those for experiments in aqueous media. For monolayers of **131**, titration with

chloride ions yielded R^2 values of 0.9529 and 0.954 (Figure 6.18). Similarly for monolayers of **136,** titration with dihydrogen phosphate and nitrate yielded R^2 values between 0.9549 and 0.9845 (Figure 6.19 and Figure 6.20).

It is possible that the organic solvent may dissolve part of the molecule from the electrode surface resulting in a less linear response. This would not be evident in aqueous media as the receptor molecules are insoluble in water.

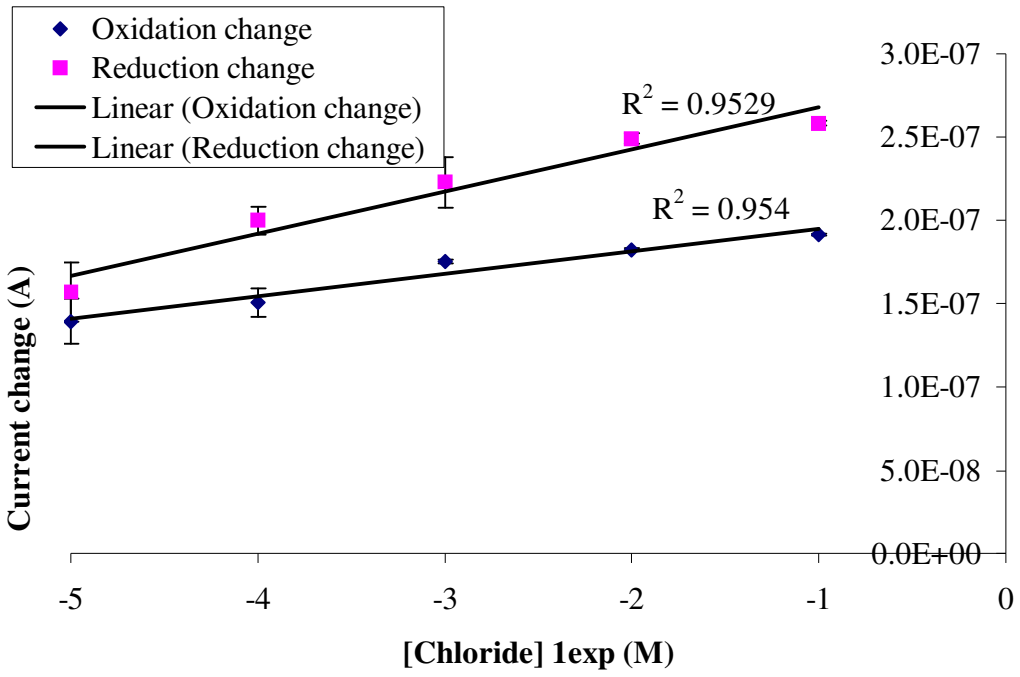

Fig. 6.18 Response of monolayers of **131** to chloride in ACN.

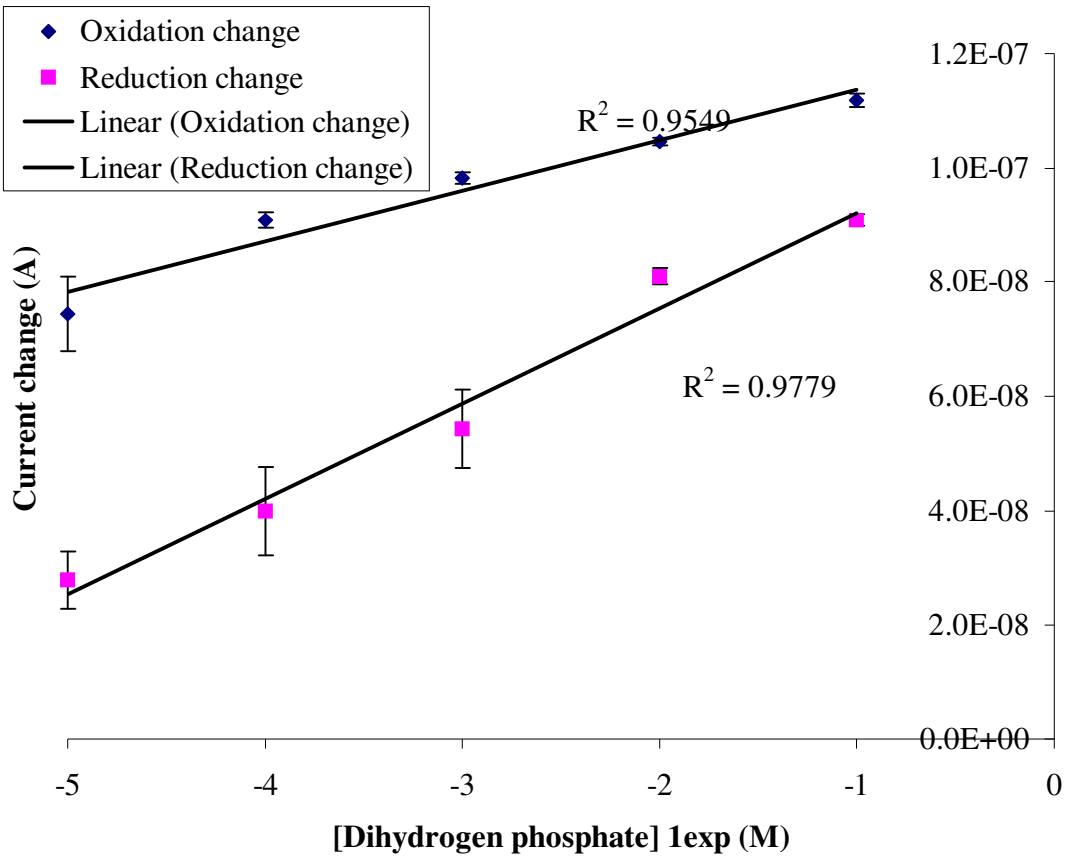

Fig. 6.19 Response of monolayers of **136** to dihydrogen phosphate in ACN.

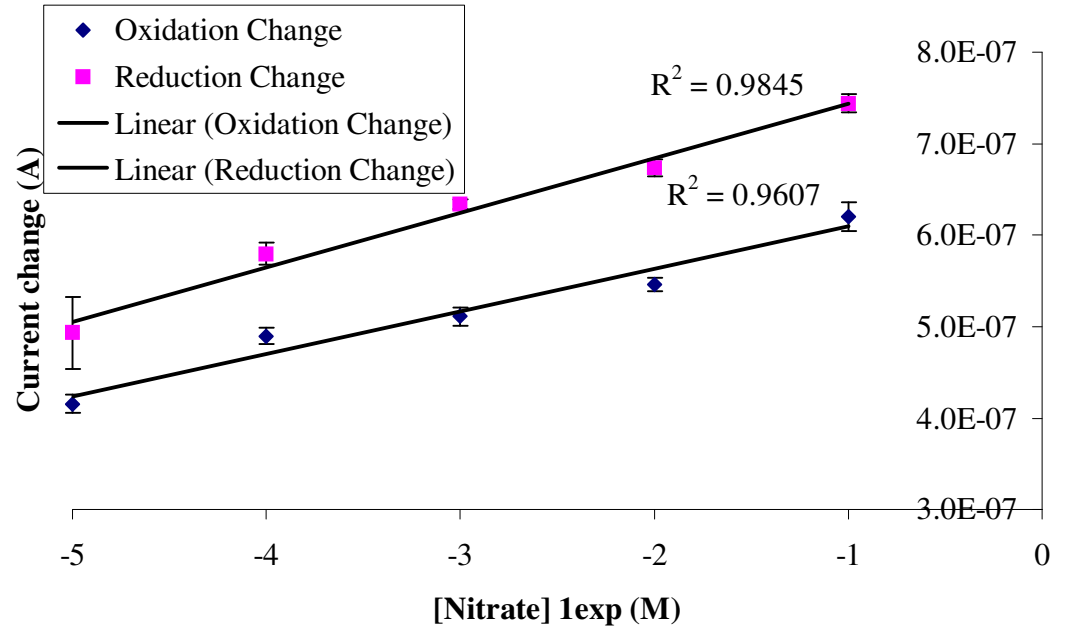

Fig. 6.20 Response of monolayers of **136** to nitrate in ACN.

6.6 Conclusions.

Whilst the detection and quantitation of cationic species has been extensively studied, the development of anion sensors is now an area of intense research due to their role in biological and environmental systems [(12)]. Research in this laboratory demonstrated the success of *N*-ferrocenoyl peptides esters as anion sensing agents. A series of recognition devices were prepared where *N*-ferrocenoyl and *N*-(ferrocenyl)benzoyl peptide esters were prepared and anchored to gold electrodes *via* a gold-sulphur bond. It was envisaged that immobilization on a surface would enable anions to be detected in aqueous electrolytes. It was initially thought that the detection event might be measured potentiometrically following a cathodic shift in the Fc/Fc^{+} redox couple. However no visible changes in redox potential were observed. Instead, the *N*-ferrocenoyl and *N*-(ferrocenyl)benzoyl peptide esters amperometrically sensed chloride, nitrate and dihydrogen phosphate anions. The magnitude of the oxidation and reduction peak currents changed dramatically during preliminary titration experiments for SAMs of each molecule **129-136**. The most sensitive molecules were then chosen for further study and monolayers of compound **131** gave a linear response to varying concentrations of chloride while **136** gave a linear response to nitrate and dihydrogen phosphate anions respectively, in the range of zero to 1×10^{-5} M .

The sensitivity of monolayers of compound **131** towards chloride may be a result of structural orientation on the gold surface. The *ortho* orientation of compound **131** may result in a binding pocket of complimentary size for the chloride anion where the amide group and the ferrocene moiety can cooperatively interact with the anion. Similarly, the response of monolayers of compound **136** towards nitrate and dihydrogen phosphate may be attributed to the two amide groups in relative proximity to the ferrocene moiety where a strong interaction between anion and receptor is possible. The amperometric recognition of adenosine nucleotides was also successfully accomplished using monolayers of compound **136**. The change in oxidation and reduction peak current was linear with respect to increasing anion concentration with nanomolar sensitivity in each case. This response may be attributed to the two amide groups in relative proximity to the ferrocene moiety where strong cooperative interaction between anion and receptor

binding sites is possible. The small degree of error following triplicate measurements indicates a high degree of reproducibility. To the best of our knowledge monolayers of compound **136** are the first ferrocene based monolayers that can amperometrically sense dihydrogen phosphate and adenosine nucleotides in aqueous media. These findings have major potential for the development of novel sensory devices capable of detecting various anionic species in water.

In future, 1,1'-*N*,*N*'-ferrocenoylbispeptide esters could be immobilized onto gold electrodes. This would create a large binding cavity and the additional amide groups would aid complexation. Also, the inclusion of a pyrrole or pyridine as a spacer groups between the ferrocene and peptide moieties would also provide additional hydrogen bonding groups and may increase sensitivity. In addition, the detection of neurologically important anions such as lactate ($CH_3CH(OH)COO^-$), pyruvate (CH_3COCOO^-) and glutamate ($HOOC–CH(NH_2)CH_2CH_2COO^-$) may also be investigated.

References.

1. Reynes, O., Bucher, C., Moutet, J-C., Royal, G., Saint-Aman, E., *Inorg. Chim. Acta.*, **2008**, *261*, 1784.
2. Beer, P. D., Gale, P. A., *Angew. Chem. Int. Ed.*, **2001**, *40*, 486.
3. Goel, A., Brennan, N., Brady, N., Kenny, P. T. M., *Biosens. Bioelectron.*, **2007**, *22*, 2047.
4. Gallagher, J. F., Kenny, P. T. M., Sheehy, M. J., *Inorg. Chem. Comm.*, **1999**, *2*, 327.
5. Gowan, R. J., Tett, P., Kennington, K., Mills, D. K., Shammon, T. M., Stewart, B. M., Greenwood, N., Flanagan, C., Devlin, M., Wither, A., *Estuarine*, *Coastal and Shelf Sci.*, **2008**, *76*, 239.
6. Mc Intyre, A. D., *Marine Pollution Bulletin*, **1995**, *31*, 147.
7. Dunne, E. J., Culleton, N., O'Donovan, G., Harrington, R., Olsen, A. E., *Ecol. Eng.*, **2005**, *24*, 221.
8. Clenaghan, C., Collins, C., Crowe, C., **2001**, *Phosphorous Regulation National Implementation Report*, EPA.
9. Bard, A. J., Faulkner, L.R., *Electrochemical Methods: Fundamentals and Applications*, **2001**, 2nd Edition, Wiley.
10. Savage, D. M., *' The Synthesis and Characterization of Novel N-Ferrocenyl Benzoyl Amino Acid and Dipeptide Derivatives'*, DCU, Ph.D, Thesis, **2003**.
11. Perez-Ruiz, T., Martinez-Lozano, C., Tomas, V., Martin, J., *Anal. Bioanal. Chem*, **2003**, *377*, 189.
12. Zhang, S., Palkar, A., Echegoyen, L., *Langmuir*, **2006**, *22*, 10732.

Experimental details

Experimental Note

All chemicals were purchased from Sigma-Aldrich and used as received. Commercial grade reagents were used without further purification. Riedel de Haën silica gel was used for flash and thin layer chromatography. Where necessary solvents were purified prior to use, dichloromethane was distilled from calcium hydride and triethylamine was distilled and stored over potassium hydroxide pellets. Melting points were determined using a Griffin melting point apparatus and are uncorrected. Infrared spectra were recorded on a Nicolet 405 FT-IR spectrometer and UV-Vis spectra on a Hewlett-Packard 8452A diode array UV-Vis spectrophotometer. NMR spectra were obtained on a Bruker AC 400 NMR spectrometer operating at 400 MHz for ^{1}H NMR and 100 MHz for ^{13}C NMR. The ^{1}H and ^{13}C NMR chemical shifts (ppm) are relative to TMS and all coupling constants (*J*) are in Hertz. Electrospray ionization mass spectra were obtained on a Micromass LCT mass spectrometer.

Electrochemistry was performed in a standard three electrode cell, at room temperature, with a polycrystalline macro-gold working electrode, Ag/AgCl reference electrode saturated with KCl and a platinum wire as a counter electrode. All solutions were degassed with N_2 and a stream of N_2 was maintained over the solution during experiments. Cyclic voltammetry experiments were performed on a CH Instruments 600a electrochemical workstation. Working electrodes were polished prior to monolayer formation by polishing with alumina (0.05 μm) followed by sonication in deionized water. The electrodes were electrochemically cleaned by scanning in 0.5 M H_2SO_4 between -0.25 and 1.45 V until stable voltammograms were obtained. The reference electrode was separated from the solution by a salt bridge filled with 0.5 M H_2SO_4 to prevent contamination of the working electrolyte with chloride ions. The area of the working electrode was determined by integration of the gold oxide reduction peak, taking the charge per square centimetre area as 390 μC for gold. Monolayers of compounds **129-136** were formed by immersing the working electrode in a solution of 0.1 mM of

compounds **129**-**136** in ethanol overnight. Cyclic voltammetry experiments were performed in 0.1 M $LiClO_4$. All experiments were performed in triplicate.

General procedures for the preparation of starting materials for N-(ferrocenyl) and N-(ferrocenoyl) cystine dimethyl esters.

1,1'-Ferrocenedicarboxylic acid 126.

1,1'-Diacetylferrocene (1.06 g, 3.9 mmol) was added to a 10% sodium hypochlorite solution (20 mls) and stirred at 45-50 ^oC for 1.5 hours. After 1.5, 2 and 3 hours sodium hypochlorite (10 mls) was added. Following the final addition of the 10% sodium hypochlorite solution the reaction was stirred for a further 2 hours. The reaction mixture was then filtered while hot and treated with bisulfite solution (5%). Dilute HCl was added and the crude product was isolated by filtration. The crude product was redissolved in sodium bicarbonate solution (5%) and refiltered. The filtrate was treated with dilute HCl and the pure product was collected by filtration as an orange solid (0.67g, 62%) m.p. (decomp.) at 260 ^oC.

^1H NMR (400 MHz) δ (d_6-DMSO): 12.32 (2H, s, -COO*H*), 4.69 {4H, s, *ortho* on (η^5-C_5H_4)}, 4.45 {4H, s, *meta* on (η^5-C_5H_4)}.

^{13}C NMR (100 MHz) δ (d_6-DMSO): 171.0, 73.4, 72.6, 71.2.

Methyl-6-ferrocenylnaphthalene-2-carboxylate 127.

Concentrated hydrochloric acid (4 mls) was added to a solution of methyl-6-aminonaphthalene-2-carboxylate (0.58 g, 2.7 mmol) in 15 mls of deionized water. Sodium nitrite (0.18 g, 2.7 mmol) in 15 mls of deionized water was then added to this solution with stirring at a temperature of less that 5 ^oC. The resulting pale yellow diazonium salt was added to ferrocene (0.50 g, 2.7 mmol) in 50 mls of diethyl ether and allowed to react for 12 hours. The reaction was then washed with water and the organic layer was dried over $MgSO_4$. The solvent was removed *in vacuo*. Column chromatography {eluant 3:2 petroleum ether (40-60 ^oC):diethyl ether} yielded the desired product as a red solid (0.12 g, 12%). m.p. 156-158 ^oC.

^{1}H NMR (400 MHz) δ (d_6-DMSO): 8.55 (1H, s, ArH), 8.11 (1H, s, ArH), 8.08 (1H, d, *J* = 8.8 Hz, ArH), 7.99-7.95 (2H, m, ArH), 7.81 (1H, dd, *J* = 1.6 Hz, *J* = 8.8 Hz, ArH), 4.91 {2H, t, *J* = 1.6 Hz, *ortho* on (η^5-C_5H_4)}, 4.46 {2H, t, *J* = 1.6 Hz, *meta* on (η^5-C_5H_4)}, 4.04 {5H, s, (η^5-C_5H_5)}, 3.91 (3H, s, -OC*H*$_3$).

^{13}C NMR (100 MHz) δ (d_6-DMSO): 166.4, 140.0, 135.4, 130.6, 130.4, 129.2, 127.8, 126.1, 125.8, 125.1, 122.7, 83.7, 69.6, 69.5, 66.8, 52.2.

6-Ferrocenylnaphthalene-2-carboxylic acid 128.

Methyl-6-ferrocenylnaphthalene-2-carboxylate (0.12 g, 0.32 mmol) in 15 mls of methanol was added to 15 mls of a 10% sodium hydroxide solution and refluxed for 3 hours. The solution was cooled in ice and concentrated HCl was added until pH 2 was reached. The product was isolated by filtration as an orange solid (0.07 g, 61%). m.p. (decomp.) at 200 ^{o}C.

^{1}H NMR (400 MHz) δ (d_6-DMSO): 12.7 (1H, s, -COO*H*), 8.55 (1H, s, ArH), 8.04 (1H, s, ArH), 8.03 (1H, d, *J* = 8.4 Hz, ArH), 7.92 (2H, s, ArH), 7.81 (1H, dd, *J* = 1.6 Hz, *J* = 8.4 Hz, ArH), 4.99 {2H, t, *J* = 1.6 Hz, *ortho* on (η^5-C_5H_4)}, 4.47 {2H, t, *J* = 1.6 Hz, *meta* on (η^5-C_5H_4)}, 4.01 {5H, s, (η^5-C_5H_5)}.

^{13}C NMR (100 MHz) δ (d_6-DMSO): 167.5, 139.7, 135.3, 130.6, 130.4, 129.1, 127.6, 127.0, 125.9, 125.5, 122.7, 83.8, 69.6, 69.5, 66.7.

Procedures for the preparation of N-(ferrocenyl)$_2$ and N-(ferrocenoyl)$_2$ cystine dimethyl esters.

{*N*-(ferrocenoyl)}$_2$-L-cystine dimethyl ester 129.

N-(3-dimethylaminopropyl)-*N'*-ethylcarbodiimide hydrochloride (0.16 g 0.84 mmol), triethylamine (2 mls) and 1-hydroxybenzotriazole (0.12 g, 0.88 mmol) were added to a solution of ferrocenecarboxylic acid (0.20 g, 0.87 mmol) in dichloromethane at 0 ^{o}C. After 30 minutes L-cystine dimethyl ester hydrochloride (0.15 g, 0.44 mmol) was added, the solution was raised to room temperature and was stirred for 48 hours. The solvent was

removed *in vacuo* and the product was purified by column chromatography (eluant ethyl acetate) and isolated as a yellow powder (0.10 g, 33%). m.p. 177-179 ^{o}C.

I.R. ν_{max} (KBr): 3446, 2920, 1740, 1635, 1490, 1049 cm^{-1}.

UV-Vis λ_{max} ACN: 435 nm.

^{1}H NMR (400 MHz) δ (*d*$_6$-DMSO): 8.19 (2H, d, *J* = 7.6 Hz, -CON*H*-), 4.84-4.82 {4H, m, *ortho* on (η^5-C_5H_4)}, 4.72-4.66 {2H, m, -C*H*(CH_2S-)}, 4.39 {4H, s, meta on (η^5-C_5H_4)}, 4.23 {10H, s, (η^5-C_5H_5)}, 3.68 (6H, s, -OC*H*$_3$), 3.22-3.11 {4H, m, -CH(C*H*$_2$S-)}.

^{13}C NMR (100 MHz) δ (*d*$_6$-DMSO): 171.3, 169.1, 75.5, 70.2, 69.4, 68.3, 52.2, 51.7, 38.8 (-ve DEPT).

Mass spectrum: found: $[M+H]^+$ 693.0472,

$C_{30}H_{33}N_2O_6S_2Fe_2$ requires: 693.0479.

1,1'-Ferrocenoyl-L-cystine dimethyl ester 130.

N-(3-dimethylaminopropyl)-*N'*-ethylcarbodiimide hydrochloride (0.34 g 1.8 mmol), triethylamine (2 mls) and 1-hydroxybenzotriazole (0.24 g, 1.8 mmol) were added to a solution of 1,1'-ferrocenedicarboxylic acid (0.20 g, 0.7 mmol) in dichloromethane at 0 ^{o}C. After 30 minutes L-cystine dimethyl ester hydrochloride (0.25 g, 0.7 mmol) was added, the solution was raised to room temperature and was stirred for 48 hours. The solvent was removed *in vacuo* and the product was purified by column chromatography (eluant ethyl acetate) and isolated as a yellow powder (0.04 g, 11%). m.p. 207-209 ^{o}C.

I.R. ν_{max} (KBr): 3438, 2921, 1747, 1645, 1494, 1451, 1050 cm^{-1}.

UV-Vis λ_{max} ACN: 431 nm.

^{1}H NMR (400 MHz) δ (*d*$_6$-DMSO): 8.28 (2H, d, *J* = 8 Hz, -CON*H*-), 4.82-4.77 {4H, m, -C*H*(CH_2S-), (η^5-C_5H_4)}, 4.65 {2H, s, (η^5-C_5H_4)}, 4.53 {2H, s, (η^5-C_5H_4)} 4.38 {2H, s, (η^5-C_5H_4)}, 3.63 (6H, s, -OC*H*$_3$), 3.03-2.98 {4H, m, -C*H*(CH_2S-)}

^{13}C NMR (100 MHz) δ (*d*$_6$-DMSO): 171.0, 168.4, 78.1, 71.0, 70.7, 70.2, 70.0, 52.2, 51.7, 38.9 (-ve DEPT).

Mass spectrum: found: $[M+H]^+$ 507.0324,

$C_{20}H_{23}N_2O_6S_2Fe$ requires: 507.0347.

{*N-ortho*-(ferrocenyl)-benzoyl}$_2$-L-cystine dimethyl ester 131.

N-(3-dimethylaminopropyl)-*N'*-ethylcarbodiimide hydrochloride (0.16 g 0.84 mmol), triethylamine (2 mls) and 1-hydroxybenzotriazole (0.12 g, 0.88 mmol) were added to a solution of *ortho*-ferrocenyl benzoic acid (0.26 g, 0.84 mmol) in dichloromethane at 0 ^{o}C. After 30 minutes L-cystine dimethyl ester hydrochloride (0.15 g, 0.44 mmol) was added, the solution was raised to room temperature and was stirred for 48 hours. The solvent was removed *in vacuo* and the product was purified by column chromatography (eluant ethyl acetate) and isolated as a yellow powder (0.05 g, 13%). m.p. 180-182 ^{o}C.

I.R. ν_{max} (KBr): 3444, 2925, 1747, 1646, 1493, 1051 cm^{-1}.

UV-Vis λ_{max} ACN: 340, 445 nm.

^{1}H NMR (400 MHz) δ (d_6-DMSO): 9.01 (2H, d, *J* = 8 Hz, -CON*H*-), 7.88 (2H, d, *J* = 7.6 Hz, ArH), 7.49 (2H, t, *J* = 7.6 Hz, ArH), 7.34-7.28 (4H, m, ArH), 4.81-4.76 {2H, m, -C*H*(CH_2S-)}, 4.73 {4H, s, *ortho* on (η^5-C_5H_4)}, 4.39 {4H, s, meta on (η^5-C_5H_4)}, 4.11 {10H, s, (η^5-C_5H_5)}, 3.77 (6H, s, -OC*H*$_3$), 3.31, {2H, dd, *J* = 4.8 Hz, *J* = 13.6 Hz, -CH(C*H*$_2$S-)}, 3.13-3.07 {2H, m, -CH(C*H*$_2$S-)}.

^{13}C NMR (100 MHz) δ (d_6-DMSO): 171.0, 169.8, 136.6, 136.2, 130.1, 129.0, 127.4, 125.4, 84.0, 69.5, 68.8, 68.3, 52.3, 51.2, 38.1 (-ve DEPT).

Mass spectrum: found: $[M+H]^+$ 845.1089,

$C_{42}H_{41}N_2O_6S_2Fe_2$ requires: 845.1105.

{*N-meta*-(ferrocenyl)-benzoyl}$_2$-L-cystine dimethyl ester 132.

N-(3-dimethylaminopropyl)-*N'*-ethylcarbodiimide hydrochloride (0.16 g 0.84 mmol), triethylamine (2 mls) and 1-hydroxybenzotriazole (0.12 g, 0.88 mmol) were added to a solution of *meta*-ferrocenyl benzoic acid (0.26 g, 0.84 mmol) in dichloromethane at 0 ^{o}C. After 30 minutes L-cystine dimethyl ester hydrochloride (0.15 g, 0.44 mmol) was added, the solution was raised to room temperature and was stirred for 48 hours. The solvent was removed *in vacuo* and the product was purified by column chromatography (eluant ethyl acetate) and isolated as a yellow powder (0.11 g, 30%). m.p. 190-192 ^{o}C.

I.R. ν_{max} (KBr): 3444, 2990, 1734, 1568, 1547, 1638, 1494 cm^{-1}.

UV-Vis λ_{max} ACN: 325, 438 nm.

^{1}H NMR (400 MHz) δ (d_6-DMSO): 9.04 (2H, d, *J* = 7.6 Hz, -CON*H*-), 8.03 (2H, s, ArH), 7.50 (4H, t, *J* = 6.4 Hz, ArH), 7.46 (2H, q, *J* = 8 Hz, ArH), 4.95-4.90 {6H, m, *ortho* on (η^5-C_5H_4), -C*H*(CH_2S-)}, 4.52 {4H, s, *meta* on (η^5-C_5H_4)}, 4.09 {10H, s, (η^5-C_5H_5)}, 3.75 (6H, s, -OC*H*$_3$), 3.52-3.30 {4H, m, -CH(C*H*$_2$S-)}.

^{13}C NMR (100 MHz) δ (d_6-DMSO): 171.1, 166.4, 139.4, 133.4, 129.2, 128.5, 124.9, 124.5, 83.9, 69.1, 66.5, 66.4, 52.3, 51.8, 38.8 (-ve DEPT).

Mass spectrum: found: $[M+H]^+$ 845.1068,

$C_{42}H_{41}N_2O_6S_2Fe_2$ requires: 845.1105.

{*N-para*-(ferrocenyl)-benzoyl}$_2$-L-cystine dimethyl ester 133.

N-(3-dimethylaminopropyl)-*N'*-ethylcarbodiimide hydrochloride (0.16 g 0.84 mmol), triethylamine (2 mls) and 1-hydroxybenzotriazole (0.12 g, 0.88 mmol) were added to a solution of *para*-ferrocenyl benzoic acid (0.26 g, 0.84 mmol) in dichloromethane at 0 ^{o}C. After 30 minutes L-cystine dimethyl ester hydrochloride (0.15 g, 0.44 mmol) was added, the solution was raised to room temperature and was stirred for 48 hours. The solvent was removed *in vacuo* and the product was purified by column chromatography (eluant ethyl acetate) and isolated as an orange powder (0.12 g, 32%). m.p. 193-195 ^{o}C

I.R. ν_{max} (KBr):3445, 2926, 1740, 1609, 1541, 1494, 1452 cm^{-1}.

UV-Vis λ_{max} ACN: 350, 450 nm.

^{1}H NMR (400 MHz) δ (d_6-DMSO): 8.90 (2H, d, *J* = 7.6 Hz, -CON*H*-), 7.74 (4H, d, *J* = 8.4 Hz, ArH), 7.57 (4H, d, *J* = 8.4 Hz, ArH), 4.85 {4H, s, *ortho* on (η^5-C_5H_4)}, 4.80-4.74 {2H, m, -C*H*(CH_2S-)}, 4.40 {4H, s, *meta* on (η^5-C_5H_4)}, 4.00 {10H, s, (η^5-C_5H_5)}, 3.79 (6H, s, -OC*H*$_3$), 3.27-3.14 {4H, m, -CH(C*H*$_2$S-)}.

^{13}C NMR (100 MHz) δ (d_6-DMSO): 171.2, 166.6, 143.3, 130.3, 127.6, 125.4, 82.9, 69.6, 69.5, 66.6, 52.3, 51.8, 38.4 (-ve DEPT).

Mass spectrum: found: $[M+H]^+$ 845.1122,

$C_{42}H_{41}N_2O_6S_2Fe_2$ requires: 845.1105.

{*N-6-ferrocenyl-2-naphthoyl*}$_2$-L-cystine dimethyl ester 134.

N-(3-dimethylaminopropyl)-*N′*-ethylcarbodiimide hydrochloride (0.05 g 0.2 mmol), triethylamine (2 mls) and 1-hydroxybenzotriazole (0.03 g, 0.2 mmol) were added to a solution of 6-ferrocenylnaphthalene-2-carboxylic acid (0.07 g, 0.2 mmol) in dichloromethane at 0 ^{o}C. After 30 minutes L-cystine dimethyl ester hydrochloride (0.4 g, 0.1 mmol) was added, the solution was raised to room temperature and was stirred for 48 hours. The solvent was removed *in vacuo* and the product was purified by column chromatography (eluant ethyl acetate) and isolated as an orange powder (0.12 g, 32%). m.p. 125-127 ^{o}C.

I.R. ν_{max} (KBr): 3444, 2926, 1745, 1620 1494, 1050 cm^{-1}.

UV-Vis λ_{max} ACN: 376, 442 nm.

^{1}H NMR (400 MHz) δ (*d*$_6$-DMSO): 9.06 (2H, d, *J* = 7.6 Hz, -CON*H*-), 8.44 (2H, s, ArH), 8.08-7.79 (10H, m, ArH), 4.97 {4H, t, *J* = 2 Hz, *ortho* on (η^5-C_5H_4)}, 4.87-4.80 {2H, m, -C*H*(CH_2S-)}, 4.46 {4H, t, *J* = 2 Hz, *meta* on (η^5-C_5H_4)}, 4.06 {10H, s, (η^5-C_5H_5)}, 3.70 (3H, s, -OC*H*$_3$), 3.07-2.93 {4H, m, -CH(C*H*$_2$S-)}.

^{13}C NMR (100 MHz) δ (*d*$_6$-DMSO): 170.7, 166.5, 139.3, 137.8, 134.3, 131.6, 128.7, 127.7, 127.4, 126.0, 125.5, 123.8, 83.9, 69.4, 66.6, 66.5, 51.8, 50.5, 37.7 (-ve DEPT).

Mass spectrum: found: $[M+H]^+$ 945.1404,

$C_{50}H_{45}N_2O_6S_2Fe_2$ requires: 945.1418.

{*N-para*-(ferrocenyl)-benzoyl-glycine}$_2$-L-cystine dimethyl ester 135.

N-(3-dimethylaminopropyl)-*N′*-ethylcarbodiimide hydrochloride (0.30 g 1.6 mmol), triethylamine (2 mls) and 1-hydroxybenzotriazole (0.22 g, 1.6 mmol) were added to a solution of *para*-(ferrocenyl) benzoic acid (0.52 g, 1.6 mmol) in dichloromethane at 0 ^{o}C. After 30 minutes (glycine)$_2$-L-cystine dimethyl ester (0.28 g, 0.88 mmol) was added, the solution was raised to room temperature and was stirred for 48 hours. The solvent was removed *in vacuo* and the product was purified by column chromatography (eluant ethyl acetate) and isolated as an orange powder (0.17 g, 20%). m.p. 144-146 ^{o}C.

I.R. ν_{max} (KBr): 3442, 2926, 1747, 1700, 1607, 1494, 1450 cm^{-1}.

UV-Vis λ_{max} ACN: 355, 450 nm.

^{1}H NMR (400 MHz) δ (*d*$_6$-DMSO): 8.70 (2H, t, *J* = 6 Hz, -CON*H*-), 8.55 (2H, d, *J* = 7.6 Hz, -CON*H*-), 7.77 (4H, d, *J* = 8.4 Hz, ArH), 7.59 (4H, d, *J* = 8.4 Hz, ArH), 4.85 {4H, s, *ortho* on (η^5-C_5H_4)}, 4.63 {2H, q, *J* = 8 Hz, -C*H*(CH_2S-)}, 4.39 {4H, s, *meta* on (η^5-C_5H_4)}, 3.99 {10H, s, (η^5-C_5H_5)}, 3.93 (4H, d, *J* = 5.2 Hz, -NHC*H*$_2$CO-), 3.77 (6H, s, -OC*H*$_3$), 3.17-3.12 {2H, m, -CH(C*H*$_2$S-)}, 2.99-2.94 {2H, m, -CH(C*H*$_2$S-)}.

^{13}C NMR (100 MHz) δ (*d*$_6$-DMSO): 170.8, 169.5, 166.5, 143.0, 130.7, 127.5, 125.4, 83.0, 69.6, 69.5, 66.5, 52.3, 51.2, 42.1 (-ve DEPT), 38.9 (-ve DEPT).

Mass spectrum: found: $[M+H]^+$ 959.1550,

$C_{46}H_{47}N_4O_8S_2Fe_2$ requires: 959.1534.

{*N*-(ferrocenoyl)-β-alanine}$_2$-L-cystine dimethyl ester 136.

N-(3-dimethylaminopropyl)-*N′*-ethylcarbodiimide hydrochloride (0.46 g 2.42 mmol), triethylamine (2 mls) and 1-hydroxybenzotriazole (0.33 g, 2.42 mmol) were added to a solution of ferrocenecarboxylic acid (0.56 g, 2.42 mmol), in dichloromethane at 0 ^{o}C. After 30 minutes (β-alanine)$_2$-L-cystine dimethyl ester (0.46 g, 1.21 mmol) was added, the solution was raised to room temperature and was stirred for 48 hours. The solvent was removed *in vacuo* and the product was purified by column chromatography (eluant ethyl acetate) and isolated as a yellow powder (0.23 g, 23%). m.p. 136-138 ^{o}C.

I.R. ν_{max} (KBr): 3444, 2926, 1740, 1622, 1547, 1494, 1452 cm^{-1}.

UV-Vis λ_{max} ACN: 440 nm.

^{1}H NMR (400 MHz) δ (*d*$_6$-DMSO): 8.54 (2H, d, *J* = 7.6 Hz, -CON*H*-), 7.80 (2H, t, *J* = 5.6 Hz, -CON*H*-), 4.76 {4H, s, *ortho* on (η^5-C_5H_4)}, 4.61-4.57 {2H, m, -C*H*(CH_2S-)}, 4.33 {4H, s, *meta* on (η^5-C_5H_4)}, 4.16 {10H, s, (η^5-C_5H_5)}, 3.64 (6H, s, -OC*H*$_3$), 3.42-3.36 (4H, m, -NHC*H*$_2$CH$_2$CO-), 3.12 {2H, dd, *J* = 5.2 Hz, *J* = 13.8 Hz, -CH(C*H*$_2$S-)}, 2.98-2.94 {2H, m, -CH(C*H*$_2$S-)} 2.46 (4H, t, *J* = 7.2 Hz, -NHCH$_2$C*H*$_2$CO-).

^{13}C NMR (100 MHz) δ (*d*$_6$-DMSO): 170.9, 170.7, 169.0, 82.7, 69.3, 68.1, 68.0, 52.7, 51.6, 39.0 (-ve DEPT), 35.5 (-ve DEPT), 35.3 (-ve DEPT).

Mass spectrum: found: $[M+H]^+$ 835.1234,

$C_{36}H_{43}N_4O_8S_2Fe_2$ requires: 835.1221.

Appendix

Abbreviations

µl	Microlitre.
µM	Micromolar.
^{o}C	Degrees Celsius.
Ala	Alanine.
ADP	Adenosine diphosphate.
AMP	Adenosine monophosphate.
ATP	Adenosine triphosphate.
Abu	2-aminobutyric acid.
ACN	Acetonitrile.
AR	Androgen receptor.
BOC	*Tert*-butoxycarbonyl.
BOP	Benzotriazolyl-1-oxy-tris-(dimethylamino)-phosphonium hexafluorophosphate.
$CDCl_3$	Deuterated chloroform.
CME	Chemically modified electrode.
CO_2	Carbon dioxide.
CV	Cyclic Voltammetry.
Da	Dalton.
DCC	Dicyclohexylcarbodiimide.
DCM	Dichloromethane.
DCU	*N, N'*-Dicyclohexylurea.
DEPT	Distortionless enhancement by polarization transfer.
DME	Dimethoxyethane.
DMSO	Dimethyl sulfoxide.
DNA	Deoxyribonucleic acid.
EC_{50}	Half maximal effective concentration.
EDC	*N*-(3-dimethylaminopropyl)-*N*′-ethylcarbodiimide hydrochloride.
E°′	Formal redox potential.
E*pa*	Anodic peak potential.
E*pc*	Cathodic peak potential.

ER	Estrogen receptor.
ESI	Electrospray ionization.
ESR	Electron spin resonance.
FACS	Fluorescence activated cell sorting.
Fc/Fc^+	Ferrocene/ferricenium redox couple.
FMOC	9-Fluorenylmethoxycarbonyl.
HAB	Harmful Algal Bloom.
HCl	Hydrochloric acid.
HMQC	Heteronuclear multiple quantum coherence.
HOBt	1-Hydroxybenzotriazole.
Hz	Hertz.
IC_{50}	Half maximal inhibitory concentration.
IR	Infrared.
ISE	Ion selective electrode.
$LiClO_4$	Lithium Perchlorate.
M	Molar.
MDR	Multi-drug resistance.
MeOH	Methanol.
$MgSO_4$	Magnesium sulphate.
MHz	Mega hertz.
ml	Millilitre.
MLCT	Metal-ligand charge transfer.
mmol	Millimole.
MS	Mass spectrometry.
mV	Millivolt.
NADH	Nicotinamide adenine dinucleotide.
$NaNO_2$	Sodium nitrite.
Nle	Norleucine.
nM	Nanomolar.
NMR	Nuclear magnetic resonance.
NSCLC	Non-small cell lung cancer.

Nva	Norvaline.
Pgp	P-glycoprotein.
ppm	Parts per million.
RBA	Relative binding affinity.
ROS	Reactive oxygen species.
RSD	Relative standard deviation.
SAM	Self assembled monolayer.
SCLC	Small cell lung cancer.
SERM	Specific estrogen receptor modulator.
$SOCl_2$	Thionyl chloride.
SOD	Superoxide dismutase.
TBAP	Tetrabutylammonium perchlorate.
TBTU	*O*-benzotriazolyl bis(dimethylamino)uronium tetrafluoroborate.
TEA	Triethylamine.
TFA	Trifluoroacetic acid.
TMS	Tetramethylsilane
TPA	Toxin producing algae
UV-Vis	Ultraviolet-Visible
V	Volt.
Z/CBz	Benzyloxycarbonyl.